On the Impact of MIMO Implementations on Cellular Networks: An Analytical Approach from a Systems Perspective

Jong-Han Kim

Dissertation submitted to the Faculty of the Virginia Polytechnic Institute and State University in partial fulfillment of the requirements for the degree of

Doctor of Philosophy
in
Electrical and Computer Engineering

Committee:
Dr. Jeffrey H. Reed (Co-Chair)
Dr. Annamalai Annamalai (Co-Chair)
Dr. William H. Tranter
Dr. Steven W. Ellingson
Dr. Michael R. Taaffe

March 19, 2007
Blacksburg, Virginia

Keywords: MIMO, Spatial Diversity, Uplink, Downlink, DS/CDMA Cellular Network, Cell Capacity, Cell Coverage, Soft Handoff, Power Control

On the Impact of MIMO Implementations on Cellular Networks: An Analytical Approach from a Systems Perspective

Jong-Han Kim

(ABSTRACT)

Multiple-input/multiple-output (MIMO) systems with the adaptive array processing technique, also referred to as *smart antennas*, have received extensive attention in wireless communications due to their ability to combat multipath fading and co-channel interference, two major channel impairments that degrade system performance. However, when smart antennas are deployed in wireless networks, careful attention is required since any defective or imperfect operation of smart antennas can severely degrade the performance of the entire network. Therefore, the evaluation of network performance under ideal and imperfect conditions is critical in the process of system design and should precede deploying smart antennas on the wireless network.

This work focuses on the development of an analytical framework to evaluate the performance of wireless networks based on popular DS/CDMA cellular systems equipped with antenna arrays. Spatial diversity at both the base station (BS) and the mobile station (MS) is investigated through both analytical analysis and simulation. The main contribution of this research is to provide a comprehensive analytical framework for examining the system level performance with multiple antennas at both the BS and the MS. Using the framework developed in this research, system capacity and coverage of the uplink (or reverse link) are investigated when antenna arrays are implemented at both the BS and the MS. In addition, the system capacity and soft handoff capability of the downlink (or forward link) are examined taking into account MIMO. Furthermore, various physical and upper layer parameters that can affect the system level performance

are taken into account in the analytical framework and their combined impact is evaluated. Finally, to validate the analytical analysis results, a system level simulator is developed and selective results are provided.

Dedication

This dissertation is dedicated with love to my heavenly Father, God, my parents, my parents in law, my lovely wife, and my two children.

Acknowledgements

First of all, I would like to give gratitude and praise to my heavenly Father, God, my Savior, Jesus Christ, and my comforter, Holy Spirit for the grace and the love throughout my life.

I thank my advisor Dr. Jeffrey H. Reed for his guidance and support to pursue research topics I am interested in. I have greatly benefited from his valuable guidance, technical inputs and encouragement. Also, my sincere appreciation goes to my co-advisor Dr. A. Annamalai. His technical knowledge, advice, and encouragement have provided me an invaluable experience and allowed me to develop my research capabilities. I would like to thank Dr. William H. Tranter, Dr. Steven W. Ellingson, and Dr. Michael R. Taaffe for serving on my committee, and for their guidance and criticism offered.

My special thanks go to Dr. Kyung Kyoon Bae who also guides me to do my research and helps me a lot to accomplish my Ph.D degree. I also thank Dr. Sang-Uoon Chung, Dr. Yong-Serk Kim, Dr. Sang-Min Bae, and Samsung Electronics for giving the opportunity and supports to finish my Ph.D study at Virginia Tech.

Life in Blacksburg becomes more joyful since I am together with my friends. I would like to thank all members of our informal group, named Max5, including Jin-Suk Park, Hyeonjoong Cho, Jong-Suk Lee, Jae-Sang Lee, Hong-Sun Lim, and Jung-Wook Suh for their friendship and valuable time we spent together. I am also thankful for the friendship of Kyou-Woong Kim, Kye-Hoon Lee, Hae-Soo Kim, Jang-Hoon Oh, Jeong-Heon Lee, Joo-Hong Lee, Brian Choi. I also thank all the members of the Korean Baptist Church of Blacksburg (KBCB), Korean ECE Student Association (KECESA), and Korean Student Association (KSA) at Virginia Tech for providing me with extra curricular activities with close fellowships.

I can’t imagine I can be here without my parents’ support. I really thank them for their love, care and sacrifices they have made for their children. I also thank my parents-in-law for their love, pray, and support. I am deeply grateful to my wife, Ji Yun Yeo. Without her love, pray, patience, and support, I would not have been able to finish my Ph.D. works. Finally, my special thanks go to my two children, Yu-Kyung and Taewook, for giving me such a joy during the tough times as a Ph.D. student.

Contents

List of Figures

List of Tables

Chapter

1 Introduction

1.1 Motivation

Multiple-input/multiple-output (MIMO) systems with the adaptive array processing technique, also referred to as *smart antenna* systems [1, 2], have received extensive attention due to their potential for combating multipath fading and co-channel interference, two major channel impairments that degrade system performance. Deploying smart antennas at the base station (BS) or access point (AP) rather than the mobile station (MS) to avoid increasing the complexity of the MS has been generally accepted as more efficient. However, the advent of high speed, low-power signal processing techniques and small RF components makes it possible to equip smart antennas at the MS [2]. Furthermore, if a smart antenna is already implemented at the BS and optimized in the conventional infrastructure, the additional implementation of a smart antenna at the BS may require re-engineering of overall system, which could be a very time-consuming and costly effort [3]. Thus, implementing a smart antenna at the MS may be an alternative and more cost-effective plan for system performance improvement. Hence, antenna arrays are becoming popular at both BSs and MSs. For example, the high speed downlink packet access (HSDPA) system in wideband CDMA standards uses

MIMO [4], and new wireless LAN standards such as IEEE 802.11n require MIMO implementation.

When smart antennas are deployed in wireless networks, careful attention is required to secure proper network operation because any defective or imperfect operation of smart antennas can severely degrade the performance of the entire network. For instance, even though space-time-coding transmit diversity shows a better performance in the link level than a single transmit antenna implementation, when employed in a high-data rate system with a greedy scheduling algorithm, the system throughput becomes worse than that achieved by a single transmit antenna [5, 6]. Likewise, the system capacity of Global Systems for Mobile (GSM) communications is significantly improved when adaptive beamforming is employed along with the frequency hopping technique rather than when only adaptive beamforming or frequency hopping is employed [7, 8]. Therefore, the evaluation of network performances is critical and should precede deploying smart antennas on the wireless network.

Wireless networks often operate in the presence of heavy interference, and multipath and shadowing lead to signal fading at the receiver. This combination of a complex system and a complicated environment leads to design and analysis problems [9]. Hence, developing an analytically tractable system model that can assist in the design process is crucial. In most cases, simulation can be a helpful tool for gaining insight into system behavior since a properly developed simulation is much like a laboratory implementation of a system. Measurements can easily be made at various points in the system under study. Furthermore, parametric studies are easily conducted since parameter values, such as filter bandwidths and signal-to-noise ratios, can be changed at will, and the effects of these changes on system performance can quickly be observed. However, simulation is not always preferable. Sometimes, even after extensive simulations, one might be unable to obtain insights on the interaction of many system parameters and complex channels. In this case, an analytical analysis might provide insight even though it may require some approximations and assumptions. Furthermore, analytical analysis can assist in solving

the simulation problems. Therefore, simulation and analytical analysis are indispensable and complementary to each other in investigating system performance and designing a system.

Thus, this dissertation presents an analytical framework to evaluate the performance of wireless networks equipped with an antenna array at both the transmitter and receiver.

1.2 Relation to the Previous Works

Basically, this research focuses on investigating the impact of MIMO on the system level performance of DS/CDMA cellular systems in terms of capacity and coverage.

Since DS/CDMA cellular systems are inherently susceptible to multiple access interference due to signals sharing the same frequency band among users, the system capacity can be straightforwardly enhanced by any reduction of interference in the system [10]. Hence, Viterbi, *et al*. showed that the soft handoff, known as macro-diversity, improves the uplink system capacity by reducing the intercell interference [11]. However, it passed over the joint impact of power control and multipath fading on the uplink system capacity which has been shown to significantly affect the interference statistics [12-14]. In addition, several studies [15-18] have shown that soft handoff expands the uplink system coverage due to macro-diversity gain. They, however, handled the system coverage separately from the system capacity despite coverage being closely connected with the system capacity in the presence of co-channel interference in cellular system.

On the other hand, in the downlink, soft handoff has been known to deteriorate the system capacity because multiple BSs allocate a channel to an MS in soft handoff [11, 19-25]. However, they all overlooked the impact of transmit power reduction from combining of the signals from multiple BSs on the system capacity. In addition, most efforts resort to simulation [22, 23, 25, 26], which usually takes too much time, and makes it complicates understanding the general behavior of the system. Note that none of

the previous efforts considered the impact of MIMO on the system performances in their analyses.

Thus, this research extends and generalizes all previous efforts by developing an analytical framework for DS/CDMA cellular systems with MIMO. This research also provides new insights on the relationship between the coverage and capacity and on the downlink soft handoff capability. In addition, performances of transmit diversity and receive diversity will be reappraised from a system perspective.

1.3 Contributions

The original contributions of this research include the following items.

1. This research provides a comprehensive mathematical framework for analyzing the impact of the transmit diversity technique on the system level performance (e.g., capacity and coverage) in the uplink DS/CDMA cellular networks, which includes understanding the impact of
    a. transmit diversity at the MS,
    b. receive diversity at the BS,
    c. general fading channel statistics with arbitrary multipath intensity profiles,
    d. user distributions in a cell,
    e. maximum transmit power allowed by the power amplifier
    f. macro diversity (soft handoff), and
    g. fast and slow power control.
2. Outage capacity and Erlang capacity of the uplink are determined using the developed analytical framework.
3. Capacity and coverage improvements of the uplink with MIMO are determined, including

a. deriving the signal-to-interference ratio (SIR) as a function of the number of users per cell as well as the fade margin to capture the relationship between the system capacity and coverage of the uplink, and

b. assessing the impact of transmit diversity at the MS on the uplink capacity and comparing the gains with receive diversity at the BS.

4. A system level simulator for the cdma2000 standard is created to investigate system level performance of transmit diversity at the MS and to analyze the performance with practical issues that are hard to capture through analytical solutions, such as

    a. the correlation between transmit antennas,

    b. the imperfect calibration of multiple transmit antennas,

    c. feedback delays and errors of closed-loop operation of power control and transmit diversity caused by mobility, and

    d. resolvable multipath combining scheme at the receiver.

5. An analytical framework is developed to assess the system capacity and soft handoff capability with MIMO for the downlink. Specifically, this framework development includes

    a. deriving the fractional power of the BS allocated to an MS with MIMO (maximal ratio transmit antenna diversity at the BS and receive diversity with maximal ratio combining at the MS), soft handoff, and fast power control;

    b. calculating outage probability of the system as a function of the number of users per cell and the percentage of MSs in soft handoff in a cell; and

    c. showing the system capacity and soft handoff capability of the downlink with MIMO.

6. The impact of MIMO channel degeneracy, known as the keyhole effect, on system outage for both the uplink and downlink is assessed.

1.4 Organization

The remainder of this dissertation is organized as follows. Chapter 2 investigates the impact of transmit diversity on the uplink DS/CDMA cellular system. Using an analytical approach, we investigate the impact of exploiting spatial diversity at both the MS and the BS on interference statistics and capacity of the uplink. Generally, spatial diversity techniques help the system achieve the required quality of service (QoS) by flattening the channel. This also results in the multiple access interference reduction in the system, hence improving capacity. Several parameters affecting capacity are considered: transmit diversity order, spatial receive diversity order, the number of multipath components, fade distribution and multiple intensity profile, maximum transmit power, soft-handoff, and user distribution.

In Chapter 3, coverage improvement in the uplink using MIMO is investigated. It is generally accepted that MIMO improves the system coverage as well as the capacity. However, exactly *how* and *how much* MIMO improves the uplink system performances is a bit controversial. Both capacity and coverage of the multiple access system depend on the SIR. Therefore, SIR outage probability is derived based on the number of users per cell and coverage.

In Chapter 4, both capacity and coverage of the uplink are evaluated through simulation. The objective of the system level simulation is not only to verify the analytical results, but also to estimate the system level performance when various practical degradation factors are considered that cannot be modeled with an analytical framework. The system level simulation can also be utilized for analyzing the impact of various communication algorithms on the system level performance. We present various simulation results that consider several practical issues such as feedback delay, mobility, power control error, and antenna correlation.

Chapter 5 discusses the system capacity and soft handoff capability of the downlink with MIMO. An analytical framework for analyzing system performances of the downlink is

developed considering MIMO, soft handoff and fast downlink power control. Using the developed analytical framework, *how* MIMO affects downlink system capacity is demonstrated.

In Chapter 6, the degeneracy of the MIMO channel, known as the *keyhole effect*, is briefly reviewed and its impact on the system performance with MIMO diversity is investigated using the analytical framework developed in the previous chapters.

Finally, this research work is summarized and concluded in Chapter 7.

Chapter

2 Capacity and Interference Statistics of Uplink DS/CDMA Cellular Systems with Transmit Diversity

2.1 Introduction

Direct sequence / code division multiple access (DS/CDMA) cellular systems are inherently susceptible to multiple access interference due to signals sharing the same frequency band among users. Hence, any reduction in interference can be directly converted into an increase in capacity [10]. Since multiple-input multiple-output (MIMO) implementations are now becoming common with the deployment of high speed downlink packet access (HSDPA) in wideband CDMA (WCDMA) systems, multiple antennas at mobile station as well as those at base station can be exploited for improving the uplink system capacity by mitigating the co-channel interference and multipath fading. The main objective of this chapter is to estimate the system capacity of the uplink DS/CDMA cellular systems in terms of outage probability when multiple antennas at mobile station are exploited for transmit diversity. In addition, we also extend the analyses presented in previous related studies [10, 12-14, 27-30] by removing the

restrictions imposed on the multipath intensity profile and fading statistics on different receiving antennas at the base stations.

For example, [10, 27-29] neglect the effect of multipath fading on interference statistics by presuming the multipath fading can be mitigated through rake combining, antenna diversity combining and error correcting coding. However, the joint effect of power control and multipath fading significantly affects interference statistics, which are closely associated with uplink capacity. Hence, [12-14, 30] have revamped the capacity analysis in [10] to account for the effects of multipath fading. Even though [12] and [14] took into account the effect of multipath fading to investigate the impact of rake combining on the system capacity, they simply assumed equal-power multipath profile for simplicity of analysis, which is not a realistic situation. In [30], exponential decayed power delay profile was assumed, but only for Rayleigh fading. [13] applied Rician fading distribution to the capacity analysis but did not consider the frequency selective fading.

- ***Contributions***

Thus, our present work extends and generalizes all the previous related studies by developing an unified mathematical framework for (a) investigating the benefits of transmit diversity, receive diversity, and multipath diversity on the reverse-link capacity (i.e., dissimilar fading statistics among the resolvable multipaths and antenna array elements); (b) providing a better understanding of the interactions between transmit diversity at the mobile stations with multipath diversity and antenna diversity at the base stations as well as power control mechanisms on the system capacity; (c) investigating the effects of fade distributions and branch correlations in spatial and multipath diversity scheme on both intercell and intracell interference statistics; (d) examining the impacts of user distribution in a cell (when users are concentrated on either the inner circle or the outer circle of each cell) on the reverse-link capacity; and finally, (e) observing the Erlang capacity

- ***Organization***

The rest of this chapter is organized as follows. In section 2.2, the system model for the analysis described. In section 2.3, the analytical expression for the fractional power of BS allocated to an MS is derived taking into account MIMO and soft handoff. In section 2.4, how to evaluate the statistics of the fractional power of BS allocated to an MS derived in the previous section are presented. In section 2.5, selective numerical results are presented. Finally, the main points of this chapter are summarized in section 2.6.

2.2 System Model

In the following subsections, the system models, including the cellular architecture for the uplink, propagation channel model, and transmit diversity technique, to analyze the system capacity, will be described in details.

2.2.1 Cell layout

The cellular communication architecture for the analysis is identical to the well-known uniform hexagonal layout with a base station (BS) at the center of every cell as in [10]. The network consists of three rings of hexagonal cells which surround the center cell as shown in Figure 2.1. Mobile stations (MS) are uniformly distributed in each cell. For soft handoff, it is assumed that handoff region is simply determined based on the distance from each BSs, that is, the multiple BSs nearest to an MS are defined as an active set, with which an MS communicate. However, transmit power of an MS is assumed to be perfectly power-controlled by the BS which provides the least average attenuation so as to compensate the channel fluctuation. The propagation channel model incorporates both long-term fading due to shadow fading effects and path loss, and short-term fading due to the multipath fading process with the arbitrary multipath intensity profile. Finally, the analysis is focused on the zeroth BS located in the center of cell layout since the hexagonal layout of the system is symmetric. For the analysis, however, the area of

system is divided into two regions, S_0 and $\overline{S}_0$ as in [28], where S_0 is defined as the soft handoff region which contains the zero[th] BS and $\overline{S}_0$ is defined as the region except S_0 as shown in Figure 2.1.

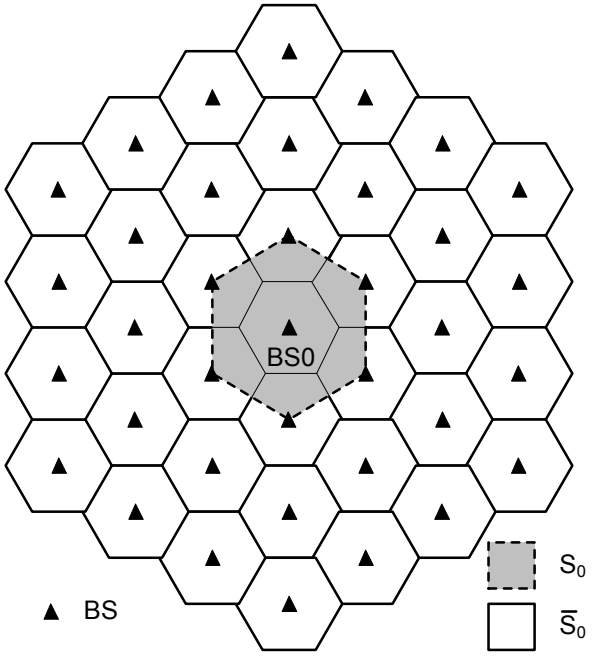

Figure 2.1: Cell layout and soft handoff region

2.2.2 Propagation channel

The propagation channel model incorporates both large-scale propagation loss and small-scale propagation loss. While large-scale propagation loss is caused by path loss between two transceivers and shadowing fading effects, small-scale propagation loss is caused by multipath fading process.

- ***Large-scale propagation loss***

Large-scale propagation loss is often referred as long-term fading or slow fading. Slow fading is generally modeled as the product of the l tḥ power of distance between transceivers and a shadowing component which is log-normally distributed. That is, for a user at a distance r from a base station, the attenuation is given by

$$L(r,u) = r^u 10^{\zeta/10} \tag{2.1}$$

where ζ is the dB attenuation due to the shadowing and Gaussian distributed with zero mean and standard deviation σ. Since our analysis involves a multiple cell system, the propagation model must take into account the dependence of the propagation losses from a mobile user to two or more base stations. Hence, the shadowing can be expressed by the sum of two components: a component in the near field of a user, which is common to all base stations, and a component which pertains solely to the receiving base station and is independent from one base station to another. That is, the random component of the dB loss due to shadowing for the i^{th} BS is given by

$$\zeta_i = a\xi + b\xi_i \quad \text{where } a^2 + b^2 = 1,\ a \le 1 \tag{2.2}$$

where all shadowing components have the zero mean and standard deviation σ. Furthermore,

$$\begin{aligned} E[\xi\xi_i] &= 0 \quad \text{for all } i \\ E[\xi_i\xi_j] &= 0 \quad \text{for all } i \neq j \end{aligned} \tag{2.3}$$

and the normalized correlation coefficient of the losses to two BSs, i and j, is

$$\frac{E[\zeta_i\zeta_j]}{\sigma^2} = a^2 = 1 - b^2 \quad \text{for all } i \neq j \tag{2.4}$$

- ***Small-scale propagation loss***

Due to the reflection by obstacles such as buildings, there are many propagation paths with different delays and different amplitudes, which are generally referred as small-scale propagation loss as compared with path loss and shadow fading. Small-scale propagation loss is also often referred short-term fading or fast fading. Hence, fast fading is generally modeled by

$$h(t,\tau) = \sum_{l=1}^{L} \alpha_l(t)\delta(t - \tau_l) \tag{2.5}$$

where $\alpha_l(t)$ and τ_l are the complex-valued path gain and time delay of the l^{th} path, respectively and L is the number of multipath. Furthermore, $\alpha_l(t)$ satisfies the following condition:

$$\sum_{l=1}^{L} E\left[|\alpha_l(t)|^2\right] = 1 \tag{2.6}$$

In our further analysis, it will be mostly assumed that $|\alpha_l(t)|$ follows Nakagami-*m* distribution since we can take into account various fading environments by only changing the parameter, m. For instance, Nakagami-*m* distribution is equivalent to Rayleigh distribution with $m = 1$ and can also be approximated to Rician distribution with the following relation of the parameter *m* of Nakagami-*m* distribution and the parameter K of Rician distribution [31].

$$m = \frac{1}{\left(1 - \frac{K^2}{(1+K)^2}\right)} \tag{2.7}$$

$$K = \frac{\sqrt{1 - 1/m}}{1 - \sqrt{1 - 1/m}} \tag{2.8}$$

However, our mathematical framework to be presented herein can handle any type of fading distribution including Nakagami-*m*, Nakagami-*q*, and Rician. Furthermore, let us assume that the maximum fading Doppler frequency is relatively low compared to the data modulation symbol rate. Then, we drop the time dependency of the path gain $\alpha_l(t)$. The probability distribution function of Nakagami-*m* is given by

$$f_{\alpha_i}(\alpha) = \frac{2}{\Gamma(m)}\left(\frac{m}{\Omega_i}\right)\alpha^{2m-1}\exp\left(-\frac{m}{\Omega_i}\alpha^2\right) \tag{2.9}$$

where

$$m = \frac{\Omega_i^2}{E\left[(\alpha_i - \Omega_i)^2\right]} \geq \frac{1}{2}, \quad \Omega_i = E\left[\alpha_i^2\right] \tag{2.10}$$

The multipath fading channel can be characterized by the power delay profile. In the analysis, we consider the standard-specific multipath profile such as Pedestrian A and Vehicular A channel shown in Table 2.1 [32].

Table 2.1: Channel models

Channel model	Average power (dB)	Relative delays (μs)
Pedestrian A channel	0,-9.7,-19.2,-22.8	0, 0.11, 0.19, 0.41
Vehicular A channel	0,-1,-9,-10,-15,-20	0, 0.31, 0.79, 1.09, 1.73, 2.51

Now, total propagation loss from a mobile i to a base station j can be denoted by

$$L_{ij} = \frac{X_{ij}}{r_{ij}^{u} 10^{\zeta_{ij}/10}} \tag{2.11}$$

where the denominator is composed of the u th power of distance and a log-normal random variable representing shadowing losses, respectively, and the numerator is a random variable modeling short-term fading loss due to multipath.

2.2.3 Transmit diversity

In third generation DS/CDMA cellular systems, such as WCDMA and cdma2000, transmit diversity techniques are adopted at the base station side for the improvement of downlink performance. Transmit diversity techniques are generally classified into the open-loop transmit diversity and closed-loop transmit diversity based on the usage of feedback to get the transmit channel information [2]. In this work, we will take into account two representative transmit diversity schemes, space-time transmit diversity for the open-loop transmit diversity, and maximal ratio transmit diversity (or transmit beamforming) for the closed-loop transmit diversity, to investigate the impact of transmit diversity at the handset on the system capacity.

- ***Open-loop transmit diversity***

In the open-loop transmit diversity, the transmit diversity does not have any information on the channels. Hence, in order to maximize the diversity, a space-time block code is devised [33] and is employed at the downlink of the third generation DS/CDMA cellular

communication standards [4, 34]. Table 2.2 shows a simple space-time block code employed at WDCMA standard for two transmit antennas.

Table 2.2: Space-time transmit diversity

	Antenna 1	Antenna 2
Symbol 1	x_1	x_2
Symbol 2	$-x_2^*$	x_1^*

where x_1 and x_2 belong to a quadrature-phase shift keying (QPSK) symbol, which are complex numbers. During symbol duration T, x_1 is transmitted from antenna 1, and x_2 from antenna 2. For the next symbol duration, $-x_2^*$ is transmitted from antenna 1, and x_1^* from antenna 2. In a multipath channel with L resolvable multipaths, the received signal from two consecutive symbol durations will be

$$r_1(t) = \sum_{k=1}^{L} \big[h_{1,k} x_1 s(t-\tau_k) + h_{2,k} x_2 s(t-\tau_k) \big] + n(t) \tag{2.12}$$

$$r_2(t) = \sum_{k=1}^{L} \big[-h_{1,k} x_2^* s(t-\tau_k) + h_{2,k} x_1^* s(t-\tau_k) \big] + n(t) \tag{2.13}$$

where $s(t)$ is the spreading sequence. Then, the output of rake finger k will be

$$\begin{aligned} r_{1,k} &= \int_{t_1}^{t_1+T} r_1(t) s^*(t-\tau_k) dt \\ &= h_{1,k} x_1 + h_{2,k} x_2 + n_{1,k} \end{aligned} \tag{2.14}$$

$$\begin{aligned} r_{2,k} &= \int_{t_1}^{t_1+T} r_1(t) s^*(t-\tau_k) dt \\ &= -h_{1,k} x_2^* + h_{2,k} x_1^* + n_{2,k} \end{aligned} \tag{2.15}$$

and the maximum likelihood estimate becomes

$$\begin{aligned} \hat{x}_1 &= \sum_{k=1}^{L} \big(h_{1,k}^* r_{1,k} + h_{2,k} r_{2,k}^* \big) \\ &= \sum_{k=1}^{L} \Big(\big| h_{1,k} \big|^2 + \big| h_{2,k} \big|^2 \Big) x_1 + \tilde{n}_1 \end{aligned} \tag{2.16}$$

$$\begin{aligned}\hat{x}_2 &= \sum_{k=1}^{L}\left(h_{2,k}^{*} r_{1,k} + h_{1,k} r_{2,k}^{*}\right) \\ &= \sum_{k=1}^{L}\left(\left|h_{1,k}\right|^2 + \left|h_{2,k}\right|^2\right) x_2 + \tilde{n}_2\end{aligned} \tag{2.17}$$

That is, space-time block coding, given in Table 2.2, provides $2L$ branch diversity similar to the maximal ratio combining at the receiver. However, note that there is a 3 dB transmit power penalty since the original transmit power is equally distributed to two transmit antenna.

- ***Closed-loop transmit diversity***

In the closed-loop transmit diversity, the transmitter has the knowledge of the channels and transmits on both antennas simultaneously but with weights chosen to optimize the signal-to-noise ratio at the receiver [35]. The closed-loop transmit diversity is also employed at the third generation WCDMA standard [4]. The received signal with weighted transmission is,

$$r(t) = \sum_{k=1}^{L}\left[w_1 h_{1,k} x \cdot s(t-\tau_k) + w_2 h_{2,k} x \cdot s(t-\tau_k)\right] + n(t) \tag{2.18}$$

The k^{th} rake finger output is,

$$r_k = \int_{t_1}^{t_1+T} r(t) s^{*}(t-\tau_k) dt = \left(w_1 h_{1,k} + w_2 h_{2,k}\right) x + n_k \tag{2.19}$$

and the maximal ratio combiner (MRC) output is

$$\begin{aligned}\hat{x} &= \sum_{k=1}^{L}\left(w_1 h_{1,k} + w_2 h_{2,k}\right)^{*} r_k \\ &= \sum_{k=1}^{L}\left\{\left\|w_1 h_{1,k} + w_2 h_{2,k}\right\|^2 x_k + \left(w_1 h_{1,k} + w_2 h_{2,k}\right) n_k\right\}\end{aligned} \tag{2.20}$$

Hence, the equivalent channel after antenna weights are applied is

$$\tilde{h}_k = w_1 h_{1,k} + w_2 h_{2,k} \tag{2.21}$$

Then, the optimum weights are chosen in such a way that the channel given in Equation (2.21) has the maximum power at the receiver. Now, let us consider the received signal vector, $\mathbf{r} = [r_1,\ldots,r_L]^T$, corresponding to L multipath components, defined as

$$\mathbf{r} = \mathbf{H} \cdot \mathbf{w} \cdot x + \mathbf{n} \tag{2.22}$$

where x is the transmit data symbol, $\mathbf{w} = [w_1,...,w_M]^T$ is the weight vector corresponding to M transmit antennas, $\mathbf{n}$ is the additive noise plus interference corresponding to L multipath components, and $\mathbf{H}$ is the channel matrix corresponding to M transmit antennas and L multipath components defined as

$$\mathbf{H} = \begin{pmatrix} h_{11} & \cdots & h_{1M} \\ \vdots & \ddots & \vdots \\ h_{L1} & \cdots & h_{LM} \end{pmatrix} \tag{2.23}$$

From the received signal, the received signal-to-interference-plus-noise ratio can be calculated as[1]

$$SINR = \mathbf{w}^H \mathbf{H}^H \mathbf{R}_{\mathbf{n}}^{-1} \mathbf{H} \mathbf{w} |x|^2 \tag{2.24}$$

where $(\bullet)^H$ denotes the Hermitian conjugate transpose operator and $\mathbf{R}_n = E[\mathbf{n}\mathbf{n}^H]$ is the noise plus interference covariance matrix. Based on the maximum signal-to-interference-plus-noise ratio criteria, the optimum weight vector can be calculated as

$$\mathbf{w}_{opt} = \max_{\mathbf{w}:\|\mathbf{w}\|^2=1} \mathbf{w}^H \mathbf{H}^H \mathbf{R}_n^{-1} \mathbf{H} \mathbf{w} \tag{2.25}$$

That is, the optimum weight vector is equivalent to the largest eigenvector of the matrix $\mathbf{H}^H \mathbf{R}_n^{-1} \mathbf{H}$ given that $\|\mathbf{w}\|^2 = 1$. If the noise plus interference term is the white Gaussian process, interference-plus-noise covariance matrix $\mathbf{R}_n$ collapses to $\sigma_n^2 \mathbf{I}$, and the optimum weight vector is calculated as

$$\mathbf{w}_{opt} = \max_{\mathbf{w}:\|\mathbf{w}\|^2=1} \mathbf{w}^H \mathbf{H}^H \mathbf{H} \mathbf{w} \tag{2.26}$$

where the optimum weight vector is the eigenvector corresponding to the largest eigenvalue of the matrix, $\mathbf{H}^H \mathbf{H}$, and the received signal-to-noise ratio becomes the largest eigenvalue of the matrix, $\mathbf{H}^H \mathbf{H}$. The matrix, $\mathbf{H}^H \mathbf{H}$, is given by

---

[1] Refer to APPENDIX for the procedure to obtain the received signal-to-interference ratio with MIMO implementation

$$\mathbf{H}^H\mathbf{H} = \begin{pmatrix} \sum_{k=1}^{L} |h_{1,k}|^2 & \cdots & \sum_{k=1}^{L} h_{1,k}h_{M,k}^* \\ \vdots & \ddots & \vdots \\ \sum_{k=1}^{L} h_{L,k}h_{1,k}^* & \cdots & \sum_{k=1}^{L} |h_{M,k}|^2 \end{pmatrix} \tag{2.27}$$

It is known that the matrix, $\mathbf{H}^H\mathbf{H}$, is the complex Wishart matrix [36, 37] for the complex Gaussian channel. Due to the difficulty of finding the probability density function of the largest eigenvalue of the matrix, $\mathbf{H}^H\mathbf{H}$, for arbitrary fade distribution and multipath profile , we exploit the bound property for the largest eigenvalue ($\lambda_{\max}$) of the matrix, $\mathbf{H}^H\mathbf{H}$ as follows

$$\frac{1}{2\sigma^2}\sum_{k=1}^{L}\sum_{l=1}^{M}|h_{l,k}|^2 \le \lambda_{\max} \le \frac{1}{\sigma^2}\sum_{k=1}^{L}\sum_{l=1}^{M}|h_{l,k}|^2 \tag{2.28}$$

The upper bound and the lower bound have the same probability function with a 3 dB difference in average signal-to-noise ratio. Since the diagonal elements of the matrix, $\mathbf{H}^H\mathbf{H}$, combine coherently while the off-diagonal elements combine incoherently, the matrix can be approximated to be a diagonal. Hence, the largest eigenvalue of the matrix, $\mathbf{H}^H\mathbf{H}$, the same as the received signal-to-noise ratio, can be approximated as

$$\lambda_{\max} \simeq \frac{1}{\sigma^2}\sum_{k=1}^{L}\sum_{l=1}^{M}|h_{l,k}|^2 \tag{2.29}$$

For $M = 2$, it gives $2L$ diversity without the 3 dB penalty of transmit power incurred in the open-loop transmit diversity case. It is shown that this theoretical expression matches well with the simulation results [38]

2.3 Interference Statistics and Outage Probability

In DS/CDMA cellular network, the quality of service (QoS) of each user can be degraded directly from the interference increase. Hence, the outage probability at a BS can be defined as follows

$$P_{out} = \Pr(I/S > \eta) \tag{2.30}$$

where I/S represents the sum of the interference power normalized by the required power, S, and η is the threshold required to maintain a certain QoS. It is known that the interference statistics follow the log-normal distribution when perfect power control is employed in the system [12, 39]. Thus, mean and variance are sufficient statistics to calculate the outage probability. Without loss of generality, total interference in DS/CDMA will be separately described by intracell interference and intercell interference.

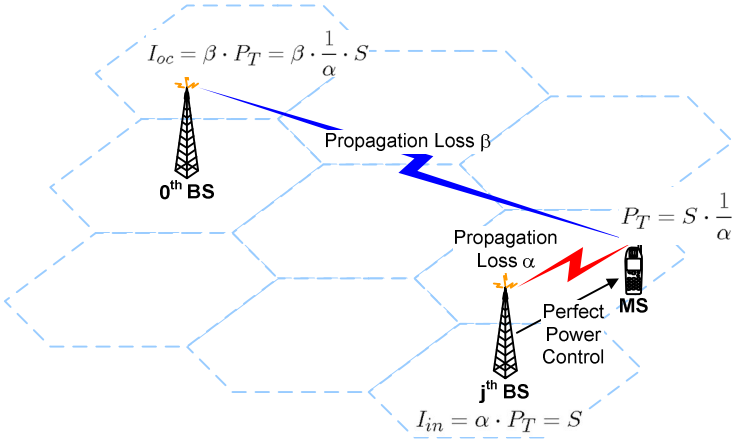

Figure 2.2: Interference model

2.3.1 Intercell interference

- ***Basic interference model***

Let us suppose that an MS (let us denote it by the k^{th} MS) communicates with the i^{th} BS as shown in Figure 2.2. If the transmit power of the k^{th} MS is perfectly power-controlled to compensate the propagation channel loss, the transmit power, P_T, of the k^{th} MS can be expressed as

$$P_T = S \cdot \frac{1}{\alpha} = S \cdot \frac{X_{ki}}{r_{ki}^{u} 10^{\zeta_{ki}/10}} \tag{2.31}$$

where S represent the target E_b / I_o satisfying the minimum bit error rate (BER) condition, and α represent the propagation channel loss between the k^{th} MS and the i^{th} BS, which consists of the short-term fading channel loss, X_{ki}, and the long-term fading channel loss, $\left(r_{ki}^{u} 10^{\zeta_{ki}/10}\right)^{-1}$, as defined in the section 2.2.2. Assuming the maximal ratio combining of the received signal from all receive antennas and closed-loop transmit diversity, described in the section 2.2.3, X_{ki} can be defined as

$$X_{ki} = \sum_{l=1}^{L_m} \sum_{m=1}^{L_r} \sum_{q=1}^{L} \left| \alpha_{l,m,q} \right|^2 \tag{2.32}$$

where $\alpha_{l,m,q}$ is the complex-valued channel gain corresponding the l^{th} multipath component of the m^{th} receive antenna and the q^{th} transmit antenna branch. If the open loop transmit diversity is employed,

$$X_{kj} = \sum_{l=1}^{L_m} \sum_{m=1}^{L_r} \sum_{q=1}^{L_t} \left| \alpha_{l,m,q} \right|^2 / L_t \tag{2.33}$$

This transmit power, P_T, becomes the *intercell interference* to the zero$^{\text{th}}$ BS. The received signal power at the zero$^{\text{th}}$ BS can be expressed as

$$I^{(k)} = P_R = P_T \cdot \beta = S \cdot \frac{\beta}{\alpha} = S \cdot \frac{r_{ki}^{u} 10^{\zeta_{ki}/10}}{r_{k0}^{u} 10^{\zeta_{k0}/10}} \frac{X_{k0}}{X_{ki}} \tag{2.34}$$

where β denotes the propagation loss between the k^{th} MS and the zero$^{\text{th}}$ BS, composed of the short-term fading channel loss, X_{k0}, and the long-term fading channel loss, $\left(r_{ko}^{u}10^{\zeta_{k0}/10}\right)^{-1}$. The normalized instantaneous intercell interference can be expressed as

$$\frac{I^{(k)}}{S} = \frac{r_{ki}^{u}10^{\zeta_{ki}/10}}{r_{k0}^{u}10^{\zeta_{k0}/10}}\frac{X_{k0}}{X_{ki}} \tag{2.35}$$

Without loss of generality, the short-term fading channel loss, X_{k0}, that is a random variable, represents the multipath fading channel loss of only one antenna branch at the zero$^{\text{th}}$ BS to estimate the performance in terms of the received signal-to-noise ratio per branch and is given by

$$X_{k0} = \sum_{l=1}^{L_m} |\alpha_l|^2 \tag{2.36}$$

where L is the number of multipath components and α_l is the complex-valued channel gain due to multipath fading.

- ***Soft handoff and voice activity***

Now, let us suppose that the transmit power of the k^{th} MS is perfectly power controlled by the j^{th} BS and is in soft handoff with N_c nearest BSs. Furthermore, the k^{th} MS transmits intermittently with the probability, $\Pr(\varepsilon_k = 1) = \nu$, which is defined as the *voice activity*. Then, the normalized instantaneous intercell interference can be expressed as

$$\frac{I^{(k)}}{S} = \varepsilon_k \frac{\min_{i\in A_k}\left\{r_{ki}^{u}10^{\zeta_{ki}/10}\right\}}{r_{k0}^{u}10^{\zeta_{k0}/10}}\frac{X_{k0}}{X_{kj}} \tag{2.37}$$

where $j = \arg\min_{i\in A_k}\left\{r_{ki}^{u}10^{\zeta_{ki}10}\right\}$ which choose the best serving BS, which provides the least average propagation loss, among the active set A_k, and ε_k is the indicator function to model the voice activity. The voice activity is also a random variable and is defined as

$$\varepsilon_k = \begin{cases} 1 & \text{when MS transmits} \\ 0 & \text{otherwise} \end{cases} \tag{2.38}$$

On the other hand, according to the region of the cellular system, S_0 and $\overline{S}_0$, which an MS belongs to, the active set, A_k, is slightly different; hence, the analysis will also be

slightly different between S_0 and $\overline{S}_0$. The intercell interference is further divided into two cases. For the intercell interference from an MS in S_0, we can use the same expression as Equation (2.37). However, for the intercell interference from an MS in $\overline{S}_0$, we need to consider another condition as follows

$$\min_{i \in \tilde{A}_k} \left\{ r_{ki}^u 10^{\zeta_{ki} 10} \right\} < r_{k0}^u 10^{\zeta_{k0}/10} \tag{2.39}$$

where $\tilde{A}_k$ is the modified active set by excluding the zero[th] BS from the original active set, A_k, because the MS in $\overline{S}_0$ has the zero[th] BS in the active set. If the MS is connected to the zero[th] BS, it will be intracell interference to the zero[th] BS; hence we have to separately handle the interference in S_0 and $\overline{S}_0$

- ***Statistics***

As previously mentioned, it is known that the interference statistics follows the log-normal distribution when the perfect power control is employed due to the occasional peak transmit power from compensating the deep fading. Hence, interference can be completely described by the mean and variance.

First, let us consider the intercell interference in S_0. The n[th] moment to calculate the mean and variance can be calculated as

$$E\left[\left(\frac{I_{oc}^{(k)}}{S}\right)_{S_0}^n\right] = E[\varepsilon_k^n] E\left[\left(\frac{\min_{i \in \tilde{A}_k} \left\{ r_{ki}^u 10^{\zeta_{ki}/10} \right\}}{r_{k0}^u 10^{\zeta_{k0}/10}}\right)^n\right] E[X_{k0}^n] E\left[\frac{1}{X_{kj}^n}\right] \tag{2.40}$$

with $\min_{i \in \tilde{A}_k} \left\{ r_{ki}^u 10^{\zeta_{ki} 10} \right\} < r_{k0}^u 10^{\zeta_{k0}/10}$ and $j = \arg\min_{i \in A_k} \left\{ r_{ki}^u 10^{\zeta_{ki} 10} \right\}$. It is assumed that the short-term fading channel loss and long-term fading channel loss are independent of each other. Then, the first expectation for the voice activity can be calculated as

$$E[\varepsilon_k^n] = \Pr(\varepsilon_k = 1) = \nu \tag{2.41}$$

The second expectation term is also easily calculated as described in [28],

$$E\left[\left(\frac{\min_{i \in \tilde{A}_k} \left\{ r_{ki}^u 10^{\zeta_{ki}/10} \right\}}{r_{k0}^u 10^{\zeta_{k0}/10}}\right)^n\right] = e^{n^2 b^2 (\beta\sigma)^2} \sum_{j \in \tilde{A}_k} \left(\frac{r_{kj}}{r_{k0}}\right)^{nu} \int_{-\infty}^{\infty} \frac{e^{-z^2/2}}{\sqrt{2\pi}} \prod_{\substack{i \in \tilde{A}_k \\ i \neq j}} Q\left(z + nb\beta\sigma + \frac{M_{kj} - M_{ki}}{b\sigma}\right) dz \tag{2.42}$$

where $\beta = \ln(10)/10$, $M_{ij} = 10u\log_{10} r_{ij}$, b is the correlation factor of shadow fadings between BSs, σ is the standard deviation of log-normal shadow fading, and $Q(y) = \int_y^\infty e^{-x^2/2}/\sqrt{2\pi}dx$. Note that Equation (2.42) is the function of M_{ki} (that is, r_{ki} , the distance between the k^{th} MS and the i^{th} BS in log-scale) and will be further used to evaluate the n^{th} moment of interference averaged over the whole system area. Now, let us think about the third and fourth expectations in Equation (2.40) that can be evaluated as

$$E[X_{k0}^n] = \int_0^\infty x^n f_{X_{k0}}(x)dx \tag{2.43}$$

and

$$E\left[\frac{1}{X_{kj}^n}\right] = \int_{u_L}^\infty \frac{1}{x^n} f_{X_{kj}}(x)dx \tag{2.44}$$

where u_L is the lower limit of X_{kj} to keep Equation (2.44) to have the solution even for one antenna branch and single path, which also can be interpreted as the upper limit of transmit power amplifier at the same time. However, since the random variables, X_{k0} and X_{kj} , are the sum of the random variables, $|\alpha_l|^2$ and $|\alpha_{l,m,q}|^2$, respectively, as shown in Equation (2.36) and (2.32), it might not be easy to find their probability density function due to the complex convolutions of each probability density function. Complex convolution of the probability density function can be circumvented by means of the moment generating function technique. Using the moment generating function, the probability density function for the sum of random variables is represented by the product of each moment generating function. Let us consider Equation (2.32) as a more general form of Equation (2.36). Its probability density function can be calculated by convolutions as follows

$$f_{X_{kj}}(x) = f_{\alpha_{1,1,1}}(x) * \cdots * f_{\alpha_{L,R,T}}(x) \tag{2.45}$$

However, the moment generating function of X_{kj} is expressed as

$$\phi_{X_{kj}}(s) = \prod_{l=1}^{L_m} \prod_{m=1}^{L_r} \prod_{q=1}^{L_t} \phi_{\alpha_{l,m,q}}(s) \tag{2.46}$$

Then, the probability density function can be obtained by the inverse Laplace transform as follows

$$f_{X_{kj}}(x) = L^{-1}\left[\phi_{X_{kj}}(s)\right] = L^{-1}\left[\prod_{l=1}^{L_m}\prod_{m=1}^{L_r}\prod_{q=1}^{L_t}\phi_{\alpha_{l,m,q}}(s)\right] \tag{2.47}$$

There are two ways to obtain the probability density function using the inverse Laplace transform. If the product of each moment generating function can be divided into the sum of known Laplace transform pairs by partial fraction expansion, we can obtain the closed form of probability density function. However, when it is impossible to express the moment generating function using the known Laplace transform pairs, we only have to evaluate the probability density function using the numerical Laplace transform technique, known as *Abate's method* [40]. For the first solution, we will describe it in more details at the later subsection. As a general solution, the probability density function by the numerical Laplace transform can be obtained as follows

$$\begin{aligned} f_{X_{kj}}(x) &= L^{-1}\left[\phi_{X_{kj}}(s)\right] \\ &\simeq \frac{e^{A/2}2^{-C}}{x}\sum_{k=0}^{C}\binom{C}{k}\left[\sum_{b=0}^{B+k}\frac{(-1)^b}{\delta_b}\mathrm{Re}\left\{\phi_{X_{kj}}\left(\frac{A+2\pi ib}{2x}\right)\right\}\right] \end{aligned} \tag{2.48}$$

where $\mathrm{Re}\{\bullet\}$ denotes the real part of complex argument, and the constants A, B, and C are arbitrarily chosen to be 30, 18, and 24, respectively, to yield an accuracy of at least 10^{-7} [41].

Now, let us consider the intercell interference in $\bar{S}_0$. Similarly, the n^{th} moment of the intercell interference in $\bar{S}_0$ can be calculated as

$$E\left[\left(\frac{I_{oc}^{(k)}}{S}\right)_{\bar{S}_0}^{n}\right] = E[\varepsilon_k^n]E\left[\left(\frac{\min_{i\in A_k}\left\{r_{ki}^u 10^{\zeta_{ki}/10}\right\}}{r_{k0}^u 10^{\zeta_{k0}/10}}\right)^n\right]E[X_{k0}^n]E\left[\frac{1}{X_{kj}^n}\right] \tag{2.49}$$

where the first, third, and fourth expectations of the right hand side are calculated by Equations (2.41), (2.43), and (2.44), respectively. However, the second expectation in Equation (2.49) is differently evaluated as described in [28],

$$E\left[\left(\frac{\min\limits_{i\in A_k}\left\{r_{ki}^{u}10^{\zeta_{ki}/10}\right\}}{r_{k0}^{u}10^{\zeta_{k0}/10}}\right)^{n}\right]=e^{n^2b^2(\beta\sigma)^2}\sum_{j\in A_k}\left(\frac{r_{kj}}{r_{k0}}\right)^{nu}\int_{-\infty}^{\infty}\frac{e^{-z^2/2}}{\sqrt{2\pi}}\prod_{\substack{i\in A_k\\ i\neq j}}Q\left(z+nb\beta\sigma+\frac{M_{kj}-M_{ki}}{b\sigma}\right)dz \quad (2.50)$$

Finally, assuming hexagonal cells with radius normalized to unity and uniform density of mobile users with $\kappa = 2K/(3\sqrt{3})$ users per unit area (where K is the number of users per cell), the mean and variance of the normalized instantaneous intercell interference can be calculated as

$$E\left[\frac{I_{oc}}{S}\right]=\iint_{S_0}E\left[\left(\frac{I_{oc}^{(k)}}{S}\right)_{S_0}\right]\kappa dA_{S_0}+\iint_{\bar{S}_0}E\left[\left(\frac{I_{oc}^{(k)}}{S}\right)_{\bar{S}_0}\right]\kappa dA_{\bar{S}_0} \quad (2.51)$$

$$Var\left[\frac{I_{oc}}{S}\right]=\iint_{S_0}Var\left[\left(\frac{I_{oc}^{(k)}}{S}\right)_{S_0}\right]\kappa dA_{S_0}+\iint_{\bar{S}_0}Var\left[\left(\frac{I_{oc}^{(k)}}{S}\right)_{\bar{S}_0}\right]\kappa dA_{\bar{S}_0} \quad (2.52)$$

where the variance of the k th MS is calculated as

$$Var\left[\left(\frac{I_{oc}^{(k)}}{S}\right)_{S_0}\right]=E\left[\left(\frac{I_{oc}^{(k)}}{S}\right)_{S_0}^{2}\right]-E\left[\left(\frac{I_{oc}^{(k)}}{S}\right)_{S_0}\right]^{2} \quad (2.53)$$

$$Var\left[\left(\frac{I_{oc}^{(k)}}{S}\right)_{\bar{S}_0}\right]=E\left[\left(\frac{I_{oc}^{(k)}}{S}\right)_{\bar{S}_0}^{2}\right]-E\left[\left(\frac{I_{oc}^{(k)}}{S}\right)_{\bar{S}_0}\right]^{2} \quad (2.54)$$

Note that all interference are independent, and two regions, S_0 and $\bar{S}_0$, are mutually exclusive.

2.3.2 Example: Nakagami-m fade distribution

First, let us consider the independent Nakagami-*m* fade distribution at each branch and multipath. The moment generating function, $\phi_l(s)$ is given by

$$\phi_l(s)=\left(1+\frac{\Omega_l}{m}s\right)^{-m} \quad (2.55)$$

where Ω_l is the average power of the l^{th} multipath. Therefore, the moment generating function of X_{kj} can be expressed as, when the multipath fading is subject to Nakagami-*m* fading,

$$\phi_{X_{kj}}(s)=\prod_{l=1}^{L_m}\left(1+\frac{\Omega_l}{m}s\right)^{-mL_tL_r} \quad (2.56)$$

for the closed-loop transmit diversity, and

$$\phi_{X_{kj}}(s) = \prod_{l=1}^{L_m}\left(1+\frac{\Omega_l}{mL_t}s\right)^{-mL_tL_r} \tag{2.57}$$

for the open-loop transmit diversity. In Equation (2.56) and (2.57), if mL_tL_r is an integer number, the probability density function of X_{kj} can be obtained in the closed form expression by the inverse Laplace transform through partial fraction expansion. Let $M = mL_tL_r$, which is an integer number, and $\lambda_l = \Omega_l / m$ for the closed loop transmit diversity, and $\lambda_l = \Omega_l /(mL_t)$ for the open-loop transmit diversity, then the moment-generating function of X_{kj} can be expanded by partial fraction expansion[2] as follows:

$$\phi_{X_{kj}}(s) = \prod_{l=1}^{L_m}(1+\lambda_l s)^{-M} = \sum_{l=1}^{L_m}\sum_{k=1}^{M}\frac{A_{l,k}}{(1+\lambda_l s)^k} \tag{2.58}$$

where

$$A_{l,k} = \frac{1}{(\lambda_l)^{n_0}}\sum_{n_1=0}^{n_0}\sum_{n_2=0}^{n_0-n_1}\cdots\sum_{n_{L_m-2}=0}^{n_0-n_1\ldots-n_{L_m-3}}\prod_{i,u=1,i\neq l}^{L_m,L_{m-1}}\binom{M+n_u-1}{n_u}\frac{\lambda_i^{n_u}}{(1-\lambda_i/\lambda_l)^{M+n_u}} \tag{2.59}$$

Then, the probability of X_{kj} is given by the inverse Laplace transform as follows:

$$\begin{aligned} f_{X_{kj}}(x) &= \sum_{l=1}^{L_m}\sum_{k=1}^{M}A_{l,k}f_l(x) \\ &= \sum_{l=1}^{L_m}\sum_{k=1}^{M}\frac{A_{l,k}}{\Gamma(k)}\left(\frac{1}{\lambda_l}\right)^k x^{k-1}\exp\left(-\frac{x}{\lambda_l}\right) \end{aligned} \tag{2.60}$$

where $\Gamma(a) = \int_0^\infty t^{a-1}e^{-t}dt$. Once the probability density function is obtained, the n^{th} moment of X_{k0} and $1/X_{kj}$ can be calculated in the closed-form solutions as follows:

$$\begin{aligned} E[X_{k0}^n] &= \sum_{l=1}^{L_m}\sum_{k=1}^{M}\frac{A_{l,k}}{\Gamma(k)}\left(\frac{1}{\lambda_l}\right)^k\int_0^\infty x^{k+n-1}e^{-x/\lambda_l}dx \\ &= \sum_{l=1}^{L_m}\sum_{k=1}^{M}A_{l,k}\left(\frac{1}{\lambda_l}\right)^k\frac{\Gamma(k+n)}{\Gamma(k)} \end{aligned} \tag{2.61}$$

and

---

[2] Refer to APPENDIX B for the procedure to obtain the coefficients, $A_{l,k}$.

$$E\left[\frac{1}{X_{kj}^{n}}\right] = \sum_{l=1}^{L_m}\sum_{k=1}^{M}\frac{A_{l,k}}{\Gamma(k)}\left(\frac{1}{\lambda_l}\right)^{k}\int_{u}^{\infty}x^{k+n-1}e^{-x/\lambda_l}dx$$
$$= \sum_{l=1}^{L_m}\left\{\sum_{k=1}^{n}\frac{A_{l,k}}{\Gamma(k)}\left(\frac{1}{\lambda_l}\right)^{k}\frac{E_{n-k+1}\left(\frac{u}{\lambda_l}\right)}{u^{n-k}} + \sum_{k=1}^{n}\frac{A_{l,k}}{\Gamma(k)}\left(\frac{1}{\lambda_l}\right)^{k}\Gamma\left(k-n,\frac{u}{\lambda_l}\right)\right\} \tag{2.62}$$

where $E_n(x) = x^{n-1}\int_x^{\infty}\frac{e^{-t}}{t^n}dt$ is the exponential integral function and $\Gamma(a,x) = \int_x^{\infty}t^{a-1}e^{-t}dt$ is the incomplete gamma function. If $|\alpha_{l,m,q}|^2$ in Equations (2.32) and (2.36) are correlated with each other and not necessarily identically distributed, that is, if there exist correlations between diversity branches such as antenna elements and rake fingers, the moment generating function of the sum of correlated random variables, $|\alpha_{l,m,q}|^2$, can be written as [42]

$$\phi_{X_{kj}}(s) = |1 + sDC|^{-m} = \prod_{i=1}^{L}(1+\lambda_i s)^{-m} \tag{2.63}$$

where $L = L_m L_t L_r$, D is the $L \times L$ diagonal matrix and is defined as $D = \mathrm{diag}(\Omega_1/m,\cdots,\Omega_L/m)$ for the closed-loop transmit diversity, or is defined as $D = \mathrm{diag}(\Omega_1/mL_t,\cdots,\Omega_L/mL_t)$ for the open-loop transmit diversity, C denotes the positive definite matrix defined by $\sqrt{R_c}$, the square root of the power correlation matrix between the diversity branches, and $\{\lambda_i\}_{i=1}^{L}$ are the eigenvalues of the matrix DC. For the correlated Nakagami-*m* fade distribution with general fading index m, the probability density function can be obtained by the numerical Laplace inversion technique given in Equation (2.48).

2.3.3 Intracell interference

- ***Basic model***

Again, let us suppose that an MS (let us denote it by the k^{th} MS) communicates with the i^{th} BS as shown in Figure 2.2. Assuming perfect power control of transmit power, the intracell interference would be constant, S, that maintains a certain QoS. That is, the received power at the i^{th} BS from the k^{th} MS can be expressed as

$$P_R = P_T \cdot \alpha = S \tag{2.64}$$

where α denote the propagation channel loss between the k th MS and the i th BS, composed of the short-term fading channel loss, X_{ki}, and the long-term fading channel loss, $r_{ki}^{u}10^{\zeta_{ki}/10}$, as defined in the section 2.2.2. Therefore, the normalized instantaneous intracell interference at the zeroth BS can be expressed as

$$\frac{I_{in}^{(k)}}{S} = 1 \tag{2.65}$$

- ***Soft handoff and voice activity***

Similar to the intercell interference, let us suppose that the k th MS is in the soft handoff with N_c nearest BSs and transmits intermittently. If the MS is connected to the other BS than the zeroth BS, it will be the intercell interference; it is the opposite case of the intercell interference in S_0. The normalized instantaneous intracell interference with soft handoff and voice activity can be expressed as

$$\frac{I_{in}^{(k)}}{S} = \varepsilon_k \cdot \phi_k \tag{2.66}$$

where ε_k is defined as Equation (2.38), and ϕ_k is the indicator function that indicates whether the k th MS is power-controlled by the zeroth BS or not. Hence, the indicator function, ϕ_k, is defined as

$$\phi_k = \begin{cases} 1 & r_{k0}^{u}10^{\zeta_{k0}/10} \le \min\limits_{i \in A_k}\left\{ r_{ki}^{u}10^{\zeta_{ki}10} \right\} \\ 0 & r_{k0}^{u}10^{\zeta_{k0}/10} > \min\limits_{i \in A_k}\left\{ r_{ki}^{u}10^{\zeta_{ki}10} \right\} \end{cases} \tag{2.67}$$

- ***Statistics***

Then, the n th moment of the normalized intracell interference can be calculated as

$$E\left[\left(\frac{I_{in}^{(k)}}{S}\right)^{n}\right] = E[\varepsilon_k^{n}] \cdot E[\phi_k^{n}] \tag{2.68}$$

where the first expectation of the right hand side can be calculated by Equation (2.41), and the second expectation of the right hand side can be evaluated as

$$
\begin{aligned}
E[\phi_k^n] &= \Pr(\phi_k = 1) \\
&= \Pr\left(r_{k0}^u 10^{\zeta_{k0}/10} \le \min_{i \in \bar{A}_k} \left\{ r_{ki}^u 10^{\zeta_{ki}10} \right\} \right) \\
&= \sum_{j \in \bar{A}_k} \int_{-\infty}^{\infty} \frac{e^{-z^2/2}}{\sqrt{2\pi}} \left[1 - Q\left(z + \frac{M_{kj} - M_{k0}}{\beta\sigma} \right) \right] \prod_{\substack{i \in \bar{A}_k \\ i \ne j}} Q\left(z + \frac{M_{kj} - M_{ki}}{b\sigma} + nb\beta\sigma \right) dz
\end{aligned}
\tag{2.69}
$$

Similar to the intercell interference, Equation (2.69) is also the function of M_{ki}. Hence, we need to average the n th moment of the intracell interference from the k th MS over the region, S_0. The mean and variance of total intracell interference can be calculated as

$$
E\left[\frac{I_{in}}{S} \right] = \iint_{S_0} E\left[\left(\frac{I_{in}^{(k)}}{S} \right) \right] \kappa dA_{S_0} \tag{2.70}
$$

$$
Var\left[\frac{I_{in}}{S} \right] = \iint_{S_0} \left\{ E\left[\left(\frac{I_{in}^{(k)}}{S} \right)^2 \right] - E\left[\frac{I_{in}^{(k)}}{S} \right]^2 \right\} k dA_{S_0} \tag{2.71}
$$

2.3.4 Outage probability

Finally, total normalized interference will be the sum of the intracell and intercell interference from all MSs in the entire system. That is, the mean and variance of total normalized interference is obtained as

$$
\begin{aligned}
m_{I/S} &= E\left[\left(\frac{I_{in}}{S} \right)_{S_0} \right] + E\left[\left(\frac{I_{oc}}{S} \right)_{S_0} \right] + E\left[\left(\frac{I_{oc}}{S} \right)_{\bar{S}_0} \right] \\
\sigma_{I/S}^2 &= Var\left[\left(\frac{I_{in}}{S} \right)_{S_0} \right] + Var\left[\left(\frac{I_{oc}}{S} \right)_{S_0} \right] + Var\left[\left(\frac{I_{oc}}{S} \right)_{\bar{S}_0} \right]
\end{aligned}
\tag{2.72}
$$

Then, the outage probability as a function of the number of users per cell, K, can be calculated as

$$
P_{out}(K) = Q\left(\frac{\ln \eta - m_Z}{\sigma_Z} \right) \tag{2.73}
$$

where $\eta = (W / R_b) / \gamma$ with the total spreading bandwidth W, the information bit rate R_b, and the required signal to interference ratio, γ, the mean and the standard deviation of the total interference, m_Z and σ_Z, respectively, can be calculated as

$$
\begin{aligned}
\sigma_Z^2 &= \ln\left(K \cdot \sigma_{I/S}^2 + K^2 \cdot m_{I/S}^2 \right) - 2\ln\left(K \cdot m_{I/S} \right) \\
m_Z &= 0.5 \ln\left(K \cdot \sigma_{I/S}^2 + K^2 \cdot m_{I/S}^2 \right) - K \cdot \sigma_{I/S}^2
\end{aligned}
\tag{2.74}
$$

2.3.5 Imperfect power control

So far, it is assumed that MS is perfectly power-controlled by BS. At times, however, the channel fluctuation is varying too fast to be compensated by the power control algorithm, in which case, it is known that the signal received at the BS still follows the short term fading distribution, and the average power of the received signal follows a log-normal distribution with a controlled standard deviation [29]. At the worst case, the power control can compensate only for the long-term fading, which can be considered as the lower bound for the imperfect power control. Then, the intercell interference from the MS in $\bar{S}_0$ and S_0 with imperfect power control can be expressed as

$$\left(\frac{I_{oc}^{(k)}}{S}\right)_{\bar{S}_0} = \varepsilon_k \frac{\min_{i\in\bar{A}_k}\left\{r_{ki}^u 10^{\zeta_{ki}/10}\right\}}{r_{k0}^u 10^{\zeta_{k0}/10}} \cdot X_{k0}\,, \tag{2.75}$$

and

$$\left(\frac{I_{oc}^{(k)}}{S}\right)_{S_0} = \varepsilon_k \frac{\min_{i\in\bar{A}_k}\left\{r_{ki}^u 10^{\zeta_{ki}/10}\right\}}{r_{k0}^u 10^{\zeta_{k0}/10}} \cdot X_{k0}, \quad r_{k0}^u 10^{\zeta_{k0}/10} \le \min_{i\in\bar{A}_k}\left\{r_{ki}^u 10^{\zeta_{ki}10}\right\}, \tag{2.76}$$

respectively, where $X_{k0} = \sum_{l=1}^{L_m} |\alpha_l|^2$ reflects only multipath fading propagation loss which represents the received signal fluctuation due to the uncompensated short-term fading. Similarly, the intracell interference also will fluctuate due to the uncompensated short-term fading, which can be expressed as

$$\left(\frac{I_{in}^{(k)}}{S}\right)_{S_0} = X_{k0} \cdot \varepsilon_k \cdot \phi_k \tag{2.77}$$

Then, each interference statistics can be straightforwardly evaluated using Equations (2.41), (2.42), (2.69), and (2.43). Finally, the outage probability in (2.73) should be modified as

$$P_{out} = \Pr\left\{\frac{I}{S\cdot\chi} > \eta\right\} \tag{2.78}$$

where χ denotes the received signal fluctuation due to the uncompensated short-term fading for a given user and defined as

$$\chi = X_{k0} \,/\, E[\,X_{k0}\,] \tag{2.79}$$

and X_{k0} follows Equation (2.32) or (2.33). Since the array gain is already taken into account in the interference term, only signal fluctuation by the short-term fading channel is considered by normalizing the random variable, X_{k0}, with its mean. Different from the perfect power control case, the total interference statistics with the imperfect power control follow the central limit theorem, hence Gaussian distribution. Consequently, Equation (2.78) can be evaluated as

$$\begin{aligned} P_{out}(K) &= \Pr\left\{\frac{I}{S} > \chi \cdot \eta\right\} \\ &= \int_0^\infty Q\left(\frac{\eta \cdot x - K \cdot m_{I/S}}{\sqrt{K}\sigma_{I/S}}\right) f_\chi(x)dx \end{aligned} \tag{2.80}$$

where $f_\chi(x)$ is the probability density function of the short-term fading random variable, χ, with a given multipath intensity profile and can be calculated as

$$f_\chi(\chi) = E[X_{k0}] \cdot f_{X_{k0}}(E[X_{k0}] \cdot \chi) \tag{2.81}$$

from $f_{X_{k0}}(x)$ by applying the technique to calculate the probability density function for the function of random variable [43].

2.4 Erlang Capacity

Thus far, we have focused on the instantaneous outage probability of the system as a measure of the system capacity, assuming that all incoming calls are admitted without any explicit call admission control. This outage probability can determine the maximum available resources of the system. However, since the users share the same frequency band in DS/CDMA cellular system, the incoming calls can cause the severe degradation of the system performance at times. Hence, it might be better block a call request when QoS of system falls below some criteria in the viewpoint of the network operator [44]. Taking into account the admission control, we can calculate the blocking probability and can estimate the number of users that can be accommodated into the system with the available resources, that is, *Erlang capacity* [45]. Thus, in this section, we specifically assess Erlang capacity of uplink DS/CDMA cellular systems taking into account: (a)

spatial transmit and receive diversity over Nakagami-*m* / Rician fading channel with arbitrary multipath intensity profile, (b) traffic distribution along with proper queuing model of each cell, and (c) call admission control scheme based on the system outage condition.

2.4.1 Traffic model

Traffic model defines the behavior of users in the system. There are two different viewpoints of traffic modeling technique widely employed in the analysis of DS/CDMA cellular system: one is independent $M/G/\infty$ queue model, and the other is independent $M/M/\infty$ queue model. While the former is usually employed when there is no explicit call admission control [27, 29, 46], the latter is used with a call admission control [44, 47, 48]. Since we will take into account a call admission control, we adopt $M/M/\infty$ queue model as a basis of the analysis. The basic assumptions for $M/M/\infty$ queue are as follows

- Call arrivals in each cell are Poisson distributed with a rate of λ.
- Call durations are exponentially distributed with average call duration of $1/\mu$
- Arrival process and departure process are independent with each other.
- Blocked call (or lost call) cleared (Furthermore, it is assumed that a blocked call reenters the system after a random interval as if it is a new call)

2.4.2 Call admission control and blocking probability

While there are various ways to control the incoming calls, we take into account the call admission control scheme introduced in [48], in which new call is blocked when the system is in outage, that is, the following interference condition occur:

$$\frac{\sum_{n=1}^{K} I^{(k)}}{S} > \eta \tag{2.82}$$

On the other hand, in our analysis, there is no soft handoff blocking since we already assumed that all MSs in the system are in the soft handoff. That is, only a new call may be blocked with the outage probability of the system in which K users are being serviced. However, the accepted calls can remain in the system through outage until their service is done. Then, the original birth-death chain can be modified as shown in Figure 2.3.

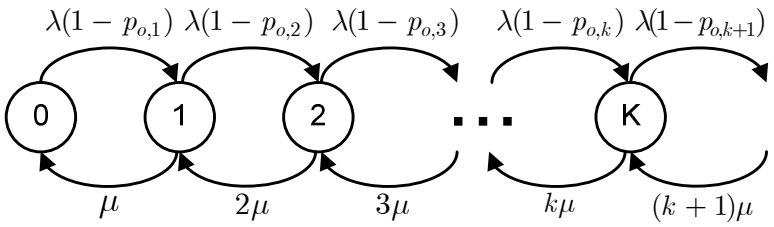

Figure 2.3: Modified birth-death process model

That is, the original call arrival rate is modified by the outage probability. Even though this call admission control scheme is very simple, it is applicable in the viewpoint of keeping the QoS of the network. Then, the blocking probability of the system can be calculated as

$$\Pr\{blocking\} = \sum_{n=1}^{\infty} p_{b,n} \cdot p_n \tag{2.83}$$

where $p_{b,n}$ is the probability of blocking a new call when n users are in the system, and p_n is the probability of that n users are in the system. Since we assume that a new call is blocked when the system is in the outage, $p_{b,n}$ is equivalent to the outage probability of the system with n users, $p_{o,n}$. The probability of that n users are in the system can be obtained by calculating the occupancy distribution of given queue.

2.4.3 Occupancy distribution

Since the call arrival rate changes according to the number of users in the system, the occupancy distribution is not simply obtained by Erlang formula; however, by solving the detailed balance equations (DBE) [49] of given queue, we can easily calculate the occupancy distribution.

$$\begin{aligned} \lambda(1-p_{o,0})p_0 &= \mu p_1 \\ &\vdots \\ \lambda(1-p_{o,k-1})p_{k-1} &= \mu p_k \\ &\vdots \end{aligned} \tag{2.84}$$

and the occupancy distribution must satisfy the stationary condition:

$$\sum_{n=1}^{\infty} p_n = 1 \tag{2.85}$$

By induction on Equation (2.84), the occupancy distribution is calculated as

$$p_k = \frac{(\lambda/\mu)^k}{k!}\left[\prod_{n=0}^{k-1}(1-p_{b,n})\right]p_0 \tag{2.86}$$

where p_0 is given by the stationary condition in Equation (2.85) as follows

$$p_0 = \left\{\sum_{k=0}^{\infty}\frac{(\lambda/\mu)^k}{k!}\left[\prod_{n=0}^{k-1}(1-p_{o,n})\right]\right\}^{-1} \tag{2.87}$$

In evaluating Equation (2.83) and (2.87), the infinite number of users will be truncated by the finite number of users that does not have much impact on the results since the arrival rate approaches to zero as the outage probability approaches to '1'.

2.5 Numerical Results

In this section, we present the numerical results for the impact of spatial diversity techniques at handset on the uplink capacity of DS/CDMA cellular systems. The system parameters assumed throughout the rest of the chapter are summarized in Table 2.3.

Table 2.3: System parameters

Parameters	Value
Spreading bandwidth (W)	1.25 MHz
Data Rate (R_b)	8 Kbps
Voice activity (ν)	0.38
Target E_b / I_0	5.6 dB
Shadowing correlation between BSs	0.5
Log-normal shadowing	$\sigma = 8\text{dB},\ m = 0$
Path loss exponent	$u = 4$
Soft handoff	3-way
Diversity order (M)	1, 2, 4, 8
Fade margin	20 dB

2.5.1 Basic results

Figure 2.4 shows the outage probability vs. the number of users per cell for one-path Nakagami-*m* fading channel with $m = 1$, where $M = L_t \times L_r$ is the diversity order with L_t transmit antennas and L_r receive antennas. M can be any combination of the number of transmit diversity and receive diversity. However, throughout the results shown in this section, it is assumed that L_r=1 because the constant intracell interference is only valid for transmit diversity and multipath diversity, which will be discussed in more detail at Chapter 3. For $m = 1$, Nakagami-*m* fade distribution is exactly the same as Rayleigh fade distribution. Now, at a specified outage probability, we can determine the number of users per cell that can be supported by the given system, that is, *system capacity*. It is observed that the system capacity is significantly improved as diversity order increases for both slow power control and fast power control. However, the relative improvements in both slow power control and fast power control by increasing diversity order decreases as the diversity order increases. Furthermore, it can be observed that systems employing fast power control achieve more capacity than those using slow power control under the same conditions, but performance gains achieved by adding higher order diversity are greater in systems employing slow power control as opposed to those using fast power control.

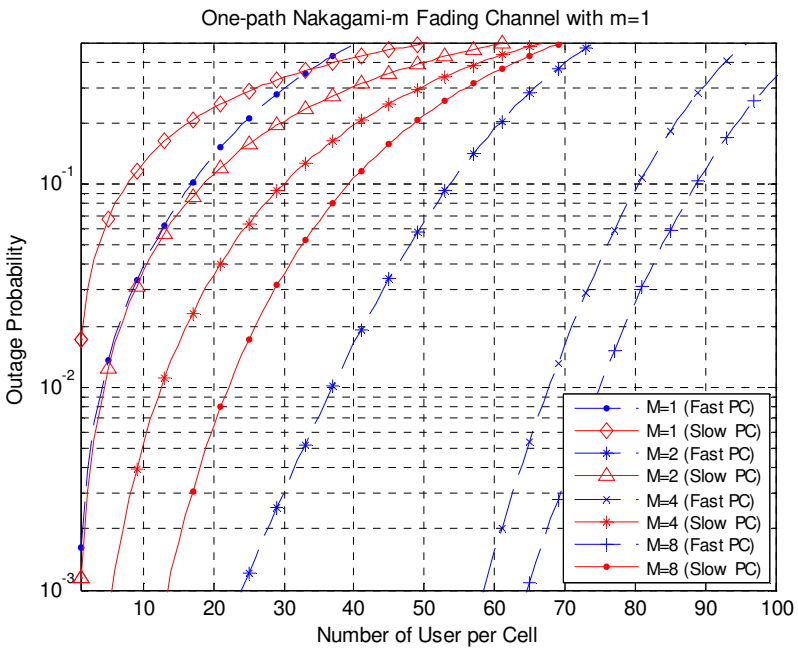

Figure 2.4: One-path Rayleigh fading channel

Table 2.4 summarize the system capacity based on the outage probability of 10^{-2}. These capacity improvements are expected to come from the reduction of intercell interference by the energy capturing effect and the channel flattening of diversity combining technique. Let us investigate the statistics of both intracell and intercell interference. As mentioned in the previous section, the interference statistics approximately follow Log-normal distribution; hence, the mean and variance are the sufficient statistics for the interference description. Table 2.5 shows the mean and variance of intracell interference and intercell interference for several spatial diversity orders, where perfect power control and Nakagami-*m* fading channel with $m = 1$ are assumed. Since perfect power control is assumed, the intracell interference power will not change by the channel fluctuation. However, the voice activity and soft handoff cause small variations in intracell interference, which is not affected by spatial diversity. It is observed that the mean and variance of intercell interference significantly decreases as diversity order increases while intracell interference does not change by diversity. From this result, it is shown that the capacity improvement comes from the significant reduction of intercell interference by

spatial diversity processing in terms of both mean and variance. On the other hand, the slow power control can be considered a bound for the imperfect power control due to the feedback delay, power control error for the same diversity order. That is, the result of any imperfect power control degrade the system performance and fall between the results of slow power control and fast power control of the same diversity order. In addition, diversity order of 1, 2, and 4 can be also considered as a bound of imperfect spatial diversity of order 2, 4, and 8, respectively.

Table 2.4: Capacity improvements by diversity

	Slow power control	% gain	Fast power control	% gain
$M = 1$			4.0	
$M = 2$	4.4		36.9	822.5 %
$M = 4$	12.6	186.4 %	67.7	83.5 %
$M = 8$	22.1	75.4 %	74.9	10.6 %

Table 2.5: Mean and variance of intracell interference and intercell interference

Diversity Order	Intracell Interference		Intercell Interference	
	Mean	Variance	Mean	Variance
$M = 1$	0.3800	0.2774	0.8742	24.628
$M = 2$	0.3800	0.2774	0.2143	1.0447
$M = 4$	0.3800	0.2774	0.0722	0.0425
$M = 8$	0.3800	0.2774	0.0309	0.0060

2.5.2 Impact of multipath profiles

Figure 2.5 and Figure 2.6 show the outage probabilities vs. the number of users for pedestrian A channel and vehicular A channel, respectively. For $m = 1$, Nakagami-*m* fade distribution is equivalent to Rayleigh fade distribution. In these results, it can be observed that the system capacities achieved by the same diversity order are larger in vehicular channel A than those in pedestrian A channel because of larger multipath diversity in vehicular A channel. However, relative gains obtained by spatial diversity are greater in pedestrian A channel than those in vehicular A channel. That is, spatial

diversity has a more positive impact in pedestrian A channel environments as compared with the spatial diversity impact in vehicular A channel since there is less path diversity available in pedestrian A channel environments than in vehicular A channel environments. From these results, it is expected that system capacity is more sensitive to the variations in the received signal which have not been compensated completely by either power control or diversity processing than to total interference caused by occasional high power transmission from other users when fast power control is employed.

Table 2.6 and Table 2.7 summarize the system capacities achieved by spatial diversity in pedestrian A channel and vehicular A channel, respectively, based on the outage probability of 10^{-2}. Furthermore, it is observed that the system capacities of fast power control achieved by the spatial diversity approach to a certain value. It is due to that as the spatial diversity order increases, both mean and variance of intercell interference approach to zero. In this case, the system capacities are determined by the number of intracell interference. That is, it is expected that the system capacities are limited by the intracell interference when high order spatial diversity is employed in the system.

Table 2.6: System capacity achieved by spatial diversity in pedestrian A channel

	Slow power control	% gain	Fast power control	% gain
$M = 1$	3.3		15.0	
$M = 2$	9.0	173.7 %	52.7	251.3 %
$M = 4$	17.3	92.2 %	69.0	30.9 %
$M = 8$	26.1	50.9 %	75.1	8.8 %

Table 2.7: System capacity achieved by spatial diversity in vehicular A channel

	Slow power control	% gain	Fast power control	% gain
$M = 1$	9.9		37.0	
$M = 2$	18.8	90.0 %	59.8	61.6 %
$M = 4$	28.2	50.0 %	70.5	17.9 %
$M = 8$	36.4	29.1 %	75.4	7.0 %

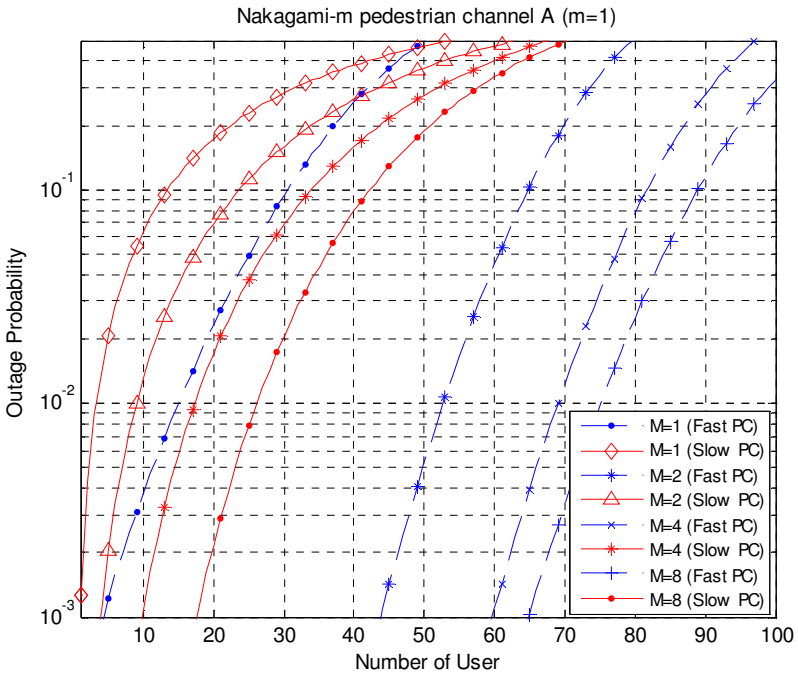

Figure 2.5: Outage probability for Nakagami-m pedestrian A channel with m=1

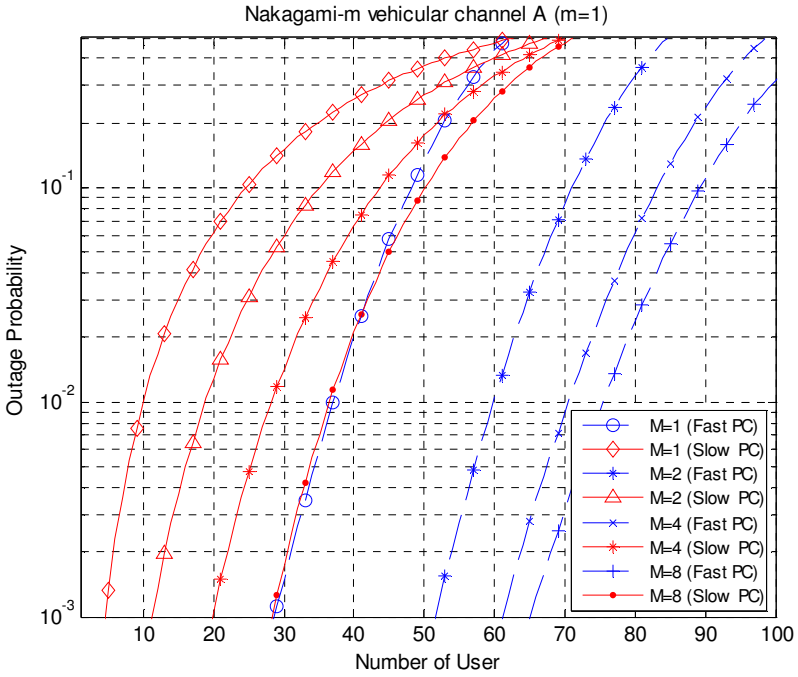

Figure 2.6: Outage probability for Nakagami-m vehicular A channel with m=1

2.5.3 Impact of fade distributions

In systems employing fast power control, reduced signal variation leads to reduced outage and interference, hence capacity improvement. Reduced interference stems from increased average received power and less frequent high power transmissions. Also, in systems using slow power control, reduced received signal variation results in reduced outage, leading to capacity increase. In this section, we investigate the effect of fading distribution on system capacity and outage probability when spatial diversity processing is employed. In Nakagami-*m* fade distribution, as the fading severity index, m, decreases, the signal variations due to the multipath fading process becomes large. Therefore, higher transmit power might be required to compensate the severe channel fluctuation, which will increase the intercell interference and result in the reduction of system capacity.

Figure 2.7 and Figure 2.8 show the outage probabilities vs. the number of users per cell for Nakagami-*m* fade distribution with $m = 0.5$ in pedestrian A channel and vehicular A channel, respectively. Nakagami-*m* fade distribution with $m = 0.5$ will show more severe fading environment. It is observed that the system capacity significantly reduces without any spatial diversity even if fast power control is applied as compared with the results shown in Figure 2.5 and Figure 2.6. However, as the spatial diversity order increases, the system capacity significantly increases. That is, the impact of spatial diversity is more positive in severe fading environment.

Figure 2.9 and Figure 2.10 show the outage probabilities vs. the number of users per cell for Nakagami-*m* fade distribution with $m = 9/5$ in pedestrian A channel and vehicular A channel, respectively. For $m = 9/5$, Nakagami-*m* fade distribution is equivalent to Rician fade distribution with $K = 2$ according to Equation (2.8). Since fading channel environments become less severe, the system capacity achieved without spatial diversity increases and becomes larger as compared with the results shown in Figure 2.7 and Figure 2.8. In addition, the relative improvements by increasing spatial diversity order are also reduced.

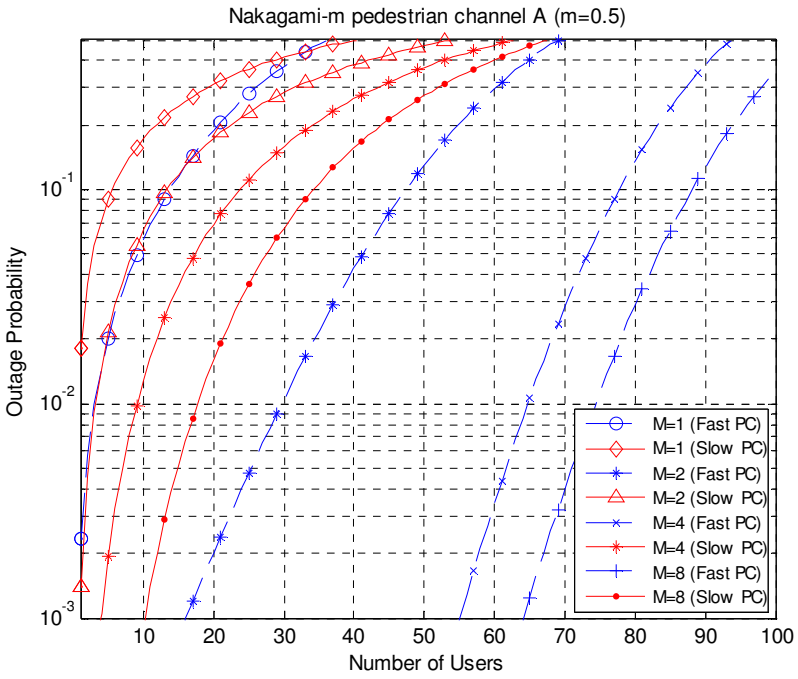

Figure 2.7: Outage probability for Nakagami-m pedestrian A channel with m=0.5

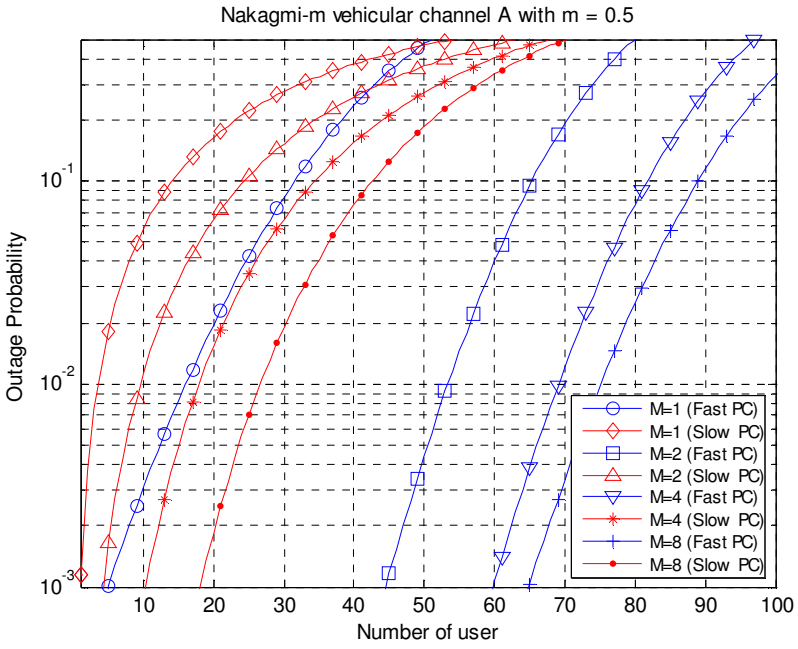

Figure 2.8: Outage probability for Nakagami-m vehicular A channel with m=0.5

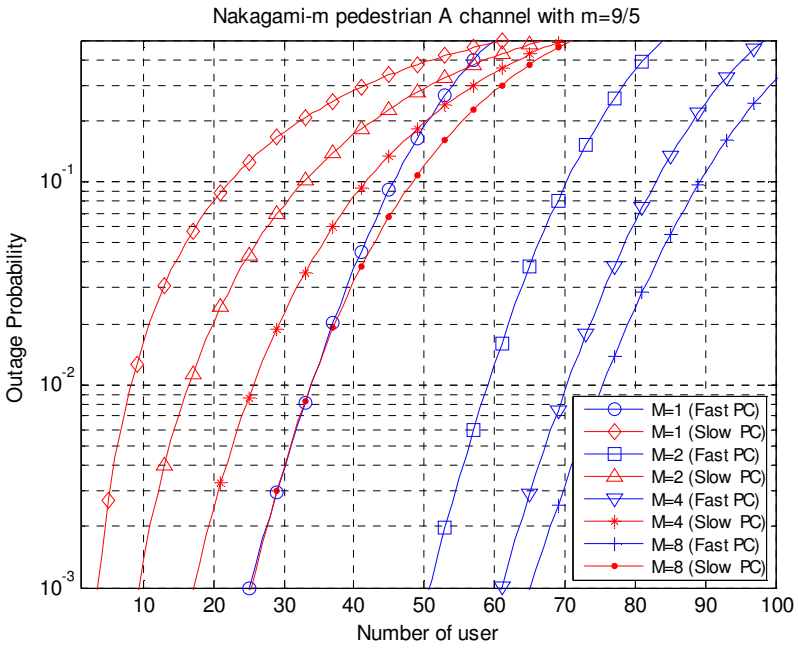

Figure 2.9: Outage probability for Nakagami-m pedestrian A channel

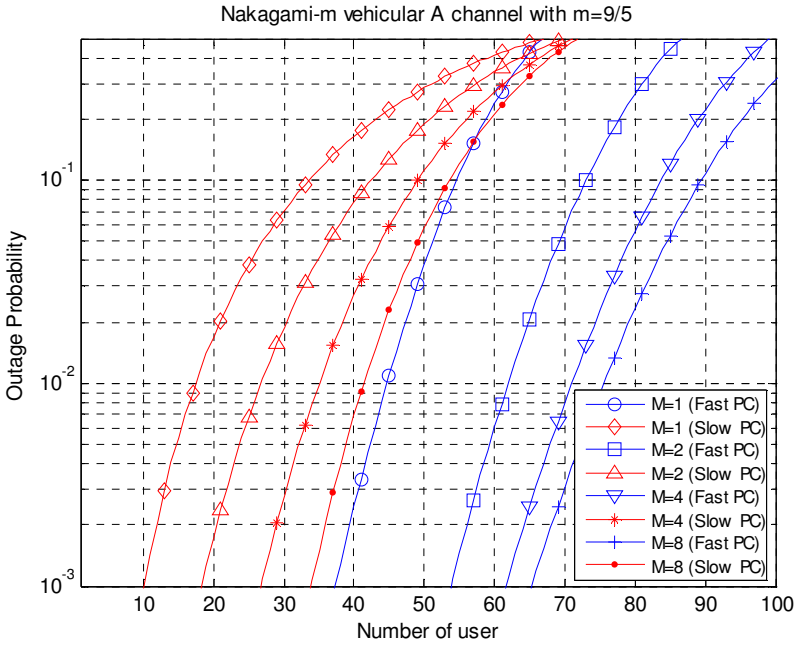

Figure 2.10: Outage probability for Nakagami-m vehicular A channel with m=9/5

The system capacities achieved by the spatial diversity from Figure 2.7 to Figure 2.9 are summarized in Table 2.8, Table 2.9, Table 2.10, and Table 2.11, respectively.

Table 2.8: System capacity achieved by spatial diversity in pedestrian A channel with m=0.5

	Slow power control	% gain	Fast power control	% gain
$M = 1$			3.0	
$M = 2$	3.2		29.7	890 %
$M = 4$	9.1	184.3 %	64.7	117.8 %
$M = 8$	17.7	94.5 %	74.3	12.9 %

Table 2.9: System capacity achieved by spatial diversity in vehicular A channel with m=0.5

	Slow power control	% gain	Fast power control	% gain
$M = 1$	3.6		16.1	
$M = 2$	9.6	166.7 %	53.4	231.7 %
$M = 4$	17.9	86.5 %	69.1	29.4 %
$M = 8$	26.6	48.6 %	75.1	8.7 %

Table 2.10: System capacity achieved by spatial diversity in pedestrian A channel with m=9/5

	Slow power control	% gain	Fast power control	% gain
$M = 1$	8.3		33.9	
$M = 2$	16.5	98.8 %	59.0	74 %
$M = 4$	25.7	55.8 %	70.0	18.6 %
$M = 8$	33.8	24.0 %	75.4	7.2 %

Table 2.11: System capacity achieved by spatial diversity in vehicular A channel with m=9/5

	Slow power control	% gain	Fast power control	% gain
$M = 1$	17.5		44.7	
$M = 2$	26.7	52.6 %	62.0	38.7 %
$M = 4$	35.0	31.1 %	71.0	14.5 %
$M = 8$	41.4	18.3 %	75.5	6.0 %

2.5.4 Impact of correlated fading channel

So far, it has been assumed that signals from each spatial diversity branch are not correlated each other. In this section, not only correlation between antenna branches, but also correlation between multipath components in channel models is considered to investigate the impact of correlation on system capacity. Correlation between antenna diversity branches is assumed to be 0.7, and inter-path correlation is assumed to be 0.3.

Figure 2.11 and Figure 2.12 shows the outage probabilities vs. the number of users per cell for correlated Nakagami-*m* fade distribution in pedestrian A and vehicular A channel, respectively. As previously mentioned, system capacity is more sensitive to received signal variations; the variations of the received signal are reduced through spatial diversity processing. The spatial diversity achieves a performance improvement by reducing the probability that each branch will experience correlated fading and by increasing the average received signal power. However, since there is a correlation between diversity branches, there is now more variation in the received signal power as compared with the uncorrelated case, and a reduced average received signal power, which both leads to a capacity loss. Even though there is a correlation between diversity branches, there is still a capacity increase in systems employing fast power control as diversity order increases, due to the energy capturing capability of the spatial diversity technique. However, it is observed that imperfect power control further degrades the system capacity when there are correlations among diversity branches. In other word, it is not easy to observe the capacity improvements by spatial diversity without fast power control if there are correlations among diversity branches.

Table 2.12 and Table 2.13summarize the system capacity achieved by the spatial diversity in pedestrian A channel and vehicular A channel, respectively, with correlated Nakagami-*m* fading channel with $m = 1$.

Table 2.12: System capacity achieved by spatial diversity in pedestrian A channel with correlated fading channel

	Slow power control	% gain	Fast power control	% gain
$M = 1$	2.6		11.0	
$M = 2$	4.8	84.6 %	42.4	285.5 %
$M = 4$	6.9	43.8 %	62.8	48.1 %
$M = 8$	8.5	23.2 %	72.0	14.6 %

Table 2.13: System capacity achieved by spatial diversity in pedestrian A channel with correlated fading channel

	Slow power control	% gain	Fast power control	% gain
$M = 1$	7.0		30.1	
$M = 2$	9.8	40.0 %	53.2	76.7 %
$M = 4$	11.8	20.4 %	66.6	25.2 %
$M = 8$	13.0	10.2 %	73.5	10.4 %

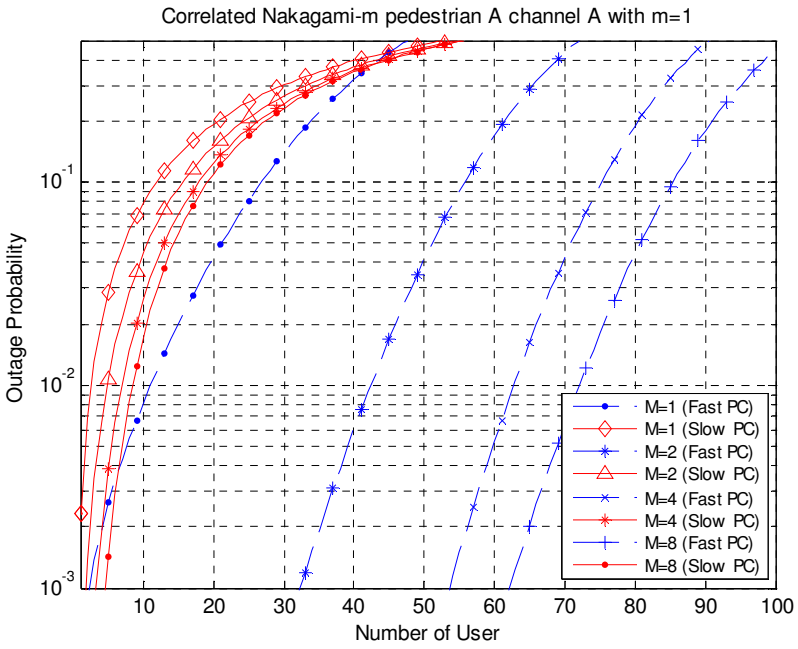

Figure 2.11: Outage probability for correlated Nakagami-m pedestrian A channel with m=1

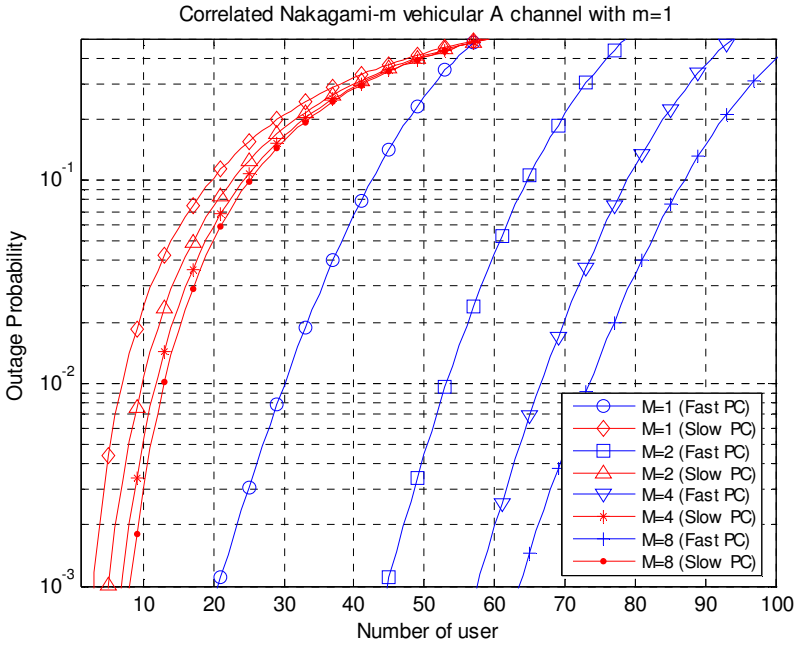

Figure 2.12: Outage probability for correlated Nakagami-m vehicular A channel with m=1

2.5.5 Impact of user distributions

Up to now, we have assumed a uniform user distribution throughout a cell; this assumption provides a general insight on the system capacity. At times, however, non-uniform user distribution throughout a cell could further deteriorate or ameliorate the system capacity, and different aspects of the capacity improvement might be observed with an interference mitigation technique. Two cases are considered including a) users are uniformly distributed in the region, $0.5 < r < 1$, b) users are uniformly distributed in the region, $0 < r < 0.5$, where r is the distance from the mobile to the BS of the cell which users belong to, and are compared with the result with uniform user distribution throughout the cell. The cell radius is assumed to be one without loss of generality. Since the user distribution determines the position of an MS, it is associated with only the path loss due to the distance between the k th MS and a BS. For the evaluation of the mean and variance of total interference with the given user distribution, Monte Carlo integration [9] is performed by uniformly placing MSs over given area as shown in Figure 2.13.

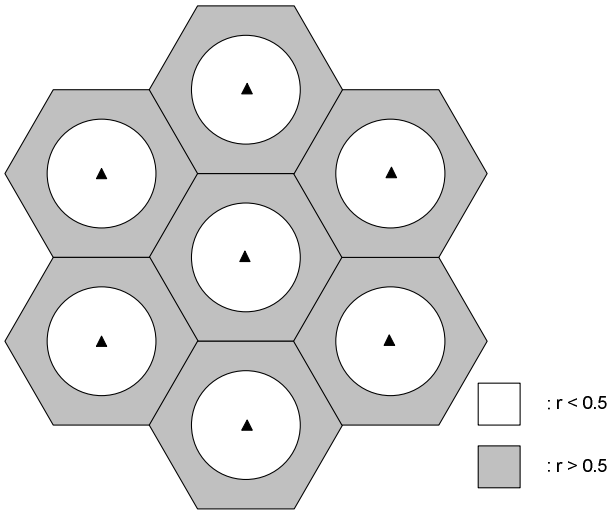

Figure 2.13: Two regions in the system divided by the cell radius

Figure 2.14 and Figure 2.15 show the outage probabilities vs. the number of users for user distribution that MSs are concentrated on the area with $r > 0.5$, that is, around cell boundaries for Nakagami-*m* pedestrian A channel, and vehicular A channel with $m = 1$, respectively. It is observed that the system capacity becomes slightly worse as compared with the system capacity when MSs are uniformly distributed in each cell shown in Figure 2.5 and Figure 2.6. It results from that MSs distributed in the outer ring of a cell region create more interference to other cells because of the relatively large path losses. As a consequence, a system loaded with MSs relatively close to the cell boundaries experiences increased interference to achieve a prescribed outage probability. Furthermore, it is observed that the relative spatial diversity improves as compared with the results of uniform user distribution.

On the other hand, when MSs are concentrated on the area with $r < 0.5$, that is, around the BS in each cell, the system capacity increases as shown in Figure 2.16 and Figure 2.17. It comes from that the average transmit power of MSs is relatively low due to the relatively small path losses and substantially reduce the other cell interference. However, it is observed that the spatial diversity gain diminishes as compared with the results of uniform user distribution. From Table 2.14 to Table 2.17, the system capacities achieved by spatial diversity for non-uniform user distributions are summarized.

Table 2.14: System capacity achieved by spatial diversity in pedestrian A channel for r>0.5

	Slow power control	% gain	Fast power control	% gain
$M = 1$	2.9		11.7	
$M = 2$	8.0	175.9 %	46.7	299.1 %
$M = 4$	15.3	91.3 %	65.1	39.4 %
$M = 8$	23.2	51.6 %	72.6	11.5 %

Table 2.15: System capacity achieved by spatial diversity in vehicular A channel for r>0.5

	Slow power control	% gain	Fast power control	% gain
$M = 1$	8.8		31.0	
$M = 2$	16.4	86.4 %	54.4	75.5 %
$M = 4$	24.5	49.4 %	66.9	23.0 %
$M = 8$	31.4	28.2 %	73.0	9.1 %

Table 2.16: System capacity achieved by spatial diversity in pedestrian A channel for r<0.5

	Slow power control	% gain	Fast power control	% gain
$M = 1$	4.7		56.8	
$M = 2$	12.9	174.5 %	76.5	34.7 %
$M = 4$	24.7	91.5 %	80.3	5.0 %
$M = 8$	37.3	51.0 %	81.5	1.5 %

Table 2.17: System capacity achieved by spatial diversity in vehicular A channel for r<0.5

	Slow power control	% gain	Fast power control	% gain
$M = 1$	14.3		70.7	
$M = 2$	26.6	86.0 %	78.2	10.6 %
$M = 4$	39.6	48.9 %	80.6	3.1 %
$M = 8$	50.9	28.5 %	81.6	1.2 %

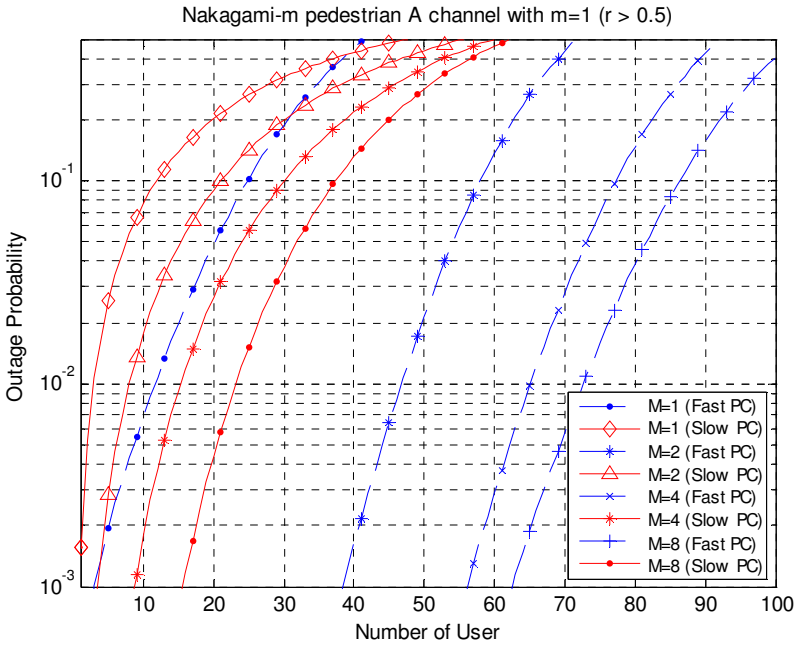

Figure 2.14: Outage probability for Nakagami-m pedestrian A channel with m=1 (r>0.5)

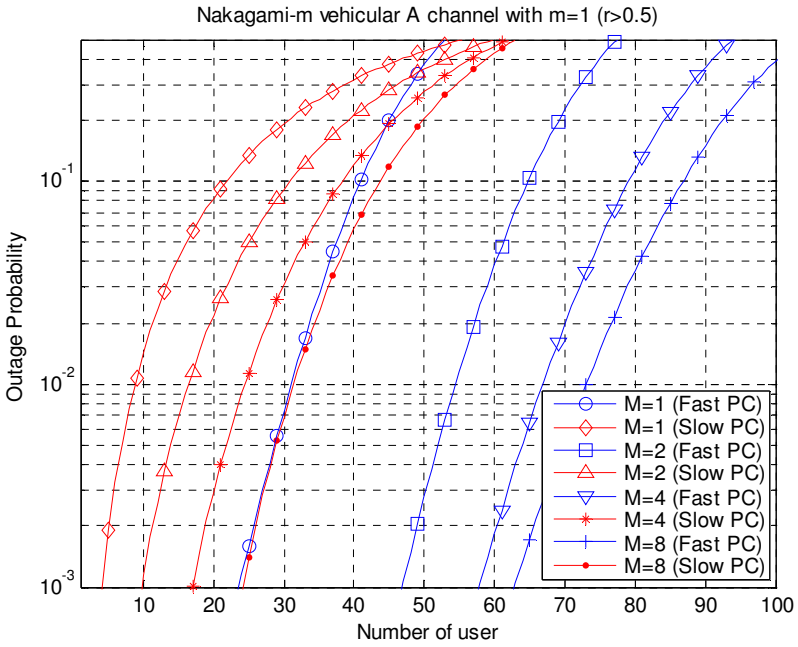

Figure 2.15: Outage probability for Nakagami-m vehicular A channel with m=1 (r>0.5)

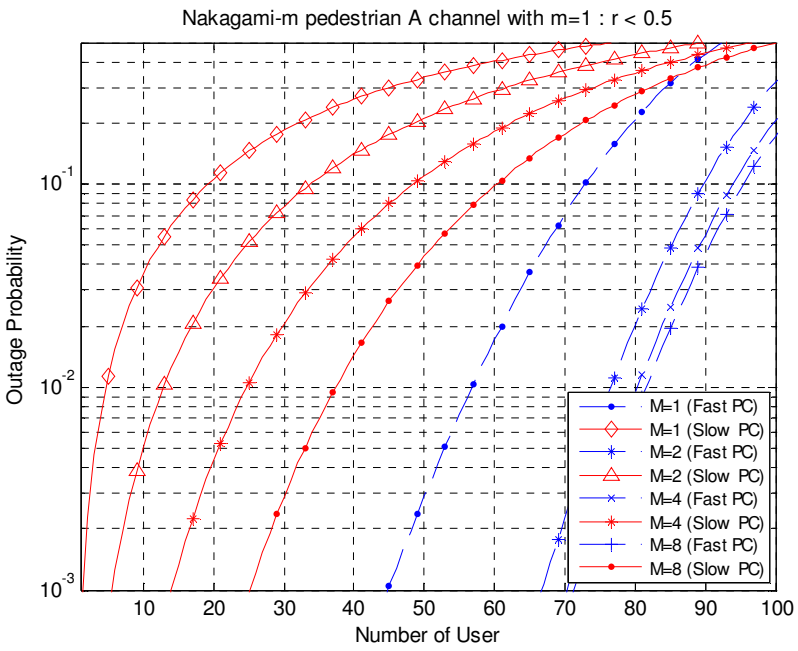

Figure 2.16: Outage probability for Nakagami-m vehicular A channel with m=1 (r<0.5)

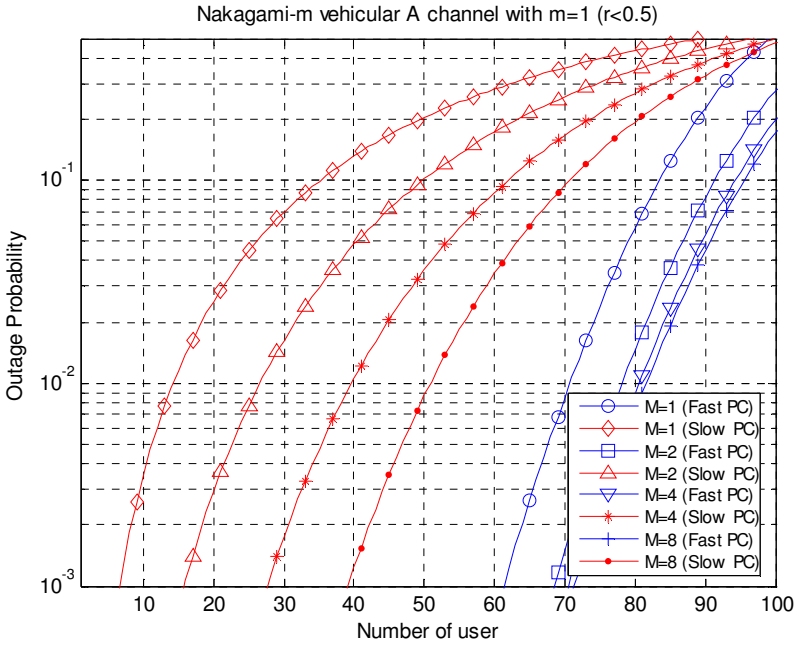

Figure 2.17: Outage probability for Nakagami-m vehicular A channel with m=1 (r>0.5)

2.5.6 Erlang capacity

Figure 2.18 and Figure 2.19 show the blocking probabilities of a new call request for Nakagami-*m* pedestrian A and vehicular A channel, respectively, with $m = 1$. $M = L_t L_r$ is the diversity order with L_t transmit antennas and L_r receive antennas. Again, for $m = 1$, Nakagami-*m* fading is equivalent to Rayleigh fading channel. As described in the previous chapter, it is assumed that the system may block a new call request when the system is in outage as a call admission control. For the threshold of the system outage, the same threshold as that to calculate the outage probability is assumed. It can be observed that the system capacity based on the blocking probability shows very similar trend to the system capacity based on the outage probability. That is,

- The system capacity substantially improved by using spatial diversity, but the amount of improvement decreases as diversity order increases.
- The system capacity improvement is greater in Pedestrian A channel than in Vehicular A channel due to the difference of number of available paths and the number of dominant paths.
- The results of slow power control can be considered as a bound of imperfect power control, that is, any imperfect power control may degrade the system capacity, and fall between the results of slow power control and fast power control.

However, it is observed that the system capacity in terms of blocking probability, expressed as the traffic intensity (λ / μ), is slightly smaller than the system capacity in terms of the outage probability in the region of smaller blocking/outage probability (less than 10^{-2}). On the other hand, at the higher blocking/outage probability region (greater than 10^{-1}), the system capacity in terms of blocking probability is better than the system capacity in terms of the outage probability. Since departure rate is larger than the arrival rate for large traffic intensity, the probability that the system states remains at the large number of users will be reduced; hence, the blocking probability will be smaller than the

outage probability that can be considered as the blocking probability without call admission control. On the other hand, for small traffic intensity, arrival rate is relatively larger than departure rate. Hence, the probability that the system state goes to the large number of users will increase, which will increase the blocking probability. It can be observed in the occupancy distributions in the system shown in Figure 2.20 which shows the occupancy distribution for both traffic intensity and states for the diversity order, M, of two. It is observed that the both traffic intensity and system states increases, the occupancy distribution reduces and vice versa.

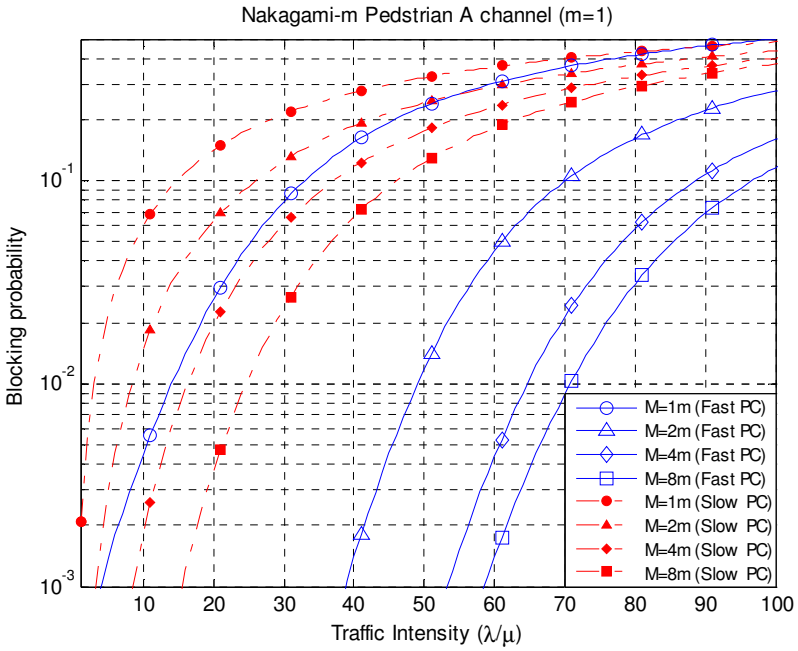

Figure 2.18: Blocking probability for Nakagami-m pedestrian A channel with m=1

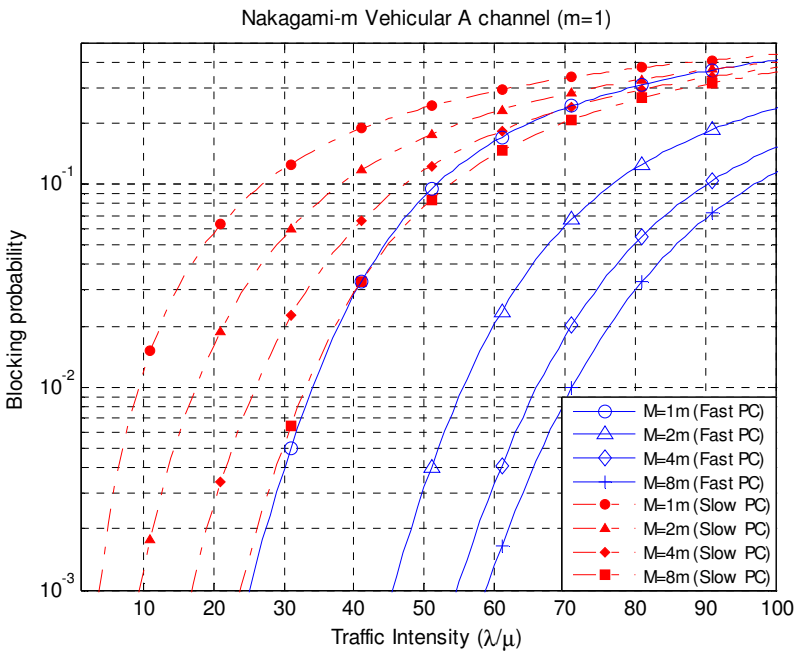

Figure 2.19: Blocking probability for Nakagami-m vehicular A channel with m=1

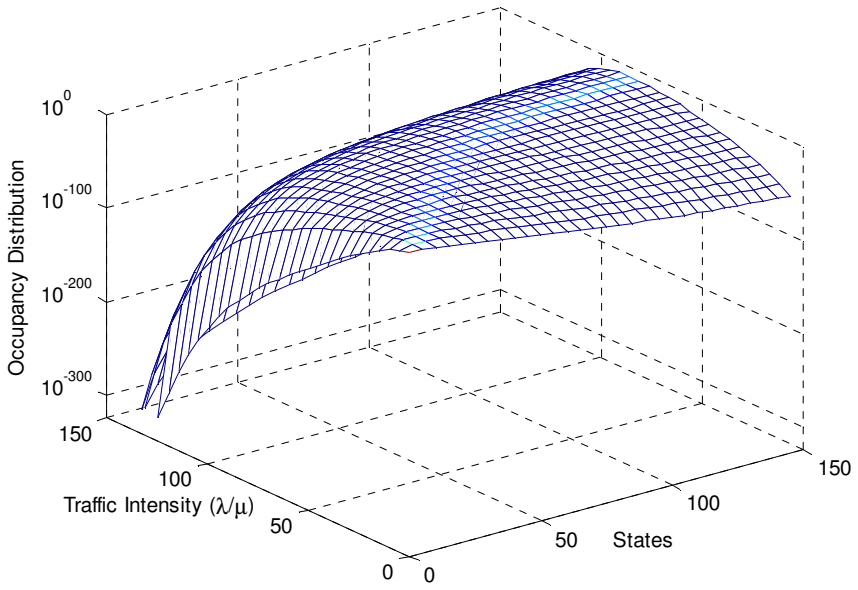

Figure 2.20: Occupancy distribution for states and traffic intensity with M=2

2.6 Chapter summary

A general mathematical framework to evaluate the impact of spatial diversity (typically, transmit diversity) processing on the system capacity of the uplink of a DS/CDMA system, and the analysis results obtained from it are presented in this chapter. By using this analytical approach, it is observed that transmit diversity at the handset can significantly improve system capacity. Key observations from this study include:

- Using transmit diversity at the handset dramatically reduces intercell interference and the fluctuation of the received signal, resulting in a significant capacity improvement for both the slow and fast power control cases;
- Spatial diversity has a greater positive impact on a system operating in environments in which the available path diversity is small;
- The impact of fade variability is reduced with respect to the system capacity and outage probability, as the spatial diversity order increases;
- The gain achievable through spatial diversity processing diminishes as the fading index increases, or equivalently, as the fading severity diminishes;
- When users are not uniformly distributed in a cell, particularly in those cases in which users are concentrated near cell boundaries, the system capacity and outage probability degrade and the relative performance gain due to spatial diversity increases;
- Systems employing fast power control achieve greater capacity than those employing slow power control when evaluated under the same conditions; However, the relative capacity increase is greater for slow power control when the antenna diversity order is increased;

- System capacity is more sensitive to variations in the received signal which have not been compensated completely by either power control or diversity processing;
- Increased inter-path correlation and antenna branch correlation reduces system capacity and increase the outage probability;
- Inter-path correlation and antenna branch correlation have a more negative impact on systems employing slow power control than systems using fast power control.

Chapter

3 Coverage of Uplink DS/CDMA with Multiple-Input Multiple-Output Implementation

3.1 Introduction

One of an attractive feature of DS/CDMA cellular systems is their ability to get into what is known as "*soft handoff*", proposed in the Telecommunication Industry Association's IS-95 standard [50]. A mobile station (MS) in soft handoff maintains simultaneous radio links with multiple base stations. Transmissions from the MS are received and processed by each of the base stations (BS) with which it maintains a radio link, known as an active set, before they are combined and passed on to the terrestrial network. Similarly, transmissions to the MS are also carried simultaneously by BSs in the active set. The MS, then, combines the signal received from these BSs using appropriate diversity techniques. Soft handoff is believed to enable the system to operate at lower power levels and/or achieve a better connection quality [15, 18, 51]. Soft handoff is also known as *base station diversity* or *macro-diversity* as compared to the diversity provided from the multipath or multi-antenna between peer-to-peer links, which is referred as a *micro-*

diversity. In many literatures [15-17, 28], it has been studied that the soft handoff (or macro-diversity) would improve the system coverage as well as the system capacity. However, it is rarely studied the ability of multiple-input multiple-output (MIMO) to improve the system coverage. In previous chapter, we have studied that MIMO can substantially improve the capacity of DS/CDMA cellular systems. However, it has been assumed that the system is well-designed so that no outage occurs by the coverage limit in the system, which may not be true in the deploying process of the cellular systems. Furthermore, the previous analysis scheme is only applicable to the system equipped with transmit diversity and multipath diversity because it is assumed that there is no intracell interference reduction, which also may not be true if we take into account the receive antenna diversity.

- ***Contributions***

Hence, in this chapter, we extends and generalizes all the previous works in several aspects: (a) derives SIR as a function of fade margin, the number of interference for the joint analysis of capacity and coverage, (b) presents how to evaluate the outage probability of the SIR based on the approximation of the interference statistics, and (c) provides analytical framework for better understanding on the impact of MIMO on the capacity, coverage, and the relationship between them. Developed analytical framework in this chapter can take into account several other parameters which can affect the system performance such as soft handoff, multipath fading with arbitrary multipath intensity profile, different fading statistics, and various user distributions.

- ***Organization***

The rest of this chapter is organized as follows. In section 3.2, how the fade margin affects the system coverage is described. In section 3.3, system coverage for the unloaded system (without considering co-channel interference) with MIMO is presented. In section 3.4, the relationship between system coverage and capacity (with co-channel

interference) are analyzed with MIMO. Finally, the main points of this chapter are summarized in section 3.5.

3.2 Coverage vs. Fade Margin

In DS/CDMA cellular systems, power control technique is essential to solve *near-far* problem. In addition, the transmit power of an MS is periodically controlled so that the instantaneous received power at the BS is maintained at a certain level satisfying a required QoS (quality of services). However, the maximum transmit power of an MS is limited by the power amplifier. Therefore, in some cases such as severe fading environments or out-of-range, the instantaneous received power at the BS might not satisfy the required power level as shown in Figure 3.1, which is generally called as the *outage*.

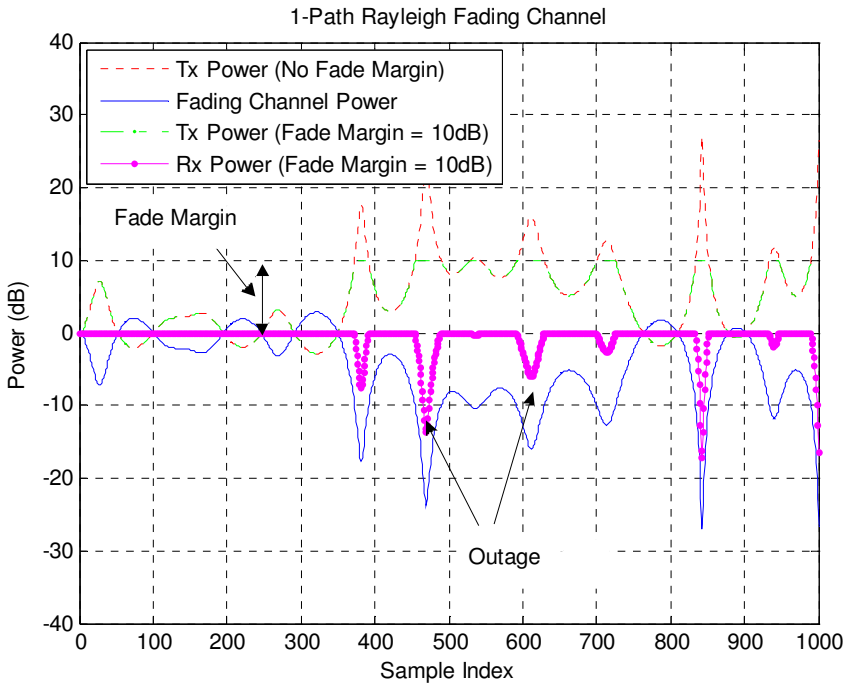

Figure 3.1: Fade margin and power control

This constraint of the maximum transmit power is generally referred as *fade margin*. Then, the outage probability can be defined as

$$P_{out} = \Pr\{P_T > \gamma\} \tag{3.1}$$

where γ denotes the fade margin and P_T denotes the transmit power of the MS. Generally, without taking into account the co-channel interference of the system, this outage probability as a function of the fade margin can be considered as the coverage metric since the outage will be obviously increased as the MS moves out far from the BS. However, taking into account the co-channel interference, we need to consider the outage probability of the signal-to-interference ratio versus the fade margin to estimate the cell coverage. First, let us investigate the outage probability of transmit power without considering the co-channel interference, which will give us an insight on the cell coverage of DS/CDMA cellular system. Next, we will examine the outage probability of the signal-to-interference ratio taking into account the co-channel interference, from which we can estimate the relation between cell coverage and capacity of the system.

3.3 Cell Coverage of Unloaded System

In this section, we present how much coverage improvements of uplink DS/CDMA cellular systems can be obtained with *micro-diversity* technique such as multipath diversity and spatial diversity techniques in conjunction with macro-diversity technique such as soft handoff. As mentioned in the previous section, we exploit fade margin analysis to evaluate the coverage improvements, which common analysis technique in many literatures [15, 16, 18, 28].

3.3.1 System model

For the estimation of the cell coverage of unloaded system, we just need to consider the cellular communication systems which consists of three BSs as shown in Figure 3.2, where the cell radius is assumed to be ‘1’ and BSs are located at the center of each cell.

For the soft handoff, it is assumed that an MS can communicate with three nearest BSs which is defined as an active set. Then, the transmit power of the MS will be changed by the power control command generated by the BS that provide the least propagation loss, which is modeled by the selection diversity. Then, the soft handoff region is simply determined by the region of gray-colored triangle in Figure 3.2. For the micro-diversity technique, we take into account multiple-input multiple-output implementation as shown in Figure 3.3, where closed loop transmit diversity at MS, and maximal ratio combining of multipath and multi-antenna branches at BS are presumed.

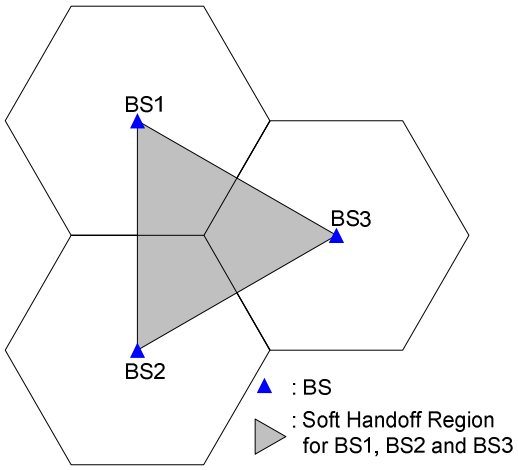

Figure 3.2: System model and soft handoff region

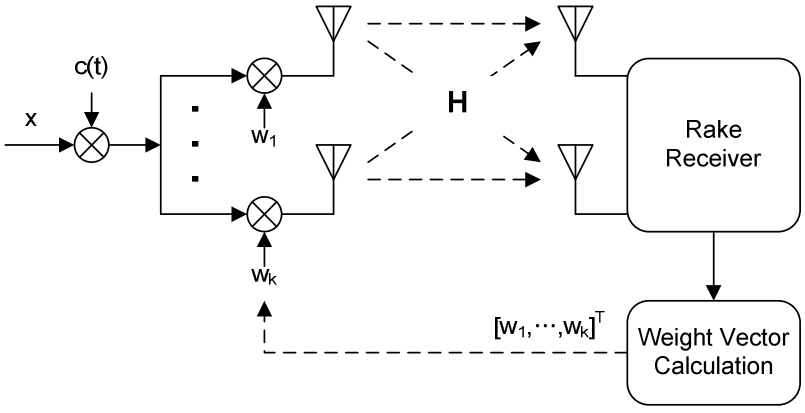

Figure 3.3: Multiple-input multiple-output implementation

3.3.2 Outage probability

Now, let us consider the outage probability of the transmit power of an MS, P_T, as a function of the fade margin, γ, as defined in Equation (3.1). Assuming the perfect power control such as the channel inversion and no macro-diversity, P_T is defined as

$$P_T = \left(\frac{X_k}{r_k^u 10^{\zeta_k/10}} \right)^{-1} \tag{3.2}$$

where r_k^u is the propagation loss due to the distance, r_k, with the power exponent, u, between MS and BS, $10^{\zeta_k/10}$ is the shadow fading channel loss, and X_k is the multipath fading loss in MIMO channel. That is, the transmit power is defined by the inverse of channel propagation losses due to both short-term and long-term fading channel. Taking into account the system given in Figure 3.3, X_k can be approximated as [38]

$$X_k \approx \sum_{l=1}^{L_t} \sum_{m=1}^{L_r} \sum_{n=1}^{L_m} \left| h_{l,m,n} \right|^2 \tag{3.3}$$

where $\left| h_{l,m,n} \right|$ represents the envelope of short-term fading that can be subject to various fading statistics such as Rayleigh, Rician, and Nakagami-*m* / -*q* distributions, and L_t, L_r, and L_m are the number of transmit antennas, receive antennas, and multipath components, respectively. If the open-loop transmit diversity such as space-time block coding technique, X_k can be expressed as

$$X_k = \sum_{l=1}^{L_t} \sum_{m=1}^{L_r} \sum_{n=1}^{L_m} \left| h_{l,m,n} \right|^2 / L_t \tag{3.4}$$

Furthermore, if macro-diversity technique (soft handoff) is employed, P_T is expressed as

$$P_T = \min_{i \in A_c(k)} \left\{ r_i^u 10^{\zeta_i/10} \right\} \cdot \frac{1}{X_k} \tag{3.5}$$

where $A_c(k)$ is the active set of MS, from which MS chooses the best serving BS that provides the least average propagation loss among N_c BSs, and ζ_i is the correlated Gaussian random variables composed of two components: one (ξ_k) in the near field of the MS that is common to all BSs, and the other (ξ_i) that pertains solely to the receiving BS and is independent from one BS to other BS. That is, ζ_i is defined as

$$\zeta_i = a\xi_k + b\xi_i, \qquad a^2 + b^2 = 1 \tag{3.6}$$

where a and b are defined as the correlation coefficients. The outage probability, then, can be calculated as

$$\begin{aligned} P_{out}^{(k)} &= \Pr(P_T > \gamma) \\ &= \Pr\left(\min_{i \in A_c(k)} \left\{ r_i^u 10^{\zeta_i/10} \right\} \cdot \frac{1}{X_k} > \gamma \right) \\ &= \Pr\left(\min_{i \in A_c(k)} \{ M_i + b\xi_i \} > \Gamma + \chi_k - a\xi_k \right) \\ &= \int_0^\infty \int_{-\infty}^\infty \prod_{i \in A_c(k)} Q\left(\frac{\Gamma + \chi_k - a\sigma z - M_i}{b\sigma} \right) f_{Z(z)dz} f_X(x) dx \end{aligned} \tag{3.7}$$

where γ is the fade margin, $\Gamma = 10\log_{10}\gamma$, $\chi_k = 10\log_{10} x$ corresponding to the short-term fading random variable, X_k, in decibel, $M_i = 10u\log_{10} r_i$, σ is the standard deviation of log-normal shadowing in decibel, and $f_Z(z)$ and $f_X(x)$ are the probability density functions of standard Gaussian random variable, z, and the multipath fading random variable, X_k, respectively. The outage probability given in Equation (3.7) is a point-wise outage probability for an MS in the soft handoff region. Most literatures [15, 16, 18, 28] just assume that MS is located at the center of soft handoff region, which corresponds to the worst case estimation of outage probability. However, it is more reasonable to take an average of point-wise outage probability over the region of interest to get an estimate of outage in the desired region. Hence, the final outage probability can be calculated as

$$\overline{P}_{out} = \iint_R P_{out}^{(k)} \cdot \kappa dR \tag{3.8}$$

where $\kappa = 2K / 3\sqrt{3}$ is a user density of uniform hexagonal shape cell with K users, and R is the region of interest corresponding to the soft handoff region in Figure 3.2.

3.3.3 Short-term fading statistics

In order to obtain the short-term fading expression given in Equation (3.3), we can apply the same method as described in the previous chapter. That is, we can evaluate the short-term fading statistics using not only the closed-form expression for Nakagami-*m* fade distribution with integer, *m*, but also the numerical inverse Laplace transform [40] for the moment generating function of the other fade distributions. Moment generating functions for several fade distributions are listed in Table 3.1 [42].

Table 3.1: PDF and MGF of signal power for common fading channels

Channel Model	PDF $f_k(\bullet)$ and MGF $\phi_k(\bullet)$ for fading signal power of the k^{th} interferer
Rayleigh	$f_k(x) = \frac{1}{\overline{p}_k}\exp\left(\frac{-x}{\overline{p}_k}\right),\ x \geq 0$ $\phi_k(s) = \frac{1}{1+s\overline{p}_k}$ where $\overline{p}_k = E[x]$ = average SNR per symbol
Rician	$f_k(x) = \frac{1+K_k}{\overline{p}_k}\exp\left[-K_k - \frac{(1+K_k)x}{\overline{p}_k}\right] I_0\left[2\sqrt{\frac{K_k(K_k+1)x}{\overline{p}_k}}\right],\ x \geq 0$ $\phi_k(s) = \frac{1+K_k}{1+K_k+s\overline{p}_k}\exp\left(\frac{-sK_k\overline{p}_k}{1+K_k+s\overline{p}_k}\right)$ where $K_k \geq 0$ is the Rician parameter
Nakagami-q	$f_k(x) = \frac{1}{\overline{p}_k\sqrt{1-b_k^2}}\exp\left[\frac{-x}{(1-b_k^2)\overline{p}_k}\right] I_0\left[\frac{b_k x}{(1-b_k^2)\overline{p}_k}\right],\ x \geq 0$ where $-1 \leq b_k = \frac{1-q_k^2}{1+q_k^2} \leq 1$ $\phi_k(s) = \frac{1}{\sqrt{[s\overline{p}_k(1+b_k)+1][s\overline{p}_k(1-b_k)+1]}}$ where $0 \leq q_k \leq \infty$ is the fading parameter
Nakagami-m	$f_k(x) = \frac{1}{\Gamma(m_k)}\left(\frac{m_k}{\overline{p}_k}\right)^{m_k} x^{m_k-1}\exp\left(\frac{-m_k x}{\overline{p}_k}\right),\ x \geq 0$ $\phi_k(s) = \left(\frac{m_k}{m_k+s\overline{p}_k}\right)^{m_k}$ where $m_k \geq 0.5$ is the fading figure

Table 3.2: System Parameters

Parameters	Value
Cell radius	1
Shadowing correlation between BSs	0.5
Log-normal shadowing	$\sigma = 8\text{dB},\ m = 0$
Path loss exponent	$u = 4$
Soft handoff	3-way
Diversity order (M)	1, 2, 4, 8
Multipath intensity profile	Pedestrian A, vehicular A, uniform

3.3.4 Numerical results

In this subsection, selective numerical results are present using the system parameters summarized in Table 3.2. Figure 3.4 shows the outage probability vs. fade margin for one-path Rayleigh fading channel, where $M = L_t L_r$ is defined as the spatial diversity order with L_t transmit antenna and L_r receive antenna. It can be observed that the fade margin is significantly reduced as spatial diversity order increases, which can be easily translated into the coverage improvements in terms of the cell radius just as in [28]. Table 3.3 shows the relative coverage improvements for Figure 3.4 according the fade margin at $\bar{P}_{out} = 0.01$. In this result, the relative margin and coverage in parentheses are the gains obtained from twice increment of diversity order. As the diversity order, M, increases by twice, the amount of coverage improvements reduces, which is general observation of diversity performance. However, the coverage is substantially improved as the diversity order. This coverage improvement comes from the energy capturing effect and the reduction of channel fluctuation by diversity combining technique.

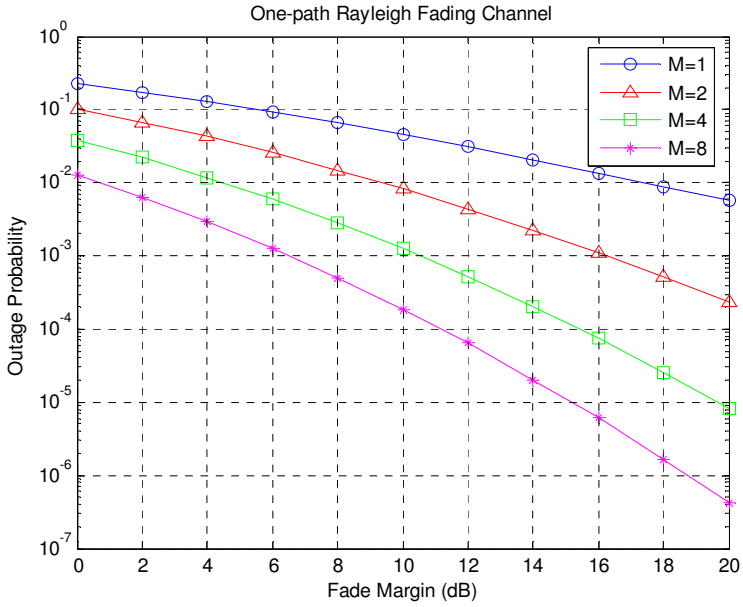

Figure 3.4: Outage probability vs. fade margin for one-path Rayleigh fading channel

Table 3.3: Relative coverage improvements

Diversity order	Fade Margin	Relative Margin	Relative Coverage
$M = 1$	17.44	0	1.00
$M = 2$	9.35	8.09	2.54
$M = 4$	4.49	12.95 (4.86)	4.44 (1.75)
$M = 8$	0.71	16.73 (3.78)	6.86 (1.54)

Figure 3.5 shows the outage probability vs. fade margin for Rician fading channel. It is observed that the outage probability of Rician fading channel is slightly improved as compared to that of Rayleigh fading channel shown in Figure 3.4. Table 3.4 summarizes the differences between Rician and Rayleigh fading channel at $\bar{P}_{out} = 0.01$. As the diversity order increases, the relative coverage difference decreases. Even for the diversity order of 8, $M = 8$, the coverage improvement might not be expected from Rayleigh fading channel to Rician fading channel.

Table 3.4: Relative coverage between Rician and Rayleigh fading channel

Diversity order	Fade Margin		Relative Margin	Relative Coverage
	Rayleigh	Rician		
M=1	17.44	16.30	1.14	1.14
M=2	9.35	8.68	0.67	1.08
M=4	4.49	4.16	0.33	1.04
M=8	0.71	0.54	0.17	1.02

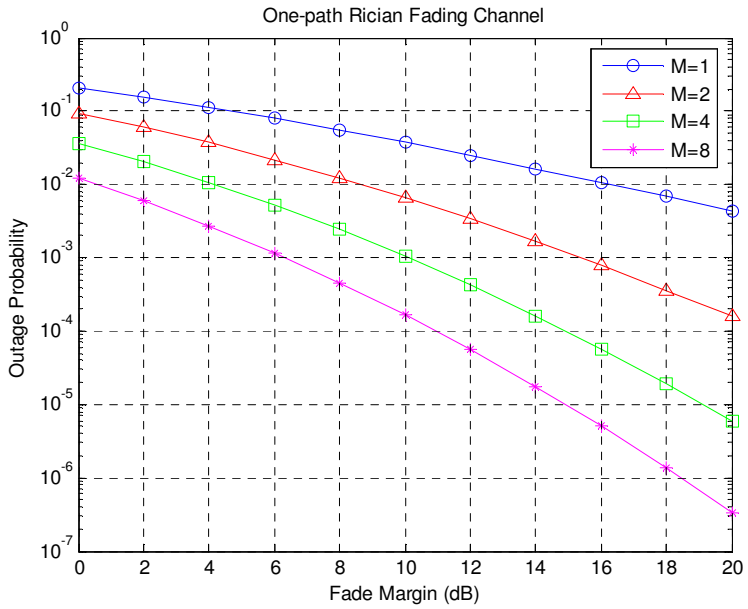

Figure 3.5: Outage probability vs. fade margin for Rician fading channel

On the other hand, Figure 3.6 shows the outage probability vs. fade margin for different number of multipath without increasing the number of antennas, where the multipath intensity profile is assumed to be uniform. It can be observed that the fade margin improves as the number of multipath increases. However, the relative gain from the multipath is small as compared with the relative gain from the multiple antennas. It is due to that we can obtain only the reduction of channel fluctuation without energy capturing effect from the multiple antennas. Table 3.5 shows the relative coverage improvements by the increased number of multipath. For the relative gain from $M = 4$ to $M = 8$ is so small that the relative coverage improvement is not much expected.

Table 3.5: Relative coverage improvements by multipath diversity

Diversity order	Fade Margin	Relative Margin	Relative Coverage
$M = 1$	17.44	0	1.00
$M = 2$	12.37	5.07	1.79
$M = 4$	10.51	6.83 (1.86)	2.19 (1.22)
$M = 8$	9.74	7.60 (0.77)	2.40 (1.09)

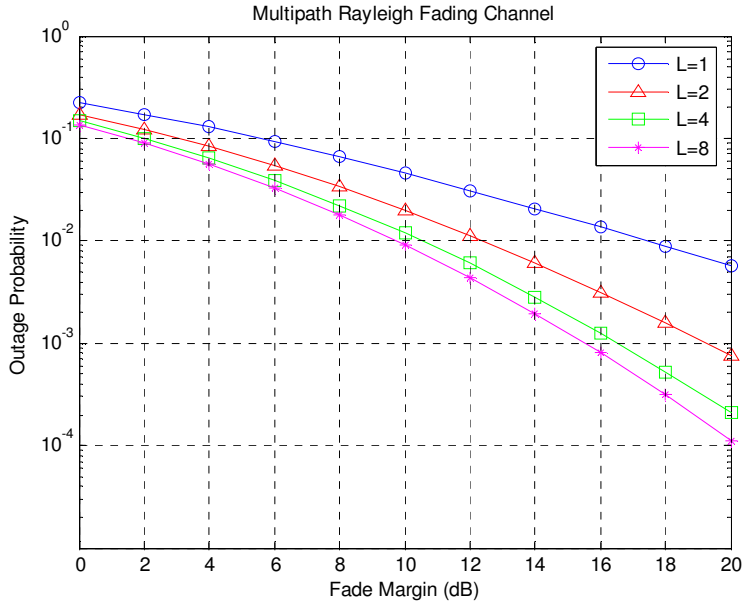

Figure 3.6: Outage probability vs. fade margin for multipath Rayleigh fading channel

Figure 3.7 and Figure 3.8 show the outage probabilities vs. fade margin (dB) for pedestrian A channel and vehicular A channel, respectively, for different spatial diversity order. Just as the results shown in Figure 3.5, it can be observed that the outage probability is significantly improved by increasing the diversity order. However, the relative gain diminishes as diversity order increases comparing with the results for one-path Rayleigh fading channel. It is due to that multipath combining process provides additional diversity capability so that the diversity gain from spatial diversity will be smaller that that without any multipath combining. Nevertheless, it is observed that the energy capturing effects (or array gain) from multiple antennas can significantly improve the outage probability.

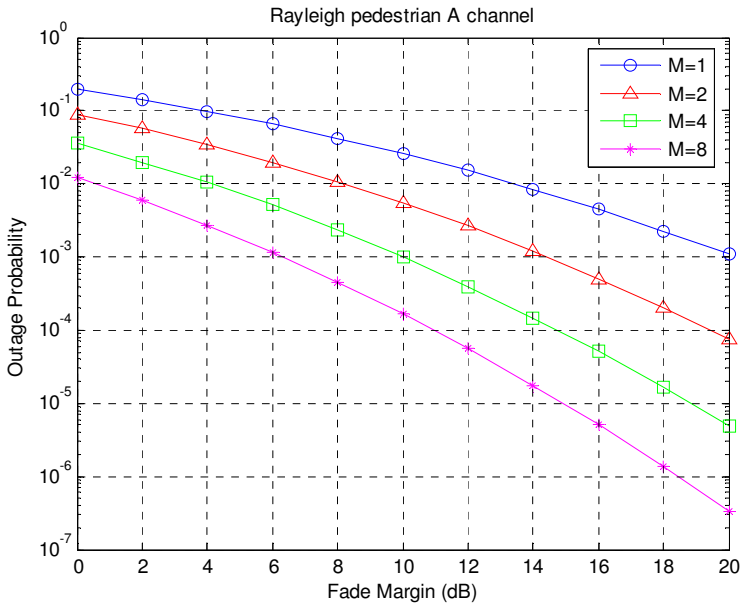

Figure 3.7: Outage probability vs. fade margin for the pedestrian A channel

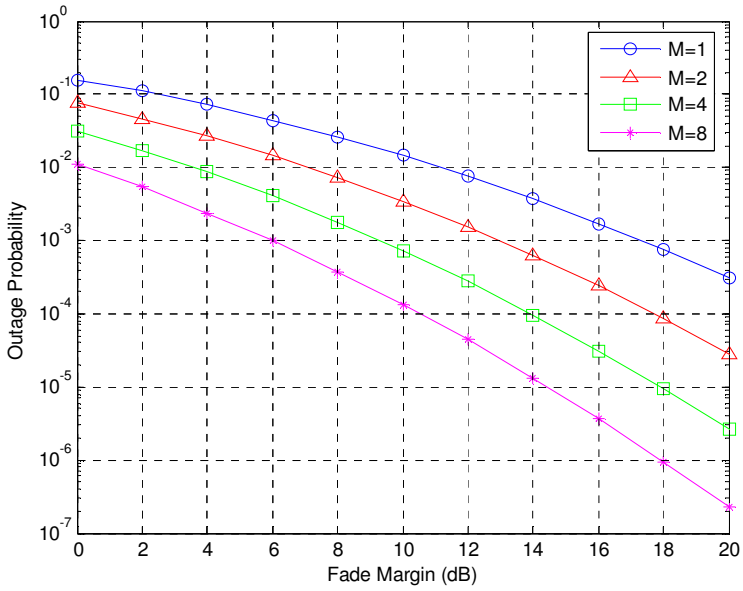

Figure 3.8: Outage probability vs. fade margin for the vehicular A channel

3.4 Cell Coverage vs. Capacity

Thus for, we have inspected the cell coverage for virtually unloaded system, assuming a single user transmitting to one of multiple BSs with no other user present, which shows the optimistic results on the cell coverage improvements with MIMO. However, cell coverage is sure to be associated with the interference when multiple co-channel interferers are present. Hence, in this section, we investigate the cell coverage for loaded system.

3.4.1 Impact of fade margin on the signal-to-interference ratio

In the presence of co-channel interference, the system outage will depend on the signal-to-interference ratio [52-56] as well as the fade margin [15-17, 27]. In multiple co-channel environments, the signal-to-interference ratio can be generally expressed as

$$\frac{S}{I} = \frac{f\left(G_l^{(0)}, P_T^{(0)}\right)}{\sum_{k=1}^{N} g\left(G_l^{(0)}, G_l^{(k)}, P_T^{(k)}\right)} \tag{3.9}$$

where $G_l^{(k)}$ is the link gain between the k^{th} transmitter and the receiver, $P_T^{(k)}$ is the transmit power for the k^{th} user, and $f(\bullet)$ and $g(\bullet)$ are the combining functions of the desired user and co-channel interference, respectively, and will be determined by the MIMO technique [53-55, 57]. Generally, the link gain consists of various factors such as the implementation loss, the antenna gain, propagation channel loss, and so on. In this analysis, we will take into account only the propagation channel loss for a simple instructive example. The combining functions will also be derived in the later section.

First, let us investigate how the fade margin affects the signal-to-interference ratio in the multiple access system. Assuming the ideal strength-based power control, the transmit power of the k^{th} MS can be expressed as

$$P_T^{(k)} = \begin{cases} \dfrac{\min\limits_{i \in A_k}\left\{ r_{ki}^{u} 10^{\zeta_{ki}/10} \right\}}{X_{kj}} & \text{if } \dfrac{\min\limits_{i \in A_k}\left\{ r_{ki}^{u} 10^{\zeta_{kj}/10} \right\}}{X_{kj}} < \gamma \\ \gamma & \text{if } \dfrac{\min\limits_{i \in A_k}\left\{ r_{ki}^{u} 10^{\zeta_{kj}/10} \right\}}{X_{kj}} \geq \gamma \end{cases} \tag{3.10}$$

where γ is the fade margin, j is the index of the BS to that the MS is connected, X_{kj} denotes the short-term fading channel loss after rake combining between the k^{th} MS and j^{th} BS, and $r_{ki}^{u}10^{\zeta_{kj}/10}$ denotes the long-term fading channel loss composed of the propagation loss and shadow fading. Furthermore, $\min_{i\in A_k}\{\bullet\}$ operator represents the soft-handoff that chooses the minimum slow fading loss between MS and BSs in the active set, A_k. That is, the transmit power of MS will be the amount of compensating for both shot-term and long-term fading channel loss. On the other hand, if the channel propagation loss to be compensated is larger than the fade margin, the transmit power will be limited by the power amplifier, which was the case we have taken into account in the previous section, assuming the single user in the system. However, for loaded system, all co-channel interference as well as the desired user's signal will behaves in such a way. If the distribution of interference term is found, the outage probability as a function of the fade margin, γ, can be evaluated as

$$\begin{aligned} P_{out}(\gamma) &= \Pr\left\{\frac{S}{I} < \eta\right\} \\ &= \Pr\left\{\frac{I}{S} > \eta^{-1},\ P_T^{(0)} < \gamma\right\} + \Pr\left\{\frac{I}{S} > \eta^{-1},\ P_T^{(0)} \geq \gamma\right\} \end{aligned} \tag{3.11}$$

where the signal-to-interference ratio, S/I, is defined as Equation (3.9), $P_T^{(0)}$ is the transmit power of the desired user and η is the required QoS. From which, we can know that there are two sources causing the system outage: one is the case that the desired signal is perfectly power controlled, but the co-channel interference deteriorate the signal-to-interference ratio; the other is that the desired signal cannot compensate the channel propagation loss regardless of the interference.

3.4.2 System model

The system model to be analyzed is the same as that taken in to account in the previous chapter: That is, the cellular communication architecture is identical to the well-known uniform hexagonal cell layout with a BS at the center of each cell as described in Figure 2.1. It is assumed that an MS communicates with the BS that provides the least average propagation loss among three nearest BS (defined as the active set) just as 3-way soft

handoff. Transmit power of an MS is periodically power-controlled so as to compensate for the channel fluctuation. The propagation channel model incorporates both long-term fading channel and short-term fading channel. The long-term fading channel is defined by the path loss and shadow fading channel loss and the short-term fading channel is defined by the multipath fading channel.

3.4.3 Signal model

In this subsection, the basic signal expression of uplink DS/CDMA cellular system is described in more detail to develop the signal-to-interference ratio expression as in Equation (3.9). It is assumed that both MS and BS are equipped with multiple transmit antennas and receive antennas. Furthermore, we do not distinguish the intracell and intercell interference here since the receiver cannot distinguish them. The difference between intracell and intercell interference will be determined by the transmit power behavior later in calculating the interference statistics.

- ***Transmitter***

First, let us consider single transmit antennas for the simplicity. In the uplink of DS/CDMA cellular system, transmit signal from the i^{th} MS can be modeled as

$$s_i(t) = \sqrt{P_T^{(i)}} \cdot a_i(t) \cdot c_i(t) \cdot e^{j(\omega_c t + \theta_i)} \tag{3.12}$$

where $\sqrt{P_T^{(i)}}$ denotes the signal gain of the i^{th} MS, $a_i(t)$ denotes the random binary data symbol assuming the binary phase shift keying, $c_i(t)$ denotes the complex pseudo noise (PN) sequence, ω_c and θ_i are the carrier frequency and random phase of local oscillator, respectively.

- ***Receiver***

Let us suppose that BS is equipped with multiple receive antennas, and rake receiver for maximal ratio combining of the signal from the multiple antennas and multipath components. First, the received signal at the j^{th} antenna of BS can be expressed as

$$r_j(t) = \sum_{i=1}^{N} \sum_{l=1}^{M_m} \alpha_{i,l,j}(t) s_i(t - \tau_{i,l}) e^{j\theta_i} \tag{3.13}$$

where j denotes the antenna index, N denotes the number of users in the system, M_m denotes the number of multipath, and $\alpha_{i,l,j}(t)$ and $\tau_{i,l}$ denote the complex channel gain and channel delay, respectively, due to the multipath fading of the j^{th} antenna and the l^{th} path for the i^{th} user. It is assumed that the channel delays suffered by each mobile's signal at multiple antennas are the same and the complex channel gain contains both fast fading and slow fading between MS and BS. Assuming the perfect synchronization[3] for each user and the slow channel variation[4], the despread symbol for user 1 from the received signal can be expressed as

$$\begin{aligned} r_{1,m,j} &= \int_0^T c_1^*(t - \tau_{1,m}) r_j(t) dt \\ &= \sqrt{P_T^{(1)}} \cdot \alpha_{1,m,j} a_1 \int_0^T c_1^*(t - \tau_{1,m}) c_1(t - \tau_{1,m}) dt \\ &\quad + \sum_{\substack{l=1 \\ l \neq m}}^{M_m} \left[\sqrt{P_T^{(1)}} \cdot \alpha_{1,l,j} \int_0^T a_1(t - \tau_{1,l}) c_1^*(t - \tau_{1,m}) c_1(t - \tau_{1,l}) dt \right] \\ &\quad + \sum_{i=2}^{N} \sum_{l=1}^{M_m} \left[\sqrt{P_T^{(i)}} \cdot \alpha_{i,l,j} e^{j\hat{\theta}_i} \int_0^T a_i(t - \tau_{i,l}) c_1^*(t - \tau_{1,m}) c_i(t - \tau_{i,l}) dt \right] \end{aligned} \tag{3.14}$$

For the long PN sequence, the autocorrelation and cross correlation in Equation (3.14) can be evaluated as

$$\int_0^T c_i^*(t - \tau_{i,m}) \cdot c_i(t - \tau_{i,m}) dt = N_T \tag{3.15}$$

---

[3] Perfect synchronization of the desired user's signal makes it possible to drop the time index from the random data symbol $a_1(t)$

[4] Assuming that the channel is slowly varying as compared to the symbol duration, we can drop the time index from the complex channel gain $\alpha_{i,l,j}(t)$.

$$\int_0^T a_i(t-\tau_{i,l}) \cdot c_1^*(t-\tau_{1,m}) \cdot c_i(t-\tau_{i,l})dt = \beta(i,l,m), \text{ for } i \neq 1 \text{ or } l \neq m \tag{3.16}$$

where T is the symbol duration, N_T is the spreading gain, and $\beta(i,l,m)$ can be approximated by complex Gaussian random process with zero mean and variance of N_T if the period of CDMA signature is large relative to the processing gain [58-60], which is valid for the uplink DS/CDMA cellular systems. With the perfect channel information assumed to be known at the BS, the demodulated symbol after the channel compensation can be expressed as

$$\begin{aligned}\hat{r}_{1,m,j} &= \sqrt{P_T^{(1)}} \cdot \left|\alpha_{1,m,j}\right|^2 a_1 \cdot N_T \\ &+\alpha_{1,m,j}^* \sum_{\substack{l=1 \\ l\neq m}}^{M_m} \left[\sqrt{P_T^{(1)}} \cdot \alpha_{1,l,j} \cdot \beta(1,l,m)\right] \\ &+\alpha_{1,m,j}^* \sum_{i=2}^{N} \sum_{l=1}^{M_m} \left[\sqrt{P_T^{(i)}} \cdot \alpha_{i,l,j} e^{j\hat{\theta}_i} \cdot \beta(i,l,m)\right]\end{aligned} \tag{3.17}$$

Finally, the combined symbol after the demodulation can be expressed as

$$\begin{aligned}y_1 &= \sum_{j=1}^{M_r} \sum_{m=1}^{M_m} \hat{r}_{1,m,j} = \sum_{j=1}^{M_r} \sum_{m=1}^{M_m} \sqrt{P_T^{(1)}} \cdot \left|\alpha_{1,m,j}\right|^2 a_1 \cdot N_T \\ &+\sum_{j=1}^{M_r} \sum_{m=1}^{M_m} \alpha_{1,m,j}^* \sum_{\substack{l=1 \\ l\neq m}}^{M_m} \left[\sqrt{P_T^{(1)}} \cdot \alpha_{1,l,j} e^{j\hat{\theta}_1} \cdot \beta(1,l,m)\right] \\ &+\sum_{j=1}^{M_r} \sum_{m=1}^{M_m} \alpha_{1,m,j}^* \sum_{i=2}^{N} \sum_{l=1}^{M_m} \left[\sqrt{P_T^{(i)}} \cdot \alpha_{i,l,j} e^{j\hat{\theta}_i} \cdot \beta(i,l,m)\right]\end{aligned} \tag{3.18}$$

where M_r denotes the number of receive antennas. In Equation (3.18), the term in the second line is referred as the *inter-path interference* and the term in the last line is known as the *other user interference*.

3.4.4 Average signal-to-interference ratio

For the estimation of average system performance, average signal-to-interference ratio will be considered by calculating average signal power and average interference power over all possible code sequences, $c_i(t)$, transmit symbols, $a_i(t)$, and random phases of local oscillator, $\hat{\theta}$. For simplicity, let us consider the single receiving antenna system.

Then, the instantaneous signal energy, P_S, and the instantaneous interference energy, P_I, averaged over all possible PN sequences, transmit symbols, and random phases, can be calculated as

$$\begin{aligned} P_s &= E\left[\left(\sum_{m=1}^{M_m}\left|\alpha_{1,m,j}\right|^2\right)^2 \cdot P_T^{(1)} \cdot a_1^2 \cdot N_T^2\right] \\ &= \left(\sum_{m=1}^{M_m}\left|\alpha_{1,m,j}\right|^2\right)^2 \cdot P_T^{(1)} \cdot N_T^2 \end{aligned} \tag{3.19}$$

$$\begin{aligned} P_I &= E\left[\left|\begin{array}{l} \displaystyle\sum_{m=1}^{M_m}\alpha_{1,m,j}^{*}\sum_{\substack{l=1\\ l\neq m}}^{M_m}\left[\sqrt{P_T^{(1)}}\cdot\alpha_{1,l,j}\cdot\beta(1,l,m)\right] \\ \displaystyle+\sum_{m=1}^{M_m}\alpha_{1,m,j}^{*}\sum_{i=2}^{N}\sum_{l=1}^{M_m}\left[\sqrt{P_T^{(i)}}\cdot\alpha_{i,l,j}e^{j\hat{\theta}_i}\cdot\beta(i,l,m)\right] \end{array}\right|^2\right] \\ &= \left(\sum_{m=1}^{M_m}\left|\alpha_{1,m,j}\right|^2\right)\left(\sum_{\substack{l=1\\ l\neq m}}^{M_m}\left[P_T^{(1)}\cdot\left|\alpha_{1,l,j}\right|^2 N_T\right]+\sum_{i=2}^{N}\sum_{l=1}^{M_m}\left[P_T^{(i)}\cdot\left|\alpha_{i,l,j}\right|^2 N_T\right]\right) \end{aligned} \tag{3.20}$$

where it is presumed that $|a_i|^2 = 1$. Finally, the average signal-to-interference ratio for the single antenna system can be expressed as

$$SIR = \frac{\left(\sum_{m=1}^{M_m}\left|\alpha_{1,m,j}\right|^2\right)P_T^{(1)}\cdot N_T}{\sum_{\substack{l=1\\ l\neq m}}^{M_m}\left[P_T^{(1)}\cdot\left|\alpha_{1,l,j}\right|^2\right]+\sum_{i=2}^{N}\sum_{l=1}^{M_m}\left[P_T^{(i)}\cdot\left|\alpha_{i,l,j}\right|^2\right]} \tag{3.21}$$

Furthermore, assuming the inter-path interference is negligible for large number of users, the average signal-to-interference ratio can be approximated as

$$SIR \approx \frac{\left(\sum_{m=1}^{M_m}\left|\alpha_{1,m,j}\right|^2\right)P_T^{(1)}\cdot N_T}{\sum_{i=2}^{N}\sum_{l=1}^{M_m}\left[P_T^{(i)}\cdot\left|\alpha_{i,l,j}\right|^2\right]} \tag{3.22}$$

- ***Receive Diversity***

Now, let us consider the multiple receive antennas. Assuming maximal ratio combining of multiple receive antenna branches, the average signal energy, P_S, and the average interference energy, P_I, can be calculated as

$$P_s = \left(\sum_{j=1}^{M_r} \sum_{m=1}^{M_m} \left| \alpha_{1,m,j} \right|^2 \right)^2 P_T^{(1)} \cdot N_T^2 \tag{3.23}$$

$$P_I = \left| \sum_{j=1}^{M_r} \sum_{m=1}^{M_m} \alpha_{1,m,j}^* \sum_{\substack{l=1 \\ l \neq m}}^{M_m} \alpha_{1,l,j} \right|^2 \cdot P_T^{(1)} \cdot N_T + \sum_{i=2}^{N} \left| \sum_{j=1}^{M_r} \sum_{m=1}^{M_m} \alpha_{1,m,j}^* \sum_{l=1}^{M_m} \alpha_{1,l,j} \cdot \beta(l,m) \right|^2 \cdot P_T^{(i)} \cdot N_T \tag{3.24}$$

where M_r denotes the number of receive antennas. Then, the signal-to-interference ratio for the multiple antenna system can be expressed as

$$SIR = \frac{\left(\sum_{j=1}^{M_r} \sum_{m=1}^{M_m} \left| \alpha_{1,m,j} \right|^2 \right)^2 \cdot P_T^{(1)} \cdot N_T}{\left| \sum_{j=1}^{M_r} \sum_{m=1}^{M_m} \alpha_{1,m,j}^* \sum_{\substack{l=1 \\ l \neq m}}^{M_m} \alpha_{1,l,j} \right|^2 \cdot P_T^{(1)} + \sum_{i=2}^{N} \left| \sum_{j=1}^{M_r} \sum_{m=1}^{M_m} \alpha_{1,m,j}^* \sum_{l=1}^{M_m} \alpha_{1,l,j} \cdot \beta(l,m) \right|^2 \cdot P_T^{(i)}} \tag{3.25}$$

Similarly, ignoring the interpath interference for the large number of users, the signal-to-interference ratio can be approximated as

$$SIR \approx \frac{\left(\sum_{j=1}^{M_r} \sum_{m=1}^{M_m} \left| \alpha_{1,m,j} \right|^2 \right)^2 \cdot P_T^{(1)} \cdot N_T}{\sum_{i=2}^{N} \left| \sum_{j=1}^{M_r} \sum_{m=1}^{M_m} \alpha_{1,m,j}^* \sum_{l=1}^{M_m} \alpha_{1,l,j} \cdot \beta(l,m) \right|^2 \cdot P_T^{(i)}} \tag{3.26}$$

- ***Transmit Diversity***

The average signal-to-interference ratio for maximal ratio transmit diversity can be easily evaluated by means of replacing the channel coefficient, $\alpha_{i,j,l}$, by the equivalent channel of transmit diversity defined as

$$\alpha_{i,j,l} = \sum_{q=1}^{M_T} w_{i,j,q} \cdot \alpha_{i,j,q,l} \tag{3.27}$$

where i is the user index, j is the index of receive antenna, and q is the index of transmit antenna. Furthermore, M_t represents the number of transmit antennas and $w_{i,j,q}$ is the weight coefficients of the q^{th} transmit antenna and is determined in such a way that the weight coefficients maximize the signal-to-noise ratio of MIMO channel as described in

the section 2.2.3. Hence, the signal-to-interference ratio with transmit diversity can be expressed as

$$SIR \approx \frac{\left(\sum_{j=1}^{M_r} \sum_{m=1}^{M_m} \left| \sum_{q=1}^{M_t} w_{1,j,q} \cdot \alpha_{1,j,q,m} \right|^2 \right)^2 \cdot P_T^{(1)} \cdot N_T}{\sum_{i=2}^{N} \left| \sum_{j=1}^{M_r} \sum_{m=1}^{M_m} \left(\sum_{q=1}^{M_t} w_{1,j,q} \cdot \alpha_{1,j,q,m} \right)^* \sum_{l=1}^{M_m} \left(\sum_{q=1}^{M_t} \hat{w}_{i,j,q} \cdot \alpha_{i,j,q,l} \right) \cdot \beta(l,m) \right|^2 \cdot P_T^{(i)}} \tag{3.28}$$

where $\hat{w}_{i,j,q}$ is determined by the connected BS, hence it will be correlated with the channel coefficients, $\alpha_{i,j,q,l}$, in the case of intracell interference and it will be uncorrelated with the channel coefficients, $\alpha_{i,j,q,l}$ in the case of intercell interference. According to the definition in Equation (3.9), the combining functions of the signal and interference, $f\left(G_l^{(0)}, P_T^{(0)}\right)$ and $g\left(G_l^{(i)}, G_l^{(i)}, P_T^{(i)}\right)$, are defined as

$$f\left(G_l^{(1)}, P_T^{(1)}\right) = \left(\sum_{j=1}^{M_r} \sum_{m=1}^{M_m} \left| \sum_{q=1}^{M_t} w_{1,j,q} \cdot G_{j,m,q}^{(1)} \right|^2 \right)^2 \cdot P_T^{(1)} \cdot N_T \tag{3.29}$$

$$g\left(G_l^{(i)}, P_T^{(i)}; i = 1, \cdots, N\right) = \left| \sum_{j=1}^{M_r} \sum_{m=1}^{M_m} \left(\sum_{q=1}^{M_t} w_{1,j,q} \cdot \alpha_{1,j,q,m} \right)^* \sum_{l=1}^{M_m} \left(\sum_{q=1}^{M_t} \hat{w}_{i,j,q} \cdot \alpha_{i,j,q,l} \right) \cdot \beta(l,m) \right|^2 \cdot P_T^{(i)} \tag{3.30}$$

3.4.5 Outage probability

In this section, we describe how to evaluate the outage probability defined in Equation (3.11) with the signal-to-interference ratio derived in Equation (3.28). For the evaluation, we will use the approximated expression for the signal-to-interference ratio and semi-analytical analysis technique for the faster evaluation. In many literatures [13, 14, 39], it is found that the interference-to-signal ratio (the inverse of the signal-to-interference ratio) at BS can be approximated by the log-normal distribution when the fast transmit power control is implemented. Hence, we will apply that log-normal approximation technique to evaluate the outage probability. Figure 3.9 shows the simulated interference-to-signal ratio for the number of users per cell of 200 and curve-fitted log-normal distribution using the mean and variance of the simulated interference-to-signal ratio. However, the mean and variance are not linearly proportional to the number of users

because of the correlation between branches and among the users that comes from the combining operation. Therefore, we need to recalculate the mean and variance for every number of users per cell to obtain the outage probability. As an alternative way to solve this problem, we made another approximation that has not much impact on the result.

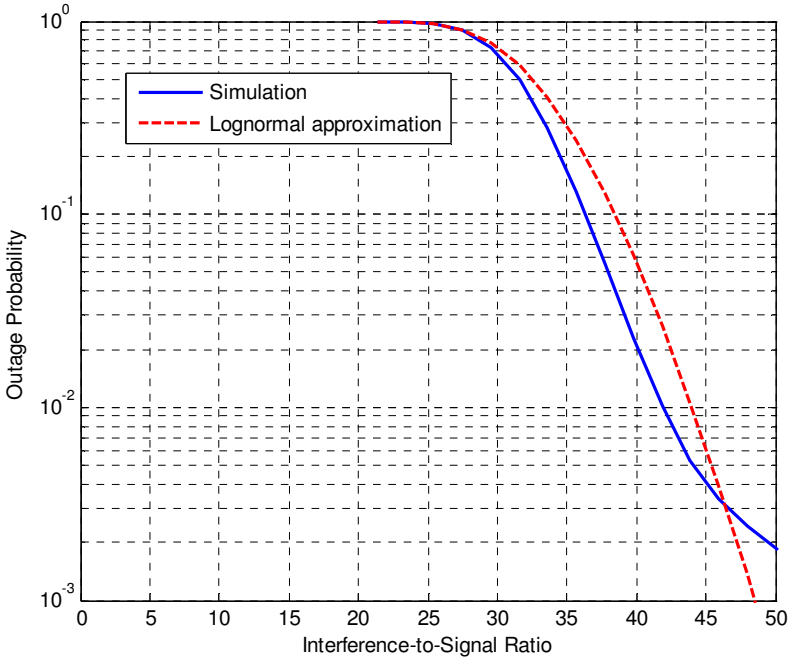

Figure 3.9: Simulated distribution and lognormal approximation for the interference-to-signal ratio

For an example, let us consider the following expression of the interference-to-signal ratio,

$$
\begin{aligned}
ISR &= \frac{\sum_{i=2}^{N}\left|\alpha_1^{(1)*}\alpha_1^{(i)}+\alpha_2^{(1)*}\alpha_2^{(i)}\right|^2 P_T^{(i)}}{\left|\left|\alpha_1^{(1)}\right|^2+\left|\alpha_2^{(1)}\right|^2\right|^2 P_T^{(1)}} \\
&= \frac{\left|\alpha_1^{(1)}\right|^2\sum_{i=2}^{N}\left|\alpha_1^{(1)}\right|^2 P_T^{(i)}+\left|\alpha_2^{(1)}\right|^2\sum_{i=2}^{N}\left|\alpha_2^{(1)}\right|^2 P_T^{(i)}}{\left|\left|\alpha_1^{(1)}\right|^2+\left|\alpha_2^{(1)}\right|^2\right|^2 P_T^{(1)}} \\
&+\frac{\sum_{i=2}^{N}\left(\alpha_1^{(1)*}\alpha_1^{(i)}\alpha_2^{(1)}\alpha_2^{(i)*}+\alpha_1^{(1)}\alpha_1^{(i)*}\alpha_2^{(1)*}\alpha_2^{(i)}\right)P_T^{(i)}}{\left|\left|\alpha_1^{(1)}\right|^2+\left|\alpha_2^{(1)}\right|^2\right|^2 P_T^{(1)}}
\end{aligned}
\tag{3.31}
$$

where the maximal ratio combination of received signal from two receive antennas is assumed, $\alpha_j^{(i)}$ represents the complex channel gain of the i^{th} user at the j^{th} receive antenna, $P_T^{(i)}$ is the i^{th} user's transmit power, and N is the number of users in the system. It is observed that the term in the last line of Equation (3.31) have the following distribution as shown in Figure 3.10, that is collected from the system level simulation for two receive antennas, where the fade margin is set to be 20 dB, the number of users per cell is assumed to be '200', and flat fading channel is assumed. Most of values are observed to be located at the very small values close to zero as compared with Figure 3.9, and other values occur very rarely even though they are very large. Based on this observation, we can assume that they have the negligible impact on the distribution of the interference-to-signal ratio. That is, we don't take them into account in evaluating the outage probabilities. It makes the problem simpler. If the desired user's channel gains, $\alpha_j^{(i)}$, are given, the interference power at one antenna branch are independent of each other. Furthermore, the log-normal approximation for the interference term at one antenna branch is still valid. Figure 3.11 shows the simulated distribution of interference term at one antenna branch and estimated log-normal distribution using the mean and variance of the simulation result. For more practically, in Figure 3.12, we compared the simulation results and the analytical results of the outage probability with / without the approximation. For the evaluation, two receive antenna diversity and one-path Rayleigh fading channel at each antenna branch are assumed, and fade margin (γ) is set to be 10 dB and 20 dB. The results, denoted by 'Simul1', shows the outage probability observed from the simulation using the original interference statistics including the last line of Equation (3.31), and the results, denoted by 'Simul2', shows the outage probability observed from the simulation using the approximated interference statistics except for the last line of Equation (3.31). We can observe small difference of the simulation results between the exact interference statistics and approximated interference statistics. However, it may not have much impact on the estimation of performance improvements by the diversity.

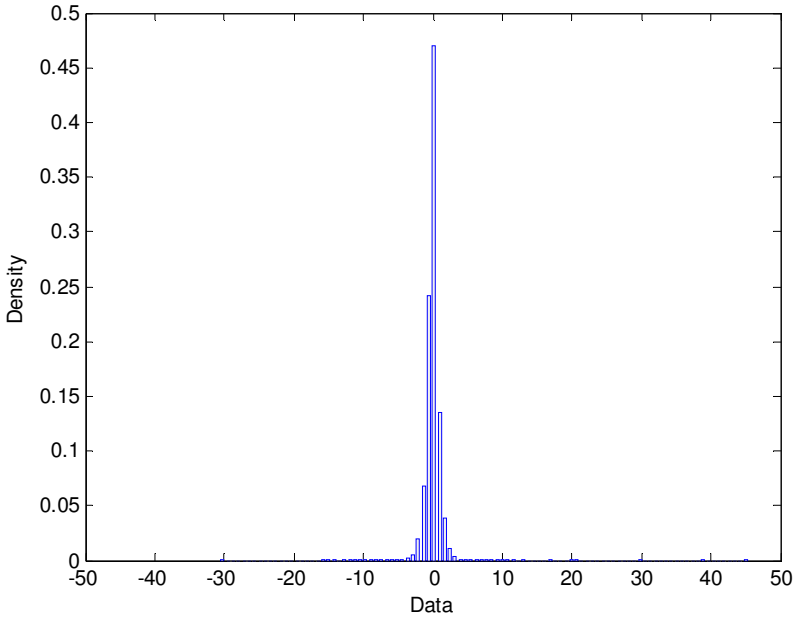

Figure 3.10: Distribution of the last terms in Equation (3.31)

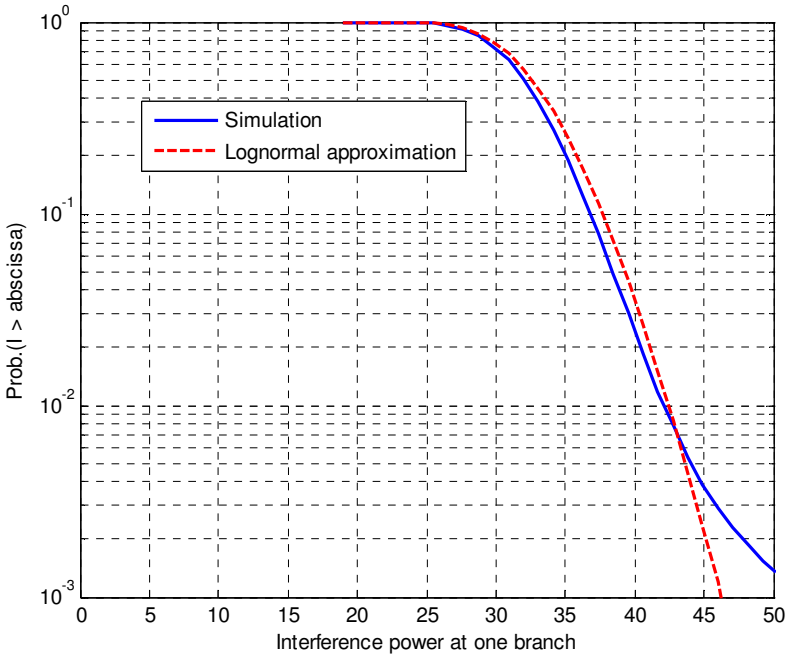

Figure 3.11: Distribution of interference at one antenna branch

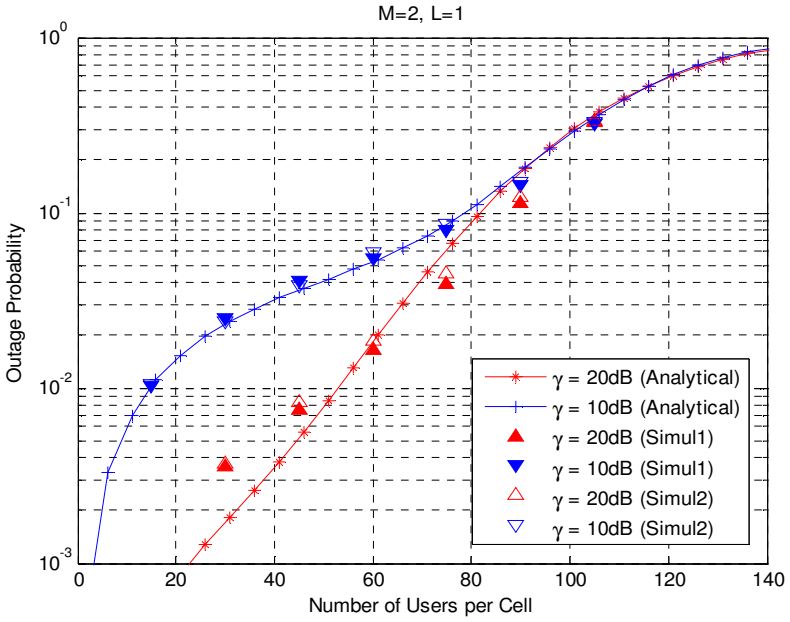

(a)

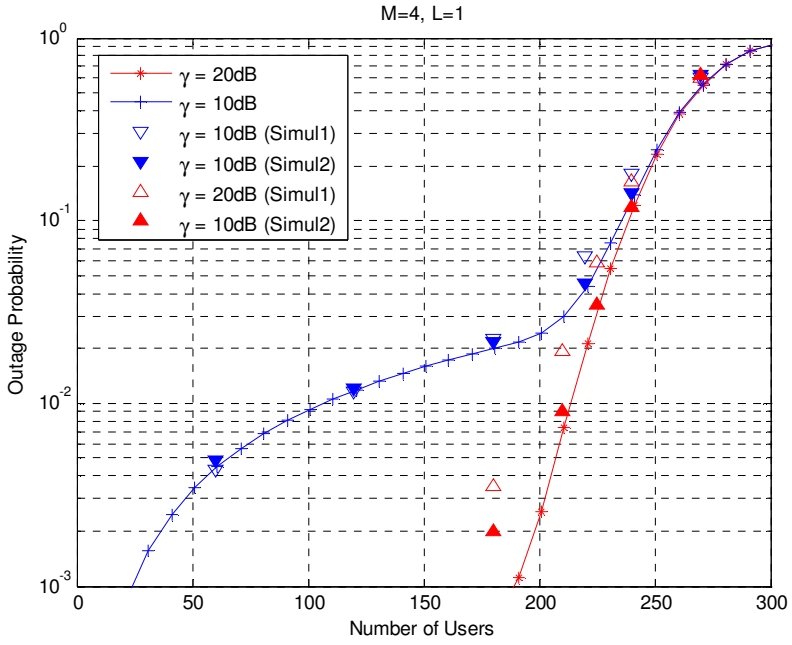

(b)

Figure 3.12: Outage probabilities with / without the approximation, (a) M = 2, (b) M = 4

Now, back to the original equation, Equation (3.28), from which interference-to-signal ratio can be approximated as

$$
\begin{aligned}
ISR &= \frac{\sum_{i=2}^{N}\left|\sum_{j=1}^{M_r}\sum_{m=1}^{M_m}\left(\sum_{q=1}^{M_t} w_{1,j,q}\cdot\alpha_{1,j,q,m}\right)^{*}\sum_{l=1}^{M_m}\left(\sum_{q=1}^{M_t}\hat{w}_{i,j,q}\cdot\alpha_{i,j,q,l}\right)\cdot\beta(l,m)\right|^2\cdot P_T^{(i)}}{\left(\sum_{j=1}^{M_r}\sum_{m=1}^{M_m}\left|\sum_{q=1}^{M_t} w_{1,j,q}\cdot\alpha_{1,j,q,m}\right|^2\right)^2\cdot P_T^{(1)}\cdot N_T} \\
&\approx \frac{\left(\sum_{j=1}^{M_r}\sum_{m=1}^{M_m}\left|\sum_{q=1}^{M_t} w_{i,j,q}\cdot\alpha_{1,j,q,m}\right|^2\cdot\sum_{i=2}^{N}\sum_{l=1}^{M_m}\left|\sum_{q=1}^{M_t}\hat{w}_{i,j,q}\cdot\alpha_{i,j,q,l}\right|^2\cdot P_T^{(i)}\right)}{\left(\sum_{j=1}^{M_r}\sum_{m=1}^{M_m}\left|\sum_{q=1}^{M_t} w_{1,j,q}\cdot\alpha_{1,j,q,m}\right|^2\right)^2\cdot P_T^{(1)}\cdot N_T}
\end{aligned}
\tag{3.32}
$$

Let us define the random variable, Z_j, as the interference term at one receive antenna branch as follows

$$
Z_j = \sum_{i=2}^{N}\sum_{l=1}^{M_m}\left|\sum_{q=1}^{M_t}\hat{w}_{i,j,q}\cdot\alpha_{i,j,q,l}\right|^2\cdot P_T^{(i)} \tag{3.33}
$$

Then, the interference-to-signal ratio can be expressed as

$$
ISR \approx \sum_{j=1}^{M_r}\frac{\sum_{m=1}^{M_m}\left|\sum_{q=1}^{M_t} w_{i,q}\cdot\alpha_{1,j,q,m}\right|^2\cdot Z_j}{\left(\sum_{l=1}^{M_r}\sum_{m=1}^{M_m}\left|\sum_{q=1}^{M_t} w_{1,q}\cdot\alpha_{1,q,m}\right|^2\right)^2\cdot P_T^{(1)}\cdot N_T} \tag{3.34}
$$

That is, the interference-to-signal ratio can be expressed as the weighted sum of log-normal random variable, Z_j, at each branch. Let us define

$$
ISR = \sum_{j=1}^{M_r} c_j\cdot Z_j = \hat{Z} \tag{3.35}
$$

Conditioned on the complex channel gain of the desired user, $\alpha_{1,m,j}$, we can expect that the interference-to-signal ratio, $\hat{Z}$, also follows the log-normal distribution by the known property that the sum of log-normal random variables is another log-normal random variable [61, 62]. Assuming that the interference terms at each receive antenna are identical, but not independent due to the same transmit power term at each receive antenna branch, the outage probability can be calculated as

$$P_{out} = \int \cdots \int Q\left(\frac{\ln \eta^{-1} - m_{\hat{Z}}(c_1,\ldots,c_{M_r})}{\sigma_{\hat{Z}}(c_1,\ldots,c_{M_r})}\right) f(c_1,\ldots,c_{M_r})\, dc_1 \cdots dc_{M_r} \tag{3.36}$$

where the mean and variance of the interference-to-signal ratio can be calculated as

$$\begin{aligned} m_{\hat{Z}}(c_1,\ldots,c_{M_r}) &= 2\ln(u_1) - 0.5\ln(u_2) \\ \sigma^2_{\hat{Z}}(c_1,\ldots,c_{M_r}) &= \ln(u_2) - 2\ln(u_1) \end{aligned} \tag{3.37}$$

with

$$\begin{aligned} u_1 &= \left(\sum_{j=1}^{M_r} c_j\right) \cdot m_Z \\ u_2 &= \left(\sum_{j=1}^{M_r} c_j^2\right) \cdot \left(m_Z^{(2)} - m_{Z_i Z_j}\right) + \left(\sum_{j=1}^{M_r} c_j\right)^2 \cdot m_{Z_i Z_j} \end{aligned} \tag{3.38}$$

In Equation (3.38), m_Z and $m_Z^{(2)}$ are the first and the second moments of Z_j, respectively, and $m_{Z_i Z_j}$ is the expectation of cross product of interference from different antenna branches, Z_i and Z_j, $i \neq j$. Furthermore, Z_j is also the sum of interference from all users in the system as follows

$$Z_j = \sum_{k=2}^{N} Z_j^{(k)} \tag{3.39}$$

Since the interference are independent of each other user, the first and the second moments of Z_j, m_Z and $m_Z^{(2)}$, can be easily calculated as

$$m_Z = E\left[\sum_{k=1}^{N} Z_j^{(k)}\right] = \sum_{k=1}^{N} E\left[Z_j^{(k)}\right] = N \cdot E\left[Z_j^{(k)}\right] \tag{3.40}$$

$$\begin{aligned} m_Z^{(2)} &= E\left[\left(\sum_{k=1}^{N} Z_j^{(k)}\right)^2\right] = E\left[\sum_{k=1}^{N}\left(Z_j^{(k)}\right)^2 + \sum_{l=1}^{N}\sum_{\substack{m=1 \\ m\neq n}}^{N} Z_j^{(l)} Z_j^{(m)}\right] \\ &= \sum_{k=1}^{N} E\left[\left(Z_j^{(k)}\right)^2\right] + \sum_{l=1}^{N}\sum_{\substack{m=1 \\ m\neq n}}^{N} E\left[Z_j^{(l)}\right] E\left[Z_j^{(m)}\right] \\ &= N \cdot E\left[\left(Z_j^{(k)}\right)^2\right] + N(N-1) \cdot E\left[Z_j^{(k)}\right]^2 \end{aligned} \tag{3.41}$$

That is, by calculating the first and the second moments of one interference source, averaged over the entire system, we can easily obtain the sum of the interference, Z_j, for different number of interference. Similarly, the expectation of the cross product of Z_i and Z_j can be calculated as

$$
\begin{aligned}
m_{Z_i Z_j} &= E\left[Z_i Z_j\right] = E\left[\left(\sum_{k=1}^{N} Z_i^{(k)}\right)\cdot\left(\sum_{m=1}^{N} Z_j^{(m)}\right)\right] \\
&= E\left[\sum_{k=1}^{N} Z_i^{(k)} Z_j^{(k)} + \sum_{l=1}^{N}\sum_{\substack{m=1 \\ m\neq l}}^{N} Z_i^{(l)} Z_j^{(m)}\right] \\
&= \sum_{k=1}^{N} E\left[Z_i^{(k)} Z_j^{(k)}\right] + \sum_{l=1}^{N}\sum_{\substack{m=1 \\ m\neq l}}^{N} E\left[Z_i^{(l)}\right] E\left[Z_j^{(m)}\right] \\
&= N\cdot E\left[Z_i^{(k)} Z_j^{(k)}\right] + N(N-1)E\left[Z_i^{(k)}\right]^2
\end{aligned}
\tag{3.42}
$$

Finally, for the integration in Equation (3.36), the joint distribution function of c_i's $(i = 1,\cdots, M_r)$ is required. However, it might not be easy to find the analytical expression for the joint distribution function of c_i's due to the correlations between receiving antenna branches and complex combination of several random variables. Note that the channel coefficients $\alpha_{1,j,q,m}$ and the transmit weight coefficients $w_{1,l,q}$ are random variables that consist of short-term fading channel coefficient and long-term fading channel coefficient. Furthermore, $P_T^{(1)}$ is also random variable correlated with $\alpha_{1,j,q,m}$ and $w_{1,l,q}$. As an alternative way to find the distribution function, we can apply semi-analytical approach for the integration in Equation (3.36). Following the conventional expression rule in Chapter 2, the coefficient c_i can be expressed as

$$
c_i = \begin{cases} \dfrac{X_d^{(i)}}{(X_d)^2}\cdot\dfrac{r_d^u 10^{\zeta_d/10}}{\gamma} & \text{if } P_T^{(1)} = \dfrac{r_d^u 10^{\zeta_d/10}}{X_d} \geq \gamma \\ \dfrac{X_d^{(i)}}{X_d} & \text{if } P_T^{(1)} = \dfrac{r_d^u 10^{\zeta_d/10}}{X_d} < \gamma \end{cases}
\tag{3.43}
$$

where $r_d^u 10^{\zeta_d/10}$ is the long-term fading channel loss between the desired MS and the zeroth BS, $X_d = \sum_{i=1}^{M_r} X_d^{(i)}$ is the short-term fading channel loss between the desired MS and the zeroth BS after combining the signal from each receiving antenna, and $X_d^{(i)}$ is the short-term fading channel loss at each receiving antenna branch and is defined as

$$
X_d^{(i)} = \left|\sum_{q=1}^{M_t} w_{1,q}\cdot h_{1,j,q,m}\right|^2
\tag{3.44}
$$

Based on Equation (3.43), the outage probability defined in Equation (3.36) is evaluated by calculating two probabilities, p_1 for $P_T^{(1)} \geq \gamma$ and p_2 for $P_T^{(1)} < \gamma$. For $P_T^{(1)} \geq \gamma$, the outage probability p_1 can be calculated as

$$p_1 = \int \cdots \int Q\left(\frac{\ln \eta^{-1} - m_{\hat{Z}}(x_1, \cdots, x_{M_r})}{\sigma_{\hat{Z}}(x_1, \cdots, x_{M_r})}\right) \cdot Q\left(\frac{M_d - \chi_d - \Gamma}{\sigma}\right) f(x_1, \cdots, x_{M_r})\, dx_1 \cdots dx_{M_r} \quad (3.45)$$

where $x_i = X_d^{(i)}$, $\chi_d = 10\log_{10}\sum_{i=1}^{M_r} x_i$, $\Gamma = 10\log_{10}\gamma$, $M_d = 10\log_{10} r_d^u$, and $m_{\hat{Z}}$ and $\sigma_{\hat{Z}}^2$ are calculated as.

$$\begin{aligned} m_{\hat{Z}} &= 2\ln u_1 - 0.5\ln u_2 \\ &= 2\ln m_Z - 0.5\ln\left(\frac{\sum_{i=1}^{M_r} x_i^2}{\left(\sum_{i=1}^{M_r} x_i\right)^2}\left(m_Z^{(2)} - m_{Z_iZ_j}\right) + m_{Z_iZ_j}\right) \end{aligned} \quad (3.46)$$

$$\begin{aligned} \sigma_{\hat{Z}}^2 &= \ln u_2 - 2\ln u_1 \\ &= \ln\left(\frac{\sum_{i=1}^{M_r} x_i^2}{\left(\sum_{i=1}^{M_r} x_i\right)^2}\left(m_Z^{(2)} - m_{Z_iZ_j}\right) + m_{Z_iZ_j}\right) - 2\ln m_Z \end{aligned} \quad (3.47)$$

, respectively. For $P_T^{(1)} < \gamma$, the outage probability p_2 can be calculated as

$$p_2 = \int \cdots \int \left[\int_0^{\infty} \left\{ Q\left(\frac{\ln \eta^{-1} - m_{\hat{Z}}(x_1, \cdots, x_{M_r})}{\sigma_{\hat{Z}}(x_1, \cdots, x_{M_r})}\right) \times f_G\left(z + \frac{\chi_d + \Gamma - M_d}{\sigma}\right) \right\} dz \right] f(x_1, \cdots, x_{M_r})\, dx_1 \cdots dx_{M_r} \quad (3.48)$$

where $f_G(z)$ is the standard Gaussian distribution function, and $m_{\hat{Z}}$ and $\sigma_{\hat{Z}}^2$ are calculated as

$$m_{\hat{Z}} = \beta(\sigma z + \chi_d) + 2\ln m_Z - 0.5\ln\left(\left(\sum_{i=1}^{M_r} x_i^2\right) \cdot \left(m_Z^{(2)} - m_{Z_iZ_j}\right) + \left(\sum_{i=1}^{M_r} x_i\right)^2 \cdot m_{Z_iZ_j}\right) \quad (3.49)$$

$$\sigma_{\hat{Z}}^2 = \ln\left(\frac{\sum_{i=1}^{M_r} x_i^2}{\left(\sum_{i=1}^{M_r} x_i\right)^2}\left(m_Z^{(2)} - m_{Z_iZ_j}\right) + m_{Z_iZ_j}\right) - 2\ln m_Z \quad (3.50)$$

Hence, we just need to generate the short-term fading random variables, $x_1, \cdots, x_{M_r}$ for the semi-analytical evaluation of outage probability.

3.4.6 Interference statistics

In this section, the statistics of the interference term, $Z_j^{(k)}$, will be described in more details. Most procedures is very similar to the section 2.3 except for that the short-term fading statistics and long-term fading statistics will not be treated independently. Without loss of generality, in the uplink DS/CDMA cellular system, interference can be classified into the intracell interference and other cell (or intercell) interference, as mentioned in the previous chapter. Intracell interference comes from the MS connected to the same BS and the other cell interference comes from the MS connected to the other BS. Furthermore, the other cell interference also can be divided into two interference sources that comes from the MS which has the zero[th] BS among the active set and the MS which has not. Therefore, they will be separately handled in this analysis.

- ***Intracell interference***

It is assumed that the reference power for the power control to be '1'. By following the notations in previous chapter, intracell interference from an MS at one receive antenna branch can be rewritten from Equation (3.33) as follows,

$$Z_j^{(k)} = I_{in}^{(k)} = P_T^{(k)} \frac{X_{k0}}{r_{k0}^u 10^{\zeta_{k0}/10}}, \qquad \min_{i \in A_k} \left\{ r_{ki}^u 10^{\zeta_{ki}/10} \right\} > r_{k0}^u 10^{\zeta_{k0}/10} \tag{3.51}$$

where X_{k0} represents the short-term propagation loss at the j[th] antenna branch between the k[th] MS and the zero[th] BS, $r_{k0}^u 10^{\zeta_{k0}/10}$ represents the long-term propagation loss between the k[th] MS and the zero[th] BS, and the condition corresponds to the soft handoff to the zero[th] BS that provides the least propagation loss among the active set, A_k. X_{k0} at jth receive antenna branch is defined as

$$X_{k0} = \sum_{m=1}^{M_m} \left| \sum_{n=1}^{M_t} w_n^{(k)} \cdot h_{j,m,n}^{(k)} \right|^2 \tag{3.52}$$

Assuming the ideal power control of channel inversion, the transmit power, $P_T^{(k)}$, can be expressed as

$$P_T^{(k)} = \begin{cases} \dfrac{r_{k0}^u 10^{\zeta_{k0}/10}}{Y_{k0}} & \text{if } \dfrac{r_{k0}^u 10^{\zeta_{k0}/10}}{Y_{k0}} < \gamma \\ \gamma & \text{if } \dfrac{r_{k0}^u 10^{\zeta_{k0}/10}}{Y_{k0}} \geq \gamma \end{cases} \tag{3.53}$$

where γ represents the transmit power limit of an MS which corresponds to the fade margin of the system, and $1/Y_{k0}$ represents the portion of transmit power that compensates for the short-term propagation loss after rake combining of the received signals from multiple receive antenna branches and multipath components at the BS. That is, Y_{k0} is represented by the principal eigenvalue of the matrix, $\mathbf{H}_{k0}^H \mathbf{H}_{k0}$ and can be expressed as

$$Y_{k0} = \sum_{l=1}^{M_r} \sum_{m=1}^{M_m} \left| \sum_{n=1}^{M_t} w_n^{(k)} \cdot h_{l,m,n}^{(k)} \right|^2 \tag{3.54}$$

where $w_n^{(k)}$ becomes the principal eigenvector of $\mathbf{H}_{k0}^H \mathbf{H}_{k0}$. Then, the n^{th} moment of the intracell interference can be calculated as

$$\begin{aligned} E\left[\left(I_{in}^{(k)}\right)^n\right] &= E\left[\left(P_T^{(k)} \frac{X_{k0}}{r_{k0}^u 10^{\zeta_{k0}/10}}\right)^n ; \min_{i \in A_k} \left\{ r_{ki}^u 10^{\zeta_{ki}/10} \right\} > r_{k0}^u 10^{\zeta_{k0}/10} \right] \\ &= E\left[\left(\frac{X_{k0}}{Y_{k0}}\right)^n ; \min_{i \in A_k} \left\{ r_{ki}^u 10^{\zeta_{ki}/10} \right\} > r_{k0}^u 10^{\zeta_{k0}/10}, \frac{r_{k0}^u 10^{\zeta_{k0}/10}}{Y_{k0}} < \gamma \right] \\ &\quad + E\left[\left(\frac{\gamma \cdot X_{k0}}{r_{k0}^u 10^{\zeta_{k0}/10}}\right)^n ; \min_{i \in A_k} \left\{ r_{ki}^u 10^{\zeta_{ki}/10} \right\} > r_{k0}^u 10^{\zeta_{k0}/10}, \frac{r_{k0}^u 10^{\zeta_{k0}/10}}{Y_{k0}} \geq \gamma \right] \end{aligned} \tag{3.55}$$

Then, the expectation at the second line of Equation (3.55) can be evaluated as

$$\begin{aligned} & E\left[\left(\frac{X_{k0}}{Y_{k0}}\right)^n ; \min_{i \in A_k} \left\{ r_{ki}^u 10^{\zeta_{ki}/10} \right\} > r_{k0}^u 10^{\zeta_{k0}/10}, \frac{r_{k0}^u 10^{\zeta_{k0}/10}}{Y_{k0}} < \gamma \right] \\ &= E\left[\left(\frac{X_{k0}}{Y_{k0}}\right)^n ; \begin{matrix} M_{k1} + b\xi_1 > M_{k0} + b\xi_0 \\ M_{k2} + b\xi_2 > M_{k0} + b\xi_0 \end{matrix}, M_{k0} + a\xi_k + b\xi_0 < \Gamma + \psi_{k0} \right] \\ &= \int_0^\infty \int_0^\infty \left[\int_{-\infty}^\infty \left(\frac{x}{y}\right)^n \begin{Bmatrix} Q\left(\dfrac{M_{k0} - M_{k1}}{b\sigma} + z_0\right) \times \\ Q\left(\dfrac{M_{k0} - M_{k2}}{b\sigma} + z_0\right) \times \\ Q\left(\dfrac{M_{k0} - \Gamma - \psi_{k0} + b\sigma z_0}{a\sigma}\right) \end{Bmatrix} f_G(z_0) dz_0 \right] f_{X,Y}(x,y) dx dy \end{aligned} \tag{3.56}$$

where $\Gamma = 10\log_{10}\gamma$, $\psi_{k0} = 10\log_{10} Y_{k0}$, and $M_{kj} = 10\log_{10} r_{kj}^u$. $Q(y) = \int_y^\infty \frac{1}{\sqrt{2\pi}} e^{-x^2/2} dx$. For the distributions of random variable, $f_G(z_0)$ is the standard Gaussian probability density function (pdf) and $f_{X,Y}(x,y)$ is the joint pdf of X_{k0} and Y_{k0} for X_{k0}/Y_{k0}. However, it

might be not easy to obtain the joint pdf of X_{k0} and Y_{k0} since X_{k0} and Y_{k0} are correlated each other. Hence, instead of finding the joint pdf of X_{k0} and Y_{k0}, we exploit Monte Carlo integration technique by generating numbers of correlated samples of X_{k0} and Y_{k0} according to their distributions. Monte Carlo integration technique can be further utilized for the evaluations of various practical issues such as quantization, feedback delay and errors, and so on, just as found in [63, 64]. Similarly, the expectation of the third line in Equation (3.55) can also be evaluated as

$$
\begin{aligned}
& E\left[\left(\frac{\gamma \cdot X_{k0}}{r_{k0}^{u} 10^{\zeta_{k0}/10}}\right)^{n};\ \min_{i\in A_k}\left\{r_{ki}^{u}10^{\zeta_{ki}/10}\right\} > r_{k0}^{u}10^{\zeta_{k0}/10}, \frac{r_{k0}^{u}10^{\zeta_{k0}/10}}{Y_{k0}} \geq \gamma\right] \\
& = E\left[\left(\frac{\gamma \cdot X_{k0}}{r_{k0}^{u} 10^{\zeta_{k0}/10}}\right)^{n}; \begin{matrix} M_{k1} + b\xi_1 > M_{k0} + b\xi_0 \\ M_{k2} + b\xi_2 > M_{k0} + b\xi_0 \end{matrix}, M_{k0} + a\xi_k + b\xi_0 \geq \Gamma + \psi_{k0}\right] \qquad (3.57) \\
& = \left(\frac{\gamma}{r_{k0}^{u}}\right)^{n} e^{\frac{n^2\beta^2\sigma^2}{2}} \int_0^{\infty}\int_0^{\infty}\int_{-\infty}^{\infty} x^{n} \begin{Bmatrix} Q\left(\frac{M_{k0}-M_{k1}}{b\sigma} + z - n\beta b\sigma\right)\times \\ Q\left(\frac{M_{k0}-M_{k2}}{b\sigma} + z - n\beta b\sigma\right)\times \\ Q\left(\frac{\Gamma + \psi_{k0} - M_{k0} - b\sigma z + n\beta\sigma^2}{a\sigma}\right) \end{Bmatrix} f_G(z)dz f_{X,Y}(x,y)dxdy
\end{aligned}
$$

where $\beta = \ln(10)/10$. Now, let us consider the expectation of cross term between each two branch, $E\left[Z_m^{(k)} Z_n^{(k)}\right]$, in Equation (3.42), which can also be easily calculated as

$$
\begin{aligned}
E\left[Z_m^{(k)} Z_n^{(k)}\right] &= E\left[\left(P_T^{(k)}\right)^2 \frac{X_{k0}^{(m)} X_{k0}^{(n)}}{\left(r_{k0}^{u}10^{\zeta_{k0}/10}\right)^2};\ \min_{i\in A_k}\left\{r_{ki}^{u}10^{\zeta_{ki}/10}\right\} > r_{k0}^{u}10^{\zeta_{k0}/10}\right] \\
&= E\left[\frac{X_{k0}^{(m)} X_{k0}^{(n)}}{Y_{k0}^2};\ \min_{i\in A_k}\left\{r_{ki}^{u}10^{\zeta_{ki}/10}\right\} > r_{k0}^{u}10^{\zeta_{k0}/10}, \frac{r_{k0}^{u}10^{\zeta_{k0}/10}}{Y_{k0}} < \gamma\right] \qquad (3.58) \\
&\quad + E\left[\gamma^2 \frac{X_{k0}^{(m)} X_{k0}^{(n)}}{\left(r_{k0}^{u}10^{\zeta_{k0}/10}\right)^2};\ \min_{i\in A_k}\left\{r_{ki}^{u}10^{\zeta_{ki}/10}\right\} > r_{k0}^{u}10^{\zeta_{k0}/10}, \frac{r_{k0}^{u}10^{\zeta_{k0}/10}}{Y_{k0}} \geq \gamma\right]
\end{aligned}
$$

Similarly, the expectation at the second line and third line of Equation (3.58) can be evaluated as

$$
\begin{aligned}
&E\left[\frac{X_{k0}^{(m)}X_{k0}^{(n)}}{Y_{k0}^2};\ \min_{i\in A_k}\left\{r_{ki}^u 10^{\zeta_{ki}/10}\right\} > r_{k0}^u 10^{\zeta_{k0}/10}, \frac{r_{k0}^u 10^{\zeta_{k0}/10}}{Y_{k0}} < \gamma\right] \\
&= \int_0^\infty\int_0^\infty\int_0^\infty \left[\int_{-\infty}^{\infty}\left(\frac{x_1x_2}{y^2}\right)\left\{\begin{array}{l} Q\left(\frac{M_{k0}-M_{k1}}{b\sigma}+z_0\right)\times \\ Q\left(\frac{M_{k0}-M_{k2}}{b\sigma}+z_0\right)\times \\ Q\left(\frac{M_{k0}-\Gamma-\psi_{k0}+b\sigma z_0}{a\sigma}\right)\end{array}\right\} f_G(z_0)dz_0\right] f_{X_1,X_2,Y}(x_1,x_2,y)dx_1dx_2dy
\end{aligned}
\tag{3.59}
$$

and

$$
\begin{aligned}
&E\left[\gamma^2\frac{X_{k0}^{(m)}X_{k0}^{(n)}}{\left(r_{k0}^u 10^{\zeta_{k0}/10}\right)^2};\ \min_{i\in A_k}\left\{r_{ki}^u 10^{\zeta_{ki}/10}\right\} > r_{k0}^u 10^{\zeta_{k0}/10}, \frac{r_{k0}^u 10^{\zeta_{k0}/10}}{Y_{k0}} \geq \gamma\right] \\
&= C\cdot\int_0^\infty\int_0^\infty\int_0^\infty\int_{-\infty}^{\infty} x_1x_2\left\{\begin{array}{l} Q\left(\frac{M_{k0}-M_{k1}}{b\sigma}+z-2\beta b\sigma\right)\times \\ Q\left(\frac{M_{k0}-M_{k2}}{b\sigma}+z-2\beta b\sigma\right)\times \\ Q\left(\frac{\Gamma+\psi_{k0}-M_{k0}-b\sigma z+2\beta\sigma^2}{a\sigma}\right)\end{array}\right\} f_G(z)dz f_{X_1,X_2,Y}(x_1,x_2,y)dx_1dx_2dy
\end{aligned}
\tag{3.60}
$$

where $C=\left(\frac{\gamma}{r_{k0}^u}\right)^2 e^{\frac{4\beta^2\sigma^2}{2}}$.

- ***Intercell interference in*** S_0

Now, let us consider intercell interference in S_0, which can be rewritten from Equation (3.33) as follows

$$
I_{oc,S_0}^{(k)} = P_T^{(k)}\frac{X_{k0}}{r_{k0}^u 10^{\zeta_{k0}/10}}, \qquad \min_{i\in A_k}\left\{r_{ki}^u 10^{\zeta_{ki}/10}\right\} < r_{k0}^u 10^{\zeta_{k0}/10} \tag{3.61}
$$

where the transmit power of MS, $P_T^{(k)}$, is defined as

$$
P_T^{(k)} = \begin{cases} \dfrac{r_{kj}^u 10^{\zeta_{kj}/10}}{Y_{kj}} & \text{if } \dfrac{r_{kj}^u 10^{\zeta_{kj}/10}}{Y_{kj}} < \gamma \\ \gamma & \text{if } \dfrac{r_{kj}^u 10^{\zeta_{kj}/10}}{Y_{kj}} \geq \gamma \end{cases} \tag{3.62}
$$

with $j=\arg\min_{i\in A_k}\left\{r_{ki}^u 10^{\zeta_{ki}/10}\right\},\ j\neq 0$. Then, the n^{th} moment of the intercell interference in S_0 can be calculated as

$$
\begin{aligned}
E\big[\, I^n_{oc,S_0} \,\big] &= E\left[\left(P_T \, \frac{X_{k0}}{r^u_{k0} 10^{\zeta_{k0}/10}} \right)^n ; \; \min_{i \in A_k} \left\{ r^u_{ki} 10^{\zeta_{ki}/10} \right\} = r^u_{kj} 10^{\zeta_{kj}/10} < r^u_{k0} 10^{\zeta_{k0}/10} \right] \\
&= E\left[\left(\frac{X_{k0}}{Y_{kj}} \frac{r^u_{kj} 10^{\zeta_{kj}/10}}{r^u_{k0} 10^{\zeta_{k0}/10}} \right)^n ; \; \min_{i \in A_k} \left\{ r^u_{ki} 10^{\zeta_{ki}/10} \right\} = r^u_{kj} 10^{\zeta_{kj}/10} < r^u_{k0} 10^{\zeta_{k0}/10}, \frac{r^u_{kj} 10^{\zeta_{kj}/10}}{Y_{kj}} < \gamma \right] \\
&\quad + E\left[\left(\frac{\gamma \cdot X_{k0}}{r^u_{k0} 10^{\zeta_{k0}/10}} \right)^n ; \; \min_{i \in A_k} \left\{ r^u_{ki} 10^{\zeta_{ki}/10} \right\} = r^u_{kj} 10^{\zeta_{kj}/10} < r^u_{k0} 10^{\zeta_{k0}/10}, \frac{r^u_{kj} 10^{\zeta_{kj}/10}}{Y_{kj}} \geq \gamma \right]
\end{aligned} \tag{3.63}
$$

The expectation at the second line can be evaluated as

$$
\begin{aligned}
&E\left[\left(\frac{X_{k0}}{Y_{kj}} \cdot \frac{r^u_{kj} 10^{\zeta_{kj}/10}}{r^u_{k0} 10^{\zeta_{k0}/10}} \right)^n ; \; \min_{i \in A_k} \left\{ r^u_{ki} 10^{\zeta_{ki}/10} \right\} = r^u_{kj} 10^{\zeta_{kj}/10} < r^u_{k0} 10^{\zeta_{k0}/10}, \frac{r^u_{kj} 10^{\zeta_{kj}/10}}{Y_{kj}} < \gamma \right] \\
&= \sum_{\substack{j \in A_k \\ j \neq i \in A_k \\ i,j \neq 0}} E\left[\left(\frac{X_{k0}}{Y_{kj}} \cdot \frac{r^u_{kj} 10^{\zeta_{kj}/10}}{r^u_{k0} 10^{\zeta_{k0}/10}} \right)^n ; \begin{matrix} M_{kj} + b\xi_j > M_{k0} + b\xi_0 \\ M_{kj} + b\xi_j > M_{ki} + b\xi_i \end{matrix}, M_{kj} + a\xi_k + b\xi_j < \Gamma + \psi_{kj} \right] \\
&= \left(\frac{r^u_{kj}}{r^u_{k0}} \right)^n e^{n^2\beta^2 b^2 \sigma^2} E\big[\, X^n_{k0} \,\big] \sum_{\substack{j \in A_k \\ j \neq i \in A_k \\ i,j \neq 0}} \int_0^\infty \left[\int_{-\infty}^\infty \frac{1}{y^n} \left\{ \begin{aligned} &Q\left(\frac{M_{kj} - M_{ki}}{b\sigma} + z + n\beta b\sigma \right) \times \\ &Q\left(\frac{M_{kj} - M_{k0}}{b\sigma} + z + 2n\beta b\sigma \right) \times \\ &Q\left(\frac{M_{kj} - \Gamma - \psi_{kj} + b\sigma z + n\beta b^2\sigma^2}{a\sigma} \right) \end{aligned} \right\} f_G(z) dz \right] f_Y(y) dy
\end{aligned} \tag{3.64}
$$

where X_{k0} and Y_{kj} are not any more correlated. Hence, those two variables can be separately calculated. Similarly, the expectation at the third line of Equation (3.63) can be evaluated as

$$
\begin{aligned}
&E\left[\left(\frac{X_{k0}}{Y_{kj}} \cdot \frac{r^u_{kj} 10^{\zeta_{kj}/10}}{r^u_{k0} 10^{\zeta_{k0}/10}} \right)^n ; \; \min_{i \in A_k} \left\{ r^u_{ki} 10^{\zeta_{ki}/10} \right\} = r^u_{kj} 10^{\zeta_{kj}/10} < r^u_{k0} 10^{\zeta_{k0}/10}, \frac{r^u_{kj} 10^{\zeta_{kj}/10}}{Y_{kj}} \geq \gamma \right] \\
&= \sum_{\substack{j \in A_k \\ j \neq i \in A_k \\ i,j \neq 0}} E\left[\left(\gamma \cdot \frac{X_{k0}}{r^u_{k0} 10^{\zeta_{k0}/10}} \right)^n ; \begin{matrix} M_{kj} + b\xi_j > M_{k0} + b\xi_0 \\ M_{kj} + b\xi_j > M_{ki} + b\xi_i \end{matrix}, M_{kj} + a\xi_k + b\xi_j \geq \Gamma + \psi_{kj} \right] \\
&= \left(\frac{\gamma}{r^u_{k0}} \right)^n e^{\frac{n^2\beta^2\sigma^2}{2}} E\big[\, X^n_{k0} \,\big] \sum_{\substack{j \in A_k \\ j \neq i \in A_k \\ i,j \neq 0}} \int_0^\infty \int_{-\infty}^\infty \left\{ \begin{aligned} &Q\left(\frac{M_{kj} - M_{ki}}{b\sigma} + z \right) \times \\ &Q\left(\frac{M_{kj} - M_{k0}}{b\sigma} + z + n\beta b\sigma \right) \times \\ &Q\left(\frac{M_{kj} - \Gamma - \psi_{kj} + b\sigma z}{a\sigma} + n\beta a\sigma \right) \end{aligned} \right\} f_G(z) dz f_Y(y) dy
\end{aligned} \tag{3.65}
$$

The expectation of the cross term of each two antenna branches can also be calculated as

$$
\begin{aligned}
E\left[Z_m^{(k)}Z_n^{(k)}\right] &= E\left[\left(P_T^{(k)}\right)^2 \frac{X_{k0}^{(m)}X_{k0}^{(m)}}{\left(r_{k0}^u 10^{\zeta_{k0}/10}\right)^2};\ \min_{i\in A_k}\left\{r_{ki}^u 10^{\zeta_{ki}/10}\right\} = r_{kj}^u 10^{\zeta_{kj}/10} < r_{k0}^u 10^{\zeta_{k0}/10}\right] \\
&= E\left[\frac{\left(r_{kj}^u 10^{\zeta_{kj}/10}\right)^2}{Y_{kj}^2}\frac{X_{k0}^{(m)}X_{k0}^{(m)}}{\left(r_{k0}^u 10^{\zeta_{k0}/10}\right)^2};\min_{i\in A_k}\left\{r_{ki}^u 10^{\zeta_{ki}/10}\right\} < r_{k0}^u 10^{\zeta_{k0}/10}, \frac{r_{kj}^u 10^{\zeta_{kj}/10}}{Y_{kj}} < \gamma\right] \\
&\quad + E\left[\gamma^2 \frac{X_{k0}^{(m)}X_{k0}^{(m)}}{\left(r_{k0}^u 10^{\zeta_{k0}/10}\right)^2};\min_{i\in A_k}\left\{r_{ki}^u 10^{\zeta_{ki}/10}\right\} < r_{k0}^u 10^{\zeta_{k0}/10}, \frac{r_{kj}^u 10^{\zeta_{kj}/10}}{Y_{kj}} \geq \gamma\right]
\end{aligned} \tag{3.66}
$$

with $j = \arg\min_{i\in A_k}\left\{r_{ki}^u 10^{\zeta_{ki}/10}\right\},\ \ j \neq 0$. The expectation at the second line and the third line of Equation (3.66) can be evaluated as

$$
\begin{aligned}
&E\left[\frac{\left(r_{kj}^u 10^{\zeta_{kj}/10}\right)^2}{Y_{kj}^2}\frac{X_{k0}^{(m)}X_{k0}^{(n)}}{\left(r_{k0}^u 10^{\zeta_{k0}/10}\right)^2};\min_{i\in A_k}\left\{r_{ki}^u 10^{\zeta_{ki}/10}\right\} < r_{k0}^u 10^{\zeta_{k0}/10}, \frac{r_{kj}^u 10^{\zeta_{kj}/10}}{Y_{kj}} < \gamma\right] = \\
&\left(\frac{r_{kj}^u}{r_{k0}^u}\right)^2 e^{4\beta^2b^2\sigma^2} E\left[X_{k0}^{(m)}\right]^2 \sum_{\substack{j\in A_k \\ j\neq i\in A_k \\ i,j\neq 0}} \int_0^\infty \int_{-\infty}^\infty \frac{1}{y^n} \left\{\begin{array}{l} Q\left(\dfrac{M_{kj}-M_{ki}}{b\sigma} + z + 2\beta b\sigma\right)\times \\ Q\left(\dfrac{M_{kj}-M_{k0}}{b\sigma} + z + 4\beta b\sigma\right)\times \\ Q\left(\dfrac{M_{kj}-\Gamma-\psi_{kj}+b\sigma z+2\beta b^2\sigma^2}{a\sigma}\right)\end{array}\right\} f_G(z)dz f_Y(y)dy
\end{aligned} \tag{3.67}
$$

and

$$
\begin{aligned}
&E\left[\gamma^2 \frac{X_{k0}^{(m)}X_{k0}^{(m)}}{\left(r_{k0}^u 10^{\zeta_{k0}/10}\right)^2};\min_{i\in A_k}\left\{r_{ki}^u 10^{\zeta_{ki}/10}\right\} < r_{k0}^u 10^{\zeta_{k0}/10}, \frac{r_{kj}^u 10^{\zeta_{kj}/10}}{Y_{kj}} \geq \gamma\right] = \\
&\left(\frac{\gamma}{r_{k0}^u}\right)^2 e^{\frac{4\beta^2\sigma^2}{2}} E\left[X_{k0}^{(m)}\right]^2 \sum_{\substack{j\in A_k \\ j\neq i\in A_k \\ i,j\neq 0}} \int_0^\infty \int_{-\infty}^\infty \left\{\begin{array}{l} Q\left(\dfrac{M_{kj}-M_{ki}}{b\sigma} + z\right)\times \\ Q\left(\dfrac{M_{kj}-M_{k0}}{b\sigma} + z + 2\beta b\sigma\right)\times \\ Q\left(\dfrac{M_{kj}-\Gamma-\psi_{kj}+b\sigma z}{a\sigma} + 2\beta a\sigma\right)\end{array}\right\} f_G(z)dz f_Y(y)dy
\end{aligned} \tag{3.68}
$$

, respectively.

- ***Intercell interference in*** $\bar{S}_0$

Intercell interference in $\bar{S}_0$, which comes from the MS connected to other BS and does not have the zero[th] BS in its active set, can be rewritten from Equation (3.33) as

$$
I_{oc,\bar{S}_0}^{(k)} = P_T^{(k)} \frac{X_{k0}}{r_{k0}^u 10^{\zeta_{k0}/10}}, \qquad \min_{i\in A_k}\left\{r_{ki}^u 10^{\zeta_{ki}/10}\right\} = r_{kj}^u 10^{\zeta_{kj}/10} \tag{3.69}
$$

where transmit power of MS, P_T, is defined as

$$P_T^{(k)} = \begin{cases} \dfrac{r_{kj}^u 10^{\zeta_{kj}/10}}{Y_{kj}} & \text{if } \dfrac{r_{kj}^u 10^{\zeta_{kj}/10}}{Y_{kj}} < \gamma \\ \gamma & \text{if } \dfrac{r_{kj}^u 10^{\zeta_{kj}/10}}{Y_{kj}} \geq \gamma \end{cases} \tag{3.70}$$

with $j = \arg\min_{i \in A_k} \left\{ r_{ki}^u 10^{\zeta_{ki}/10} \right\}$. Then, the n^{th} moment of the other cell interference in $\overline{S}_0$ can be evaluated as

$$\begin{aligned} E\left[\left(I_{oc,S_0}^{(k)} \right)^n \right] &= E\left[\left(P_T^{(k)} \frac{X_{k0}}{r_{k0}^u 10^{\zeta_{k0}/10}} \right)^n ; \ \min_{i \in A_k} \left\{ r_{ki}^u 10^{\zeta_{ki}/10} \right\} = r_{kj}^u 10^{\zeta_{kj}/10} \right] \\ &= E\left[\left(\frac{X_{k0}}{Y_{kj}} \cdot \frac{r_{kj}^u 10^{\zeta_{kj}/10}}{r_{k0}^u 10^{\zeta_{k0}/10}} \right)^n ; \ \min_{i \in A_k} \left\{ r_{ki}^u 10^{\zeta_{ki}/10} \right\} = r_{kj}^u 10^{\zeta_{kj}/10}, \frac{r_{kj}^u 10^{\zeta_{kj}/10}}{Y_{kj}} < \gamma \right] \\ &\quad + E\left[\left(\frac{\gamma \cdot X_{k0}}{r_{k0}^u 10^{\zeta_{k0}/10}} \right)^n ; \ \min_{i \in A_k} \left\{ r_{ki}^u 10^{\zeta_{ki}/10} \right\} = r_{kj}^u 10^{\zeta_{kj}/10}, \frac{r_{kj}^u 10^{\zeta_{kj}/10}}{Y_{kj}} \geq \gamma \right] \end{aligned} \tag{3.71}$$

where the first expectation of the right hand side (RHS) can be evaluated as

$$\begin{aligned} & E\left[\left(\frac{X_{k0}}{Y_{kj}} \cdot \frac{r_{kj}^u 10^{\zeta_{kj}/10}}{r_{k0}^u 10^{\zeta_{k0}/10}} \right)^n ; \ \min_{i \in A_k} \left\{ r_{ki}^u 10^{\zeta_{ki}/10} \right\} = r_{kj}^u 10^{\zeta_{kj}/10}, \frac{r_{kj}^u 10^{\zeta_{kj}/10}}{Y_{kj}} < \gamma \right] \\ &= \sum_{\substack{j \in A_k \\ j \neq i, l \in A_k \\ i \neq l}} E\left[\left(\frac{X_{k0}}{Y_{kj}} \cdot \frac{r_{kj}^u 10^{\zeta_{kj}/10}}{r_{k0}^u 10^{\zeta_{k0}/10}} \right)^n ; \begin{matrix} M_{kj} + b\xi_j > M_{kl} + b\xi_l \\ M_{kj} + b\xi_j > M_{ki} + b\xi_i \end{matrix}, M_{kj} + a\xi_k + b\xi_j < \Gamma + \psi_{kj} \right] \end{aligned} \tag{3.72}$$

$$= \left(\frac{r_{kj}^u}{r_{k0}^u} \right)^n e^{n^2\beta^2 b^2 \sigma^2} E[\, X_{k0}^n \,] \sum_{\substack{j \in A_k \\ j \neq i, l \in A_k \\ i \neq l}} \int_0^\infty \int_{-\infty}^\infty \frac{1}{y^n} \left\{ \begin{aligned} & Q\left(\frac{M_{kj} - M_{ki}}{b\sigma} + z + n\beta b\sigma \right) \times \\ & Q\left(\frac{M_{kj} - M_{kl}}{b\sigma} + z + n\beta b\sigma \right) \times \\ & Q\left(\frac{M_{kj} - \Gamma - \psi_{kj} + b\sigma z + n\beta b^2\sigma^2}{a\sigma} \right) \end{aligned} \right\} f_G(z) dz f_Y(y) dy$$

Similarly, the second expectation of RHS can be evaluated as

$$
\begin{aligned}
&E\left[\left(\frac{X_{k0}}{Y_{kj}}\cdot\frac{r_{kj}^{u}10^{\zeta_{kj}/10}}{r_{k0}^{u}10^{\zeta_{k0}/10}}\right)^{n};\ \min_{i\in A_k}\left\{r_{ki}^{u}10^{\zeta_{ki}/10}\right\}=r_{kj}^{u}10^{\zeta_{kj}/10},\frac{r_{kj}^{u}10^{\zeta_{kj}/10}}{Y_{kj}}\geq\gamma\right]\\
&=\sum_{\substack{j\in A_k\\ j\neq i\in A_k\\ i,j\neq 0}}E\left[\left(\gamma\cdot\frac{X_{k0}}{r_{k0}^{u}10^{\zeta_{k0}/10}}\right)^{n};\begin{matrix}M_{kj}+b\xi_j>M_{kl}+b\xi_l\\ M_{kj}+b\xi_j>M_{ki}+b\xi_i\end{matrix},M_{kj}+a\xi_k+b\xi_j\geq\Gamma+\psi_{kj}\right] \qquad (3.73)\\
&=\left(\frac{\gamma}{r_{k0}^{u}}\right)^{n}e^{\frac{n^2\beta^2\sigma^2}{2}}E[\,X_{k0}^{n}\,]\sum_{\substack{j\in A_k\\ j\neq i\in A_k\\ i,j\neq 0}}\int_{-\infty}^{\infty}\left\{\begin{matrix}Q\left(\frac{M_{kj}-M_{ki}}{b\sigma}+z\right)\times\\ Q\left(\frac{M_{kj}-M_{kl}}{b\sigma}+z\right)\times\\ Q\left(\frac{M_{kj}-\Gamma-\psi_{kj}+b\sigma z}{a\sigma}+n\beta a\sigma\right)\end{matrix}\right\}f_G(z)dz
\end{aligned}
$$

and the cross term of each two antenna branches can also be calculated as

$$
\begin{aligned}
E\left[\,Z_m^{(k)}Z_n^{(k)}\,\right]&=E\left[\left(P_T^{(k)}\right)^2\frac{X_{k0}^{(m)}X_{k0}^{(m)}}{\left(r_{k0}^{u}10^{\zeta_{k0}/10}\right)^2};\ \min_{i\in A_k}\left\{r_{ki}^{u}10^{\zeta_{ki}/10}\right\}=r_{kj}^{u}10^{\zeta_{kj}/10}\right]\\
&=E\left[\frac{\left(r_{kj}^{u}10^{\zeta_{kj}/10}\right)^2}{Y_{kj}^2}\frac{X_{k0}^{(m)}X_{k0}^{(m)}}{\left(r_{k0}^{u}10^{\zeta_{k0}/10}\right)^2};\ \min_{i\in A_k}\left\{r_{ki}^{u}10^{\zeta_{ki}/10}\right\}=r_{kj}^{u}10^{\zeta_{kj}/10},\frac{r_{kj}^{u}10^{\zeta_{kj}/10}}{Y_{kj}}<\gamma\right] \qquad (3.74)\\
&\quad+E\left[\gamma^2\frac{X_{k0}^{(m)}X_{k0}^{(m)}}{\left(r_{k0}^{u}10^{\zeta_{k0}/10}\right)^2};\ \min_{i\in A_k}\left\{r_{ki}^{u}10^{\zeta_{ki}/10}\right\}=r_{kj}^{u}10^{\zeta_{kj}/10},\frac{r_{kj}^{u}10^{\zeta_{kj}/10}}{Y_{kj}}\geq\gamma\right]
\end{aligned}
$$

The second line and third line of Equation (3.74) can also be evaluated as

$$
\begin{aligned}
&E\left[\frac{\left(r_{kj}^{u}10^{\zeta_{kj}/10}\right)^2}{Y_{kj}^2}\frac{X_{k0}^{(m)}X_{k0}^{(m)}}{\left(r_{k0}^{u}10^{\zeta_{k0}/10}\right)^2};\ \min_{i\in A_k}\left\{r_{ki}^{u}10^{\zeta_{ki}/10}\right\}=r_{kj}^{u}10^{\zeta_{kj}/10},\frac{r_{kj}^{u}10^{\zeta_{kj}/10}}{Y_{kj}}<\gamma\right]=\\
&\left(\frac{r_{kj}^{u}}{r_{k0}^{u}}\right)^2e^{4\beta^2b^2\sigma^2}E\left[\,X_{k0}^{(m)}\,\right]^2\sum_{\substack{j\in A_k\\ j\neq i,l\in A_k\\ i\neq l}}\int_{0}^{\infty}\int_{-\infty}^{\infty}\frac{1}{y^n}\left\{\begin{matrix}Q\left(\frac{M_{kj}-M_{ki}}{b\sigma}+z+2\beta b\sigma\right)\times\\ Q\left(\frac{M_{kj}-M_{kl}}{b\sigma}+z+2\beta b\sigma\right)\times\\ Q\left(\frac{M_{kj}-\Gamma-\psi_{kj}+b\sigma z+2\beta b^2\sigma^2}{a\sigma}\right)\end{matrix}\right\}f_G(z)dzf_Y(y)dy
\end{aligned} \qquad (3.75)
$$

and

$$E\left[\gamma^2 \frac{X_{k0}^{(m)} X_{k0}^{(m)}}{\left(r_{k0}^u 10^{\zeta_{k0}/10}\right)^2};\ \min_{i\in A_k}\left\{r_{ki}^u 10^{\zeta_{ki}/10}\right\} = r_{kj}^u 10^{\zeta_{kj}/10}, \frac{r_{kj}^u 10^{\zeta_{kj}/10}}{Y_{kj}} \geq \gamma\right] =$$

$$\left(\frac{\gamma}{r_{k0}^u}\right)^2 e^{\frac{4\beta^2\sigma^2}{2}} E\left[X_{k0}^{(m)}\right]^2 \sum_{\substack{j\in A_k \\ j\neq i\in A_k \\ i,j\neq 0}} \int_{-\infty}^{\infty} \left\{\begin{array}{l} Q\left(\frac{M_{kj}-M_{ki}}{b\sigma}+z\right)\times \\ Q\left(\frac{M_{kj}-M_{kl}}{b\sigma}+z\right)\times \\ Q\left(\frac{M_{kj}-\Gamma-\psi_{kj}+b\sigma z}{a\sigma}+2\beta a\sigma\right) \end{array}\right\} f_G(z)dz \tag{3.76}$$

, respectively.

3.4.7 Numerical Results

In this section, the numerical results for the impact of MIMO on the capacity and coverage of the uplink DS/CDMA cellular systems. Table 3.6 shows the system parameters for the evaluation. The desired user is placed on the cell boundary for the worst case scenario. Without loss of generality, the required signal level and the cell radius are assumed to be '1'. As previously mentioned, Monte Carlo integration technique will be applied for the integration related to the short-term fading by generating 10^6 samples according to the distribution of random variables.

Table 3.6: System Parameters

Parameters	Value
Spreading bandwidth (W)	1.25 MHz
Data Rate (R_b)	8 Kbps
Voice activity (ν)	0.38
Target E_b / I_o	5.6 dB
Shadowing correlation between BSs	0.5
Log-normal shadowing	$\sigma = 8\text{dB},\ m = 0$
Path loss exponent	$u = 4$
Soft handoff	3-way
Diversity order (M)	1, 2, 4, 8
Multipath intensity profile	Uniform

- ***Basic Results***

Figure 3.13 shows the outage probability as a function of the number of users with two receive antenna. Fade limit is set to be 10 dB. Total outage probability is the sum of two probabilities, p_1 and p_2. p_1 corresponds to the outage probability of the case that the signal-to-interference ratio falls below the threshold although the desired signal level satisfies the required signal level, and p_2 corresponds to the outage probability of the case where the signal-to-interference ratio falls below the threshold as the transmit power of the desired signal does not meet the required signal level as described in Equation (3.45) and Equation (3.48), respectively. It is shown that the analytical result of the outage probability defined in Equation (3.11) is well matched with the simulation result. Furthermore, it is expected that the outage probabilities are depending on the p_1 when the number of users in the system are small; while it depends on the p_2 when the number of users in the system is large. This trend of the outage probability is thought to be due to the assumption of the strength-based power control. When the number of users in the system is small, interference variation will be small. Hence, the signal-to-interference ratio will depend on the signal variation. On the other hand, when there is large number of users in the system, the interference variation will be relatively larger than the signal variation. Therefore, the signal-to-interference ratio will be more affected by the interference variation.

Figure 3.14 shows the outage probabilities for the different number of receive antennas (M). Fade limit is set to be 10 dB and 1-path Rayleigh fading channel is assumed. As expected, the outage probability significantly improves as the number of receive antenna increases. Generally, this diversity gain comes from the energy capturing effect of spatially separated receive antenna as well as the reduction of the channel fluctuation by combining multiple independent signal received by multiple receive antennas. Furthermore, the intercell interference reduction is observed as the diversity order increases, which is a different observation as compared with the results in Chapter 2.

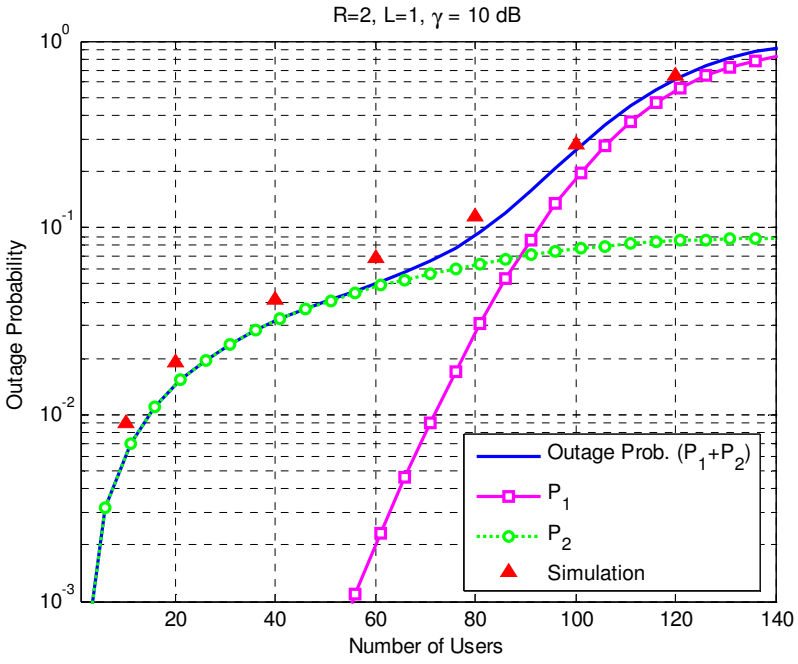

Figure 3.13: Outage probability vs. the number of users per cell for two receive antennas

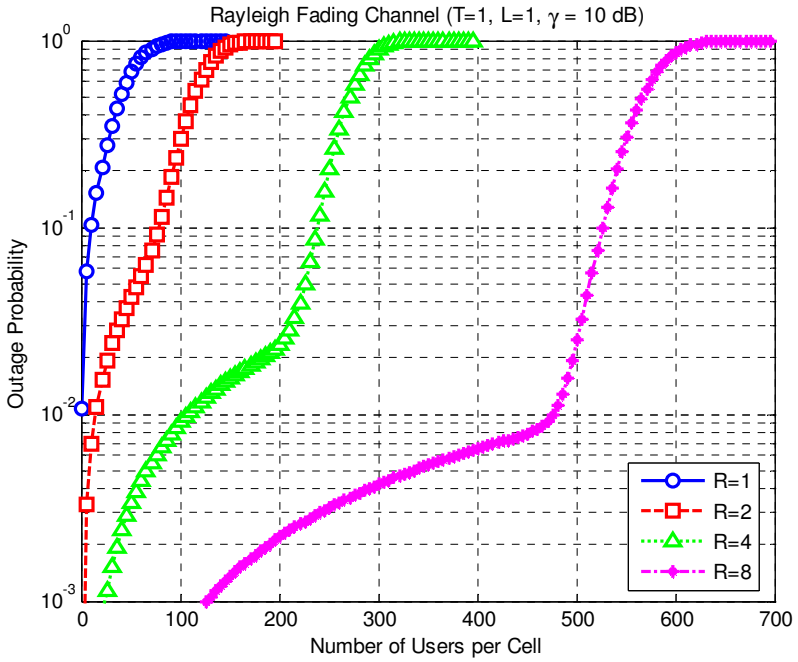

Figure 3.14: Outage probability vs. the number of users per cell for different number of receive antennas ($\gamma = 10\text{dB}$, $L = 1$)

In Chapter 2, it has been presumed that the intracell interference is always constant and does not change regardless of diversity technique. Generally, the assumption of the constant intracell interference is not wrong for the multipath diversity and transmit diversity without receive diversity. However, because of the non-coherent combining of signals from each branch in the receive antenna, intracell interference is also reduced, which is shown with simple examples in Appendix. Table 3.7 shows that the mean as well as the variance of the interference-to-signal ratio per branch decreases as the diversity order increases. However, the relative reduction by the increased diversity is more pronounced in the intercell interference statistics as compared with intracell interference statistics.

Table 3.7: Statistics of the interference-to-signal ratio for the different number of receive antennas ($\gamma = 10\text{dB}$, $L = 1$)

	Intracell interference		Intercell interference	
	Mean	Variance	Mean	Variance
M=1	0.365	0.262	0.725	16.193
M=2	0.186	0.098	0.189	0.568
M=4	0.093	0.031	0.067	0.038
M=8	0.047	0.0088	0.029	0.0057

Figure 3.15 shows the outage probability of the system versus the number of users per cell for different number of receive antennas. Fade margin is set to be 20 dB and Rayleigh fading channel with one resolvable multipath component is assumed. As expected, because of the increased fade margin (corresponding to the reduction of cell radius) the outage probability improves as compared with those shown in Figure 3.14 for the same diversity order. It is also observed that the probability p_2 decreases due to the increased fade margin. Note that p_2 is defined by the outage probability of that the signal-to-interference falls below as the transmit power of desired users does not meet the required signal level due to the limit of fade margin.

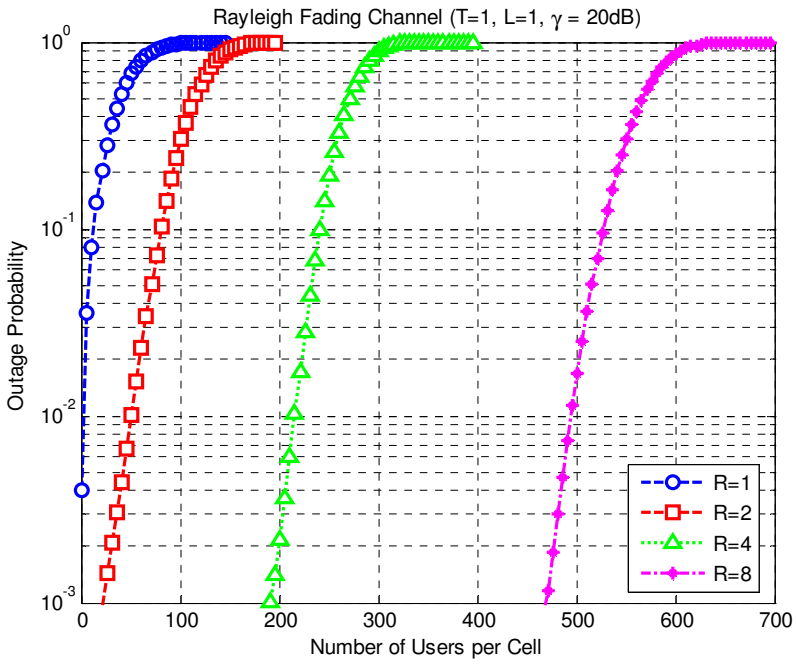

Figure 3.15: Outage probability vs. the number of users per cell for different number of receive antennas ($\gamma = 20\text{dB}$, $L = 1$)

Figure 3.16 and Figure 3.17 shows the outage probabilities versus the number of users per cell for different number of receive antennas for the fade margin of 10 dB and 20 dB, respectively. For the evaluation of the system performances in the frequency selective channel, Rayleigh fading channel with two resolvable multipath components is assumed. Because of the increased resolvable multipath components, it is observed that the outage probability improves as compared with the results shown in Figure 3.14 and Figure 3.15 for the same diversity order. However, as the diversity order increases, the amount of improvement decreases as compared with the results shown in Figure 3.14 and Figure 3.15. It is thought to be due to that the interference variation is sufficiently flattened by large order of spatial diversity so that additional diversity gain obtained from combining the resolvable multipath has the less impact on the system. Furthermore, the multipath combining does not provide any array gain as the spatial diversity.

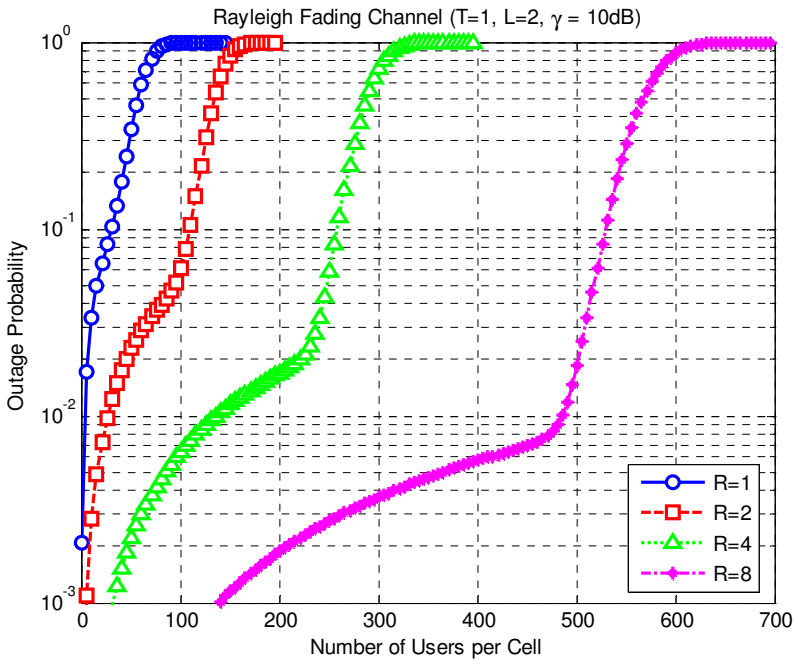

Figure 3.16: Outage probability vs. the number of users per cell for different number of receive antennas ($\gamma = 10\text{dB}$, $L = 2$)

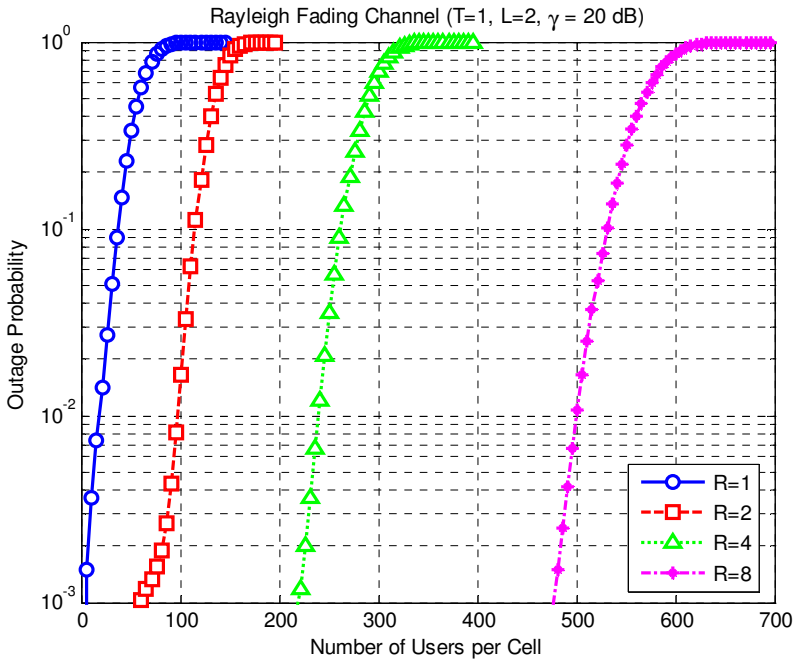

Figure 3.17: Outage probability vs. the number of users per cell for different number of receive antennas ($\gamma = 20\text{dB}$, $L = 2$)

On the other hand, Figure 3.18 shows the outage probability vs. the number of users per cell for two transmit antenna diversity of. Fade limit is also set to be 10 dB. It is shown that the analytical result are well-matched with the simulation results for the case of transmit diversity. Just as the result of two receive antenna diversity, it can be observed that the total outage probability consists of two probabilities, p_1 and p_2. However, as compared to the same diversity order with receive antennas, the improvements of outage probability vs. the number of users per cell is smaller because of that the intracell interference is not reduced with transmit diversity only. The interference statistics are shown in Table 3.8 for the same order of transmit antenna diversity as that of receive antenna diversity. Since the intracell interference statistics are not changed by the transmit diversity, the system capacity achievable by the large number of transmit antennas will eventually approach to that of the single cell system.

Table 3.8: Statistics of the interference-to-signal ratio for the different number of transmit antennas

	Intracell interference		Intercell interference	
	Mean	Variance	Mean	Variance
M=1	0.365	0.262	0.725	16.193
M=2	0.373	0.269	0.200	0.849
M=4	0.374	0.270	0.069	0.049
M=8	0.374	0.270	0.029	0.0067

Figure 3.19 and Figure 3.21 show the outage probabilities versus the number of users per cell for different number of transmit antennas and the fade margins of 10 dB and 20 dB. Rayleigh fading channel with one resolvable multipath component is assumed for the evaluation of the system performance in a frequency flat fading channel. It can be observed that outage probability improves as the diversity order increases. However, because of the intracell interference, which is not changed by transmit diversity, the relative improvements by increasing diversity order is observed to diminishes as compared with the results shown in Figure 3.14 Figure 3.15.

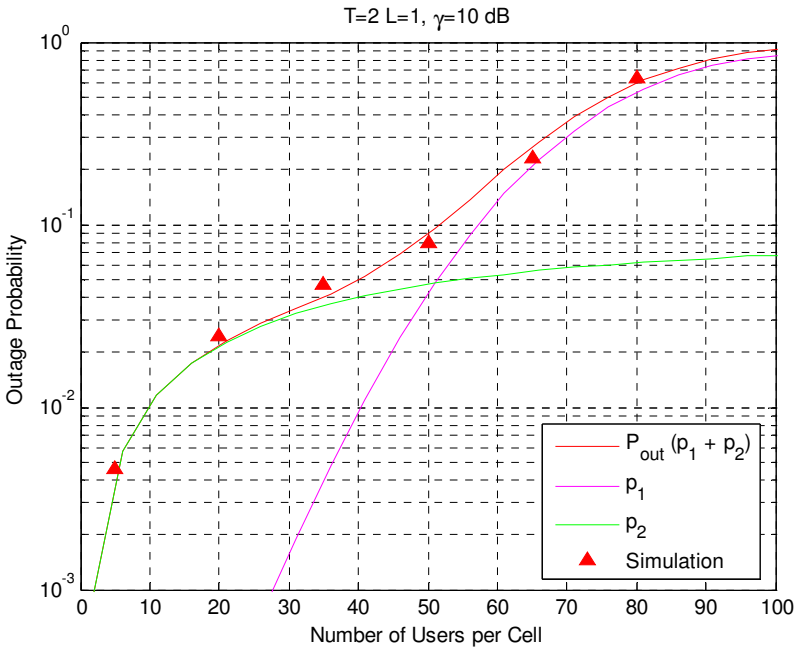

Figure 3.18: Outage probability vs. the number of users per cell for two transmit antennas

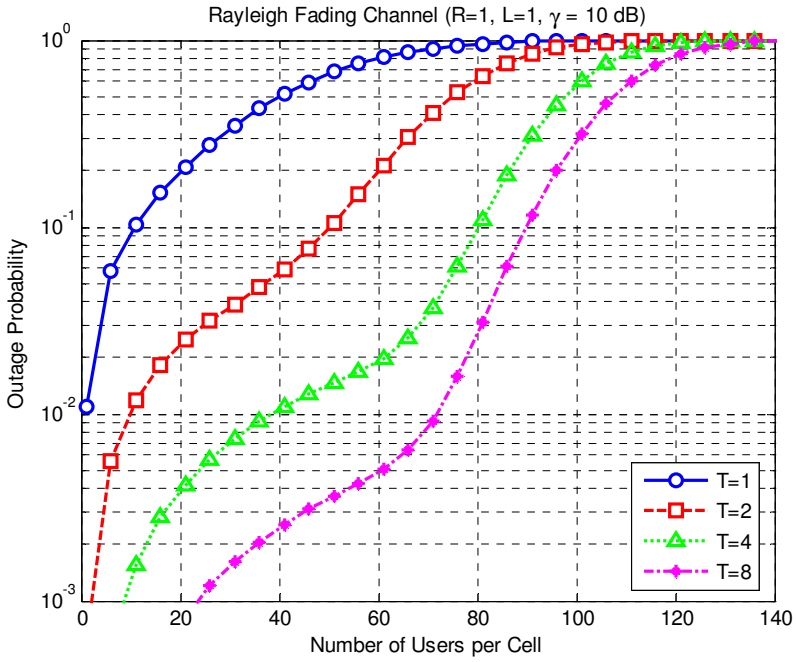

Figure 3.19: Outage probability vs. the number of users per cell for different number of transmit antennas ($\gamma = 10\text{dB}$, $L = 1$)

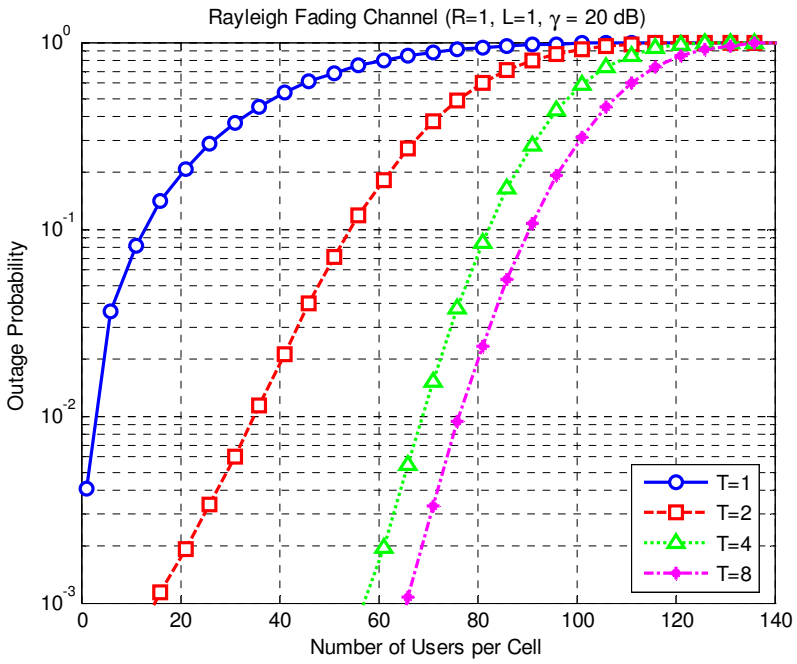

Figure 3.20: Outage probability vs. the number of users per cell for different number of transmit antennas ($\gamma = 20\text{dB}$, $L = 1$)

Figure 3.21 and Figure 3.22 shows the outage probabilities versus the number of users per cell for different number of transmit antennas and the fade margins of 10 dB and 20 dB. For the evaluation of the system performances in the frequency selective fading channel, Rayleigh fading channel with two resolvable multipath components (L=2) is assumed. As observed in the system level simulations of closed loop transmit diversity in the fading channel with multiple resolvable multipath components, the performance of transmit diversity is expected to diminishes in the frequency selective channel due to the discrepancy of diversity order and the number of transmit weight coefficients. However, for the low order of transmit diversity (T=1 and T=2), the outage probabilities slightly improve as compared with the results shown in Figure 3.19 and Figure 3.20. However, for the high order of transmit diversity (T=4 and T=8), the outage probabilities is observed to deteriorate due to the multiple resolvable multipath components.

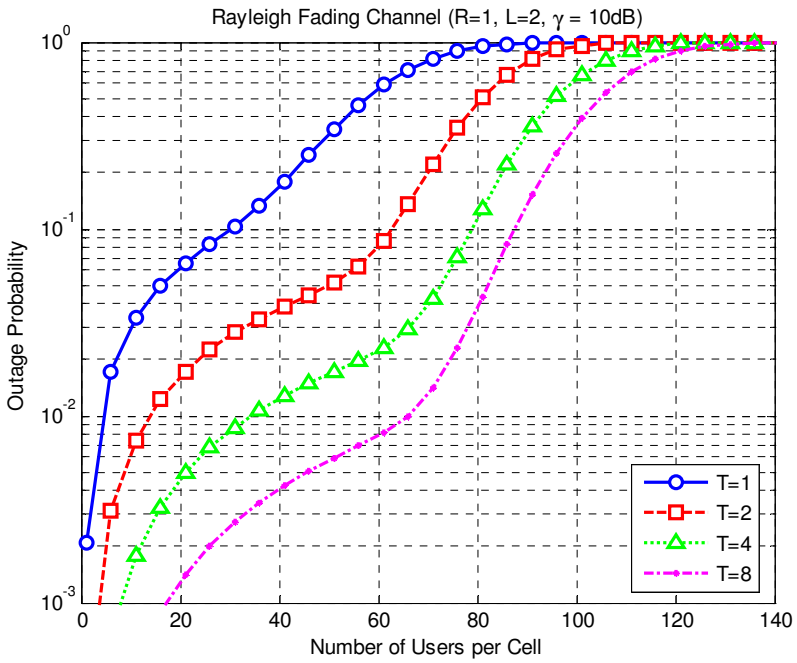

Figure 3.21: Outage probability vs. the number of users per cell for different number of transmit antennas ($\gamma = 10\text{dB}$, $L = 2$)

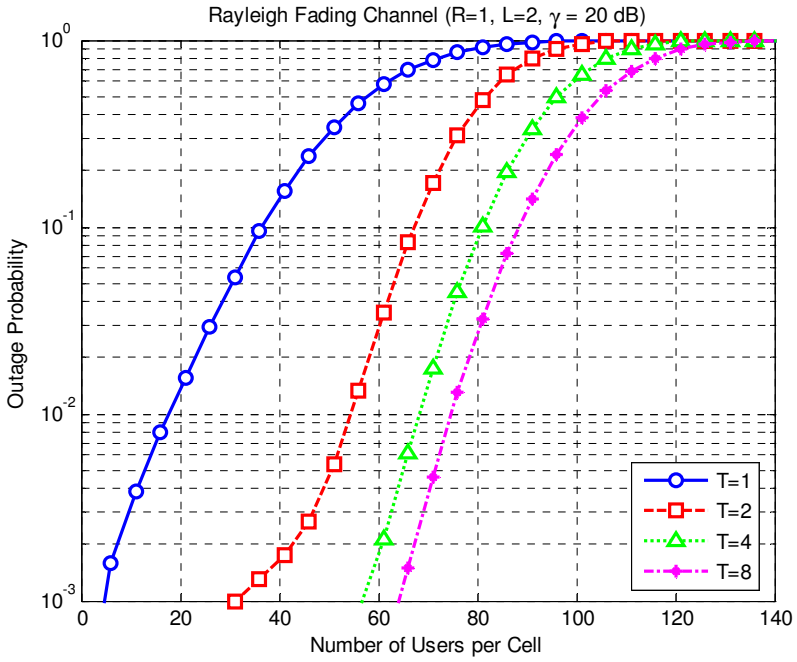

Figure 3.22: Outage probability vs. the number of users per cell for different number of transmit antennas ($\gamma = 20\text{dB}$, $L = 2$)

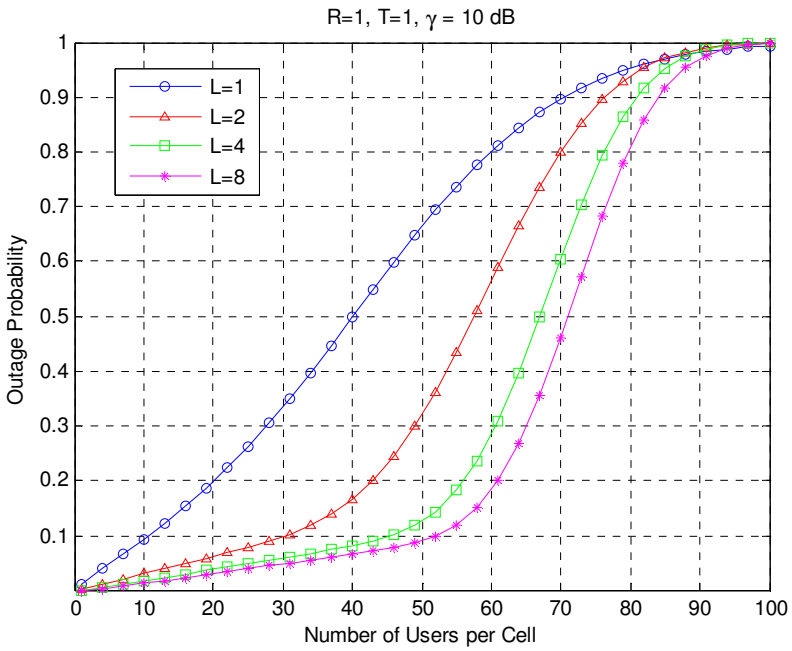

Figure 3.23: Outage Probability vs. the number of users per cell for the different number of multipath components

Figure 3.23 shows the outage probabilities for the different number of multipath (L). Fade limit is set to be 10 dB and the number of receive and transmit antennas is fixed to be one. As expected, the outage probabilities are improved as the number of multipath increases. However, the amount of improvement is small as compared with the results for the different number of the receive antennas since there is no reduction in the statistics of the intracell interference in multipath combining just as those in transmit diversity. In addition, the reduction in the statistics of the intercell interference is small in multipath combining as compared with the spatial diversity combining. Eventually, the capacity of multipath combining only will approach to the capacity of single cell system by the reduction of only intercell interference. Table 3.9 shows the interference-to-signal ratio for the different number of multipath. It is observed that mean and variance of intercell interference are reduced while those of intracell interference are not. As compared with the interference statistics in Table 3.8, the relative reduction of mean and variance of intercell interference by the increment of the number of multipath is small.

Table 3.9: Statistics of the interference-to-signal ratio for the different number of multipath

	Intracell interference		Intercell interference	
	Mean	Variance	Mean	Variance
L=1	0.365	0.262	0.725	16.193
L=2	0.370	0.267	0.363	1.340
L=4	0.372	0.268	0.263	0.334
L=8	0.373	0.269	0.227	0.184

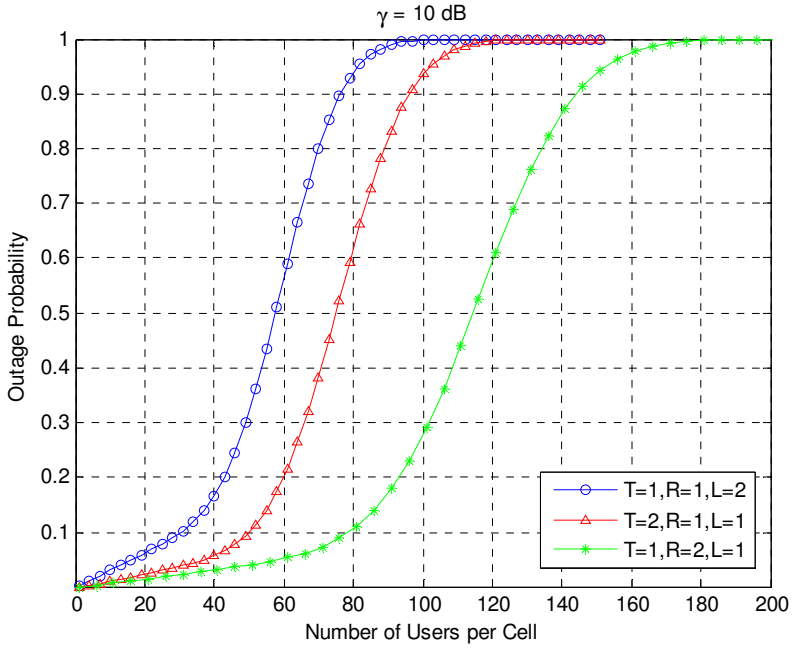

Figure 3.24: Outage probability vs. the number of users per cell for two branch diversity

More comprehensively, Figure 3.24 shows the outage probabilities for two branch diversity. As expected, the receive diversity outperforms transmit diversity and multipath diversity. Furthermore, spatial diversity also outperforms multipath diversity, as mentioned in the above.

- ***Capacity vs. coverage***

Let us consider the number of users vs. fade margin. As mentioned in the section 0, the relative improvements of fade margin can be easily translated into the coverage improvements. Figure 3.25 shows the outage probability vs. the number of users per cell for different fade margins with receive diversity. It can be observed that the outage probability increases as the fade margin decreases, in other words, the outage occurrence of the received signal increases as the cell radius increases without changing the fade margin; hence, the system capacity is reduced by increasing cell radius. In different point of view, the system capacity can be improved by increasing the fade margin without changing the cell radius or reducing the cell radius without changing fade margin. However, increasing the fade margin or reducing cell radius is not always positive. For example, large fade margin can increase the peak power of the interference, which would decrease the system capacity. That is, if cell radius is too small, interference from other MSs would increase. It can be observed above 80 users and the outage probability of 10^{-1} in Figure 3.25. Figure 3.26 shows the outage probability vs. the number of users per cell for different fade margin with transmit diversity, which also shows the outage probability improves as the fade margin increases, that is, cell coverage reduces. In addition, it can be more easily observed that large fade margin diminishes the system capacity in the case of transmit diversity as compared with the receive diversity case shown in Figure 3.25, which is due to that the receive diversity reduces the intracell interference as well as the intercell interference while transmit diversity reduces only the intracell interference.

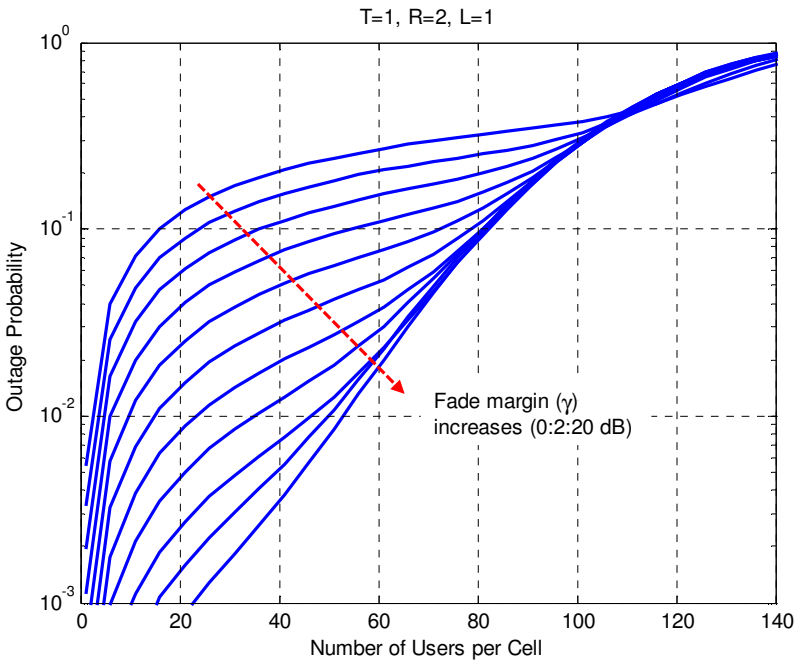

Figure 3.25: Outage probability vs. the number of users per cell for different fade margins with receive diversity

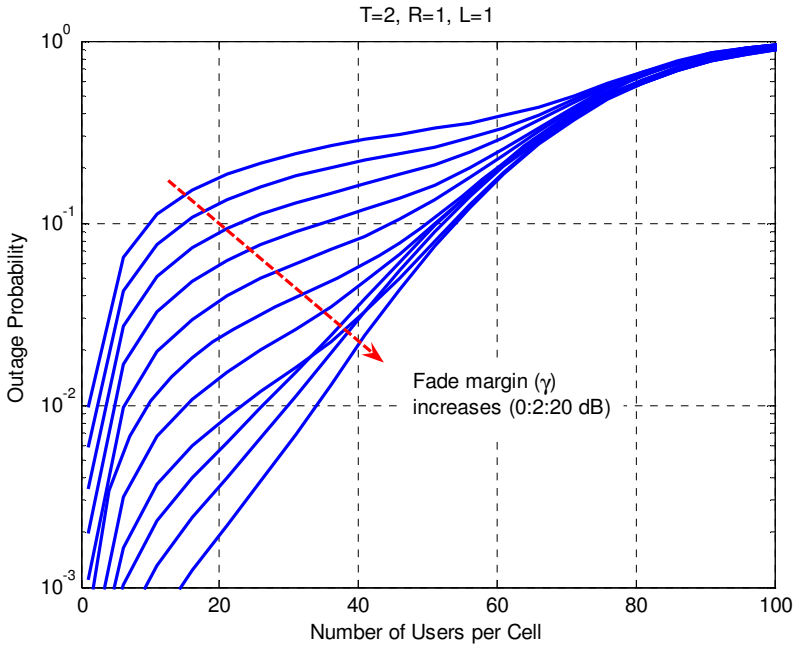

Figure 3.26: Outage probability vs. the number of users per cell for different fade margins with transmit diversity

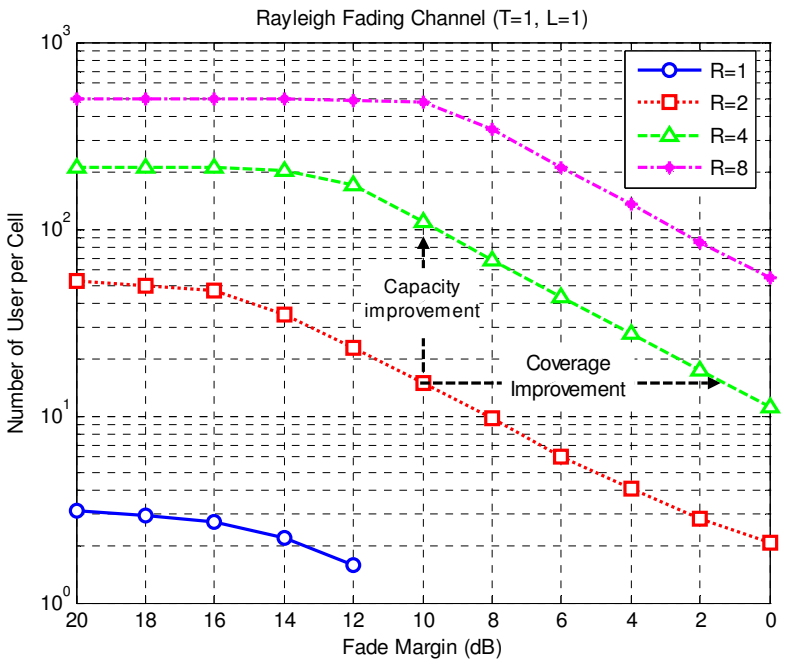

Figure 3.27: Number of users per cell vs. fade margin for different number of receive antennas with one resolvable multipath

Figure 3.27 shows the number of users per cell versus fade margin based on the outage probability of 10^{-2}. It is assumed that the number of transmit antennas is one (T=1) and the number of resolvable multipath components is one (L=1). It is observed that the supportable number of users per cell diminishes as the fade margin decreases. As mentioned before, fade margin constrains the maximum transmit power of MS, which results in reducing the cell coverage. Hence, the cell capacity decreases as the fade margin decreases. However, by increasing the number of the receive antenna, it is observed that coverage is dramatically improved as shown in Figure 3.27. For instance, from the point at 10 dB fade margin and two receive antennas, we can observe the capacity improvement by increasing the number of the receive antennas without changing the cell coverage. On the other hand, from the same point, we can observe the coverage improvement by increasing the number of the receive antennas while maintaining the same capacity. Note that the reduction of fade margin can be translated into the coverage improvement in this analysis. Furthermore, it can be observed that the supportable number of users per cell does not any more increases above a certain value of the fade

margin. It is expected that the channel fluctuation is almost compensated above that fade margin. Then, the signal-to-interference ratio will be mostly dependent on the number of interferers under the same environment. Hence, the capacity of DS/CDMA cellular system is not expected to increases even though the cell radius decreases below a certain radius, which can be considered as a *capacity limit*. Furthermore, spatial diversity is expected to reduce the channel fluctuation. Thus, the capacity limit is reached at a lower fade margin as the diversity order increases. In different viewpoint, it is also expected that spatial diversity can provide the great capacity improvements that cannot be achieved without spatial diversity.

Figure 3.28 shows the number of users per cell versus the fade margin for different number of receive antennas implemented at BS. For the evaluation of the system performance under frequency selective channel, two resolvable multipath components are taken into account with equal power delay profiles. It is also assumed that the number of transmit antennas at MS is one (T=1). The number of users per cell is determined given outage probability of 10^{-2} .). Similar results to those shown in Figure 3.27 can be observed:

- The cell capacity increases as the fade margin increases; however, the cell capacity does not increase as the fade margin increases above a certain fade margin.
- The cell capacity for given fade margin (that is, coverage) or the coverage given the number of users per cell improves as the number of transmit antennas increases

However, because of the multipath diversity, it is observed that the cell capacity given fade margin or fade margin given the number of users are significantly improved as compared with the results shown in Figure 3.27.

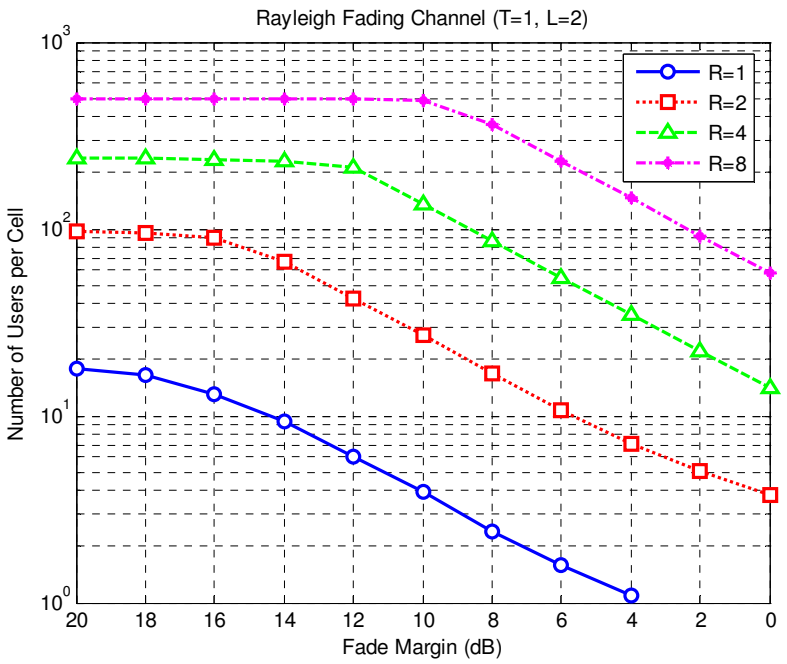

Figure 3.28: Number of users per cell vs. fade margin for different number of receive antennas with two resolvable multipaths

Figure 3.29 and Figure 3.30 show the number of users per cell versus fade margin based on the outage probability of 10^{-2} for different number of transmit antennas implemented at MS. It is assumed that the number of receive antennas at MS is one (R=1) and the number of resolvable multipath components is one (L=1) in Figure 3.29 and is two (L=2) in Figure 3.30 corresponding to the frequency flat fading channel and frequency selective fading channel, respectively. Similar results to those obtained by receive diversity can be observed:

- The cell capacity increases as the fade margin increases; however, the cell capacity does not increase as the fade margin increases above a certain fade margin.

- The cell capacity for given fade margin (that is, coverage) or the coverage given the number of users per cell improves as the number of transmit antennas increases

However, since the statistics of intracell interference is not changed regardless of increasing the number of transmit antennas at MS, the relative improvements of cell capacity given fade margin or the fade margin given the number of users per cell by transmit diversity are smaller than those achieved by receive diversity shown in Figure 3.27 and Figure 3.28.

Furthermore, the similar performance differences of transmit diversity is observed according to the number of resolvable multipath components:

- For the high order of transmit diversity (T=4 and T=8), the cell capacity achieved in frequency selective fading channel, given the fade margin or the fade margin given the number of users per cell, diminishes as compared with those achieved in frequency flat fading channel, since the number of transmission path is larger than the number of transmit weight coefficients. Therefore, the channel power are spread over multiple eigenvalues.

- For the low order of transmit diversity (T=1 and T=2), however, the cell capacity achieved in frequency selective channel, given the fade margin or the fade margin given the number of users per cell, slightly improves since the impact of multipath diversity is greater than the that of transmit diversity with small number of transmit antennas

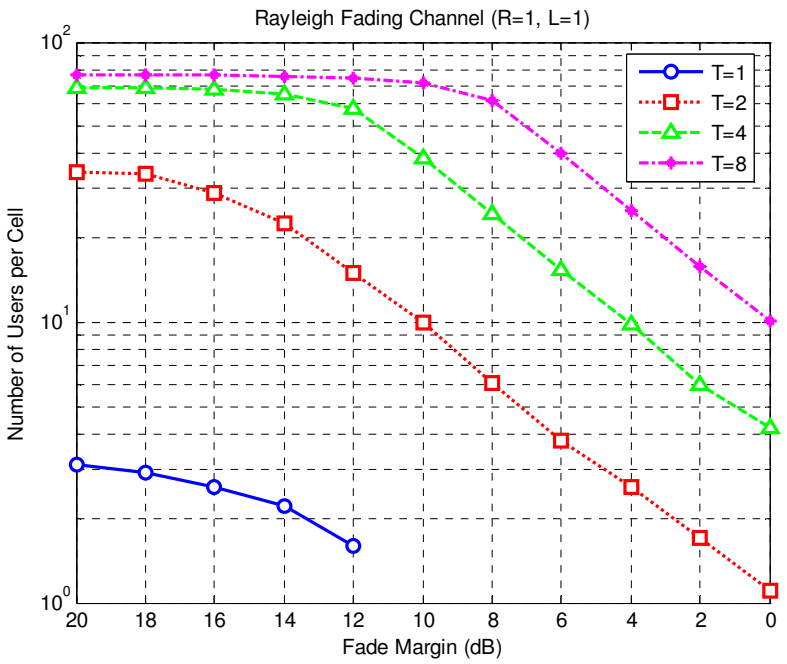

Figure 3.29: Number of users per cell vs. fade margin for different number of transmit antennas

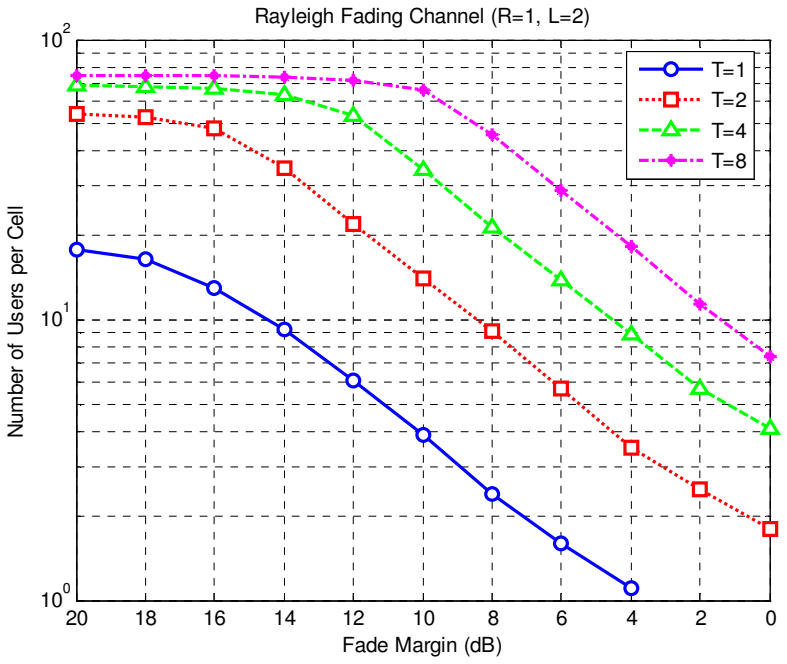

Figure 3.30: Number of users per cell vs. fade margin for different number of transmit antennas and two resolvable multipaths

Figure 3.31 and Figure 3.32 show the number of users per cell versus the fade margin with two transmit antennas in frequency flat fading channel and frequency selective channel, respectively. Following observations are made:

- The relative capacity and/or coverage improvements by adding transmit antenna are smaller than those by receive diversity with the same diversity order (e.g. T=2, R=2 vs. T=1, R=4).
- Nevertheless, the transmit diversity still shows great improvement in both coverage and capacity over the system without transmit diversity (e.g. T=2, R=2 vs. T=1, R=2).
- However, the relative improvement by transmit diversity decreases as the receive diversity order increases.

Table 3.10 summarizes the capacity achievable by spatial diversity in Figure 3.31 for the fixed fade margin, that is, without changing the cell radius, where 'T' denotes the number of transmit antennas, 'R' denotes the number of receive antennas, and 'M' denotes the diversity order. The fade margin is assumed to be 12 dB.

Table 3.10: The number of users per cell achievable by spatial diversity for fixed cell radius

	T=1, R=M	T=2, R=M/2
M=1	1.6	
M=2	23.3	15.2
M=4	170.5	88.1
M=8	488.4	266.9

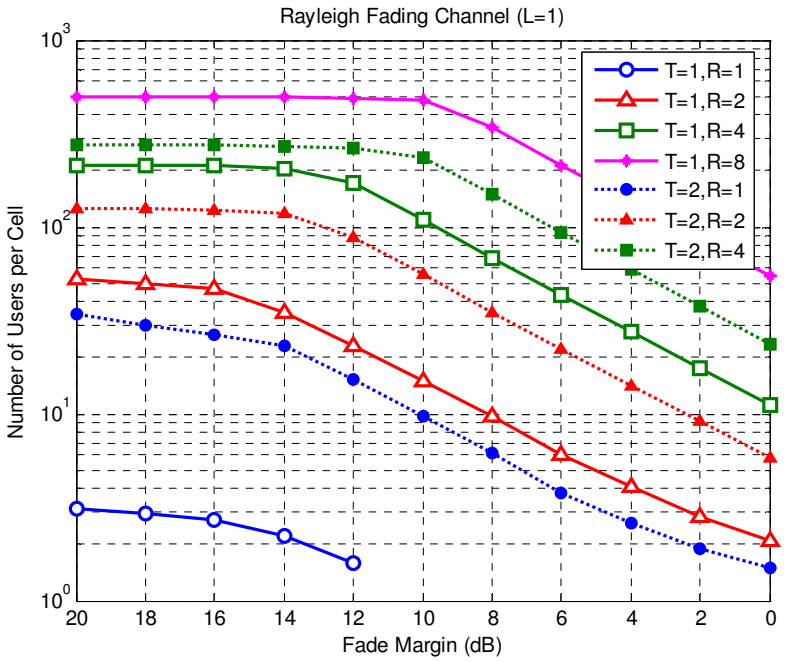

Figure 3.31: Number of users per cell vs. fade margin for different diversity order with one resolvable multipath

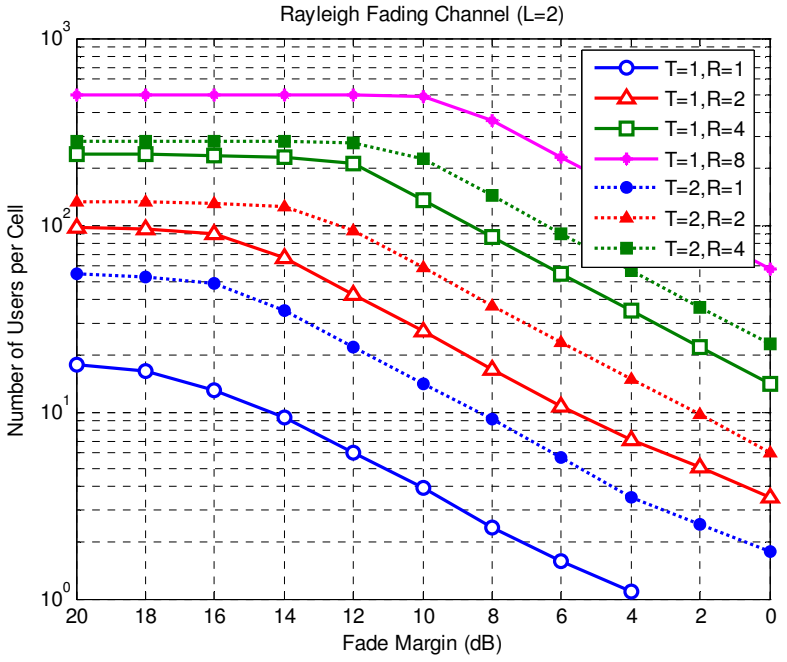

Figure 3.32: Number of users per cell vs. fade margin for different diversity order with two resolvable multipaths

Now, let us consider different path loss exponent other than '4'. Figure 3.33 shows the number of users per cell versus fade margin for different number of users per cell with the path loss exponent of '5'. Since the larger path loss exponent increase the propagation loss from the interferer to the BS, the interference becomes less significant; on the other hand, power control keeps the desired user's signal power at the required signal level. Hence, the received SIR improves, which results in the system capacity improvement. It can be observed that the system capacities shown in Figure 3.33 are slightly improved as compared with that in Figure 3.31 for all diversity configurations. Therefore, we can easily expect that smaller path loss exponent will reduce the system capacity.

Table 3.11 summarizes the relative coverage improvements, by spatial diversity with co-channel interference in terms of cell radius, based on Figure 3.31. The first column represents the number of users per cell achieved by spatial diversity corresponding to the relative coverage of '1' and fade margin, γ, in parenthesis. For example, in the second row, the number of users per cell in the first column is achieved by 'T=1, R=1' with the fade margin of 20 dB, and in the fourth row, the number of users per cell in the first column is achieved by 'T=2, R=2' with the fade margin of 18 dB. The fade margin is determined based on the value above which the capacity does not increase for the same diversity order. From this table, the coverage improvements as well as the capacity improvements by spatial diversity are more easily observed.

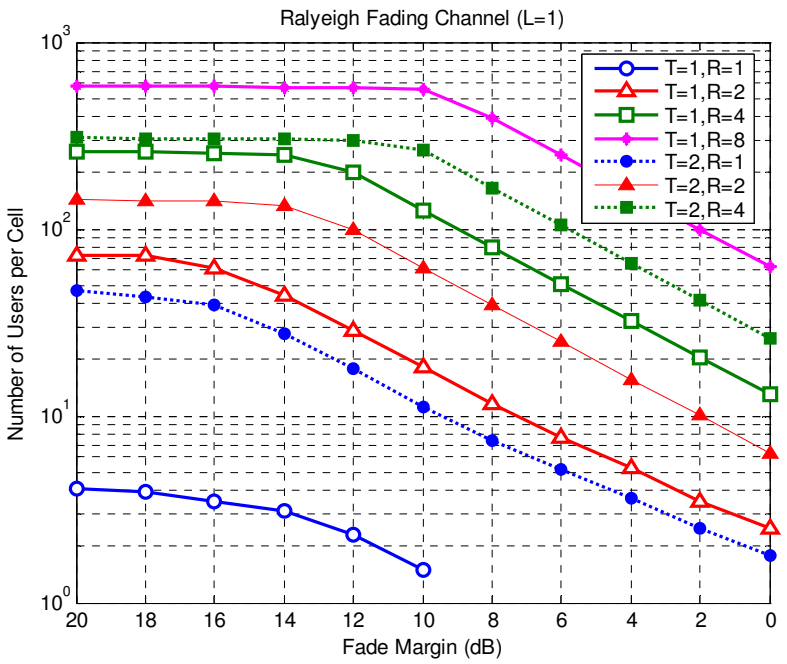

Figure 3.33: Number of users per cell vs. fade margin for different diversity order with path loss exponent of '5'

Table 3.11: Relative coverage improvements with co-channel interference

K (γ)	T=1, R=1	T=2, R=1	T=1, R=2	T=2, R=2	T=1, R=4	T=2, R=4	T=1, R=8
3 (20 dB)	1.0	5.6	7.5				
34 (20 dB)		1.0	2.0	4.0	5.6	8.4	
52 (18 dB)			1.0	2.7	3.8	5.6	7.9
126 (16 dB)				1.0	1.9	2.8	4.0
215 (14 dB)					1.0	1.8	2.5
274 (12 dB)						1.0	1.8
496 (10 dB)							1.0

3.5 Chapter Summary

In this chapter, we have investigated the impact of MIMO on the system coverage of uplink DS/CDMA cellular system and trade-off between coverage and capacity.

- Without any co-channel interference (virtually unloaded systems), the system coverage depends on the statistics of the desired signal. It is shown that MIMO could significantly improve the system coverage for unloaded system.
- However, when there is co-channel interference, system coverage apparently depends on the signal-to-interference ratio, from which we have derived the relation between the coverage and capacity with MIMO.
- It is also shown that the receive antenna diversity outperforms the transmit antenna diversity when the system employs perfect (or fast) power control.
- Furthermore, by employing semi-analytical approach in the analytical framework developed in this chapter, we can readily estimate the system performance with various smart antenna techniques.

Chapter

4 System Level Simulations of Uplink of DS/CDMA Cellular Systems

4.1 Introduction

Wireless cellular systems often operate in the presence of heavy interference and, in addition, multipath and shadowing lead to signal fading at the receiver. The combination of complex system operations in a complicated environments leads to design and analysis problems that might not be analytically tractable using traditional (non-simulation based) analysis techniques [9]. In this situation, simulation can be a valuable tool for gaining insight into system behavior. A properly developed simulation is much like a laboratory implementation of a system. Measurements can easily be made at various points in the system under study. Furthermore, parametric studies are easily conducted since parameter values, such as filter band-widths and signal-to-noise ratios, can be changed at will and the effects of these changes on system performance can quickly be observed.

However, simulation is not always preferable. Sometimes, even after extensive simulations, it is not easy to get insights on what parameters impact system performance and how fading channels impact proper selection of system parameters. In this situation, analytical analysis might be able to provide easier and better insight. Therefore,

simulation and analytical analysis are both indispensable and complementary to each other. In this chapter, the system level simulation methodology and the structure of system simulator are described in detail, and selective simulation results are presented and compared with the analytical results from previous chapters.

- ***Contributions***

The objective of the system level simulation is not only to verify the previous analysis results, but also to estimate the system capacity by introducing various degradation factors which are difficult (if it is not impossible) to model analytically. The system level simulation can be further utilized for analyzing the impact of various communication algorithms on the system capacity.

- ***Organization***

The rest of this chapter is organized as follows. In section 4.2, the system model for the analysis described. In section 4.3, the specifications for developing the system simulator are presented. In section 4.4, simulation flow is detailed along with the implemented algorithms. In section 4.5, the method for the interference measurement in the simulator is described. In section 4.6, selective simulation results are presented. Finally, the main points of this chapter are summarized in section 4.7.

4.2 System Model

The system model for the theoretical analysis and system simulation such as cell layout and channel models is basically the same as the section 2.2. Hence, it will be briefly described in this chapter. The cellular communication architecture for our analysis is identical to the well-known uniform hexagonal layout with a base station (BS) at the center of every cell as in [28]. That is, the network consists of three rings of hexagonal cells which surround the center cell, and mobile stations (MS) are uniformly distributed in each cell. It is assumed that an MS communicates with the BS which provides the least

average attenuation among three nearest BSs (3-way soft handoff). While an MS is assumed to be perfectly power-controlled so as to compensate for the channel fluctuations in the analysis, it is power-controlled in a fixed step by the feedback from the BS in our simulation. Therefore, the feedback latency and error can be taken into account to reflect practical situations. The propagation channel model incorporates both long-term fading and short-term fading process with arbitrary multipath intensity profiles. Typically, the standardized multipath channel model such as 'Pedestrian channel A' or 'Vehicular channel A' is considered in both the analysis and simulation. The analysis is focused on the zeroth BS located in the center of cell layout since the hexagonal layout of the system is symmetric. However, the area of system is divided into two regions, S_0 and $\overline{S}_0$, where S_0 is defined as the soft handoff region which includes the zeroth BS and $\overline{S}_0$ as the region except S_0. This region will be different according to the number of BSs participating in the soft handoff.

4.3 Specifications

To validate the analysis results, most system parameters of the simulation are set to the same as those of analytical framework in Chapter 2. Table 4.1 shows the basic specification of the system level simulator currently implemented.

Table 4.1: Specification of system level simulator

Parameters	Specification
Number of cells *	Up to 37 corresponding to 3-tier of hexagonal cells
Number of users / cell *	Only limited by memory allocation
Cell radius	Normalized to 1 (no dimension)
Sector/cell	No sectorization
Antenna gain	Omni directional
Supporting handoff	Hard handoff / 3-way soft handoff
Voice activity	0.38 (ON-OFF traffic / Flexible data rate based on the standard specified Markov chain probability)
Propagation loss	Multipath Rayleigh fading channel, Log-normal shadowing, and path loss
Channel model	ITU-R channel model
MS transmit diversity	Up to 2 antennas – optimum /equal gain combining
BS receive diversity	Up to 4 antennas – maximal ratio combining
Multipath combining	Maximal ratio combining of all possible multipath / resolvable multipath based on link level simulator
Power control	Channel inversion / fixed step power control based on the received signal strength
Mobile Velocity	3 ~ 120 Km/h

* In the system level simulator, the number of cells and the number of users/cell are critical factors for the memory allocation. Even though the maximum number of cells are 37 corresponding to 3-tier of hexagonal cells, all simulation results in this Chapter are performed with 19 cells (corresponding to 2-tier of hexagonal cells). Also, the maximum number of users per cell is set to 100. It is due to the excessive simulation time resulting from large memory allocation and frequent paging operations during simulation.

4.4 Simulation Flow

The basic flow of the system level simulation follows the simulation steps described in [65]. First, all BSs are placed on the center of each cell and the specified number of MSs per cell are uniformly dropped in each cell. For the soft handoff, each MS determines the BS, which provides the least average attenuation, to communicate with. Then, each MS in the entire system is power controlled by each BS to which it is connected. The reference power for the power control is assumed to be '1'. For every simulation turn, which corresponds to 1.25ms power control unit, the power control function calculates the received signal power attenuated by the long-term and short-term propagation losses, compares it with the reference power and updates the transmit power of MS. After updating all MSs' transmit power, total interference is calculated by collecting transmit powers from all the mobile stations to the zeroth BS, taking into account the signal power attenuation by propagation loss. In the flowchart and the simulation code, the measurement of total interference and power control is performed in the same function. The collected total interference is compared with the reference value for determining the system outage. The main flowchart is shown in Figure 4.1. Each process in the flow chart will be described in the following subsection.

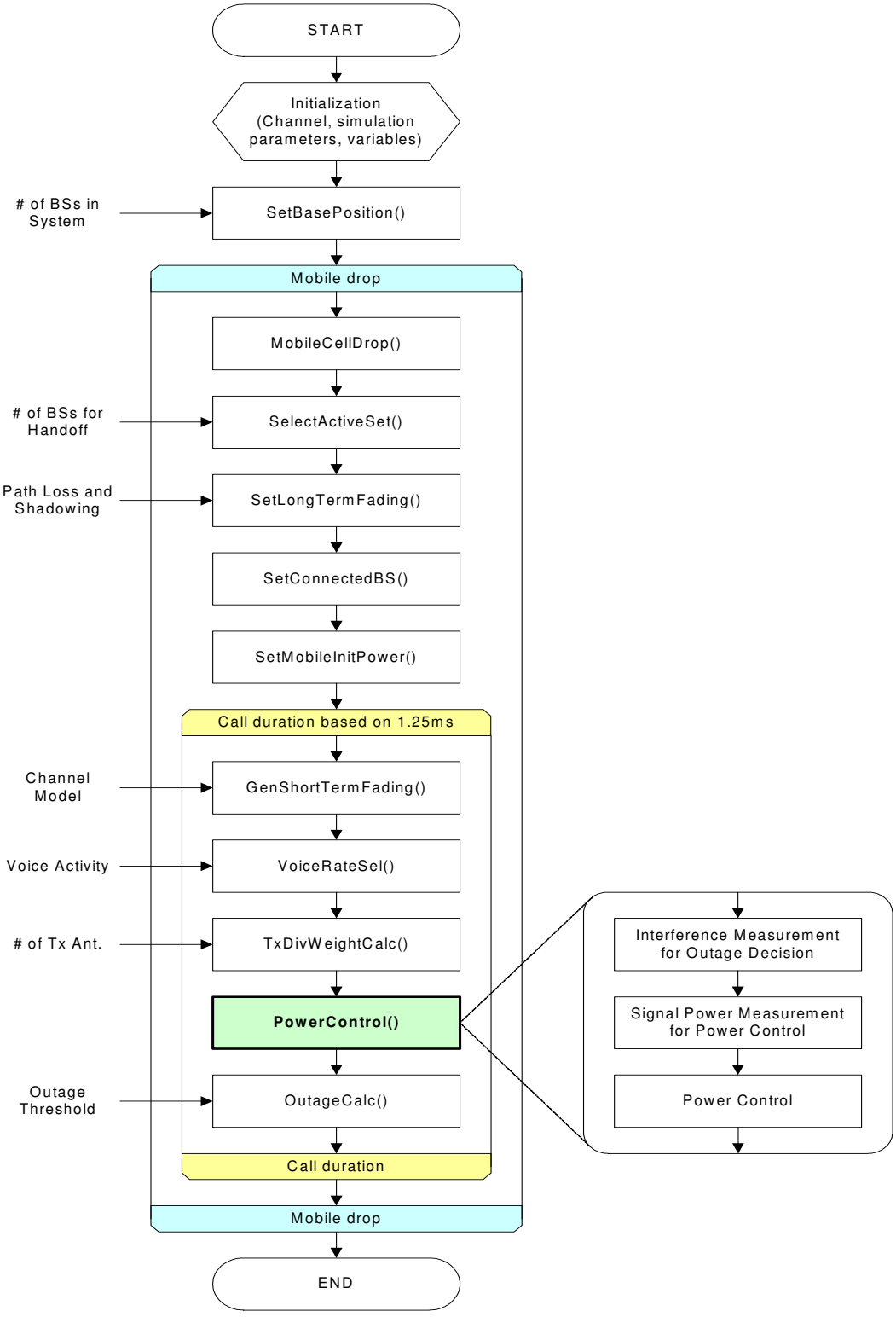

Figure 4.1: Flow chart of the system simulator

4.4.1 Initialization

In this process, the following operations are performed.

- Memory allocation
- Simulation parameter setting: refer to Table 4.1 for the changeable parameters.
- Channel initialization: the filter to generate Rayleigh fading is initialized.
- Initialization of mobile station structure: the parameters associated with each MS are initialized. Each MS can have different parameters, such as the number of transmit antennas, the number of BS receive antennas, mobile velocity and channel environments. However, all MSs are currently set to have the same parameters for the simplicity of the simulation.

4.4.2 Setup the position of base stations

In this process, the positions of all BSs in the system are determined in the system. The position of BS is given by the X-Y coordinates based on the origin where the zeroth BS is located as shown in Figure 2.1.

4.4.3 Drop the mobile station

In this process, the positions of MSs in each cell are determined by dropping the MSs uniformly in a cell. The positions of MSs are given by the X-Y coordinates based on the origin which is the position of the zeroth BS just as the determination of the positions of BSs. The simplest way to generate the position of MSs in each cell is to add the position of each BS to the position of MSs generated by the uniform distribution satisfying Equation (4.1) corresponding to the zeroth cell. Then, by adding the position of each BS, we can distribute MSs into the entire area of the system.

$$(x,y) = \begin{cases} |y| < \dfrac{\sqrt{3}}{2} & \text{for } |x| < 0.5 \\ |y| < \sqrt{3}\,(1-|x|) & \text{for } |x| \geq 0.5 \end{cases} \tag{4.1}$$

4.4.4 Selection of active set

In this process, the active set of each MS are determined based on the distance between each MS and the surrounding BSs. Referring to Figure 4.2, the active set of MS1 will be BS1, BS2, and BS3 and that of MS2 will be BS2, BS3, and BS4. MS is power controlled by the BS which provides the least average attenuation (defined as the connected BS) among the active set.

4.4.5 Generating the long-term fading: SetLongTermFading

In this process, the large-scale propagation losses between each MS and all BSs in the system are generated according to path loss and log-normal shadowing loss. The path loss is proportional to the m^{th} power of the distance between MS and BS. On the other hand, the log-normal shadowing is dependent of antenna heights of BS and MS, and terrain features such as building obstructions and trees surrounding BS and MS. Let us suppose that cellular system is deployed in urban area, where the antenna height of BS is relatively higher than that of MS and MS is surrounded by lots of local clutter of scatters such as buildings and trees. It has been reported that log-normal shadowing losses between different BSs observed at MS have some correlation while log-normal shadowing losses between different MSs are uncorrelated when those are observed at BS unless the angle of arrival difference are small [10, 66-68]. Therefore, in this simulator, correlated log-normal shadowing losses are modeled as shown in Figure 4.3. That is, log-normal shadowing losses from an MS to BS0 and BS1 are correlated. However, log-normal shadowing losses from BS0 to MS1 and MS2 are uncorrelated.

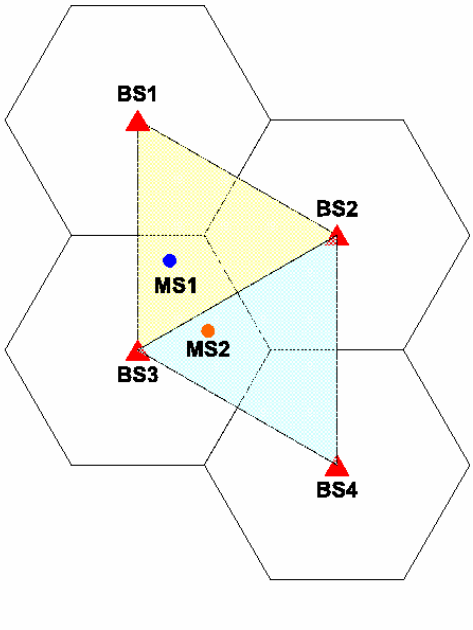

Figure 4.2: Active set

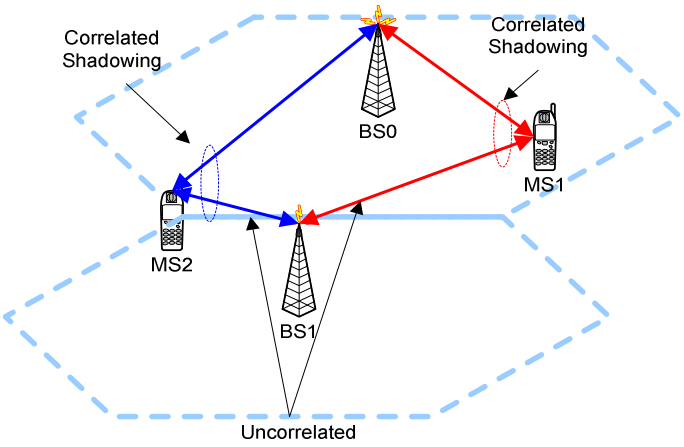

Figure 4.3: Correlated log-normal shadowing

4.4.6 Select the connected base station: SetConnectedBS

In this process, each MS chooses one BS, which provides the least attenuation among its active set based on the large-scale propagation loss including log-normal shadowing and path loss.

4.4.7 Open-loop power control: SetMobileInitPower

In this process, the initial transmit power of each MS is determined based on the large-scale propagation loss just as the open loop power control in the system. In the simulation, the initial transmit power is set to the inverse of the large-scale propagation loss. This helps initialize power control before counting the system outage. This initial power control insures the initial transmit power reflects the current channel gain so that system outage statistics are representative of steady state behavior.

4.4.8 Generating the short-term fading channel: GenShortTermFading

In this process, the multipath Rayleigh fading is generated for all possible links in the system. To generate Rayleigh fading samples, the well-known filtered Gaussian method [45] is used. For the generation of the correlated fading samples, the method proposed in [69] is used. In [69], the desired covariance matrix for the correlated Rayleigh fading sample is defined and is translated into the covariance matrix for colored complex Gaussian samples. Using the covariance matrix for the colored complex Gaussian sample, we can determine the transformation matrix for the independent complex Gaussian samples by the Cholesky decomposition

4.4.9 Voice activity: VoiceRateSel

In this process, the voice activity is determined. Two kinds of voice activity model are implemented; ON/OFF traffic and variable rate traffic. ON/OFF traffic model assumes

that an MS transmits signal discontinuously with a certain probability. Variable rate traffic is to model the practical systems such as IS-95 or cdma2000, where the data rate is changed according to the voice activity which subsequently changes the transmit power. Variable rate traffic can be easily modeled by Markov chain with a state transition probability [70]. In this simulator, Markov chain is not implemented, but the data rate is determined according to the state probability of each state. The state probability for the variable rate voice traffic is shown in Table 4.2.

Table 4.2: The state probability to model the variable rate voice traffic

Data rate	State probability	Transmit power ratio
9600	0.294	1
4800	0.039	0.5
2400	0.072	0.25
1200	0.595	0.125

4.4.10 Transmit diversity: TxDivWeightCalc

In this process, the transmit weight vector is calculated if the transmit diversity is enabled. The optimum transmit weight vector is the eigenvector corresponding to the largest eigenvalue of the matrix $\mathbf{H}^H\mathbf{H}$, where $\mathbf{H}$ is the channel coefficient matrix of each diversity and multipath branches and $(\bullet)^H$ represents Hermitian transpose operation as described in the section 2.2.3. For the equal gain combining, the transmit weight vector is calculated by taking only the phase information from the optimum weight vector as follows

$$w_{k,egc} = \frac{w_{k,opt}}{|w_{k,opt}|}, \quad k = 1,2 \tag{4.2}$$

where $w_{k,egc}$ and $w_{k,opt}$ are transmit weight coefficients of the equal gain closed-loop transmit diversity and the optimum closed-loop transmit diversity, respectively, for the k^{th} transmit antenna.

4.4.11 Fast power control: PowerControl

In this process, the total interference is measured at the zeroth BS, and the received power at each BS, which each MS is connected to, is measured for the power control for all MSs. Based on the received power at each BS, the transmit power of each MS is updated. The measurement methods for total interference and the received power are described in the following sections in more detail.

Two power control methods are implemented; one is the channel inversion and the other is the fixed step power control. The channel inversion power control for transmit power of MS is determined by the inverse of the channel propagation loss as follows

$$P_{transmit} = \frac{1}{(L_F \cdot S_F)} \tag{4.3}$$

where L_F and S_F are the long-term fading loss, which includes the log-normal shadow fading and path losses, and the short-term fading loss, respectively. This channel inversion power control is implemented to verify the analysis results where perfect power control is assumed.

The fixed step power control is also implemented to emulate the realistic power control scheme, where the received signal from MS are compared with the reference value and the power control command is fed back to the MS to change the transmit power of MS.

4.4.12 Counting the system outage: OutageCalc

In this process, the system outage is determined by comparing the amount of interference measured at the zeroth BS and the outage threshold. The outage probability is calculated by the number of system outage divided by total simulation runs.

4.5 Calculation of Received Signal and Interference Power

4.5.1 Received signal

The received signal power calculation is different according to whether the transmit diversity is applied or not. The received signal power with receive diversity only is calculated as

$$P_R = P_T \cdot \alpha \cdot \beta \cdot \sum_{i=1}^{L_r} \sum_{j=1}^{L_m} \left| h_{i,j} \right|^2 \tag{4.4}$$

where P_T is the transmit power of mobile station, α is the voice activity, β represents the long-term propagation loss and $h_{i,j}$ is the short-term fading channel response of j^{th} multipath component at i^{th} receive antenna with L_m multipaths and L_r receive antennas. On the other hand, the received signal power with both receive diversity and transmit diversity is calculated as

$$P_R = P_T \cdot \alpha \cdot \beta \cdot \sum_{i=1}^{L_r} \sum_{j=1}^{L_m} \left| h_{i,j,1} \cdot w_1 + h_{i,j,2} \cdot w_2 \right|^2 \tag{4.5}$$

where w_1 and w_2 are the weight vectors for two transmit antennas and $h_{i,j,1}$ and $h_{i,j,2}$ are the short-term fading channel response of the j^{th} multipath component at the i^{th} receive antenna corresponding to the first and second transmit antenna, respectively. The transmit weight vectors, w_1 and w_2 will be obtained based on maximizing the received signal power at the receiver. However, in calculating the received signal power for the power control, voice activity is not applied (that is, always $\alpha = 1$ in calculating the received signal power) for the proper power control operation when the voice is deactivated. The voice activity is applied only to the total interference measurement for checking the system outage.

On the other hand, when the resolvable multipath combining is enabled, the fractional multipath components among L_m multipath components will be combined. The resolvable multipath components are determined by the sampling resolution of the receiver and are the same as those implemented in the link simulator. The resolvable

multipath components for Pedestrian channel A and Vehicular channel A are shown in Table 4.3. Note that the resolvable multipath combining is also applied to the intracell interference measurement since we have assumed that the intracell interference is not changed in terms of its mean. However, in the intracell interference measurement, all possible multipaths are taken into account.

Table 4.3: Resolvable multipath components for Pedestrian and Vehicular channel A

Channel model	Resolvable multipath	Total number of multipath
Pedestrian channel A	1 (1st path only)	4
Vehicular channel A	4 (1st, 2nd, 4th, 6th paths)	6

4.5.2 Interference power

Total interference power is measured at the zeroth BS as shown in Figure 4.4. Based on the assumption in the analytical framework of Chapter 2, interference measurement will be different between intercell interference and intracell interference. Theoretically, the interference cannot be differentiated by intracell and intercell. However, for the purpose of validating the analytical results presented in Chapter 2, the measurement method between the intracell and intercell interference is distinguished in the simulator. For the purpose of validating the results shown in Chapter 3, the measurement method does not need to be distinguished.

Intercell interference is calculated as

$$I_{oc} = \sum_{i=1}^{N} \sum_{j=1, j \notin BS_0}^{K} \left(P_{T(i,j)} \cdot \alpha_{i,j} \cdot \beta_{i,j} \sum_{k=1}^{L_m} \left| h_{i,j,k} \right|^2 \right) \tag{4.6}$$

where N and K are the number of base stations in the entire system and the number of users in a cell, respectively, $P_{T(i,j)}$, $\alpha_{i,j}$ and $\beta_{i,j}$ are the transmit power, voice activity factor, and long-term propagation loss of the j^{th} user in the i^{th} cell, respectively, and $h_{i,j,k}$ represents the short-term fading channel response of the k^{th} multipath component for the j^{th} user in the i^{th} cell. On the other hand, the intracell interference with the receive diversity only is calculated as

$$I_{in} = \sum_{i=1}^{N} \sum_{j=1, j \in BS_0}^{K} \left(P_{T(i,j)} \cdot \alpha_{i,j} \cdot \beta_{i,j} \cdot \sum_{k=1}^{L_r} \sum_{l=1}^{L_m} \left| h_{i,j,k,l} \right|^2 \right) \tag{4.7}$$

where $h_{i,j,k,l}$ represents the short-term fading channel response of the l^{th} multipath component at the k^{th} receive antenna for the j^{th} user in the i^{th} cell. The intracell interference with both the receive diversity and transmit diversity is calculated as

$$I_{in} = \sum_{i=1}^{N} \sum_{j=1, j \in BS_0}^{K} \left(P_{T(i,j)} \cdot \alpha_{i,j} \cdot \beta_{i,j} \sum_{k=1}^{L_r} \sum_{l=1}^{L_m} \left| h_{i,j,k,l,1} w_{i,j,1} + h_{i,j,k,l,2} w_{i,j,2} \right|^2 \right) \tag{4.8}$$

where $h_{i,j,k,l,1}$ and $h_{i,j,k,l,2}$ are the short-term fading channel responses of the l^{th} multipath component at the k^{th} receive antenna for the j^{th} user in the i^{th} cell, corresponding to the first and second transmit antenna, respectively, and $w_{i,j,1}$ and $w_{i,j,2}$ are the antenna weights of the first and second transmit antenna, respectively, for the j^{th} user in the i^{th} cell. The total interference is the sum of I_{in} and I_{oc} calculated by Equation (4.6), (4.7), and (4.8). Then, the total interference is directly compared with the reference value for deciding the system outage without normalization, since the reference value for the power control is set to '1'.

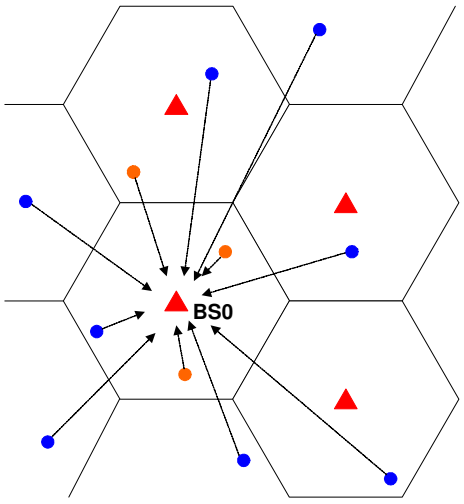

Figure 4.4: Interference measurement

4.6 Simulation Results

In this section, a set of simulation results, which can show the impact of transmit diversity technique at the handset on the uplink DS/CDMA system capacity, with practical scenarios, is present and is compared with the analytical results presented in Chapter 2. First, we verify the validity of both simulation and analytical results by comparing the simulation results with the analytical results obtained under the same condition. Then, we present several simulation results with practical scenarios such as feedback delay and errors, resolvable multipath combining, transmit power constraint, imperfect power control and so on, and compare them with the basic results without errors. System parameters for the simulations basically the same as the analytical analysis and are summarized in Table 4.4

Table 4.4: System parameters

Parameters	Value
Spreading bandwidth (W)	1.25 MHz
Data Rate (R_b)	8 Kbps
Voice activity (ν)	0.38
Target E_b / I_0	5.6 dB
Shadowing correlation between BSs	0.5
Log-normal shadowing	$\sigma = 8\text{dB},\ m = 0$
Path loss exponent	$u = 4$
Soft handoff	3-way
Diversity order (M)	1, 2, 4, 8
Fade margin	20 dB

Figure 4.5 shows the basic simulation results, compared with the analysis results for one-path Rayleigh fading channel where mobile velocity is set to 3 Km/h and perfect power control like channel inversion is assumed. It is observed that the simulation results without any diversity (in both spatial and time) are matching well with the analytical estimates. However, it is observed that the simulation results with the spatial diversity

shows small deviations from the analytical estimates, which is expected to come from the log-normal approximation in the analysis. Lognormal approximation for the sum of interferences is based on the occasional peak power of the interference occurred by the perfect power control. However, applying spatial diversity will reduce those peak powers, which results in small differences between the analysis and simulation results. In Figure 4.6 and Figure 4.7, the complimentary cumulative distribution functions (CCDF) of interference collected from the simulator without spatial diversity and with spatial diversity, respectively, are shown and are compared with the theoretical log-normal distributions with the estimated mean and variance from the simulation results. It can be observed that the log-normal approximation deviates from the simulated results at the small probability below 10^{-3}. If our typical interest region is focused on the probability around 10^{-2}, we can still apply the log-normal approximation regardless of this deviation just as other literatures [12, 14].

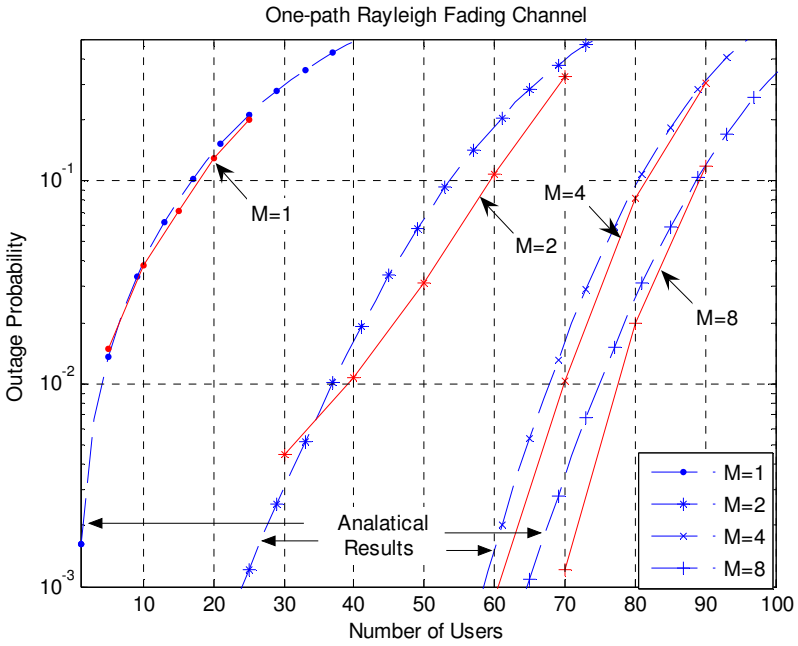

Figure 4.5: Simulation results for one-path Rayleigh fading channel

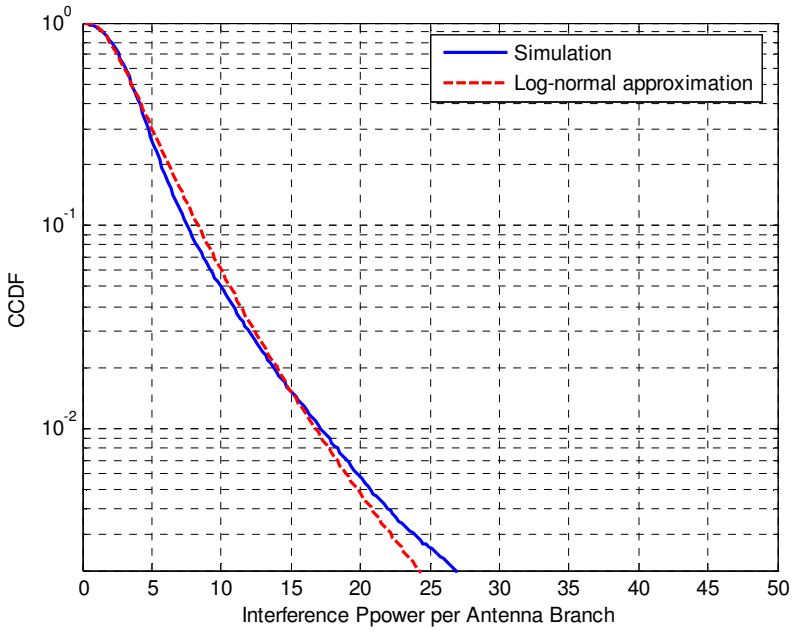

Figure 4.6: Log-normal approximation without diversity

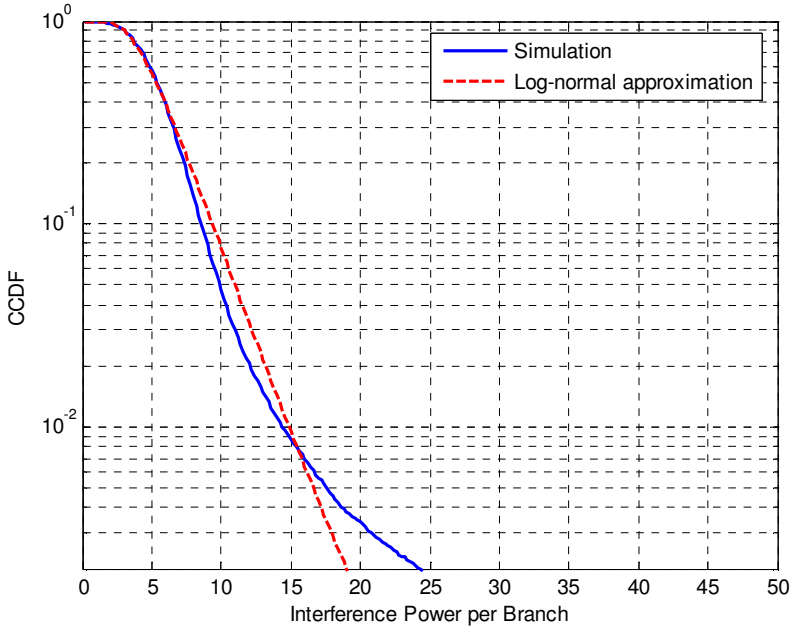

Figure 4.7: Log-normal approximation with spatial diversity

Now, let us consider the Pedestrian A channel of the standard specified channel. The simulation results and analytical results are compared in Figure 4.8, where the mobile velocity is set to 3 Km/h and fixed step power control is performed by changing the transmit power of MS in the unit of 0.5 dB step size according to the received signal power. All multipath components in the channel model are combined in the simulations for the sake of comparison with the analytical estimates where all multipath components are combined at the receiver. Furthermore, in this simulation, the received signal power from MSs at each BS is measured based on the approximated analytical expression developed in Equation (2.32) for comparison between the analytical results and simulation results, with standard specified channel profiles. Even though the log-normal approximation for both spatial and multipath diversity is only valid for the higher outage probability, usually, above 10^{-3}, it is observed that the analytical results (dotted line) are relatively well-matched with the simulation results (solid line). On the other hand, the simulation results with the exact implementation of transmit diversity show more deviation from the analytical results due to the increased number of multipath components as compared to 1-path Rayleigh fading channel model as shown in Figure 4.9, where 'T' denotes the number of transmit antennas. Since transmit weight vector tries to exploit higher dimension in signal space to maximize the signal-to-noise ratio at the receiver in multipath fading channel, the actual performance gains of using transmit diversity diminish as compared to the analytical estimates. However, these differences between the results of actual transmit diversity and analytical estimates are tolerable taking into account the number of users, and are reduced as the diversity order increases.

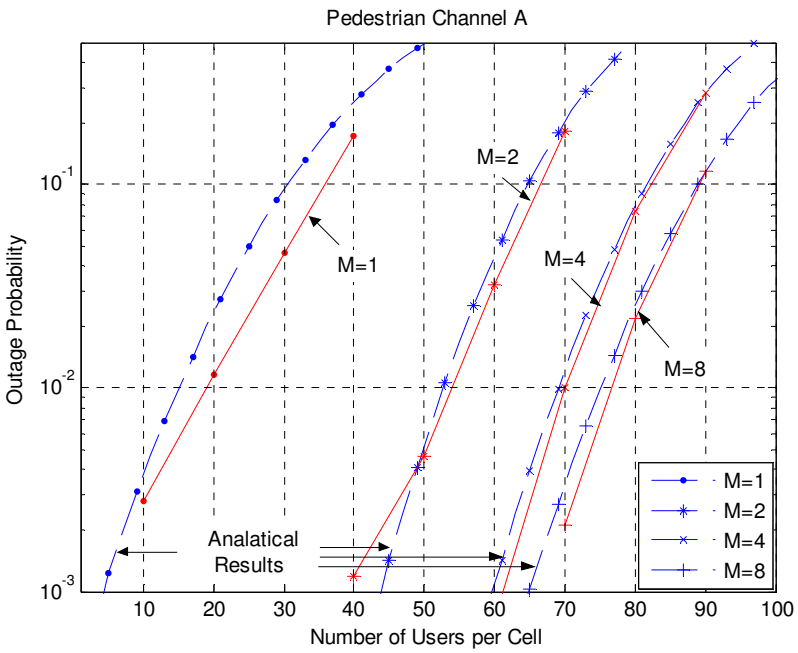

Figure 4.8: Outage probability vs. the number of users per cell for Pedestrian A channel

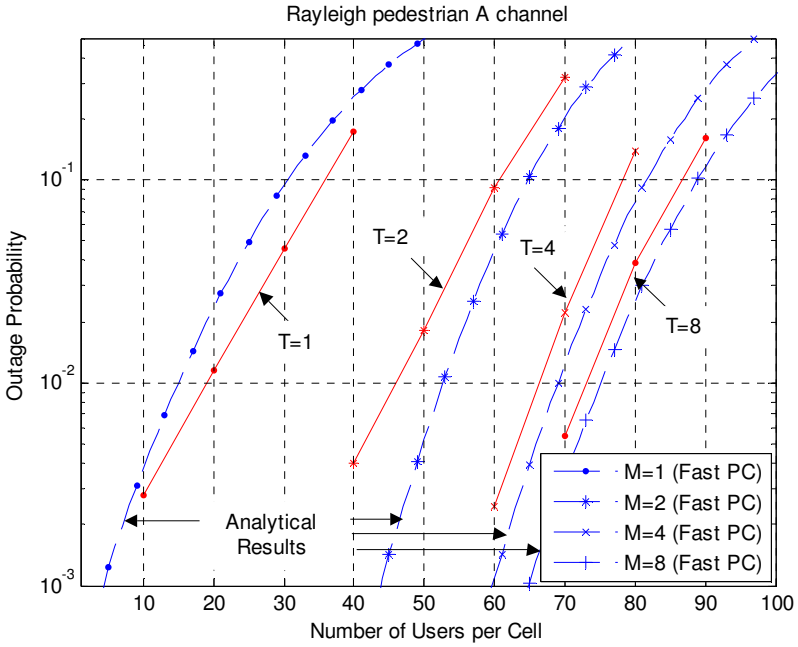

Figure 4.9: Outage probabilities vs. the number of users per cell for Pedestrian A channel with transmit diversity ('T': the number of transmit antennas)

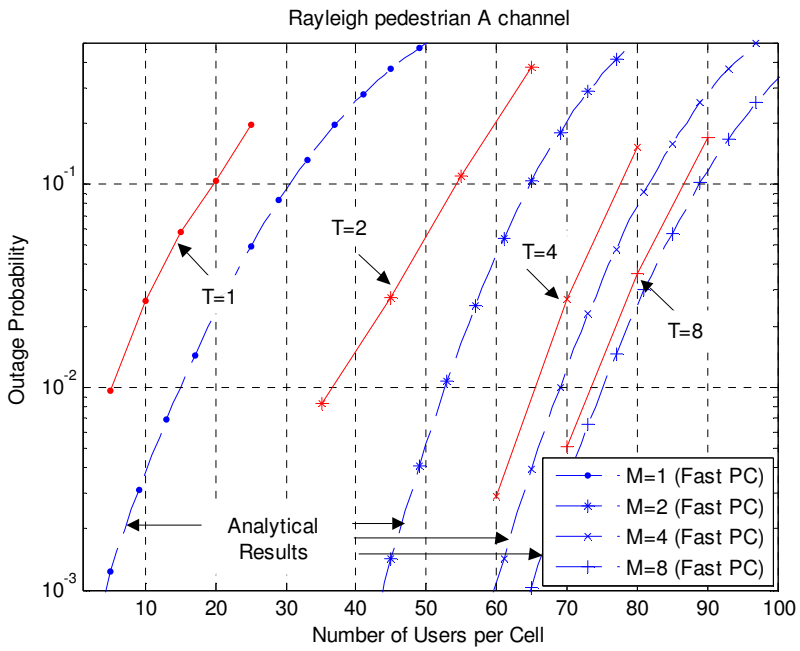

Figure 4.10: Outage probability vs. the number of users per cell for Pedestrian A channel with resolvable multipath combining ('T': the number of transmit antennas)

For more practical situations, let us consider the resolvable multipath combining scheme at the receiver. The simulation results for Pedestrian A channel with resolvable multipath combining are shown in Figure 4.10. From now on, the calculation of the received signal power from MSs at BS follows Equation (4.6), (4.7), and (4.8). Just as before, the dotted lines are the analytical results where all multipath components in the Pedestrian A channel model are combined. It is observed that the simulation results show more deviation from the analytical estimates. However, since the resolvable multipath component is only one in Pedestrian A channel, the system performance are very similar to those in 1-path Rayleigh fading channel in Figure 4.5. Due to the partial energy capturing of received signal at the receiver from combining only the resolvable multipath components in the simulations, the system capacities are observed to is a little bit decreased as compared with those in one-path Rayleigh fading channel. However, one resolvable path in Pedestrian A channel is a dominant path, that is, its power is much larger than that of other irresolvable multipath components; hence, capacity differences are not so large.

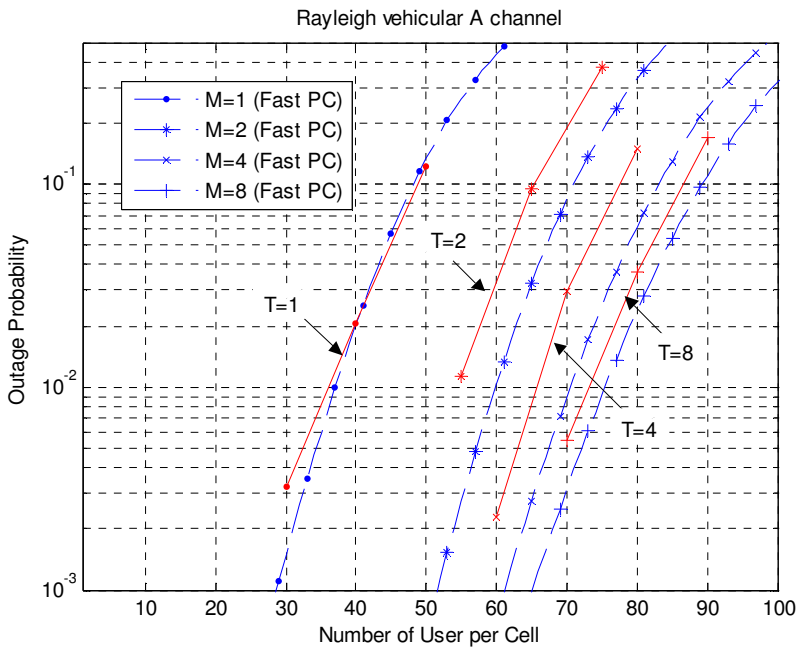

Figure 4.11: Outage probability vs. the number of users per cell for Vehicular A channel, low mobility, and all multipath combining

For Vehicular A channel, it is observed that the similar results to the results of Pedestrian A channel. Figure Figure 4.11 shows the simulation results for Vehicular A channel. Fixed step power control and feedback delay of two power control group is presumed. Furthermore, the mobile velocity is assumed to be 3 Km/h so that power control loop and transmit weight vector feedback can compensate for the channel variation. As expected, the simulation results with transmit diversity show some deviations from the analytical estimates because the dimension of transmit weight vector is smaller than that of channels between MS and BS for transmit weight vector to compensate for. Taking into account that dimension of transmit weight vector smaller than channel dimension, analytical estimates shows relatively accurate estimates.

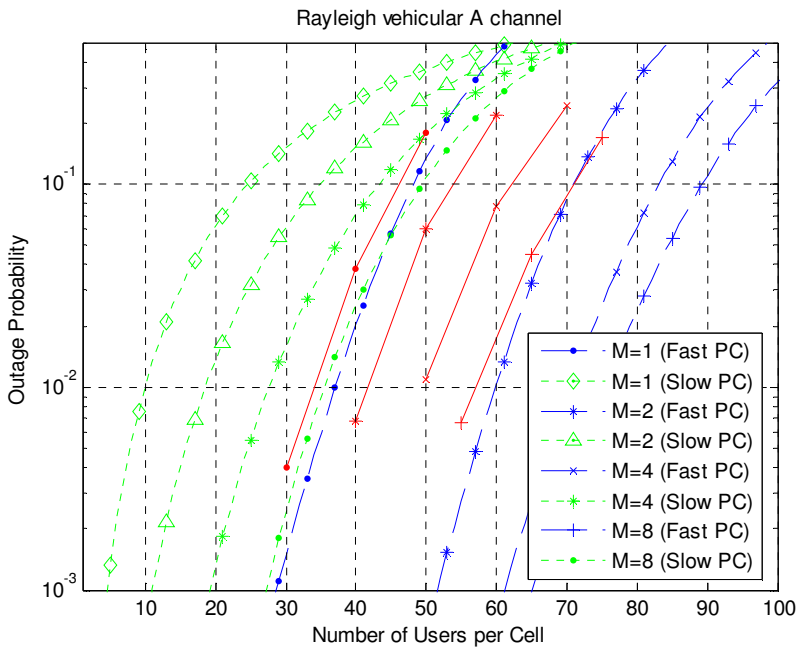

Figure 4.12: Outage probability vs. the number of users per cell for Vehicular A channel, high mobility, and all multipath combining

On the other hand, if we consider the higher mobility, the analytical estimates would show more deviations from the simulation results because mobility is not considered in the analytical results. However, those estimate error might be bounded by the slow power control results as mentioned in Chapter 2. Figure 4.12 shows the simulation results with high mobility of MS, where the mobile velocity is assumed to 30 Km/h. Simulation results shows much more deviations from the analytical estimates due to the feedback error of power control and transmit weight vector, but are much better than the analytical estimates with slow power control. In addition, transmit diversity still shows capacity improvements as diversity order increases even though the feedback delays and errors of power control and transmit diversity weight vector due to the high mobility as observed in analytical estimates of slow power control. Furthermore, the performance degradation due to high mobility gets more severe as mobile velocity increases.

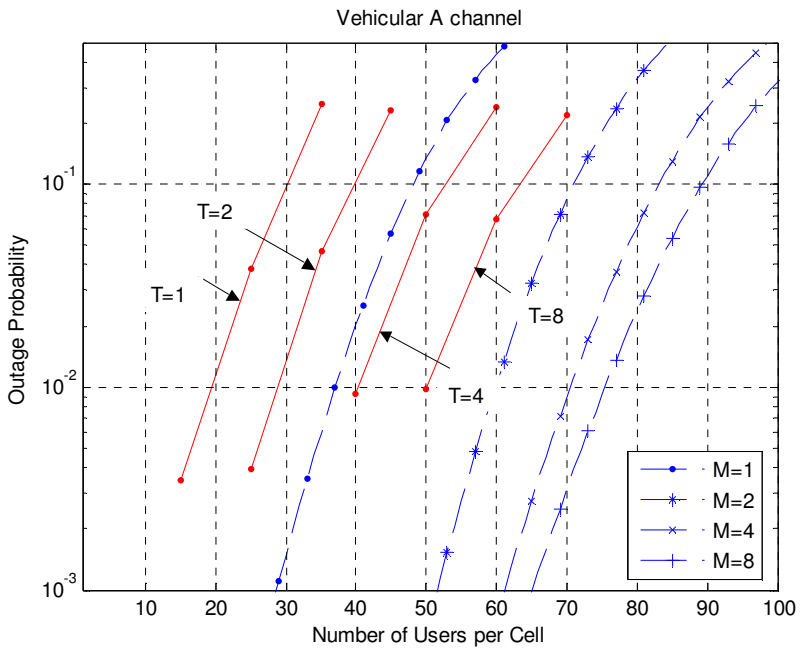

Figure 4.13: Outage probability vs. the number of users per cell for Vehicular A channel, high mobility, and resolvable multipath combining

Now, let us consider the resolvable multipath combining in Vehicular A channel. Figure shows the simulation results for Vehicular A channel with resolvable multipath combining, where the fixed step power control and the mobile velocity of 30 Km/h is assumed. Feedback delay is assumed to be two power control group. However, different from Pedestrian A channel, there are four resolvable multipath components in Vehicular A channel, but one dominant path as shown in Table 4.3. Hence, the system capacity would be more severely degraded by uncaptured channel power due to resolvable multipath combining scheme at the receiver as shown in Figure 4.13. Nevertheless, performance improvements by transmit diversity is still observed just as analytical estimates of slow power control.

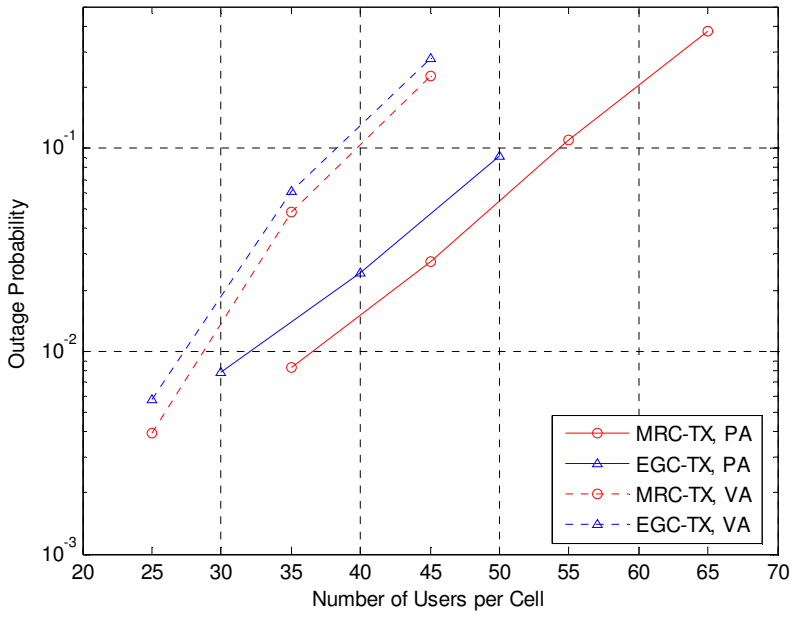

Figure 4.14: Outage probability vs. the number of users per cell with equal gain transmit diversity

In Figure 4.14, performances of equal gain transmit diversity is compared with those of maximal ratio transmit diversity with two transmit antennas, where 'MRC-TX' denotes the maximal ratio transmit diversity, 'EGC-TX' denotes the equal gain transmit diversity, 'PA' denotes the Pedestrian A channel, and 'VA' denotes the Vehicular A channel. Mobile velocity is assumed to be 3 Km/h for the Pedestrian A channel, and is assumed to be 30 Km/h for the Vehicular A channel. Furthermore, resolvable multipath combining and fixed step power control is assumed. Equal gain transmit diversity is a sort of sub-optimum technique in such a case that the amount of feedback information is limited so that only phase information is fed back to the transmitter. As expected, the performances of equal gain transmit diversity is worse than those of maximal ratio transmit diversity in both Pedestrian A channel and Vehicular A channel. However, it is observed that the performance degradation is smaller in Vehicular A channel than in Pedestrian A channel. It is thought to be due to that phase information is more robust against to errors than the amplitude information, and thus phase modulation is preferable than amplitude modulation.

A more practical case is when there is correlation between transmit antenna branches. Generally, if the multiple transmit antennas are separately placed more than half wavelength (for handheld terminal, a quarter wavelength assuming rich scattering environment), each signal from multiple antennas is known to experience independent fading. In practice, however, there is always some amount of correlation even if antenna spacing is more than half wavelength. So, it is necessary to evaluate the impact of correlation on the performance of transmit diversity technique. Figure 4.15 and Figure 4.16 show the outage probability vs. the number of users per cell in Pedestrian A channel and Vehicular A channel, respectively, for several correlation coefficients, ρ. Just as before, fixed step power control and resolvable multipath combining is assumed, and mobile velocity is assumed to be 3 Km/h for Pedestrian A channel and is assumed to be 30 Km/h for Vehicular A channel. Since there is only one resolvable path in Pedestrian A channel, the performance degrades more quickly as the correlation increases, as compared with those in Vehicular A channel which has four resolvable multipath components which are independent of each other. From these results, it is expected that the impact of correlation among transmit antennas on the system capacity will diminish as the number of independent multipath components increases. Furthermore, in Figure 4.16, it is observed that the fully correlated transmit antennas show better performance than partially correlated transmit antennas. Since the number of multipath in the vehicular channel is large, the dimension of channel space is larger than the dimension of transmit weight vector. Thus, the obtained transmit weight vector cannot fully compensate for the channel space even if it maximize the received signal to noise ratio. However, correlation between transmit antennas works on reducing the channel space. Hence, performance of transmit antennas improve as the correlation between transmit antennas increases. For an extreme case in which the correlation between transmit antennas is '1', the dimension of channel space reduce to '1', and closed loop transmit diversity will behave like beam-forming. The array gain will provide an SNR expected for beam-forming, and this SNR will be better than that of closed loop transmit diversity with several multipath components.

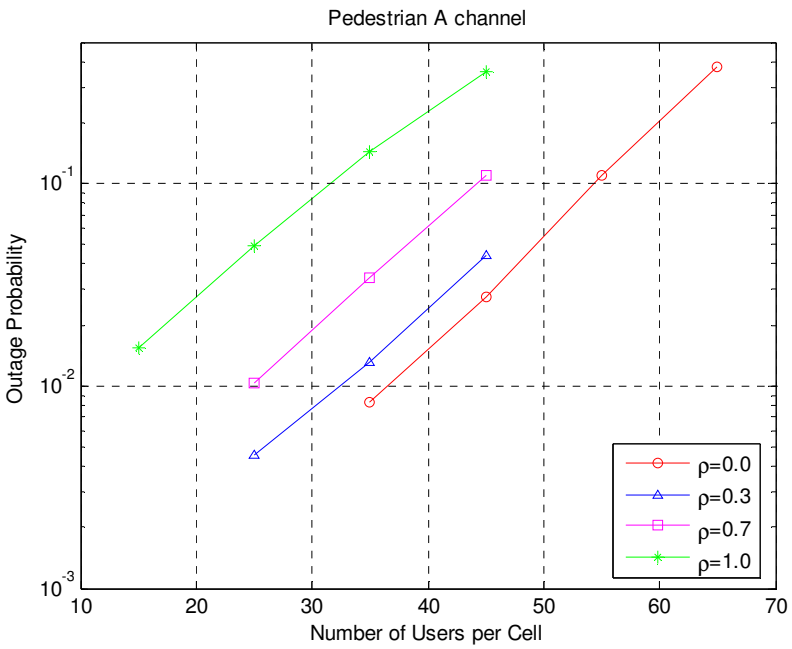

Figure 4.15: Outage probability vs. the number of users per cell with correlated transmit antennas for Pedestrian A channel

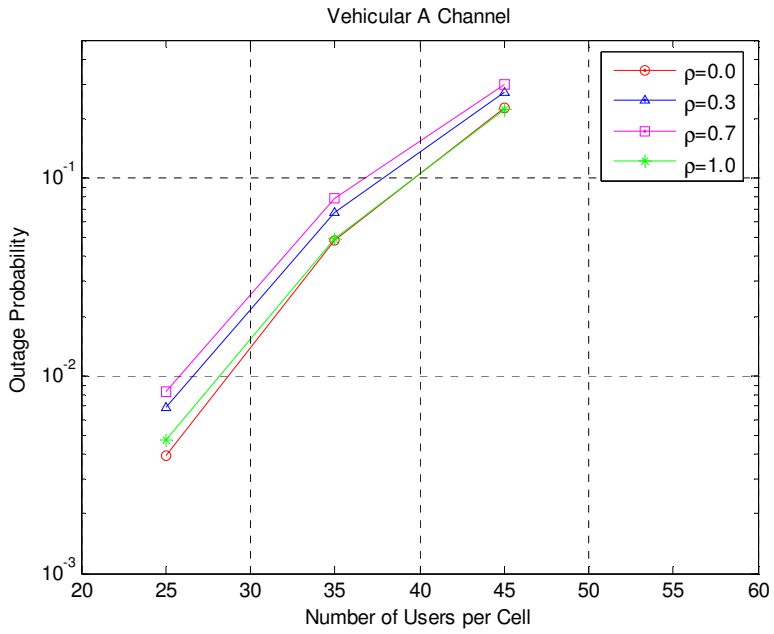

Figure 4.16: Outage probability vs. the number of users per cell with correlated transmit antennas for Vehicular A channel

4.7 Chapter Summary

In this chapter, the system level simulator for the uplink DS/CDMA cellular system has been developed to validate the analytical results and to evaluate the impact of several practical implementation issues on the system capacity. Practical implementation issues listed below have been taken into account and evaluated:

- Imperfect power control: it includes the feedback delay and error of power control command. Its impact on the system capacity are taken into account along with feedback delay of transmit weight vector and resolvable multipath combining. It is observed that the impact of imperfect power control in the vehicular channel with high mobility is more pronounced than that in the pedestrian channel with low mobility.

- Feedback delay of transmit weight vector: feedback delay of transmit weight vector deteriorates the performance of closed loop transmit diversity. Similar to the imperfect power control, the impact of the feedback delay of transmit weight vector in the vehicular channel with high mobility is more pronounced than that in the pedestrian channel with low mobility.

- Resolvable multipath combining: it only combines the resolvable multipath components in multipath intensity profile; hence, the overall system performances are degraded due to the uncaptured channel power and reduced multipath diversity. On the other hand, it reduces the channel space where transmit weight coefficients are calculated; hence, the performance of transmit diversity improves since available channel power is more concentrated on the largest eigenvalue.

- Mobile velocity: for closed-loop transmit diversity technique, mobile velocity is a critical factor which causes performance degradation along with the feedback delay of any closed loop operation in the system. In vehicular channel

environment, mobile velocity of 30 Km/h cause severe degradations of system capacity as compared to the same environments with a slow mobile velocity.

- Equal gain transmit diversity: when the amount of feedback is constrained, equal gain transmit diversity, which is sub-optimum, can be useful. Its performance is slightly degraded as compared with the performance of the optimum transmit diversity. However, it provides a comparable performance to optimum transmit diversity.

- Correlated transmit antennas: correlated transmit antennas are another source degrading the performance of transmit diversity. However, as the eigenspread of composite channel matrix increases, correlated antennas provide array gain, resulting in better performance than that of a system which tries to exploit transmit diversity.

Chapter

5 Soft Handoff in Downlink DS/CDMA Cellular Systems with MIMO

5.1 Introduction

Soft handoff in the uplink of DS/CDMA cellular systems is known to be helpful in improving system capacity, coverage and link performance. On the other hand, studies have shown that soft handoff in the downlink deteriorates system capacity because multiple cells participating in the soft handoff allocate their fractional power to the same user [11, 19-25]. However, these studies overlooked the effects of transmit power reduction from combining of multiple copy of signal from the multiple cells. In addition, research [26, 71] shows that there exists a tradeoff between power reduction by soft handoff and fractional power allocation to the same users by multiple cells: this affects the system capacity. However, most papers resort to the simulation [22, 23, 25, 26], which usually takes too much time to obtain the reliable results. A few studies have used the analytical analysis [11, 19, 21, 24, 71]; however, the results only provide the performance bounds for the system capacity [11, 19] and do not explain the relationship between the soft handoff capacity and power reduction by soft handoff [24]. In addition, some studies take into account only large-scale fading for the simplicity [11, 21, 71],

which is not sufficient to fully understand system performance. Finally, all the studies referenced above did not take into account MIMO in the analysis of the system performance.

- ***Contributions***

The objectives of this research are (a) to develop an analytical framework for the analysis of the system performances of downlink DS/CDMA cellular system with MIMO and soft handoff, (b) to demonstrate how MIMO affects the system behaviors in terms of downlink system capacity, (c) to provide the better understanding of the relationship between the power reduction and the capacity impairment by soft handoff, and (d) to investigate the impact of MIMO on power, system capacity, and soft handoff in the downlink.

- ***Organization***

The rest of this chapter is organized as follows. In section 5.2, the system model for the analysis described. In section 5.3, the analytical expression for the fractional power of BS allocated to an MS is derived taking into account MIMO and soft handoff. Section 5.4 shows how to evaluate the statistics of the fractional power of BS allocated to an MS derived in the previous section. Section 5.5 presents selective numerical results. Finally, the main points of this chapter are summarized in section 0.

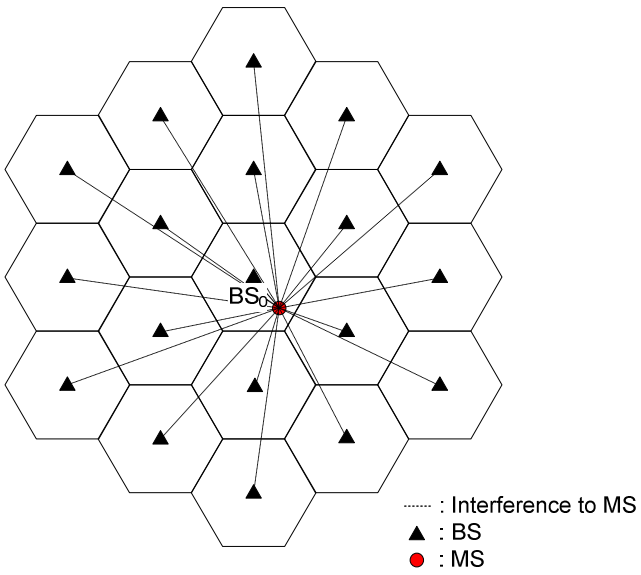

Figure 5.1: Cell layout and interference in the downlink DS/CDMA cellular system

5.2 System Model

In the following subsections, the system models, including the cellular architecture of downlink DS/CDMA system, soft handoff process and MIMO will be described in detail.

5.2.1 Cellular architecture

The cellular communication system for our analysis will be modeled by the well-known uniform hexagonal layout with a BS at the center of every cell. The entire system consists of two tiers of hexagonal cells which surround the center cell as shown in Figure 5.1. It is assumed that MSs are uniformly distributed in the system and all BSs transmit at the same total power level. Alternatively, an MS receives interference from a few concentrated large sources (BSs) rather than many distributed small ones (MSs). Soft handoff process is assumed to be similar to US IS-95 standard [50], where soft handoff region is determined by parameters such as T_{ADD} and T_{DROP} as shown in Figure 5.2, where T_{ADD} is the threshold to add an BS to the active set, and T_{DROP} is the threshold to drop an BS from active set. However, in our analysis, the handoff region is defined based on the distance from the BS for analytical simplicity. That is, an MS located outside the

handoff boundary R_h, is considered to be in soft handoff mode with neighboring BSs as shown in Figure 5.3. Hence, MSs at the triangle region in Figure 5.3 would communicate BSs, A, B, and C during the soft handoff. This assumption is a viable one considering that the pilot signal measurements are averaged out over a period of time. This averaging period is assumed to be long enough to counter slow and fast fadings, leaving path loss due to distance only. Hence, the active set is defined as the multiple nearest BSs for the MSs in the soft handoff region, the same as that in the uplink. However, unlike the soft handoff in the uplink, all BSs in the active set allocate a fractional power for the same MS which then combines these signals using maximal ratio combining (MRC).

5.2.2 Outage probability

The total transmit power on the downlink of DS/CDMA cellular system is shared among multiple users [11], for which a small fraction of this power is allocated to the i^{th} MS, denoted by ϕ_i. Since the total available power at the BS is limited, we impose the following constraint on the summation of the fractional powers allocated to all MSs:

$$\sum_{i=1}^{K} \phi_i < \eta \tag{5.1}$$

where K is the number of users connected to the BS, and η is the available power for the user traffic excluding the power allocated to the common channels such as pilot, paging, and sync channels.

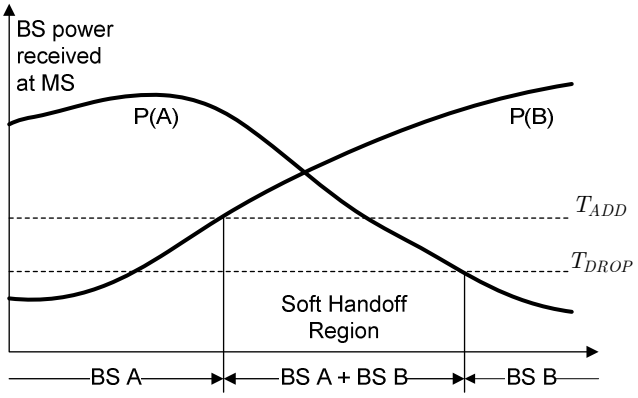

Figure 5.2: Handoff process

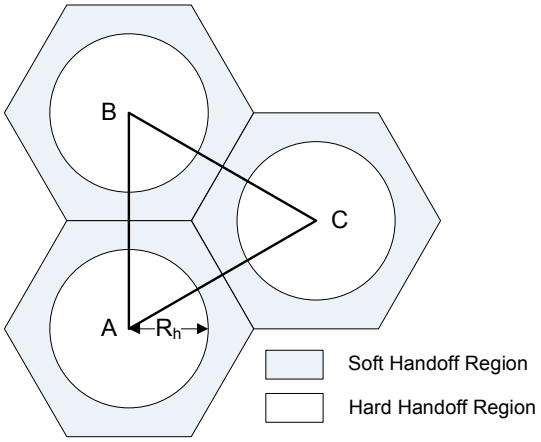

Figure 5.3: Handoff regions

Hence, the outage probability of downlink DS/CDMA cellular system can be defined as

$$P_{out} = \Pr\left\{\sum_{i=1}^{K} \phi_i \cdot \nu_i > \eta\right\} \tag{5.2}$$

where ν_i is the voice activity of the i^{th} MS and is assumed to be Bernoulli random process with probability of ν. A few studies show a possibility that the distribution of the fractional power of BS allocated to each MS can be approximated by a known distribution such as Gamma distribution or Log-normal distribution [19, 24, 72]. If uniform user distribution is assumed in the entire system, the fractional power of BS allocated to each MS, ϕ_i, can be considered an independent and identical random process, ϕ. Then, the outage probability can be evaluated as

$$P_{out} = \sum_{n=1}^{K} \Pr\left\{\sum_{i=1}^{n} \phi > \eta\right\} \binom{K}{n} \nu^n \cdot (1-\nu)^{K-n} \tag{5.3}$$

In this research, it will be shown that the fractional power of BS allocated to each MS, ϕ, is well approximated by Log-normal distribution assuming perfect downlink power control. Then, outage probability can be evaluated as

$$P_{out} = \sum_{n=1}^{K} Q\left(\frac{\eta - m_{\phi(n)}}{\sigma_{\phi(n)}}\right) \binom{K}{n} \nu^n \cdot (1-\nu)^{K-n} \tag{5.4}$$

where $m_{\phi(n)}$ and $\sigma_{\phi(n)}$ are the mean and standard deviation of $\phi(n) = \sum_1^n \phi$.

5.3 Fractional power of BS allocated to MS with power control

In the uplink DS/CDMA cellular system, fast power control is implemented to compensate for the multipath fading loss. It is shown that fast power control improves the uplink system capacity when power control rate is fast enough to follow channel fluctuation. Even for the downlink, fast transmit power control is shown to increase the system capacity [23, 25], and has become an essential technique for all 3rd generation standards [4, 34]. That is, the fractional power of BS allocated to MS is power controlled

by MS based on the received signal-to-interference-plus-noise ratio (SINR), similar to the uplink.

5.3.1 Signal-to-Interference Ratio

Assuming that background noise (primarily of thermal origin) is negligible as compared to the total signal power (including all users' signals) received from all BSs, the SIR can be used for the analysis instead of SINR. First, let us consider the received SIR at the MS for a single transmit and single receive antenna without soft handoff.

- ***Transmitter***

Let us start with the k^{th} user's signal at the l^{th} BS, $s_l^{(k)}(t)$

$$s_l^{(k)}(t) = \sqrt{P_l^{(k)}} \cdot a_l^{(k)}(t) \cdot w_l^{(k)}(t) \cdot c_l(t) \tag{5.5}$$

where $\sqrt{P_l^{(k)}}$ denotes the signal gain allocated to the k^{th} user at the l^{th} BS, $a_l^{(k)}(t)$ denote the random binary data symbol assuming the binary phase shift keying, $w_l^{(k)}$ denotes the orthogonal code allocated to the k^{th} user, and $c_l(t)$ denotes the complex pseudo noise (PN) sequence. Then, the transmit signal from the l^{th} BS can be expressed as

$$s_l(t) = \sum_{k=1}^{K} s_l^{(k)}(t) = \sum_{k=1}^{K} \sqrt{P_l^{(k)}} \cdot a_l^{(k)}(t) \cdot w_l^{(k)}(t) \cdot c_l(t) \cdot e^{j(\omega_c t + \theta_l)} \tag{5.6}$$

where K is the number of users per cell, and ω_c and θ_l are the carrier frequency and the random phase of local oscillator, respectively.

- ***Receiver***

Let us take into account the receive structure shown in Figure 5.4, and investigate the demodulation procedure of the *k*th user in the zeroth cell.

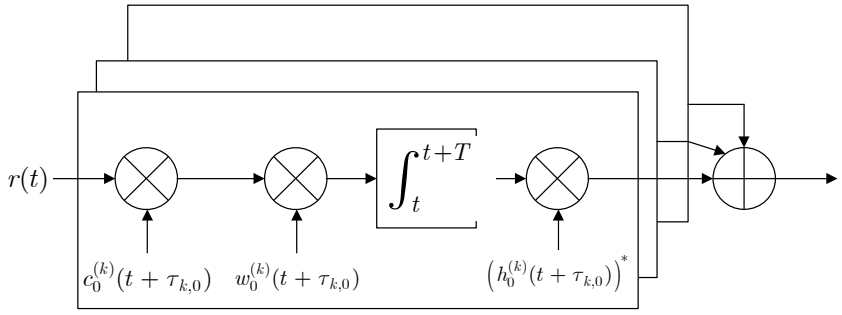

Figure 5.4: Receiver structure of MS

The received signal at the k^{th} user in the zero$^{\text{th}}$ cell can be expressed as

$$\begin{aligned} r_0^{(k)}(t) &= \sum_{l=0}^{M}\sum_{m=1}^{L} \alpha_{l,m}^{(k)}(t-\tau_{l,m})\cdot s_l(t-\tau_{l,m})\cdot e^{j\hat{\theta}_l} + n_k(t) \\ &= \sum_{l=0}^{M}\sum_{m=1}^{L}\sum_{n=1}^{K} \alpha_{l,m}^{(k)}(t-\tau_{l,m})\cdot s_l^{(n)}(t-\tau_{l,m})\cdot e^{j\hat{\theta}_l} + n_k(t) \\ &= \sum_{l=0}^{M}\sum_{m=1}^{L}\sum_{n=1}^{K} \alpha_{l,m}^{(k)}(t-\tau_{l,m})\cdot \sqrt{P_l^{(n)}}\cdot a_l^{(n)}(t-\tau_{l,m})\cdot w_l^{(n)}(t-\tau_{l,m})\cdot c_l(t-\tau_{l,m})e^{j\hat{\theta}_l} + n_k(t) \end{aligned} \tag{5.7}$$

where $\alpha_{l,m}^{(k)}$ is the complex channel gain corresponding to the m^{th} multipath component between the k^{th} MS and the l^{th} BS, composed of long-term fading and short-term fading channel loss, $n_k(t)$ is the thermal background noise at the receive antenna of the k^{th} MS, and $\hat{\theta}_l$ is the phase difference of local oscillator between the transmitter and receiver. Assuming the perfect synchronization[5] of each multipath component and slowly varying channel as compared to the symbol duration, the despread symbol, obtained by complex PN sequence $c_0(t)$ and the Walsh code $w_0^{(k)}$ for the k^{th} MS at the zeroth cell, can be expressed as

[5] Perfect synchronization makes it possible to drop the time index from the random data symbol of the desired user $a_0^{(l)}$

$$
\begin{aligned}
r_{0,q}^{(k)} &= \int_{t}^{t+T} r_0^{(k)}(t)\cdot w_l^{(0)}(t-\tau_{0,q})\cdot c_0^{*}(t-\tau_{0,q})dt \\
&= \alpha_{l,q}^{(k)}\cdot\sqrt{P_0^{(k)}}\cdot a_0^{(k)}\cdot N_T \\
&\quad+\sum_{\substack{m=1\\ m\neq q}}^{L}\sum_{n=1}^{K}\alpha_{0,n}^{(k)}\cdot\sqrt{P_0^{(k)}}\cdot\Phi_{0,m,n} \\
&\quad+\sum_{l=1}^{M}\sum_{m=1}^{L}\sum_{n=1}^{K}\alpha_{l,q}^{(k)}\cdot\sqrt{P_l^{(k)}}\cdot\Phi_{l,m,n}\cdot e^{j\hat{\theta}_l}
\end{aligned}
\tag{5.8}
$$

where T is the symbol duration, N_T denotes the spreading gain obtained by the auto correlation of the complex PN sequence and Walsh code, and $\Phi_{l,m,n}$ is the random process defined by the cross correlation of the complex PN sequence, Walsh code, and random binary data symbol. Given the complex PN sequence $c_0(t-\tau_{0,q})$ and Walsh code $w_0^{(n)}(t-\tau_{0,q})$, the random process $\Phi_{l,m,n}$ can be defined as

$$
\Phi_{l,m,n} = \int_{t}^{t+T} a_{l,m}^{(n)}(t-\tau_{l,m})\cdot w_l^{(n)}(t-\tau_{l,m})\cdot c_l(t-\tau_{l,m})\cdot w_0^{(n)}(t-\tau_{0,q})\cdot c_0^{*}(t-\tau_{0,q})dt \tag{5.9}
$$

For a long PN sequence relative to the symbol duration, $\Phi_{l,m,n}$ can be approximated by complex Gaussian random process with zero mean and variance of N_T [58-60]. Assuming the perfect channel information at the receiver, the demodulated symbol after channel compensation can be expressed as

$$
\begin{aligned}
\tilde{r}_{0,q}^{(k)} &= \left|\alpha_{0,q}^{(k)}\right|^2\cdot\sqrt{P_0^{(k)}}\cdot a_0^{(k)}\cdot N_T + \\
&\quad+\left(\alpha_{0,q}^{(k)}\right)^{*}\cdot\sum_{\substack{m=1\\ m\neq q}}^{L}\sum_{\substack{n=1\\ n\neq k}}^{K}\alpha_{0,m}^{(k)}\cdot\sqrt{P_0^{(k)}}\cdot\Phi_{0,m,n} \\
&\quad+\left(\alpha_{0,q}^{(k)}\right)^{*}\cdot\sum_{l=1}^{M}\sum_{m=1}^{L}\sum_{n=1}^{K}\alpha_{l,m}^{(k)}\cdot\sqrt{P_l^{(k)}}\cdot\Phi_{l,m,n}\cdot e^{j\hat{\theta}_l}
\end{aligned}
\tag{5.10}
$$

Finally, the multipath combined symbol after the demodulation can be expressed as

$$
\begin{aligned}
\tilde{r}_0^{(k)} &= \sum_{q=1}^{L}\left|\alpha_{0,q}^{(k)}\right|^2\cdot\sqrt{P_0^{(k)}}\cdot a_0^{(k)}\cdot N_T + \\
&\quad+\sum_{q=1}^{L}\left(\alpha_{0,q}^{(k)}\right)^{*}\cdot\sum_{\substack{m=1\\ m\neq q}}^{L}\sum_{n=1}^{K}\alpha_{0,m}^{(k)}\cdot\sqrt{P_0^{(k)}}\cdot\Phi_{0,m,n} \\
&\quad+\sum_{q=1}^{L}\left(\alpha_{0,q}^{(k)}\right)^{*}\cdot\sum_{l=1}^{M}\sum_{m=1}^{L}\sum_{n=1}^{K}\alpha_{l,m}^{(k)}\cdot\sqrt{P_l^{(k)}}\cdot\Phi_{l,m,n}\cdot e^{j\hat{\theta}_l}
\end{aligned}
\tag{5.11}
$$

Now, let us take into account the instantaneous SIR averaged over random processes $\Phi_{l,m,n}$ and $\hat{\theta}_l$ for the performance evaluation. The instantaneous signal energy P_S is calculated as

$$\begin{aligned} P_S &= E\left[\left|\sum_{q=1}^{L}\left|\alpha_{0,q}^{(k)}\right|^2 \cdot \sqrt{P_0^{(k)}} \cdot a_0^{(k)} \cdot N_T\right|^2\right] \\ &= \left(\sum_{q=1}^{L}\left|\alpha_{0,q}^{(k)}\right|^2\right)^2 \cdot P_0^{(k)} \cdot N_T^2 \end{aligned} \tag{5.12}$$

where it is assumed that $\left|a_0^{(k)}\right|^2 = 1$. The instantaneous interference energy P_I is calculated as

$$\begin{aligned} P_I &= E\left[\left|\begin{array}{l} \sum_{q=1}^{L}\left(\alpha_{0,q}^{(k)}\right)^* \cdot \sum_{\substack{m=1 \\ m\neq q}}^{L}\sum_{n=1}^{K}\alpha_{0,m}^{(k)} \cdot \sqrt{P_0^{(n)}} \cdot \Phi_{0,m,n} \\ +\sum_{q=1}^{L}\left(\alpha_{0,q}^{(k)}\right)^* \cdot \sum_{l=1}^{M}\sum_{m=1}^{L}\sum_{n=1}^{K}\alpha_{l,m}^{(k)} \cdot \sqrt{P_l^{(n)}} \cdot \Phi_{l,m,n} \cdot e^{j\hat{\theta}_l} \end{array}\right|^2\right] \\ &= N_T \cdot \left(\sum_{q=1}^{L}\left|\alpha_{0,q}^{(k)}\right|^2 \cdot \sum_{\substack{m=1 \\ m\neq q}}^{L}\sum_{n=1}^{K}\left|\alpha_{0,m}^{(k)}\right|^2 \cdot P_0^{(k)} + \sum_{q=1}^{L}\left|\alpha_{0,q}^{(k)}\right|^2 \cdot \sum_{m=1}^{L}\sum_{l=1}^{M}\sum_{n=1}^{K}\left|\alpha_{l,m}^{(k)}\right|^2 \cdot P_l^{(n)}\right) \end{aligned} \tag{5.13}$$

where $E[\bullet]$ is the statistical expectation over the random processes, $\Phi_{0,m,n}$, $\Phi_{l,m,n}$, and $\hat{\theta}_l$. In Equation (5.13), the last term consists of the l^{th} BS's user signal except the zeroth BS is generally referred as the intercell interference, and the sum of user's signal powers $\sum_{n=1}^{K} P_l^{(n)}$ from the *l*th BS can be simply replaced by the total transmit power of the l^{th} BS P_l. Then, Equation (5.13) can be expressed as

$$P_I = N_T \cdot \left(\sum_{q=1}^{L}\left|\alpha_{0,q}^{(k)}\right|^2 \cdot \sum_{\substack{m=1 \\ m\neq q}}^{L}\sum_{n=1}^{K}\left|\alpha_{0,m}^{(k)}\right|^2 \cdot P_0^{(k)} + \left(\sum_{q=1}^{L}\left|\alpha_{0,q}^{(k)}\right|^2\right) \cdot \sum_{l=1}^{M}\left(\sum_{m=1}^{L}\left|\alpha_{l,m}^{(k)}\right|^2\right) \cdot P_l\right) \tag{5.14}$$

Then, the instantaneous signal-to-interference ratio (γ_{k0}) can be expressed as

$$\gamma_{k0} = \frac{P_S}{P_I} = \frac{\left(\sum_{q=1}^{L}\left|\alpha_{0,q}^{(k)}\right|^2\right)^2 \cdot P_0^{(k)} \cdot N_T}{\sum_{q=1}^{L}\left|\alpha_{0,q}^{(k)}\right|^2 \cdot \sum_{\substack{m=1 \\ m\neq q}}^{L}\sum_{n=1}^{K}\left|\alpha_{0,m}^{(k)}\right|^2 \cdot P_0^{(k)} + \left(\sum_{q=1}^{L}\left|\alpha_{0,q}^{(k)}\right|^2\right) \cdot \sum_{l=1}^{M}\left(\sum_{m=1}^{L}\left|\alpha_{l,m}^{(k)}\right|^2\right) \cdot P_l} \tag{5.15}$$

In Equation (5.15), the first term in the denominator corresponds to the interference from the same cell and is generally referred as *intracell interference*, and the second term in the denominator correspond to the interference from the other cell and is referred as *intercell interference* [11, 17, 24]. The ratio of intracell interference power over signal power is also referred as *non-orthogonality factor* [11]. Non-orthogonality factor is an important parameter evaluating the system performance of downlink DS/CDMA cellular system [11, 24, 73-75]. Assuming that orthogonal spreading code is employed, non-orthogonal factor goes to zero in single-path environment, which is ideal situation for the intracell interference reduction. However, multipath fading channel will introduce interference which is not orthogonal among the same cell users; hence, non-orthogonality factor will have some value or distribution. For the analytical tractability, intracell interference power is generally assumed to be a constant value by simply adopting mean value [11, 24]. Now, let us consider the following expression for the received SIR,

$$\gamma_{k0} = \frac{P_0^{(k)} \cdot N_T}{C_{NOF} \cdot P_0 + \dfrac{\sum_{l=1}^{M}\sum_{m=1}^{L}\left|\alpha_{l,m}^{(k)}\right|^2 \cdot P_j}{\left(\sum_{q=1}^{L}\left|\alpha_{0,q}^{(k)}\right|^2\right)}} \tag{5.16}$$

where C_{NOF} is the channel gain ratio of intracell interference and signal power defined as

$$C_{NOF} = \frac{\sum_{q=1}^{L}\left|\alpha_{k0}^{(q)}\right|^2\left(\sum_{m=1,m\neq q}^{L}\sum_{n=1}^{K}\left|\alpha_{0,m}^{(k)}\right|^2 \cdot P_0^{(k)}\right)}{\left(\sum_{p=1}^{L}\left|\alpha_{0,p}^{(k)}\right|^2\right)^2 \cdot P_0} \tag{5.17}$$

Suppose that the fractional power of BS allocated to MS is small and the number of users per cell is large, the following approximation holds

$$\sum_{m=1,m\neq q}^{L}\sum_{n=1}^{K}\left|\alpha_{0,m}^{(k)}\right|^2 \cdot P_0^{(k)} \approx \sum_{m=1}^{L}\left|\alpha_{0,m}^{(k)}\right|^2 \cdot P_0 \tag{5.18}$$

and C_{NOF} becomes constant '1'; otherwise, C_{NOF} will have relatively small variance as compared to that of intracell interference because the numerator and denominator are strongly correlated. Thus, C_{NOF} will be assumed to be constant in the subsequent analysis.

Finally, this received SIR is compared to the required SIR for given QoS, and power control command is delivered from MS to BS, which will adjust the power allocation to MS at BS. Assuming perfect power control at steady state, the fractional power of BS allocated to the k^{th} MS can be expressed as

$$P_0^{(k)} = \frac{\gamma_T}{N_T} \cdot \left(C_{NOF} \cdot P_0 + \frac{\sum_{j=1}^{M} \sum_{m=1}^{L} \left| \alpha_{j,m}^{(k)} \right|^2 \cdot P_j}{\sum_{q=1}^{L} \left| \alpha_{0,q}^{(k)} \right|^2} \right) \tag{5.19}$$

This power allocation expression can easily be extended for MIMO systems with soft handoff as described in the following subsection.

5.3.2 Multiple-Input Multiple-Output

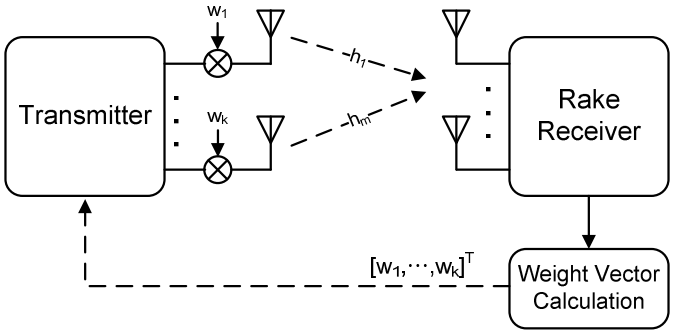

Figure 5.5: MIMO configuration

Let us take into account MIMO configuration of system as shown in Figure 5.5, where T transmit antennas are implemented at BS and R receive antennas are implemented at MS. Similar to the uplink DS/CDMA cellular system, it is assumed that maximal ratio transmit diversity is performed by closed loop transmit diversity and signals received at each receive antennas are coherently combined by maximal ratio combining technique. Assuming that rake receive at MS can combine signals from all possible diversity branches, the received SIR can be expressed as

$$\gamma_{k0} = \frac{\left|\sum_{r=1}^{R}\sum_{q=1}^{L}\left|\sum_{t=1}^{T} w_{0,t}^{(k)} \cdot \alpha_{0,t,q,r}^{(k)}\right|^2\right|^2 \cdot P_0^{(k)} \cdot N_T}{\left\{\begin{array}{l}\sum_{q=1}^{L}\sum_{m=1,m\neq q}^{L}\left|\sum_{r=1}^{R}\left(\sum_{t=1}^{T} w_{0,t}^{(k)} \cdot \alpha_{0,t,q,r}^{(k)}\right)^* \sum_{n=1}^{K}\sum_{t'=1}^{T} w_{0,t'}^{(n)} \cdot \alpha_{0,t',m,r}^{(k)}\sqrt{P_0^{(n)}}\right|^2 \cdots \\ +\sum_{j=1}^{M}\sum_{q=1}^{L}\sum_{m=1}^{L}\left|\sum_{r=1}^{R}\left(\sum_{t=1}^{T} w_{0,t}^{(k)} \cdot \alpha_{0,t,q,r}^{(k)}\right)^* \sum_{t'=1}^{T} \alpha_{j,t',m,r}^{(k)}\right|^2 \cdot \frac{P_j}{T}\end{array}\right\}} \tag{5.20}$$

where $w_{kj}^{(t)}$ is the weight coefficient of the t^{th} transmit antenna from the j^{th} BS to the k^{th} MS, $\alpha_{k0}^{(m,r,t)}$ is the channel coefficient of the m^{th} multipath component between the t^{th} transmit antenna and the r^{th} receive antenna from the k^{th} MS to the zero$^{\text{th}}$ BS, and transmit power of BS is assumed to be equally distributed to multiple transmit antennas so that total transmit power of BS, P_j, is divided by the number of antennas T. Then, similar to Equation(5.19), the received SIR can be expressed as

$$\gamma_{k0} = \frac{P_0^{(k)} \cdot N_T}{\left\{C_{NOF} \cdot \frac{P_0}{T} + \frac{\sum_{j=1}^{M}\sum_{q=1}^{L}\sum_{m=1}^{L}\left|\sum_{r=1}^{R}\left(\sum_{t=1}^{T} w_{0,t}^{(k)} \cdot \alpha_{0,t,q,r}^{(k)}\right)^* \sum_{t'=1}^{T} \alpha_{j,t',m,r}^{(k)}\right|^2 \cdot \frac{P_j}{T}}{\left|\sum_{r=1}^{R}\sum_{q=1}^{L}\left|\sum_{t=1}^{T} w_{0,t}^{(k)} \cdot \alpha_{0,t,q,r}^{(k)}\right|^2\right|^2}\right\}} \tag{5.21}$$

Thus, the fractional power of BS to allocated to MS can be expressed as

$$P_0^{(k)} = \frac{\gamma_{k0}}{N_T} \cdot \left(C_{NOF} \cdot \frac{P_0}{T} + \frac{\sum_{j=1}^{M}\sum_{q=1}^{L}\sum_{m=1}^{L}\left|\sum_{r=1}^{R}\left(\sum_{t=1}^{T} w_{0,t}^{(k)} \cdot \alpha_{0,t,q,r}^{(k)}\right)^* \sum_{t'=1}^{T} \alpha_{j,t',m,r}^{(k)}\right|^2 \cdot \frac{P_j}{T}}{\left|\sum_{r=1}^{R}\sum_{q=1}^{L}\left|\sum_{t=1}^{T} w_{0,t}^{(k)} \cdot \alpha_{0,t,q,r}^{(k)}\right|^2\right|^2} \right) \tag{5.22}$$

5.3.3 Soft handoff

Finally, let us take into account the effect of soft handoff in the received SIR expression of downlink DS/CDMA cellular system. In the uplink DS/CDMA cellular system, multiple BSs in the active set receive the same signal from MS and choose the signal correctly decoded, which is modeled by the selection diversity choosing the signal suffering the least propagation loss. However, in the downlink DS/CDMA cellular system, multiple BSs in the active set transmit the same signal to MS, and the MS

combines these signals using various combining techniques. Maximal ratio combining technique is the usual combining technique for the MS. Assuming that MS is equipped with sufficient number of rake fingers to combine signals from all diversity sources like multipath, receive antennas, and multiple BSs in the active set, the received SIR can be expressed as

$$\gamma_{k0} = \frac{\left|\sum_{s\in A_k}\sum_{r=1}^{R}\sum_{q=1}^{L}\left|\sum_{t=1}^{T} w_{s,t}^{(k)}\cdot\alpha_{s,t,q,r}^{(k)}\right|^2\sqrt{P_s^{(k)}}\right|^2\cdot N_T}{\left\{\begin{array}{l}\sum_{s\in A_k}\left\{\sum_{q=1}^{L}\sum_{m=1,m\neq q}^{L}\left|\sum_{r=1}^{R}\left(\sum_{t=1}^{T} w_{s,t}^{(k)}\cdot\alpha_{s,t,q,r}^{(k)}\right)^*\sum_{n=1}^{K}\sum_{t'=1}^{T} w_{s,t'}^{(n)}\cdot\alpha_{s,t',m,r}^{(k)}\sqrt{P_s^{(n)}}\right|^2\cdots\right. \\ \left.+\sum_{j\notin A_k}\sum_{q=1}^{M}\sum_{m=1}^{L}\sum_{r=1}^{L}\left|\sum_{r=1}^{R}\left(\sum_{t=1}^{T} w_{s,t}^{(k)}\cdot\alpha_{s,t,q,r}^{(k)}\right)^*\sum_{t'=1}^{T}\alpha_{j,t',m,r}^{(k)}\right|^2\cdot\frac{P_j}{T}\right\}\end{array}\right.} \tag{5.23}$$

where A_k is the active set of the k^{th} MS and $P_s^{(k)}$ is the fractional power of the s^{th} BS allocated to the k^{th} MS. During soft handoff, the fractional power of each BS, in the active set, allocated to the MS will be slightly different due to the propagation loss and other factors such as power control error and other users' power allocation in the BS. However, for the purpose of analysis, $P_s^{(k)}$ can be assumed to be an identical random process [11, 19, 24] assuming the same cell loading in the active set. Then, the received SIR can be expressed as

$$\gamma_{k0} = \frac{\left|\sum_{s\in A_k}\sum_{r=1}^{R}\sum_{q=1}^{L}\left|\sum_{t=1}^{T} w_{s,t}^{(k)}\cdot\alpha_{s,t,q,r}^{(k)}\right|^2\right|^2\cdot P_0^{(k)}\cdot N_T}{\left\{\begin{array}{l}\sum_{s\in A_k}\sum_{q=1}^{L}\sum_{m=1,m\neq q}^{L}\left|\sum_{r=1}^{R}\left(\sum_{t=1}^{T} w_{s,t}^{(k)}\cdot\alpha_{s,t,q,r}^{(k)}\right)^*\sum_{n=1}^{K}\sum_{t'=1}^{T} w_{s,t'}^{(n)}\cdot\alpha_{s,t',m,r}^{(k)}\sqrt{P_s^{(n)}}\right|^2\cdots\right. \\ \left.+\sum_{s\in A_k}\sum_{j\notin A_k}^{M}\sum_{q=1}^{L}\sum_{m=1}^{L}\left|\sum_{r=1}^{R}\left(\sum_{t=1}^{T} w_{s,t}^{(k)}\cdot\alpha_{s,t,q,r}^{(k)}\right)^*\sum_{t'=1}^{T}\alpha_{j,t',m,r}^{(k)}\right|^2\cdot\frac{P_j}{T}\right\}\end{array}\right.} \tag{5.24}$$

where the total power of BSs in the active set is assumed to be the same. Finally, the fractional power of BSs, in the active set, allocated to the k^{th} MS can be expressed as

$$P_0^{(k)} = \frac{\gamma_{k0}}{N_T} \cdot \left(C_{NOF} \cdot \frac{P_0}{T} + \frac{\sum_{s \in A_k} \left\{ \sum_{j \notin A_k}^{M} \sum_{q=1}^{L} \sum_{m=1}^{L} \left| \sum_{r=1}^{R} \left(\sum_{t=1}^{T} w_{s,t}^{(k)} \cdot \alpha_{s,t,q,r}^{(k)} \right)^* \sum_{t'=1}^{T} \alpha_{j,t',m,r}^{(k)} \right|^2 \cdot \frac{P_j}{T} \right\}}{\left| \sum_{s \in A_k} \sum_{r=1}^{R} \sum_{q=1}^{L} \left| \sum_{t=1}^{T} w_{s,t}^{(k)} \cdot \alpha_{s,t,q,r}^{(k)} \right|^2 \right|^2} \right) \quad (5.25)$$

Equation (5.25) is the final expression for the fractional power of BS allocated to an MS. This is a key result used for the subsequent analyses.

5.3.4 Log-normal approximation

As mentioned in the previous section, the fractional power of BS allocated to MS will be approximated by log-normal distribution for the calculation of outage probability of the system. Let us revisit the outage condition in Equation (5.1) with the fractional power of BS allocated to MS in Equation (5.25) as follows

$$\sum_{k=1}^{K} \left(C_{NOF} \cdot \frac{P_0}{T} + \frac{\sum_{s \in A_k} \left\{ \sum_{j \notin A_k}^{M} \sum_{q=1}^{L} \sum_{m=1}^{L} \left| \sum_{r=1}^{R} \left(\sum_{t=1}^{T} w_{s,t}^{(k)} \cdot \alpha_{s,t,q,r}^{(k)} \right)^* \sum_{t'=1}^{T} \alpha_{j,t',m,r}^{(k)} \right|^2 \cdot \frac{P_j}{T} \right\}}{\left| \sum_{s \in A_k} \sum_{r=1}^{R} \sum_{q=1}^{L} \left| \sum_{t=1}^{T} w_{s,t}^{(k)} \cdot \alpha_{s,t,q,r}^{(k)} \right|^2 \right|^2} \right) > \eta \cdot \frac{N_T}{\gamma_{k0}} \quad (5.26)$$

Since $C_{NOF} \cdot P_0 / N_t$ is constant value, Equation (5.26) can be expressed as

$$\sum_{k=1}^{K} \frac{\sum_{s \in A_k} \left\{ \sum_{j \notin A_k}^{M} \sum_{q=1}^{L} \sum_{m=1}^{L} \left| \sum_{r=1}^{R} \left(\sum_{t=1}^{T} w_{s,t}^{(k)} \cdot \alpha_{s,t,q,r}^{(k)} \right)^* \sum_{t'=1}^{T} \alpha_{j,t',m,r}^{(k)} \right|^2 \cdot \frac{P_j}{T} \right\}}{\left| \sum_{s \in A_k} \sum_{r=1}^{R} \sum_{q=1}^{L} \left| \sum_{t=1}^{T} w_{s,t}^{(k)} \cdot \alpha_{s,t,q,r}^{(k)} \right|^2 \right|^2} > \eta' \quad (5.27)$$

where $\eta' = \eta \cdot N_T / \gamma_{k0} - K \cdot C_{NOF} \cdot P_0 / T$. Then, it can be observed that the left-hand side (LHS) in Equation (5.27) has the identical form of intercell interference in the uplink DS/CDMA cellular system except MRC for the soft-handoff; hence, it is expected to be easily approximated by Log-normal distribution just as the interference in the uplink DS/CDMA cellular system. For the log-normal approximation, let us define the random variable y_k as

$$y_k = \frac{\sum_{s\in A_k}\left\{\sum_{j\notin A_k}^{M}\sum_{q=1}^{L}\sum_{m=1}^{L}\left|\sum_{r=1}^{R}\left(\sum_{t=1}^{T} w_{s,t}^{(k)}\cdot\alpha_{s,t,q,r}^{(k)}\right)^{*}\sum_{t'=1}^{T}\alpha_{j,t',m,r}^{(k)}\right|^{2}\cdot\frac{P_j}{T}\right\}}{\left|\sum_{s\in A_k}\sum_{r=1}^{R}\sum_{q=1}^{L}\left|\sum_{t=1}^{T} w_{s,t}^{(k)}\cdot\alpha_{s,t,q,r}^{(k)}\right|^{2}\right|^{2}} \tag{5.28}$$

where the channel coefficient $\alpha_{ks}^{(q,r,t)}$ is expanded into the short-term fading channel coefficient h and long-term fading channel coefficient $r^{-m}10^{\zeta/10}$. Hence, the random variable y_k is the function of another random variables such as h, r and ζ. Assuming uniform distribution of MSs in the system, the random variable y_k can be considered the identical and independent random. Let us further define the random variable Z as

$$Z = \sum_{k=1}^{K} y_k \tag{5.29}$$

From the fact that the sum of log-normal random variable is also log-normal random variable, the random variable Z can also be considered log-normal random variable.

For the simple verification, the simulated distributions and log-normal approximated distributions of Z are compared for several representative configurations in Figure 5.6, where T, R, and L denote the number of transmit antennas, receive antennas, and multipath components, respectively. For the short-term fading channel, Rayleigh fading channel is assumed. It is observed that the distribution of Z is well-approximated by log-normal distribution in our interested region of probability $(> 10^{-3})$ except the cases of one-path Rayleigh fading channel $(L = 1)$ without any micro diversity such as antenna diversity and multipath diversity. Further simulated and approximated distributions of Z for $K = 10$ are plotted in Figure 5.7. Similarly, the log-normal distribution well approximates the simulated distribution within our interested region of probability.

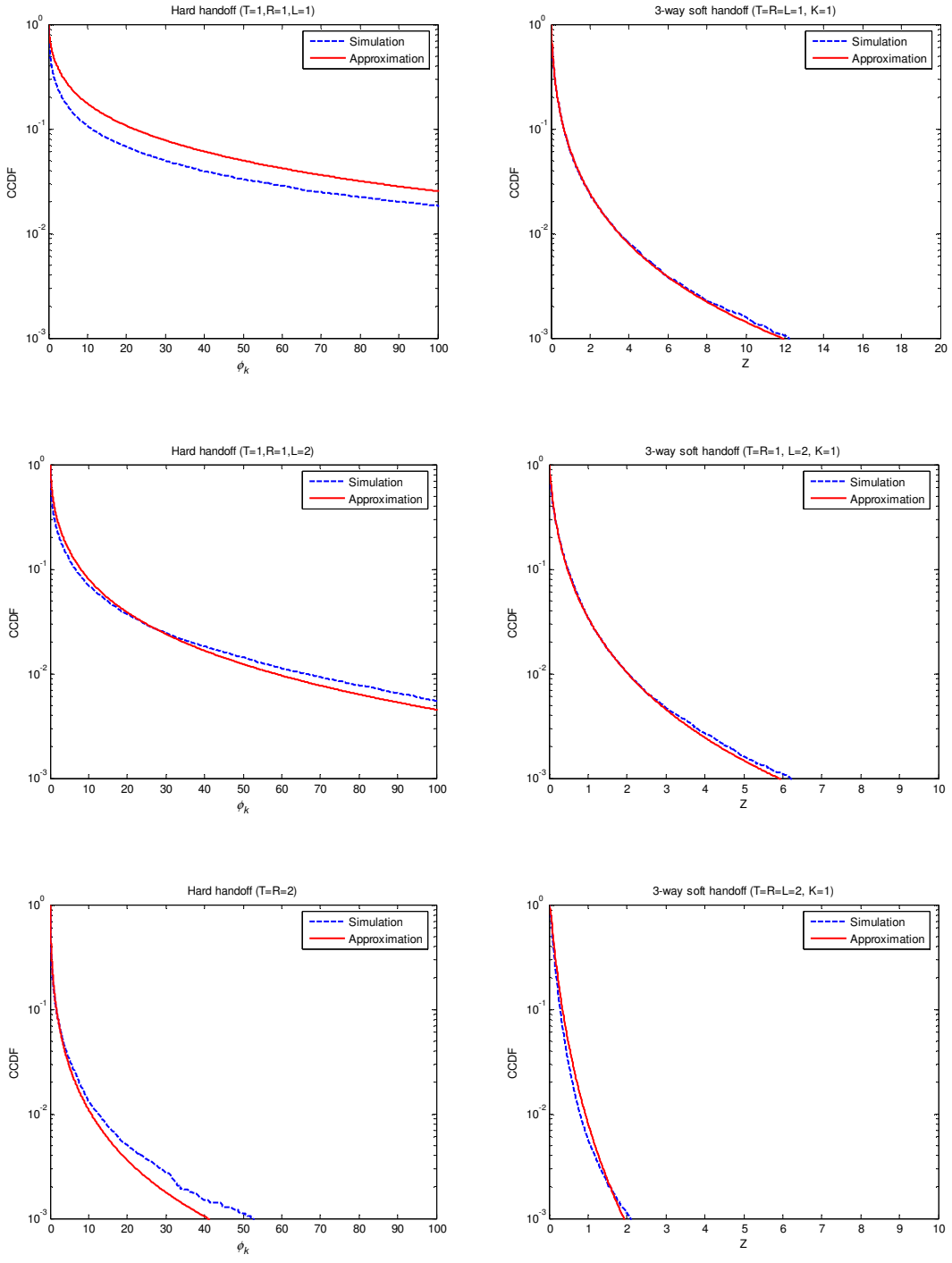

Figure 5.6: Simulated and approximated distributions of Z_k for several configurations with $K = 1$

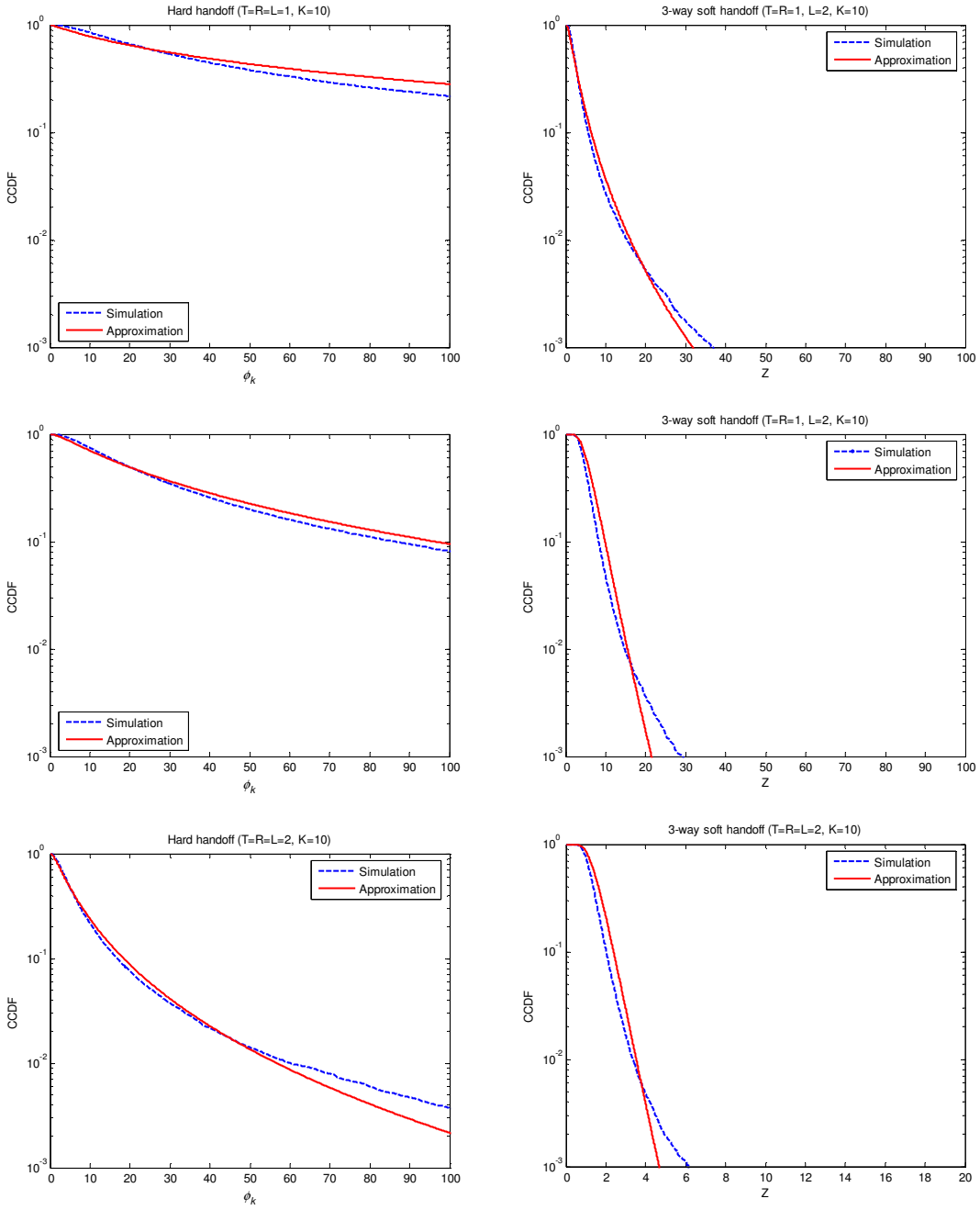

Figure 5.7: Simulated and approximated distributions of Z_k for several configurations with $K = 10$

5.4 Statistics of the fractional power of BS allocated to MS

In the previous section, it was shown that the fractional power of BS allocated to MS can be approximated by the log-normal distribution. Note that the sufficient statistics for log-normal distribution are mean and variance. Hence, this section shows how to estimate the mean and variance. Without loss of generality, the fractional power of BS allocated to an MS can be divided into the non-orthogonality factor and intercell interference factor.

5.4.1 Intercell interference

Let us consider the n^{th} moment of Equation (5.28) to calculate the mean and variance of intercell interference factor.

$$E[\,y_k^n\,] = E\left[\frac{\displaystyle\sum_{s\in A_k}\left\{\sum_{j\notin A_k}^{M}\sum_{q=1}^{L}\sum_{m=1}^{L}\left|\sum_{r=1}^{R}\left(\sum_{t=1}^{T}w_{s,t}^{(k)}\cdot h_{s,t,q,r}^{(k)}\right)^{*}\sum_{t'=1}^{T}h_{j,t',m,r}^{(k)}\right|^{2n}\cdot\left(\frac{10^{(\zeta_{s,k}+\zeta_{j,k})/10}}{r_{s,k}^{u}\cdot r_{j,k}^{u}}\right)^{n}\cdot\frac{P_j^n}{T^n}\right\}}{\displaystyle\left|\sum_{s\in A_k}\sum_{r=1}^{R}\sum_{q=1}^{L}\left|\sum_{t=1}^{T}w_{s,t}^{(k)}\cdot h_{s,t,q,r}^{(k)}\right|^{2}\right|^{2n}\cdot\left(\frac{10^{\zeta_{s,k}/10}}{r_{s,k}^{u}}\right)^{2n}}\right] \tag{5.30}$$

where $r_{j,k}^{u}$ and $10^{\zeta_{j,k}/10}$ denote the path loss with the exponent of u and the log-normal shadow fading loss, respectively, between the k^{th} MS and the j^{th} BS, and $h_{s,t,q,r}^{(k)}$ denotes the short-term fading channel loss of the t^{th} transmit antenna and the q^{th} multipath and the r^{th} receive antenna between the k^{th} MS and the s^{th} BS. Since $\zeta_{j,k} = a\cdot\xi_k + b\cdot\xi_j$, Equation (5.30) can be reformed as

$$E[\,y_k^n\,] = E\left[\frac{\displaystyle\sum_{s\in A_k}\left\{\sum_{j\notin A_k}^{M}\sum_{q=1}^{L}\sum_{m=1}^{L}\left|\sum_{r=1}^{R}\left(\sum_{t=1}^{T}w_{s,t}^{(k)}\cdot h_{s,t,q,r}^{(k)}\right)^{*}\sum_{t'=1}^{T}h_{j,t',m,r}^{(k)}\right|^{2n}\cdot\left(\frac{10^{b(\xi_s+\xi_j)/10}}{r_{s,k}^{u}\cdot r_{j,k}^{u}}\right)^{n}\cdot\frac{P_j^n}{T^n}\right\}}{\displaystyle\left|\sum_{s\in A_k}\sum_{r=1}^{R}\sum_{q=1}^{L}\left|\sum_{t=1}^{T}w_{s,t}^{(k)}\cdot h_{s,t,q,r}^{(k)}\right|^{2}\right|^{2n}\cdot\left(\frac{10^{b\xi_s/10}}{r_{s,k}^{u}}\right)^{2n}}\right] \tag{5.31}$$

- ***Hard handoff***

First, let us take into account hard handoff case in which the number of active set is one. Since the long-term fading channel loss and short-term fading channel loss can be assumed to be independent, Equation (5.31) can be expressed as

$$
\begin{aligned}
E[\,y_k^n\,] &= E\left[\frac{\sum_{j=1}^{M}\sum_{q=1}^{L}\sum_{m=1}^{L}\left|\sum_{r=1}^{R}\left(\sum_{t=1}^{T} w_{0,t}^{(k)}\cdot h_{0,t,q,r}^{(k)}\right)^{*}\sum_{t'=1}^{T} h_{j,t',m,r}^{(k)}\right|^{2n}\cdot\left(\frac{10^{b\xi_j/10}}{r_{j,k}^{u}}\right)^{n}\cdot\frac{P_j^n}{T^n}}{\left|\sum_{r=1}^{R}\sum_{q=1}^{L}\left|\sum_{t=1}^{T} w_{0,t}^{(k)}\cdot h_{0,t,q,r}^{(k)}\right|^{2}\right|^{2n}\cdot\left(\frac{10^{b\xi_0/10}}{r_{0,k}^{u}}\right)^{n}}\right] \\
&= \sum_{j=1}^{M}\frac{P_j^n}{T^n}E\left[10^{\frac{nb(\xi_j-\xi_0)}{10}}\right]E\left[\left(\frac{r_{0,k}^{u}}{r_{j,k}^{u}}\right)^{n}\right]E\left[\frac{\sum_{q=1}^{L}\sum_{m=1}^{L}\left|\sum_{r=1}^{R}\left(\sum_{t=1}^{T} w_{0,t}^{(k)}\cdot h_{0,t,q,r}^{(k)}\right)^{*}\sum_{t'=1}^{T} h_{j,t',m,r}^{(k)}\right|^{2n}}{\left|\sum_{r=1}^{R}\sum_{q=1}^{L}\left|\sum_{t=1}^{T} w_{0,t}^{(k)}\cdot h_{0,t,q,r}^{(k)}\right|^{2}\right|^{2n}}\right] \qquad (5.32) \\
&= \frac{1}{T^n}E\left[10^{\frac{nb(\xi-\xi_0)}{10}}\right]E\left[\frac{\sum_{q=1}^{L}\sum_{m=1}^{L}\left|\sum_{r=1}^{R}\left(\sum_{t=1}^{T} w_{t}^{(k)}\cdot h_{t,q,r}^{(k)}\right)^{*}\sum_{t'=1}^{T} h_{t',m,r}^{(k)}\right|^{2n}}{\left|\sum_{r=1}^{R}\sum_{q=1}^{L}\left|\sum_{t=1}^{T} w_{t}^{(k)}\cdot h_{t,q,r}^{(k)}\right|^{2}\right|^{2n}}\right]\cdot\sum_{j=1}^{M}P_j^n E\left[\left(\frac{r_{0,k}^{u}}{r_{j,k}^{u}}\right)^{n}\right]
\end{aligned}
$$

where it is assumed that the shadow fading channel and short-term fading channel has identical distributions at every cell. Assuming the independent Rayleigh fading distributions for the short-term fading channel, Equation (5.32) can be further simplified as [76, 77]

$$
\begin{aligned}
E[\,y_k^n\,] = \frac{1}{T^n}\left(\sum_{j=1}^{M}P_j^n E\left[\left(\frac{r_{0,k}^{u}}{r_{j,k}^{u}}\right)^{n}\right]\right)E\left[10^{\frac{nb(\xi-\xi_0)}{10}}\right]E\left[\left|\sum_{r=1}^{R}\sum_{q=1}^{L}\left|\sum_{t=1}^{T} w_{t}^{(k)}\cdot h_{t,q,r}^{(k)}\right|^{2}\right|^{-n}\right]\times \\
E\left[\left(\frac{\sum_{q=1}^{L}\sum_{m=1}^{L}\left|\sum_{r=1}^{R}\left(\sum_{t=1}^{T} w_{t}^{(k)}\cdot h_{0,t,q,r}^{(k)}\right)^{*}\sum_{t'=1}^{T} h_{t',m,r}^{(k)}\right|^{2}}{\left|\sum_{r=1}^{R}\sum_{q=1}^{L}\left|\sum_{t=1}^{T} w_{t}^{(k)}\cdot h_{t,q,r}^{(k)}\right|^{2}\right|^{n}}\right)^{n}\right] \qquad (5.33)
\end{aligned}
$$

The sum of the expectation of path losses depends on the location of a MS and can be evaluated by Monte Carlo integration technique. Assuming the same total power of every

BS in the system, the first and second moments of the sum of path losses by Monte Carlo integration result in

$$\begin{aligned} \sum_{j=1}^{M} E\left[\frac{r_{0,k}^{u}}{r_{j,k}^{u}}\right] &= 0.416 \\ \sum_{j=1}^{M} E\left[\left(\frac{r_{0,k}^{u}}{r_{j,k}^{u}}\right)^{2}\right] &= 0.156 \end{aligned} \tag{5.34}$$

which will be commonly used in evaluating the statistics of intracell interference with hard handoff. The expectation of shadow fading channel loss in Equation (5.33) can be also simply calculated as

$$\begin{aligned} E\left[10^{\frac{nb(\xi-\xi_0)}{10}}\right] &= \int_{-\infty}^{\infty} e^{nb\beta\xi} \frac{1}{\sqrt{2\pi\sigma_\xi}} e^{-\xi^2/2\sigma_\xi^2} d\xi \cdot \int_{-\infty}^{\infty} e^{nb\beta\xi_0} \frac{1}{\sqrt{2\pi\sigma_{\xi_0}}} e^{-\xi_0{}^2/2\sigma_{\xi_0}^2} d\xi_0 \\ &= \exp\left(n^2 b^2 \beta^2 \sigma^2\right) \end{aligned} \tag{5.35}$$

In addition, assuming L-equal gain multipath profile, the last expectation in Equation (5.33) can be simply expressed by the n^{th} moment of a chi-square distribution with $2L$ degree of freedom, scaled by $(2L)^n$ [76, 77]. Let us define X as

$$X = \frac{\sum_{m=1}^{L}\sum_{q=1}^{L}\left|\sum_{r=1}^{R}\left(\sum_{t=1}^{T} w_t^{(k)} \cdot h_{0,t,q,r}^{(k)}\right)^{*}\sum_{t'=1}^{T} h_{t',m,r}^{(k)}\right|^2}{\left|\sum_{r=1}^{R}\sum_{q=1}^{L}\left|\sum_{t=1}^{T} w_t^{(k)} \cdot h_{t,q,r}^{(k)}\right|^2\right|^n} \tag{5.36}$$

Then, the n^{th} moment of X can be calculated as

$$\begin{aligned} E[X^n] &= \frac{1}{(2L)^n}\int_0^{\infty} x^n f_X(x) dx \\ &= \frac{\Gamma(L+n)}{L^n \cdot \Gamma(L)} \end{aligned} \tag{5.37}$$

where $f_X(x) = \frac{e^{-x/2}(x/2)^{L-1}}{2\cdot\Gamma(L)}$ is the pdf of chi-square distribution with $2L$ degree of freedom and $\Gamma(a) = \int_0^{\infty} t^{a-1}e^{-t}dt$ is the gamma function. Finally, let us define the random variable Y as the received signal combined by maximal ratio combining technique as follows

$$Y = \sum_{r=1}^{R}\sum_{q=1}^{L}\left|\sum_{t=1}^{T} w_t^{(k)} \cdot h_{t,q,r}^{(k)}\right|^2 \tag{5.38}$$

It is known that the random variable Y is the largest eigenvalue of complex Wishart matrix $\mathbf{H}^H\mathbf{H}$ for given MIMO in flat Rayleigh fading channel where $\mathbf{H}$ is complex Gaussian channel matrix defined as

$$\mathbf{H} = \begin{bmatrix} h_{1,1} & \cdots & h_{1,T} \\ \vdots & \ddots & \vdots \\ h_{R,1} & \cdots & h_{R,T} \end{bmatrix} \tag{5.39}$$

The probability density function of Y can be expressed as [36]

$$f_Y(y) = \frac{1}{\prod_{i=1}^{Q}(Q-i)!(P-i)!}\frac{d}{dy}\det \mathbf{S}(y) \tag{5.40}$$

where $Q = \min\{T,R\}$, $P = \max\{T,R\}$, and $\mathbf{S}(y)$ is defined by $Q \times Q$ Hankel matrix of which element in the k^{th} row and l^{th} column is given by

$$S_{k,l}(y) = \Gamma(P-Q+k+l-1, y) \tag{5.41}$$

where $\Gamma(k+1,y)$ for $k = 0,1,2,\ldots$, and $y > 0$ is the incomplete gamma function having the representation as

$$\begin{aligned} \Gamma(k+1,y) &= \int_0^y t^k e^{-t} dt \\ &= k!\left[1 - e^{-y}\sum_{m=0}^{k}\frac{u^m}{m!}\right] \end{aligned} \tag{5.42}$$

Hence, the n^{th} moment of the inverse of received signal can be evaluated as

$$E\left[\frac{1}{Y^n}\right] = \int_{\gamma^{-1}}^{\infty}\frac{1}{y^n} f_Y(y) dy \tag{5.43}$$

where γ is the fade limit to guarantee the existence of the first moment of Y^{-1} without any diversity scheme and can be considered as a fade margin to limit the factional power of BS allocated to an MS. For the frequency selective Rayleigh fading channel with L-equal gain multipath profile, the n^{th} moment of Y^{-1} can be calculated by means of normalizing Y by L^n as

$$E\left[\frac{1}{Y^n}\right] = L^n\int_{\gamma^{-1}}^{\infty}\frac{1}{y^n} f_Y(y) dy \tag{5.44}$$

and by extending the channel matrix $\mathbf{H}$ as

$$\mathbf{H} = \begin{bmatrix} h_{1,1} & \cdots & h_{1,T} \\ \vdots & \ddots & \vdots \\ h_{RL,1} & \cdots & h_{RL,T} \end{bmatrix} \tag{5.45}$$

which will affect calculating the probability density function of Y.

- ***Soft handoff***

Now, let us take into account the soft handoff case where the number of BSs in the active set is larger than one. Equation (5.31) can be expressed as

$$E[y_k^n] = \sum_{j \notin A}^{M} E\left[\frac{\left\{ \sum_{s \in A_k} \sum_{q=1}^{L} \sum_{m=1}^{L} \left| \sum_{r=1}^{R} \left(\sum_{t=1}^{T} w_{s,t}^{(k)} \cdot h_{s,t,q,r}^{(k)} \right)^* \sum_{t'=1}^{T} h_{j,t',m,r}^{(k)} \right|^{2n} \left(\frac{10^{b\xi_s/10}}{r_{s,k}^u} \right)^n \left(\frac{10^{b\xi_j/10} \cdot P_j}{r_{j,k}^u \cdot T} \right)^n \right\}}{\left| \sum_{s \in A_k} \sum_{r=1}^{R} \sum_{q=1}^{L} \left| \sum_{t=1}^{T} w_{s,t}^{(k)} \cdot h_{s,t,q,r}^{(k)} \right|^2 \cdot \left(\frac{10^{b\xi_s/10}}{r_{s,k}^u} \right) \right|^{2n}} \right] \tag{5.46}$$

Assuming that the short-term fading channel has the independent Rayleigh fading distribution with L equal-power multipath profile, the same argument used in Equation (5.36) can be applied to Equation (5.46). Let us define the random variable X_j as

$$X_j = \frac{\left\{ \sum_{s \in A_k} \sum_{q=1}^{L} \sum_{m=1}^{L} \left| \sum_{r=1}^{R} \left(\sum_{t=1}^{T} w_{s,t}^{(k)} \cdot h_{s,t,q,r}^{(k)} \right)^* \sum_{t'=1}^{T} h_{j,t',m,r}^{(k)} \right|^{2n} \left(\frac{10^{b\xi_s/10}}{r_{s,k}^u} \right)^n \right\}}{\left| \sum_{s \in A_k} \sum_{r=1}^{R} \sum_{q=1}^{L} \left| \sum_{t=1}^{T} w_{s,t}^{(k)} \cdot h_{s,t,q,r}^{(k)} \right|^2 \cdot \left(\frac{10^{b\xi_s/10}}{r_{s,k}^u} \right) \right|^{n}} \tag{5.47}$$

Then, the random variable X_j can be simply represented by the chi-square distribution with $2L$ degree of freedom, scaled by $(2L)^n$. Since X_j and ξ_j are assumed to be independently distributed in the system, Equation (5.46) can be expressed as

$$E[y_k^n] = E[X^n] E\left[10^{b\xi/10}\right] \sum_{j \notin A}^{M} \frac{P_j^n}{T^n} E\left[\frac{\left(\frac{1}{r_{j,k}^u} \right)^n}{\left| \sum_{s \in A_k} \sum_{r=1}^{R} \sum_{q=1}^{L} \left| \sum_{t=1}^{T} w_{s,t}^{(k)} \cdot h_{s,t,q,r}^{(k)} \right|^2 \cdot \left(\frac{10^{b\xi_s/10}}{r_{s,k}^u} \right) \right|^n} \right] \tag{5.48}$$

where $E[X^n]$ can be evaluated by Equation (5.37) and $E\left[10^{b\xi/10}\right]$ can be evaluated as

$$E\left[10^{nb\xi_j/10}\right] = \exp\left(\frac{n^2 \beta^2 b^2 \sigma^2}{2} \right) \tag{5.49}$$

For the last expectation, it may be difficult (or impossible) to obtain the closed form solution as in the hard handoff case because the path losses from the BSs are correlated each other according to the location of MS. Given the location of MS, however, it is observed that the denominator in the last expectation can be well-approximated by log-normal distribution. Hence, Equation (5.48) can be evaluated as

$$E\left[y_k^n \mid r_{0,k}^u \cdots r_{M,k}^u\right] = E\left[X^n\right] \cdot E\left[10^{b\xi/10}\right] \cdot \left(\sum_{j \notin A}^{M} \frac{P_j^n}{T^n} r_{j,k}^{-nu}\right) \times E\left[\left|\sum_{s \in A_k} \sum_{r=1}^{R} \sum_{q=1}^{L} \left|\sum_{t=1}^{T} w_{s,t}^{(k)} \cdot h_{s,t,q,r}^{(k)}\right|^2 \cdot \left(\frac{10^{b\xi_s/10}}{r_{s,k}^u}\right)\right|^{-n}\right]. \tag{5.50}$$

Let us define the random variable Z as

$$Z = \sum_{s \in A_k} \sum_{r=1}^{R} \sum_{q=1}^{L} \left|\sum_{t=1}^{T} w_{s,t}^{(k)} \cdot h_{s,t,q,r}^{(k)}\right|^2 \cdot \frac{10^{b\xi_s/10}}{r_{s,k}^u} \tag{5.51}$$

Then, the n^{th} moment of the inverse of Z, given the location of an MS, can be evaluated as

$$E\left[Z^{-n} \mid r_{0,k}^u \cdots r_{M,k}^u\right] = \int_0^\infty \frac{1}{z^n} f_Z(z) dz = \exp\left(-n m_z + \frac{n^2 \sigma_Z^2}{2}\right) \tag{5.52}$$

where $f_Z(z)$ is the probability density function of the random variable Z, and m_Z and σ_Z^2 are the mean and variance of the random variable $\ln Z$, respectively. m_Z and σ_Z^2 can be obtained as

$$\begin{aligned} m_Z &= 2\ln u_1 - 0.5 \ln u_2 \\ \sigma_Z^2 &= \ln u_2 - 2 \ln u_1 \end{aligned} \tag{5.53}$$

where u_1 and u_2 are the first and the second moment of the random variable Z given the location of an MS. The n^{th} moment of Z given $r_{s,k}$ can be evaluated as

$$\begin{aligned} u_n &= E\left[Z^n \mid r_{0,k}^u \cdots r_{M,k}^u\right] \\ &= E\left[\left(\sum_{s \in A_k} \sum_{r=1}^{R} \sum_{q=1}^{L} \left|\sum_{t=1}^{T} w_{s,t}^{(k)} \cdot h_{s,t,q,r}^{(k)}\right|^2 \cdot \frac{10^{b\xi_s/10}}{r_{s,k}^u}\right)^n\right] \\ &= E\left[10^{nb\xi_s/10}\right] \cdot E\left[\left(\sum_{r=1}^{R} \sum_{q=1}^{L} \left|\sum_{t=1}^{T} w_{s,t}^{(k)} \cdot h_{s,t,q,r}^{(k)}\right|^2\right)^n\right] \left(\sum_{s \in A_k} r_{s,k}^{-nu}\right) \end{aligned} \tag{5.54}$$

Note that the long-term shadow fading and short-term fading are independent and the long-term shadow fading is assumed to be identically distributed in the system. In Equation (5.54), the first expectation can be easily evaluated by Equation (5.49), and the second expectation can be evaluated as

$$E\left[\left(\sum_{r=1}^{R}\sum_{q=1}^{L}\left|\sum_{t=1}^{T} w_{s,t}^{(k)} \cdot h_{s,t,q,r}^{(k)}\right|^2\right)^n\right] = \int_0^\infty y^n f_Y(y)dy \tag{5.55}$$

where $f_Y(y)$ can be found in Equation (5.40) which is the probability density function of largest eigenvalue of the complex Wishart matrix defined in Equation (5.45). Note that the n^{th} moment of y_k obtained in this soft handoff case is a function of the location of an MS. Finally, the n^{th} moment of y_k can be evaluated by averaging $E[y_k \mid r_{0,k} \ldots r_{0,M}]$ over the predefined area as

$$E[y_k^n] = E\left[E[y_k^n \mid r_{0,k} \cdots r_{M,k}]\right] \tag{5.56}$$

5.4.2 Intracell interference

In this analysis, intracell interference is defined by non-orthogonality factor C_{NOF} which is given as follows

$$C_{NOF} = \frac{\sum_{s\in A_k}\sum_{q=1}^{L}\sum_{m=1,m\neq q}^{L}\left|\sum_{r=1}^{R}\left(\sum_{t=1}^{T} w_{s,t}^{(k)} \cdot h_{s,t,q,r}^{(k)}\right)^* \sum_{n=1}^{K}\sum_{t'=1}^{T} w_{s,t'}^{(n)} \cdot h_{s,t',m,r}^{(k)} \sqrt{\frac{P_s^{(n)}}{T}}\right|^2 \cdot \left(\frac{10^{b\xi_s/10}}{r_{s,k}^u}\right)^2}{\left|\sum_{s\in A_k}\sum_{r=1}^{R}\sum_{q=1}^{L}\left|\sum_{t=1}^{T} w_{s,t}^{(k)} \cdot h_{s,t,q,r}^{(k)}\right|^2 \frac{10^{b\xi_s/10}}{r_{s,k}^u}\right|^2} \tag{5.57}$$

Ideally, the non-orthogonality factor will be zero for frequency flat fading channel. However, under multipath fading environments or soft handoff, orthogonality will not be guaranteed among the signal comes from the serving BSs. In this case, intracell interference will be a random variable. However, the variance of intracell interference is much smaller than that of intercell interference since the numerator and denominator given in Equation (5.57) are strongly correlated. Therefore, in this analysis, only the mean value of C_{NOF} will be reflected. Assuming large number of users, that is, a small

fraction of power of BS is allocated to an MS, the non-orthogonality factor given in Equation (5.57) can be approximated as

$$C_{NOF} \approx E\left[\frac{\sum_{s\in A_k}\sum_{q=1}^{L}\sum_{m=1}^{L}\left|\sum_{r=1}^{R}\left(\sum_{t=1}^{T} w_{s,t}^{(k)}\cdot h_{s,t,q,r}^{(k)}\right)^{*}\sum_{t'=1}^{T} h_{s,t',m,r}^{(k)}\right|^{2}\frac{P_s}{T}\cdot\left(\frac{10^{b\xi_s/10}}{r_{s,k}^{u}}\right)^{2}}{\left|\sum_{s\in A_k}\sum_{r=1}^{R}\sum_{q=1}^{L}\left|\sum_{t=1}^{T} w_{s,t}^{(k)}\cdot h_{s,t,q,r}^{(k)}\right|^{2}\frac{10^{b\xi_s/10}}{r_{s,k}^{u}}\right|^{2}}\right] \tag{5.58}$$

- ***Hard Handoff***

First, let us simply take into account the non-orthogonality factor without soft handoff, Equation (5.58) can be expressed as

$$C_{NOF} \approx \frac{P_0}{T}\cdot E\left[\frac{\sum_{q=1}^{L}\sum_{m=1}^{L}\left|\sum_{r=1}^{R}\left(\sum_{t=1}^{T} w_{0,t}^{(k)}\cdot h_{0,t,q,r}^{(k)}\right)^{*}\left(\sum_{t'=1}^{T} h_{0,t',m,r}^{(k)}\right)\right|^{2}}{\left|\sum_{r=1}^{R}\sum_{q=1}^{L}\left|\sum_{t=1}^{T} w_{0,t}^{(k)}\cdot h_{0,t,q,r}^{(k)}\right|^{2}\right|^{2}}\right] \tag{5.59}$$

Since the numerator and denominator is strongly correlated, it may be difficult (or impossible) to directly estimate the expectation by calculating joint probability distribution function. In this analysis, the following property of expectation is used as a simple estimate of the expectation in Equation (5.59). It is known that if the random variable, X/Y and Y are stochastically independent and all the moments of X, Y and X/Y exist then, for every *n*, the *n*th order moment of X/Y is exactly equal to the ratio of the *n*th order moments of X and Y [78]. That is,

$$E\left[\left(\frac{X}{Y}\right)^{n}\right] = \frac{E[X^n]}{E[Y^n]} \tag{5.60}$$

If random variable Y is strictly positive and all its moments are nonzero, the simple proof can be shown as follows: Since X/Y and Y are assumed to be stochastically independent,

$$E[X^n] = E\left[\left(\frac{X}{Y}Y\right)^{n}\right] = E\left[\left(\frac{X}{Y}\right)^{n}\right]E[Y^n] \tag{5.61}$$

Hence,

$$E\left[\left(\frac{X}{Y}\right)^n\right] = \frac{E[X^n]}{E[Y^n]} \tag{5.62}$$

Note that even though the denominator and numerator in Equation (5.59) are strongly correlated, their ratio and the denominator are uncorrelated since the strong correlation between the denominator and numerator forces the ratio to be constant while the denominator has large variation. Hence, Equation (5.59) can be evaluated as

$$C_{NOF} \approx \frac{P_0}{T} \frac{E\left[\left|\sum_{q=1}^{L}\sum_{m=1}^{L}\left|\sum_{r=1}^{R}\left(\sum_{t=1}^{T} w_{0,t}^{(k)} \cdot h_{0,t,q,r}^{(k)}\right)^*\left(\sum_{t'=1}^{T} h_{0,t',m,r}^{(k)}\right)\right|^2\right|^2\right]}{E\left[\left|\sum_{r=1}^{R}\sum_{q=1}^{L}\left|\sum_{t=1}^{T} w_{0,t}^{(k)} \cdot h_{0,t,q,r}^{(k)}\right|^2\right|^2\right]} \tag{5.63}$$

where the denominator follows the complex Wishart distribution and can be evaluated by Equation (5.55). On the other hand, the numerator can be evaluated as

$$E[\bullet] = \sum_{q=1}^{L}\sum_{m=1}^{L} E\left[\left|\sum_{r=1}^{R}\left(\sum_{t=1}^{T} w_{0,t}^{(k)} \cdot h_{0,t,q,r}^{(k)}\right)^*\left(\sum_{t'=1}^{T} h_{0,t',m,r}^{(k)}\right)\right|^2\right] \tag{5.64}$$

Without transmit diversity, Equation (5.64) can be calculated as

$$\begin{aligned} E[\bullet] &= \sum_{q=1}^{L}\sum_{m=1}^{L} E\left[\left|\sum_{r=1}^{R}\left(h_{0,q,r}^{(k)}\right)^*\left(h_{0,m,r}^{(k)}\right)\right|^2\right] \\ &= \sum_{q=1}^{L} E\left[\left|\sum_{r=1}^{R}\left|h_{0,q,r}^{(k)}\right|^2\right|^2\right] + \sum_{q=1}^{L}\sum_{\substack{m=1 \\ m\neq q}}^{L} E\left[\left|\sum_{r=1}^{R}\left(h_{0,q,r}^{(k)}\right)^*\left(h_{0,m,r}^{(k)}\right)\right|^2\right] \\ &= L \cdot \frac{R(R+1)}{L^2} + L(L-1)\frac{R}{L^2} \\ &= \frac{R^2}{L} + R \end{aligned} \tag{5.65}$$

For transmit diversity implemented, Equation (5.64) can be evaluated as

$$\begin{aligned} E[\bullet] = &\sum_{q=1}^{L} E\left[\left|\sum_{r=1}^{R}\left(\sum_{t=1}^{T} w_{0,t}^{(k)} \cdot h_{0,t,q,r}^{(k)}\right)^*\left(\sum_{t'=1}^{T} h_{0,t',q,r}^{(k)}\right)\right|^2\right] \\ &+\sum_{q=1}^{L}\sum_{\substack{m=1 \\ m\neq q}}^{L} E\left[\left|\sum_{r=1}^{R}\left(\sum_{t=1}^{T} w_{0,t}^{(k)} \cdot h_{0,t,q,r}^{(k)}\right)^*\left(\sum_{t'=1}^{T} h_{0,t',m,r}^{(k)}\right)\right|^2\right] \end{aligned} \tag{5.66}$$

where the first expectation may not be easily calculated because of the product of correlated random variables. In this analysis, the following Cauchy-Schwarz inequality will be used

$$\left|\sum_{i=1}^{n} f_i^* g_i\right|^2 \le \left(\sum_{i=1}^{n} |f_i|^2\right)\left(\sum_{i=1}^{n} |g_i|^2\right) \tag{5.67}$$

Then, the first expectation in right hand side (RHS) of Equation (5.66) can be estimated by

$$\sum_{q=1}^{L} E\left[\left|\sum_{r=1}^{R}\left(\sum_{t=1}^{T} w_{0,t}^{(k)} \cdot h_{0,t,q,r}^{(k)}\right)^*\left(\sum_{t'=1}^{T} h_{0,t',q,r}^{(k)}\right)\right|^2\right] \le E\left[\sum_{q=1}^{L}\left|\sum_{r=1}^{R}\left|\sum_{t=1}^{T} w_{0,t}^{(k)} \cdot h_{0,t,q,r}^{(k)}\right|^2\right|^2\right] \tag{5.68}$$

The second expectation in RHS of Equation (5.66) can be evaluated as

$$\begin{aligned} E\left[\left|\sum_{r=1}^{R}\left(\sum_{t=1}^{T} w_{0,t}^{(k)} \cdot h_{0,t,q,r}^{(k)}\right)^*\left(\sum_{t'=1}^{T} h_{0,t',m,r}^{(k)}\right)\right|^2\right] &= E\left[\sum_{r=1}^{R}\left|\sum_{t=1}^{T} w_{0,t}^{(k)} \cdot h_{0,t,q,r}^{(k)}\right|^2\left|\sum_{t'=1}^{T} h_{0,t',m,r}^{(k)}\right|^2\right] \\ &= \sum_{r=1}^{R} E\left[\left|\sum_{t=1}^{T} w_{0,t}^{(k)} \cdot h_{0,t,q,r}^{(k)}\right|^2\right] E\left[\left|\sum_{t'=1}^{T} h_{0,t',m,r}^{(k)}\right|^2\right] \\ &= \frac{T}{L} \cdot \sum_{r=1}^{R} E\left[\left|\sum_{t=1}^{T} w_{0,t}^{(k)} \cdot h_{0,t,q,r}^{(k)}\right|^2\right] \end{aligned} \tag{5.69}$$

Finally, Equation (5.66) can be evaluated as

$$\begin{aligned} E[\bullet] &\le E\left[\sum_{q=1}^{L}\left|\sum_{r=1}^{R}\left|\sum_{t=1}^{T} w_{0,t}^{(k)} \cdot h_{0,t,q,r}^{(k)}\right|^2\right|^2\right] + \frac{T}{L} \cdot \sum_{q=1}^{L}\sum_{\substack{m=1 \\ m\neq q}}^{L}\sum_{r=1}^{R} E\left[\left|\sum_{t=1}^{T} w_{0,t}^{(k)} \cdot h_{0,t,q,r}^{(k)}\right|^2\right] \\ &\le E\left[\left|\sum_{q=1}^{L}\sum_{r=1}^{R}\left|\sum_{t=1}^{T} w_{0,t}^{(k)} \cdot h_{0,t,q,r}^{(k)}\right|^2\right|^2\right] + \frac{T}{L}\sum_{\substack{m=1 \\ m\neq q}}^{L} E\left[\sum_{q=1}^{L}\sum_{r=1}^{R}\left|\sum_{t=1}^{T} w_{0,t}^{(k)} \cdot h_{0,t,q,r}^{(k)}\right|^2\right] \\ &\approx E\left[\lambda_{\max}^2\right] + \frac{T(L-1)}{L} \cdot E\left[\lambda_{\max}\right] \end{aligned} \tag{5.70}$$

where $E[\lambda_{\max}]$ is the first order moment of the largest eigenvalue of complex Wishart matrix and can be evaluated by Equation (5.55) with $n = 1$. $E\left[\lambda_{\max}^2\right]$ is the second order moment of the largest eigenvalue of complex Wishart matrix and can be evaluated by Equation (5.55) with $n = 2$.

- ***Soft Handoff***

For the soft handoff, the same procedure to calculate the coefficient for the non-orthogonality factor can be applied. Hence, Equation (5.58) can be calculated as

$$C_{NOF} \approx \frac{E\left[\sum_{s\in A_k}\sum_{q=1}^{L}\sum_{m=1}^{L}\left|\sum_{r=1}^{R}\left(\sum_{t=1}^{T} w_{s,t}^{(k)} \cdot h_{s,t,q,r}^{(k)}\right)^{*}\sum_{t'=1}^{T} h_{s,t',m,r}^{(k)}\right|^{2}\frac{P_s}{T}\cdot\left(\frac{10^{b\xi_s/10}}{r_{s,k}^{u}}\right)^{2}\right]}{E\left[\left|\sum_{s\in A_k}\sum_{r=1}^{R}\sum_{q=1}^{L}\left|\sum_{t=1}^{T} w_{s,t}^{(k)} \cdot h_{s,t,q,r}^{(k)}\right|^{2}\right|^{2}\left(\frac{10^{b\xi_s/10}}{r_{s,k}^{u}}\right)^{2}\right]} \tag{5.71}$$

For a given $r_{s,k}$, Equation (5.71) can be expressed as

$$\begin{aligned} C_{NOF}\,|\,r_{s,k} &\approx \frac{\frac{P_s}{T}E\left[\sum_{q=1}^{L}\sum_{m=1}^{L}\left|\sum_{r=1}^{R}\left(\sum_{t=1}^{T} w_{s,t}^{(k)} \cdot h_{s,t,q,r}^{(k)}\right)^{*}\sum_{t'=1}^{T} h_{s,t',m,r}^{(k)}\right|^{2}\right]\cdot E\left[10^{2b\xi_s/10}\right]\cdot\sum_{s\in A_k}\frac{1}{r_{s,k}^{2u}}}{E\left[\left|\sum_{r=1}^{R}\sum_{q=1}^{L}\left|\sum_{t=1}^{T} w_{s,t}^{(k)} \cdot h_{s,t,q,r}^{(k)}\right|^{2}\right|^{2}\right]\cdot E\left[10^{2b\xi_s/10}\right]\cdot\sum_{s\in A_k}\frac{1}{r_{s,k}^{2u}}} \\ &= \frac{E\left[\sum_{q=1}^{L}\sum_{m=1}^{L}\left|\sum_{r=1}^{R}\left(\sum_{t=1}^{T} w_{s,t}^{(k)} \cdot h_{s,t,q,r}^{(k)}\right)^{*}\sum_{t'=1}^{T} h_{s,t',m,r}^{(k)}\right|^{2}\right]}{E\left[\left|\sum_{r=1}^{R}\sum_{q=1}^{L}\left|\sum_{t=1}^{T} w_{s,t}^{(k)} \cdot h_{s,t,q,r}^{(k)}\right|^{2}\right|^{2}\right]} \end{aligned} \tag{5.72}$$

That is, C_{NOF} with soft handoff is independent of $r_{s,k}$, and is the same as that obtained for hard handoff.

5.5 Numerical Results

In this section, selective results for the given analytical framework are presented. System parameters for the analysis are summarized in Table 5.1.

5.5.1 Impact of micro-diversity on the capacity of downlink DS/CDMA cellular systems

In this section, the capacity of downlink DS/CDMA cellular systems is presented with multipath diversity and spatial diversity, implementation.

Figure 5.8 shows outage probabilities versus the number of users per cell for different number of multipath components without any spatial diversity. It is assumed that rake receiver can resolve all existing multipath components. Outage probability improves as the number of resolvable multipath increases, because of multipath diversity.

In Figure 5.9, outage probability versus the number of users per cell is plotted for different number of receive antennas. It is assumed that all MSs are in hard handoff and the constant C_{NOF} related to the non-orthogonality factor is assumed to be zero. It is observed that the outage probability significantly improves as the number of receive antenna increases as compared to the results in Figure 5.8 because of the array gain from the multiple antennas as well as diversity gain. The statistics of intercell interference, normalized by signal for multipath diversity and receive diversity, are shown in Table 5.2. It can be observed that the mean and variance of the normalized interference decreases as diversity order increases in both multipath and receive diversity. However, the reduction of the normalized interference is more pronounced in receive diversity due to the array gain from multiple receive antennas. Furthermore, in single path environments, orthogonality among the same cell users is preserved so that there is no intracell interference, while the orthogonality among the same cell users in multipath environments does not maintained.

Table 5.1: System Parameters

Parameters	Value
Spreading bandwidth (W)	1.25 MHz
Data Rate (R_b)	8 Kbps
Voice activity (ν)	0.4
Target E_b / I_0	5.6 dB
Shadowing correlation between BSs	0.5
Log-normal shadowing	$\sigma = 8\text{dB},\ m = 0$
Path loss exponent	$u = 4$
Soft handoff	2 and 3-way
Diversity order (M)	1, 2, 4, 8
Multipath profile	uniform

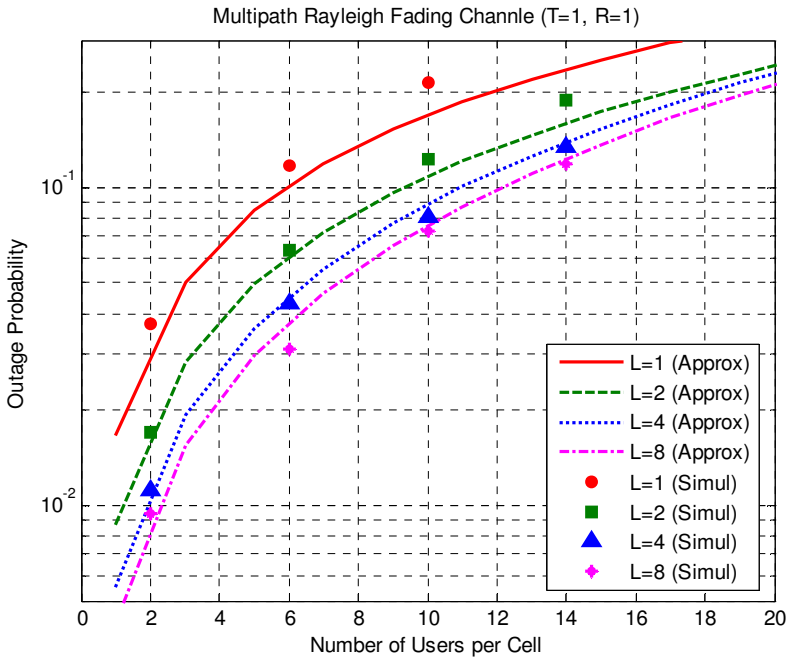

Figure 5.8: Outage probability vs. the number of users per cell for different number of resolvable multipath

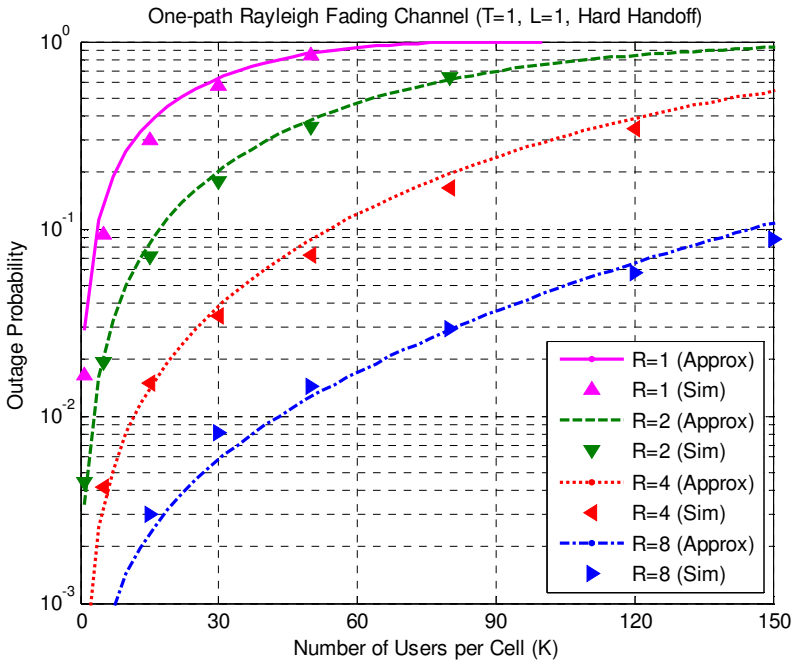

Figure 5.9: Outage probability vs. the number of users per cell for different number of receive antennas

Table 5.2: Mean and variance of the interference for different number of antennas

Diversity order	Multipath diversity		Receive diversity	
	Mean	Variance	Mean	Variance
M=1	9.179	26201.	9.179	26201.
M=2	4.501	3540.1	2.251	1112.5
M=4	3.031	452.08	0.758	45.552
M=8	2.598	230.49	0.325	6.4844

For the same configurations as those in Figure 5.9, transmit diversity shows the same performance as the receive diversity. Since the constant C_{NOF} is assumed to be zero in this results, the performance of transmit diversity can be determined by the statistics of normalized intercell interference. Table 5.3 summarizes the means and variances of the normalized intercell interference for different number of receive antennas and transmit antennas. It is observed that the mean and variance for transmit diversity and receiver diversity is the same for the same diversity order (M). Therefore, if there is no intracell interference, transmit diversity and receive diversity show the same performance in the downlink. Furthermore, the mean and variance are significantly reduced by increasing diversity order.

Now, let us take into account the non-zero value of C_{NOF} which means that orthogonality among users in the same cell is not preserved even for a one-path Rayleigh fading channel. Figure 5.10 shows the outage probabilities versus the number of users per cell for a different number of receive antennas, where C_{NOF} is set to '1' for all diversity order. Due to the nonzero value of C_{NOF}, the system performances are slightly degraded as compared to those in Figure 5.9. However, it is still observed that receive diversity at MS significantly improves the system performance.

Table 5.3: Mean and variance of the intercell interference for different number of antennas

Diversity order	Receive diversity		Transmit diversity	
	Mean	Variance	Mean	Variance
M=1	9.179	26201.	9.179	26201.
M=2	2.251	1112.5	2.251	1112.5
M=4	0.758	45.552	0.758	45.552
M=8	0.325	6.4844	0.325	6.4844

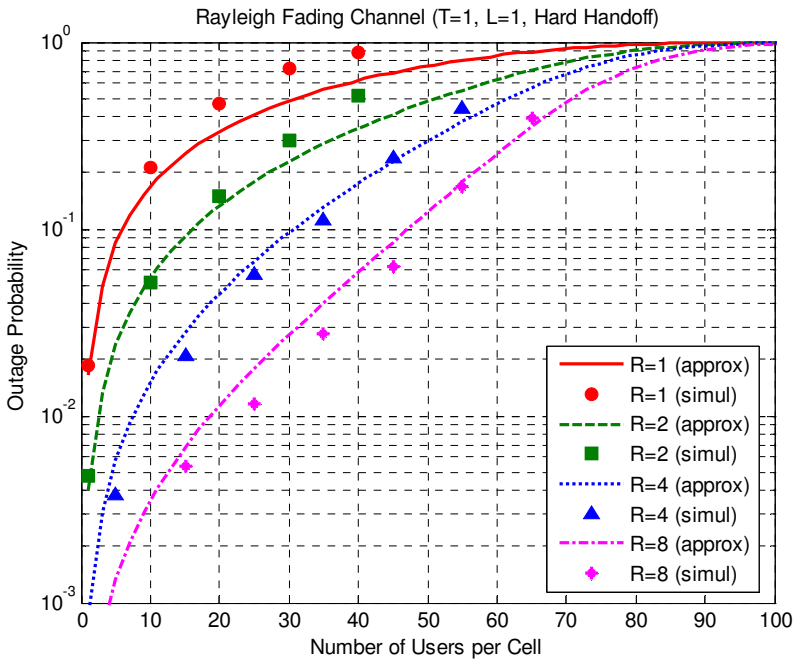

Figure 5.10: Outage probability vs. the number of users per cell for different number of receive antennas with non-orthogonal intracell interference

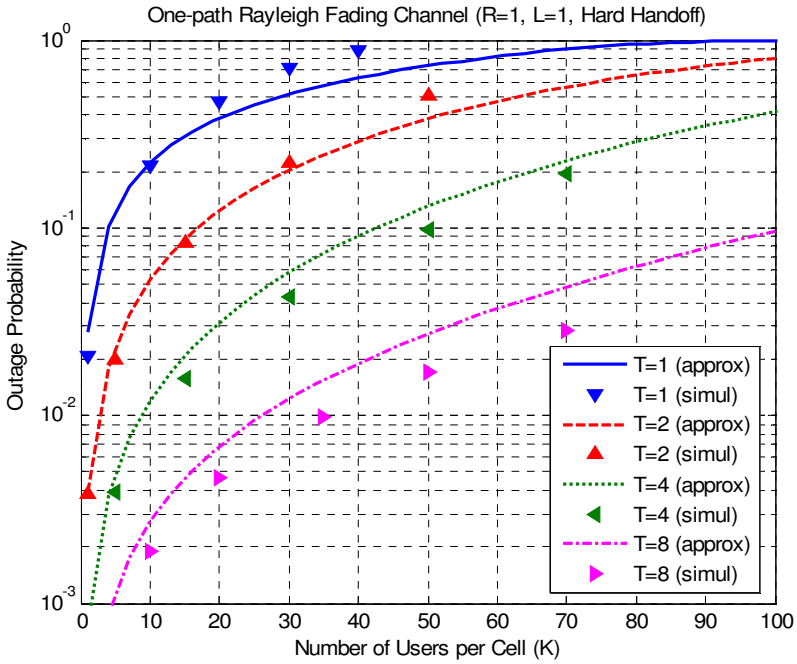

Figure 5.11: Outage probability vs. the number of users per cell for different number of transmit antennas with non-orthogonal intracell interference

On the other hand, for the condition of $C_{NOF} \neq 0$, transmit diversity at the downlink shows different performance from receive diversity. This is shown in Figure 5.11. It can be observed that the performance improvement by transmit diversity is greater than that by receive diversity. This is different observation from the link-level (point-to-point) performance of transmit diversity and receive diversity. Note that maximal ratio transmit diversity and receive diversity with MRC show the same performance in link level. It can be clearly observed in the distribution of the received signal power and the distribution of the received SIR at MS with either receive diversity or transmit diversity as shown in Figure 5.12 and Figure 5.13. For the comparison of difference between intracell interference, received signal power and received SIR are measured by simulating a single cell DS/CDMA cellular system for MISO and SIMO configurations with the diversity order of two. Random spreading code is applied to each user to simulate of non-orthogonality between users at the same BS. Ten users are simulated to investigate the impact of intracell interference from other users. It can be apparently observed that both transmit diversity and receive diversity has the same distributions of the received signal power as shown in Figure 5.12. This observation has been conventionally made in the link level; hence, the performance between transmit diversity and receive diversity cannot observed. However, if we consider interference from other users, received SIR with transmit diversity is observed to be at higher SIR than that of receive diversity as shown in Figure 5.13. Therefore, the intracell interference with transmit diversity is smaller than that with receive diversity.

Furthermore, trend of performance difference between transmit diversity and receive diversity in the downlink is also different from that in the uplink observed in Chapter 3. Note that, in the uplink, receive diversity at BS shows better system performance than transmit diversity at MS. In the uplink, the performance difference between transmit diversity and receive diversity is due to that additional intracell interference reduction performed by receive diversity. Similarly, in the downlink DS/CDMA cellular system, the intracell interference differently behaves according to the location of diversity implementation. In the downlink, if transmit diversity is implemented at BS, the intracell

interferences are incoherently transmitted from BS, thus, incoherently combined at MS. On the other hand, if receive diversity is implemented at MS, intracell interference are coherently combined at MS. This can be more clearly understood if we compare transmit beamforming and receive beamforming in the downlink. Transmit beamforming at BS adaptively forms a beam to each user in the same cell while the receive diversity cannot differentiate other users in the same cell with multiple antennas.

For the results shown in Figure 5.10 and Figure 5.11, the mean values (C_{NOF}) of the intracell interference are summarized in Table 5.4. From these results, it can be observed that the intracell interference decreases almost linearly as the number of transmit diversity increases because of interference rejection property by transmit diversity.

Table 5.4: Mean of the intracell interference for different number of antennas

Diversity order	Transmit diversity	Receive diversity
M=1	1.000	1.000
M=2	0.500	1.000
M=4	0.250	1.000
M=8	0.125	1.000

Now, let us investigate the performances of transmit diversity and receive diversity in downlink with multipath diversity under frequency selective channel. It is assumed that there exist two resolvable equal gain multipath components. Each multipath component follows Rayleigh fading distribution and independent of each other. Figure 5.14 and Figure 5.15 shows the outage probabilities versus the number of users per cell for different number of receive antennas and transmit antennas, respectively. Because of due to the increased resolvable multipath components, receive diversity provides slightly improved outage probability as compared with those in Figure 5.10. Given a outage probability of 10^{-2}, the system capacity can be determined and is summarized in Table 5.5.

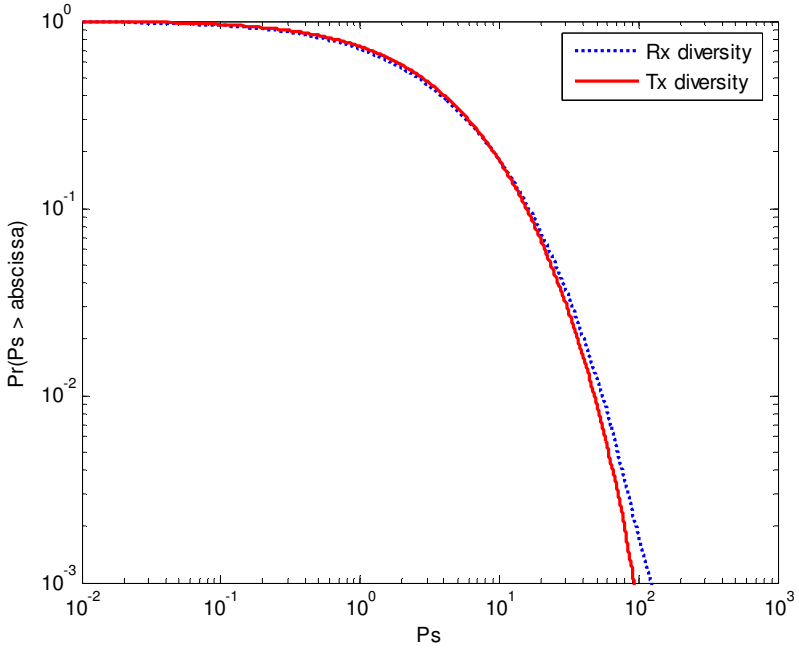

Figure 5.12: Complementary cumulative distribution functions of received signal power at MS

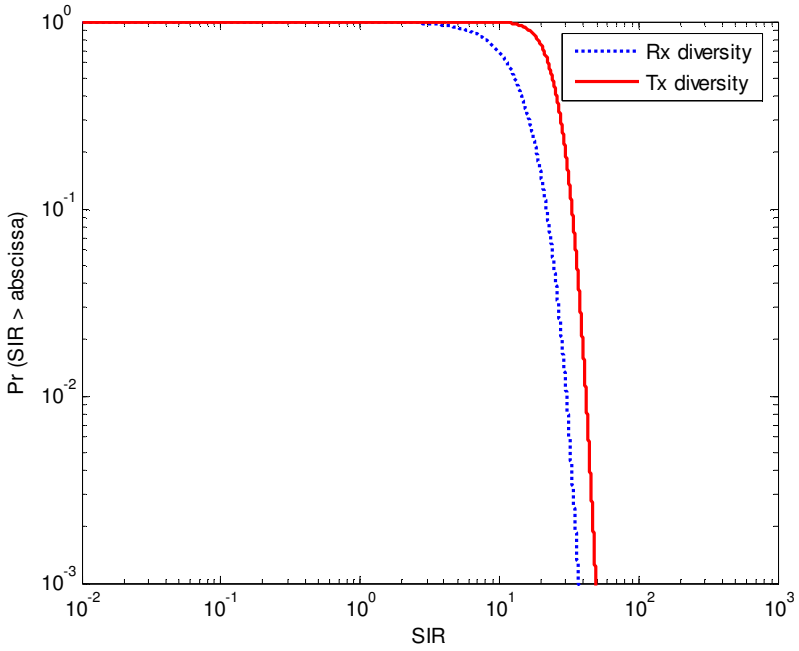

Figure 5.13: Complementary cumulative distribution functions of received signal-to-interference ratio at MS

On the other hand, when the transmit diversity is implemented, the outage probabilities are slightly deteriorated as compared with those in frequency flat fading channel in spite of the additional multipath diversity. It is likely due to that the number of transmit weight coefficients are smaller than the dimension of transmit channel due to the increased resolvable multipath components. Since transmit weight vector tries to exploit higher dimension in signal space to maximize the SNR at the receiver in multipath fading channel, the received SNR with transmit diversity will be worse than the SNR with receive diversity for the same diversity order. Furthermore, the intracell interference with transmit diversity also slightly increases due to the increased resolvable multipath components while that with receive diversity are reduced by resolvable multipath components. The intracell and intercell interference with transmit diversity and receive diversity are summarized in Table 5.6.

Table 5.5: Cell capacity with transmit diversity and receive diversity under frequency flat and frequency selective channel

	Transmit Diversity		Receive Diversity	
	L=1	L=2	L=1	L=2
M=1		1.2		1.2
M=2	2.8	3.2	2.5	3.8
M=4	8.8	7.9	7.5	10.4
M=8	26.2	19.3	18.7	26.4

Table 5.6: Statistics of intracell and intercell interference with transmit and receive diversity for different diversity order

	Transmit Diversity			Receive Diversity		
	Intracell	Intercell Interference		Intracell	Intercell Interference	
	C_{NOF}	Mean	Variance	C_{NOF}	Mean	Variance
M=1	1.000	4.501	3540.1	1.000	4.501	3540.1
M=2	0.613	1.756	185.73	0.800	1.516	136.08
M=4	0.371	0.852	33.870	0.667	0.650	19.348
M=8	0.218	0.440	8.2467	0.588	0.303	3.8621

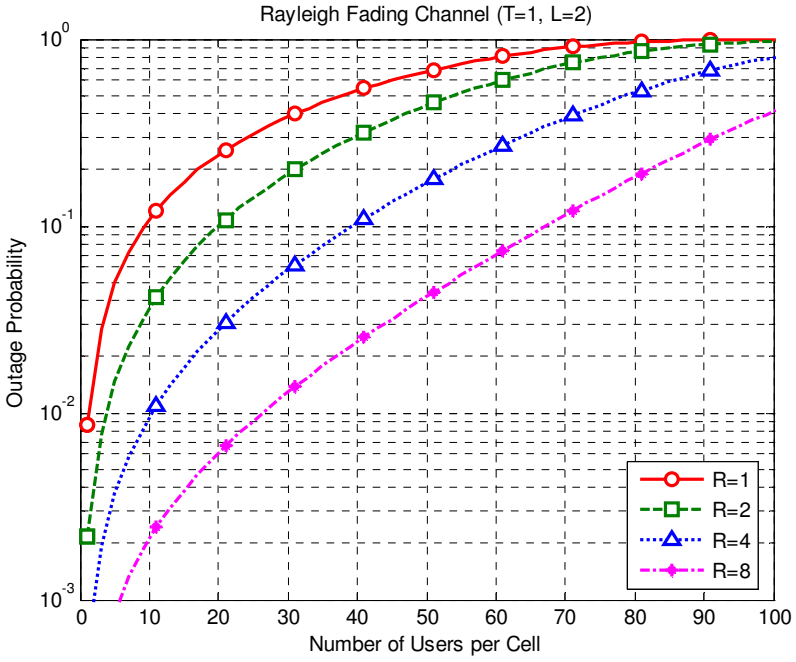

Figure 5.14: Outage probability vs. the number of users per cell for different number of receive antennas in frequency selective channel (L=2)

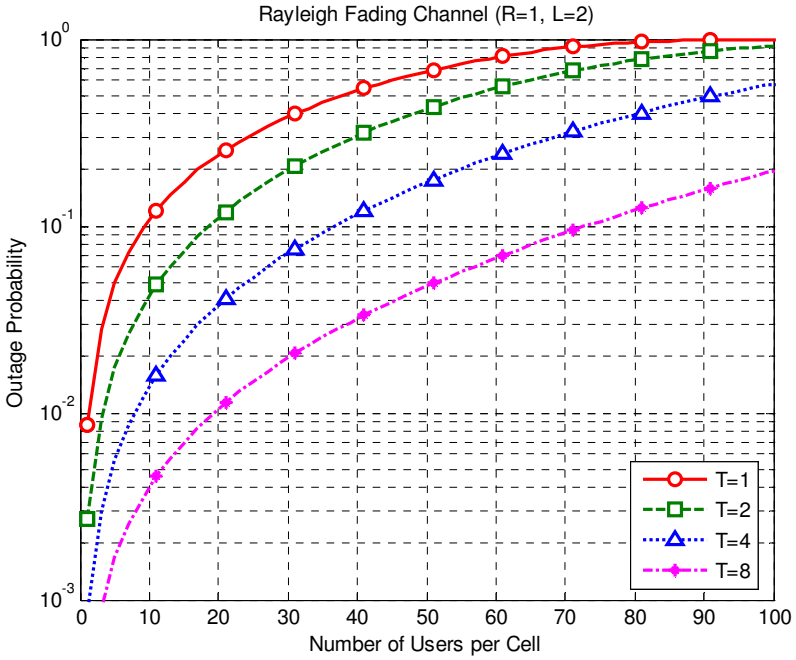

Figure 5.15: Outage probability vs. the number of users per cell for different number of transmit antennas in frequency selective channel (L=2)

Figure 5.16 shows the outage probabilities versus the number of users per cell for different number of transmit antennas at BS, and with two receive antennas at MS. It is assumed that the number of resolvable multipath components is one, i.e. frequency flat fading channel. It can be observed that transmit diversity at BS significantly improves the outage probability of the system even when there are two receive antennas at MS. However, the outage probability is worse than that achieved by either receive diversity only or transmit diversity only with the same diversity order in Figure 5.14 and Figure 5.15. The system performance under frequency selective channel with two resolvable multipath components is shown in Figure 5.17. The receiver is assumed to combine all the resolvable multipath components. Again, it is observed that transmit diversity improves the outage probability of the system. However, the outage probability is inferior to that achieved by either receive diversity only or transmit diversity only with the same diversity order. Furthermore, the system performance under the frequency selective channel are worse than those under frequency flat fading channel due to eigenvalue spread by transmit diversity behavior over multiple receive diversity branches. For the comparison, the number of users per cell for an outage probability of 10^{-2} is summarized in Table 5.7.

Table 5.7: Cell capacity of transmit diversity with two receive antennas

	Transmit diversity with two receive antennas	
	L=1	L=2
M=2 (T=1)	2.5	3.8
M=4 (T=2)	6.7	7.6
M=8 (T=4)	16.6	15.0
M=16 (T=8)	41.6	31.4

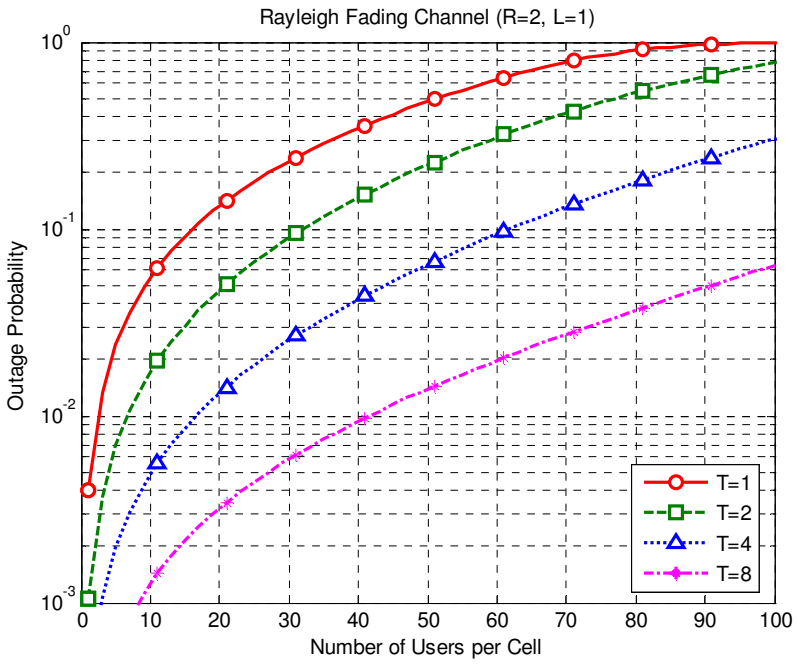

Figure 5.16: Outage probability vs. the number of users per cell with two receive antennas for different number of transmit antenna

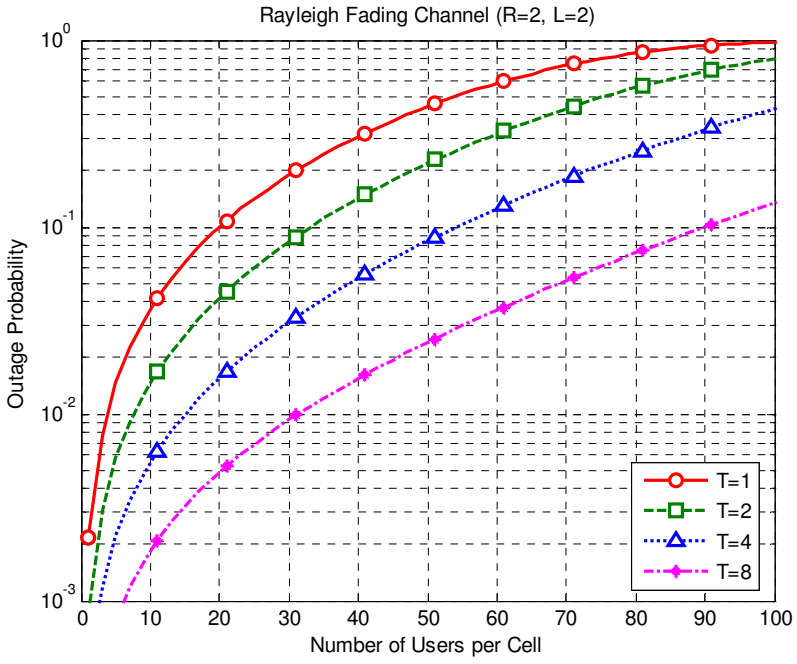

Figure 5.17: Outage probability vs. the number of users per cell with two receive antennas and two resolvable multipath components for different number of transmit antennas

5.5.2 Impact of soft handoff on the capacity of downlink DS/CDMA cellular systems

Now, let us investigate how soft handoff affects the system capacity of the downlink. Generally, diversity combining of signals from multiple BSs in the active set and power control will reduce the fractional power allocation of BS to an MS. This reduction of the fractional power allocation of BS is expected to improve the supportable number of users in a cell. Figure 5.18 shows the impact soft handoff on the outage probability of the downlink for different number of BSs in active set. It is assumed that there is no microscopic diversity such as multipath diversity and antenna diversity. It is assumed that all MSs in each cell communicate with all BSs in the active set. It is observed that system capacity is significantly improved by increasing the number of BS in the active set. However, downlink soft handoff naturally consumes the channel resources of BSs in the active set, that is, the BSs in the active set assign their channel to the same MS in soft handoff, and allocate a fractional power to the same MS in soft handoff. Thus, the actual system capacity may be less than the system capacity shown in Figure 5.18. Figure 5.19 shows the outage probability versus the number of users per cell taking into account BSs in the active set assign a channel to the same MS. It is observed that the outage probability of soft handoff is significantly degraded. Nevertheless, it is observed that there is still a soft handoff gain at low outage probability or for a small number of users. However, at high outage probability or for a large number of users, the outage probability of soft handoff quickly gets worse. Thus, capacity gain from the soft handoff in the downlink is obtained for systems with low outage probability.

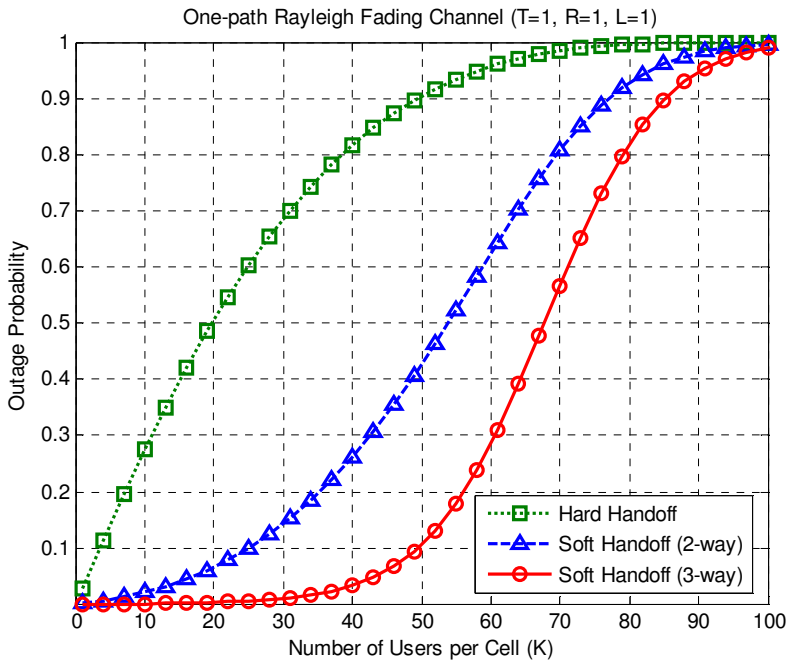

Figure 5.18: Outage probability vs. the number of users per cell for different size of active set

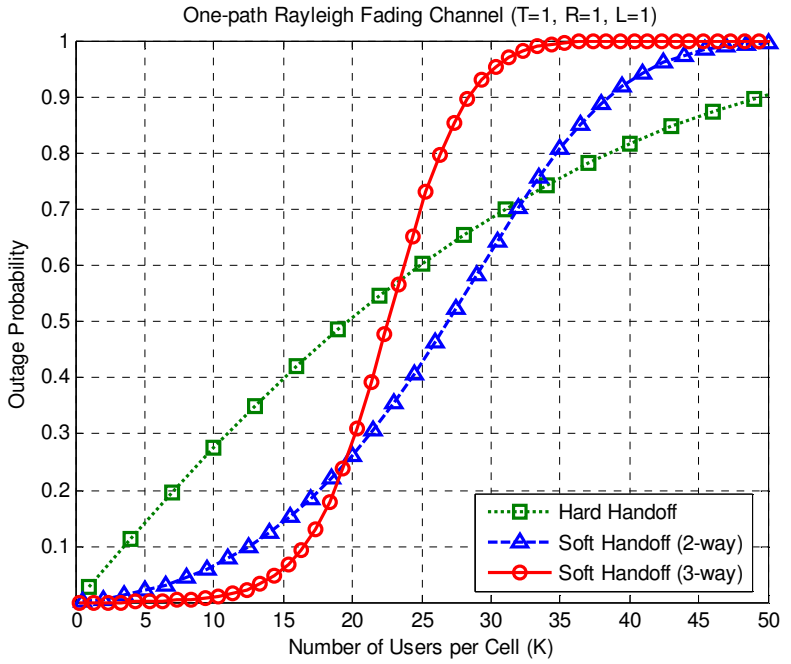

Figure 5.19: Outage probability vs. the number of users per cell for different size of active set (normalized by the size of active set)

Figure 5.20 shows the outage probability versus the number of users per cell when all MSs in the system are in soft handoff. The number of BSs in the active set is assumed to be '3'. The number of users per cell is normalized by the number of BSs participating in soft handoff. Comparing with the results observed in Figure 5.10, it is observed that the system capacity with one receive antenna significantly improves due to the diversity gain from the soft handoff. However, the improvement of outage probability with multiple receive antennas is observed to be not as much as the improvement of outage probability with one receive antenna in spite of the soft handoff gain shown in Figure 5.18. It is due to that multiple channel resources of BSs in the active set are consumed by the same MS.

Now, examine the plot shown in Figure 5.20, where the outage probability versus the number of users per cell are plotted for different number of transmit antennas with 3-way soft handoff. The number of users per cell is normalized by the number of BSs participating in soft handoff. Different from the results shown in Figure 5.21, it is observed that the outage probability significantly improves as the number of transmit antenna increases even though multiple channel resources of BSs in the active set are consumed by the same MS. In addition, the improvement of the outage probability by transmit diversity is greater that those observed in Figure 5.11. Basically, these improvement results from the intracell interference reduction by transmit diversity. Therefore, it can be concluded that the impact of intracell interference reduction is larger in soft handoff than that without soft handoff when the transmit diversity is implemented in the downlink.

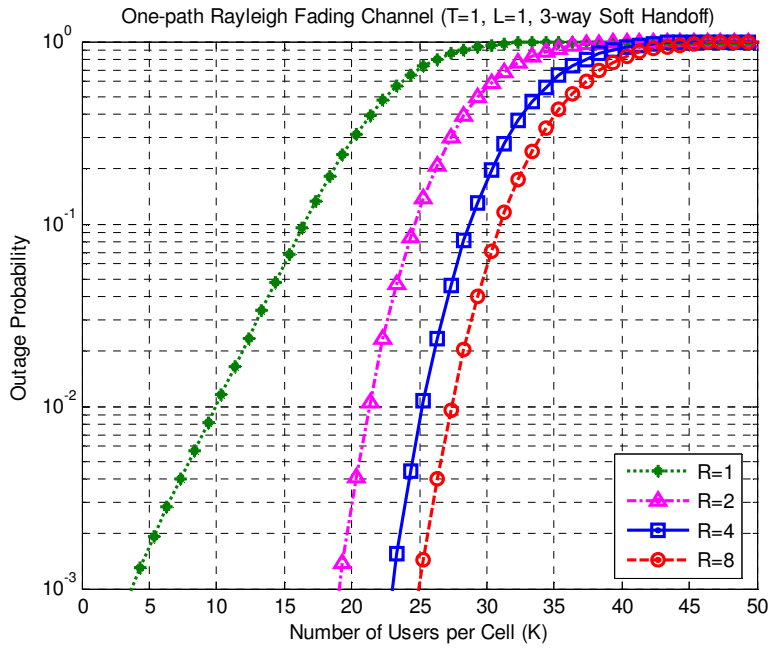

Figure 5.20: Outage probability vs. the number of users per cell for different number of receive antennas with soft handoff

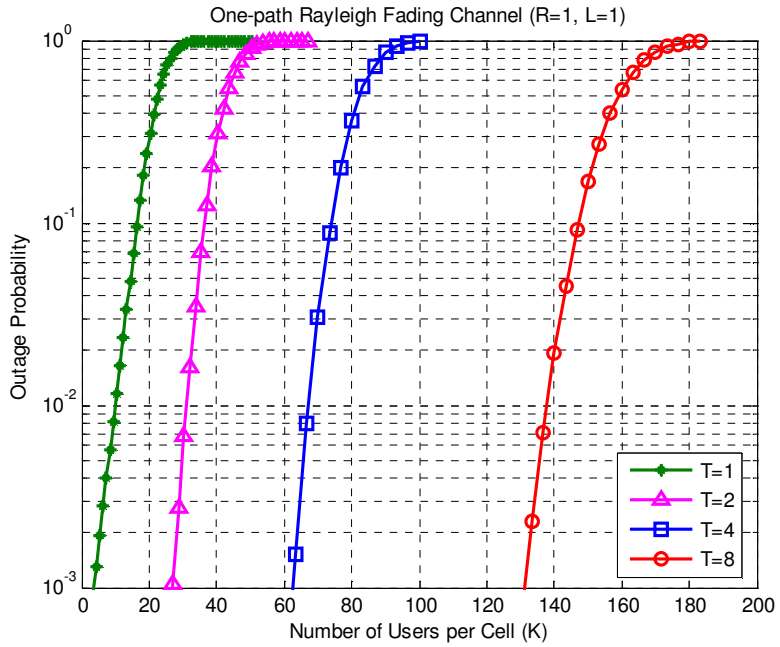

Figure 5.21: Outage probability vs. the number of users per cell for different number of transmit antennas

Now, let us consider the change of the soft handoff region in a cell. The soft handoff region will be determined by the soft handoff thresholds, T_{ADD} and T_{DROP}, shown in Figure 5.2. As described in the system model, it is assumed that soft handoff region is determined by the path loss between MS and BS. Then, the soft handoff region will be placed at the outer ring of cell as shown in Figure 5.3. Without taking into account the multiple channels are consumed by the same MS, the system capacity will increases as the ratio of MSs in soft handoff to the total number of MSs increases as shown in Figure 5.22, where the number of receive antennas at MS is set to '2', and one-path Rayleigh fading channel and 3-way soft handoff are presumed.

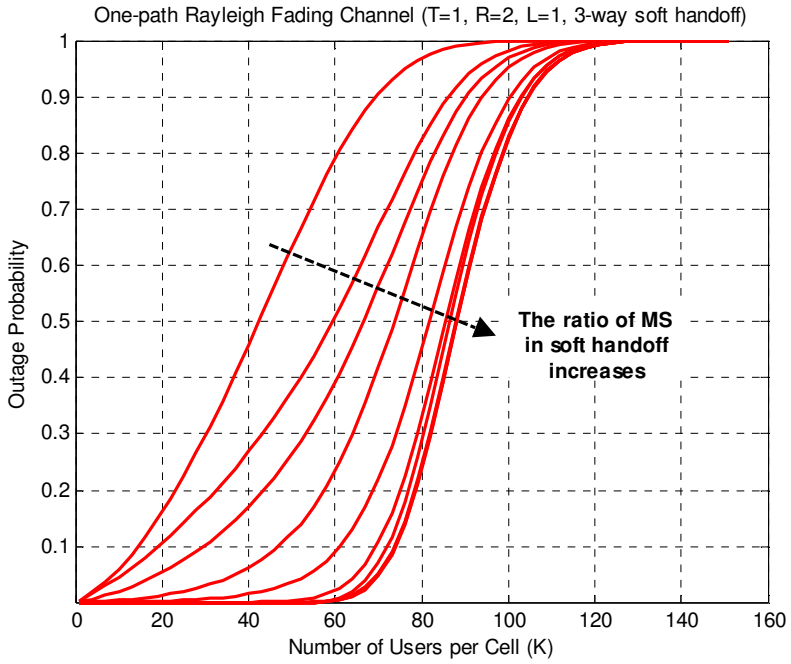

Figure 5.22: Outage probability vs. the number of users per cell for different ratio of MSs in soft handoff.

For given outage probability (for example, $P_{out} = 10^{-2}$), the supportable numbers of users per cell can be determined for the different ratio of MSs in soft handoff. Then, the relationship between system capacity for a given outage probability and soft handoff ratio can be drawn as shown in Figure 5.23. Without taking into account that each BS in the active set assigns a channel to the same MS, the system capacity is observed to increases with the ratio of MSs in soft handoff. However, it is observed that the system capacity reaches a limit with increasing number of MSs in soft handoff. This is due to the intercell interference decreasing as the soft handoff ratio increases. The system outage depends on the intracell interference once the intercell interference is sufficiently suppressed. Note that the intracell interference is the same for given diversity order regardless of the handoff. Furthermore, it is observed that the ratio of MSs in soft handoff, at which the capacity is saturated, decrease as the number of receive antennas increases. This is due to that the intercell interference is more rapidly reduced by both soft handoff and receive diversity. Note that system capacity shown in Figure 5.23 did not take into account the channel resources consumed at other cells by soft handoff.

Taking into account that the neighboring BSs in the active set assign a channel to the same MS, system capacity versus the ratio of MSs in soft handoff is plotted in Figure 5.24. It is observed that the system capacity increases to a certain ratio of MSs in soft handoff, after which it decreases. The system capacity versus the ratio of MSs in soft handoff is a convex function and the maximum points varies depending on the number of receive antennas. Therefore, in order to maximize the system capacity with soft handoff technique employed in the system, it is critical to choose the optimal soft handoff threshold.

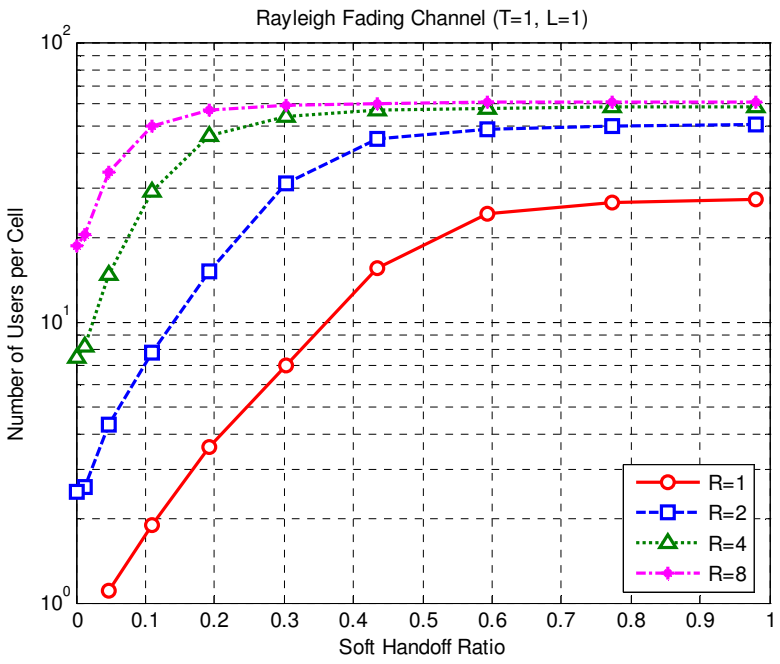

Figure 5.23: Cell capacity vs. soft handoff ratio (considering only power reduction by soft handoff) for different number of receive antennas

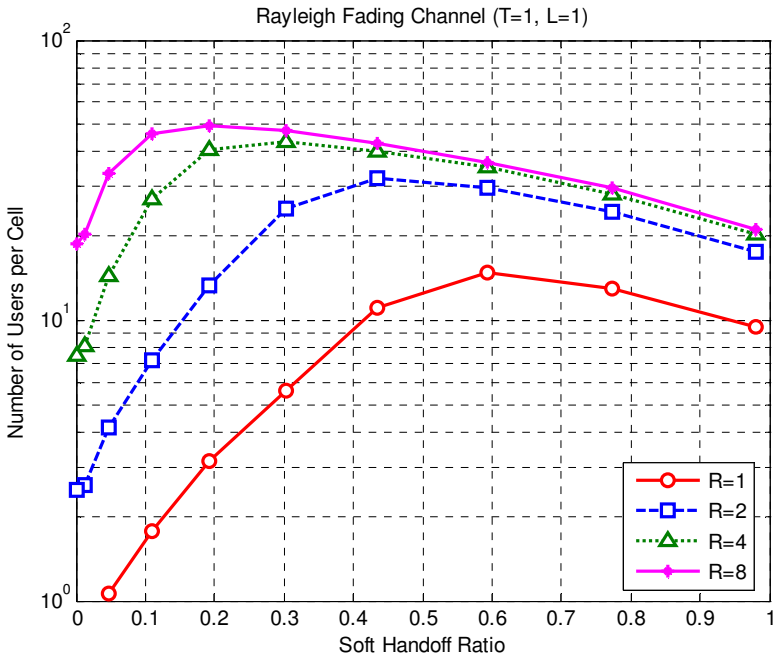

Figure 5.24: Cell capacity vs. soft handoff ratio (considering both power reduction and channel assignment) for different number of receive antennas

Figure 5.25 shows the number of users per cell versus the ratio of MSs in soft handoff for different number of transmit antennas. This figure does not take into account that the multiple channels are assigned by multiple BSs in the active set to the same user in soft handoff. It is assumed that MS is equipped with one receive antenna and there is only one resolvable multipath components. Comparing Figure 5.25 to Figure 5.23, relative capacity improvement by transmit diversity is greater that that by receive diversity. This is due to the intracell interference reduction provided by transmit diversity.

Taking into account the channel assignment to the same MS by multiple BSs in the active set and the reduction of the fractional power of BS allocated to MS by soft handoff, the same trend of cell capacity versus the soft handoff ratio as that in Figure 5.24 is observed. That is, the supportable number of users per cell begins to decrease as the ratio of MSs in soft handoff increases after a certain soft handoff ratio. However, it can be observed that the soft handoff ratio for the maximum cell capacity is slightly shifted to a large value when transmit diversity is implemented. For example, the maximum cell capacity is achieved at a soft handoff ratio of 0.3 with four receive antennas; while the maximum cell capacity is achieved at a soft handoff ratio of 0.4 with four transmit antennas. Also, the maximum cell capacity is achieved at a soft handoff ratio of 0.2 with eight receive antennas; while the maximum cell capacity is achieved at a soft handoff ratio of 0.3 with eight transmit antennas. It is likely due to the different amounts of intracell interference for the two cases. However, for the diversity order of two, there is little difference in the soft handoff ratio to obtain maximum cell capacity. From these results, it can be concluded that as diversity order increases capacity is more sensitive to the soft handoff ratio.

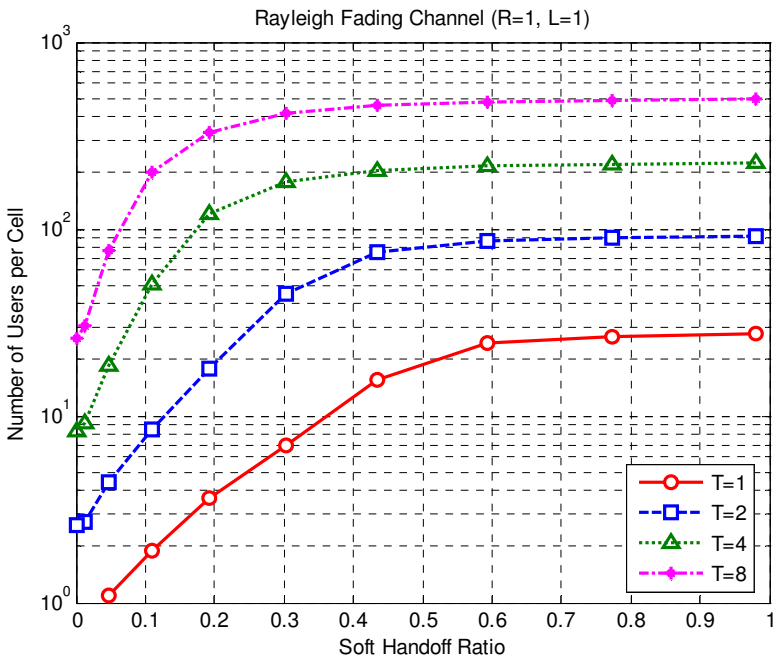

Figure 5.25: Cell capacity vs. soft handoff ratio (considering only power reduction by soft handoff) for different number of transmit antennas

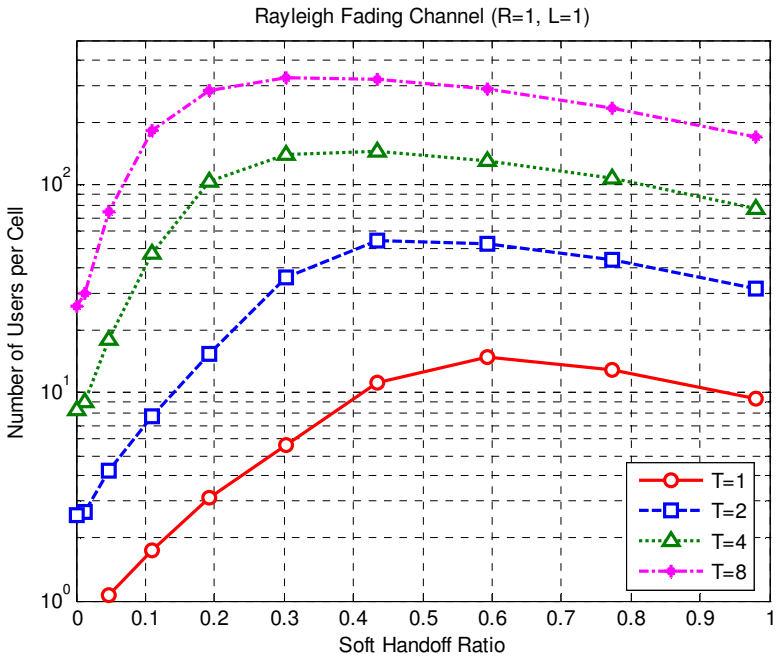

Figure 5.26: Cell capacity vs. soft handoff ratio (considering only power reduction by soft handoff) for different number of transmit antennas

Now, let us examine the system performance for the frequency selective channel environments. It is assumed that there are two resolvable multipath components with identical and independent Rayleigh fading distributions. Figure 5.27 shows the cell capacity versus the soft handoff ratio taking into account only the reduction of fractional power of BSs by soft handoff for different number of receive antennas. It can be observed that because of the multipath diversity the cell capacity significantly improves as the soft handoff ratio increases as compared to the results shown in Figure 5.23.

Figure 5.28 shows cell capacity versus soft handoff ratio taking into account both fractional power reduction and the consumption of multiple channel resources by an MS in soft handoff for different number of receive antennas. As compared with the results shown in Figure 5.24, the soft handoff ratio for the maximum cell capacity is observed to be shifted to a small value when the order of spatial diversity is small. For instance, for one receive antenna, the maximum cell capacity with one resolvable multipath component is achieved when a soft handoff ratio is 0.6; while the maximum cell capacity with two resolvable multipath components is achieved when a soft handoff ratio is about 0.55. Also, for two receive antennas, the maximum cell capacity with one resolvable multipath component is achieved when a soft handoff ratio is 0.4; while the maximum cell capacity with two resolvable multipath components is achieved when a soft handoff ratio is 0.3. However, for large diversity order, the soft handoff ratio for the maximum capacity is not observed to be shifted as much as that with small diversity orders. That is, the impact of multipath diversity on capacity is more pronounced for the small diversity order.

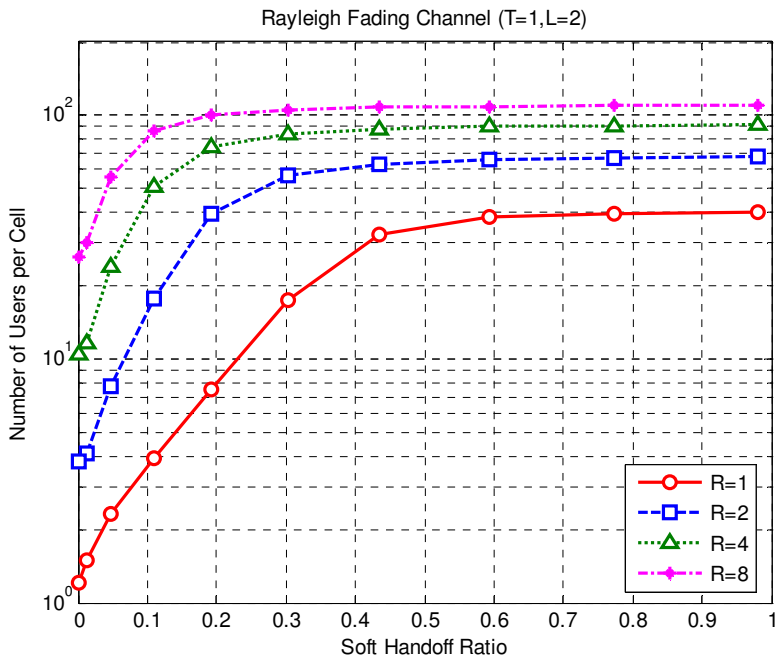

Figure 5.27: Cell capacity vs. soft handoff ratio (considering only power reduction by soft handoff) for different number of receive antennas and two resolvable multipaths

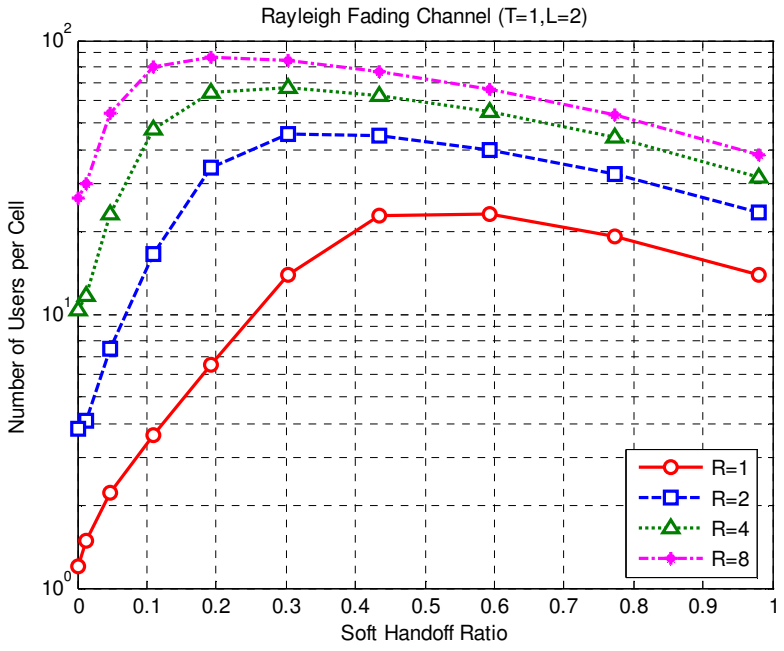

Figure 5.28: Cell capacity vs. soft handoff ratio (considering both power reduction and channel assignment) for different number of receive antennas and two resolvable multipaths

Figure 5.29 shows cell capacity versus soft handoff ratio in a cell under frequency selective fading channel for different number of transmit antennas, where only the fractional power reduction of BS by soft handoff is taken into account. It is assumed that two resolvable multipath components are combined at the rake receiver. Because of multiple resolvable multipath components, the performance of transmit diversity is degraded as shown in Figure 5.15; hence, the supportable number of users per cell is observed to be reduced as compared with the results shown in Figure 5.25 for the same number of transmit antennas except for T=1, since the channel power is spread over multiple eigenvalues. However, it can still be observed that the cell capacity is significantly improved by transmit diversity without any spatial diversity implementation at the receiver. It is also observed that the cell capacity is saturated above a certain soft handoff ratio.

Figure 5.30 shows cell capacity versus soft handoff ratio for different number of transmit antennas, taking into account both the fractional power reduction of BS and the consumptions of multiple channel resources by an MS in soft handoff. Hence, the cell capacity decreases above a certain soft handoff ratio in a cell. Similar trends are observed as shown in Figure 5.28 for the soft handoff ratio at which the maximum capacity is achieved. That is, the soft handoff ratio for the maximum cell capacity is observed to be shifted to a lower value when the number of transmit antennas is small (T=1 and T=2); while the soft handoff ratio for the maximum cell capacity is not observed to be shifted by multipath diversity when the number of transmit antennas are large (T=4 and T=8).

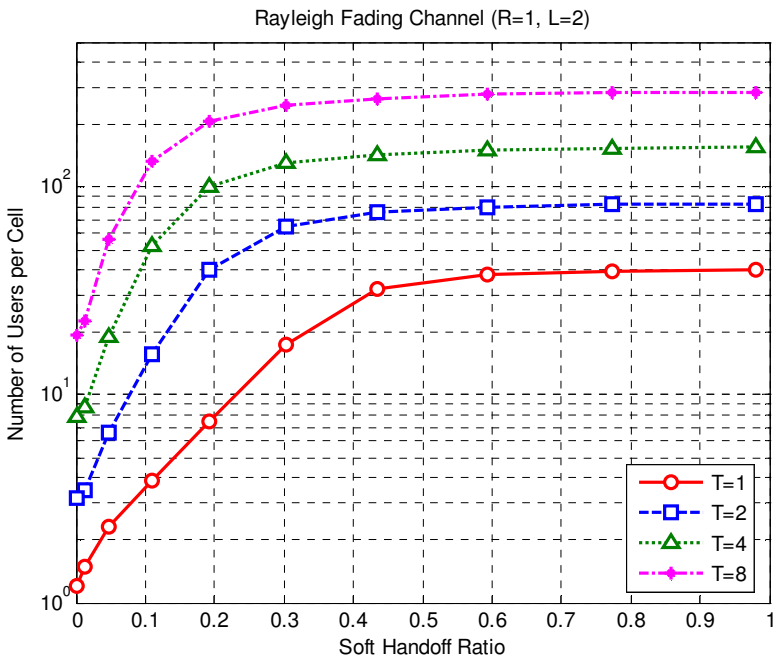

Figure 5.29: Cell capacity vs. soft handoff ratio (considering only power reduction by soft handoff) for different number of transmit antennas and two resolvable multipaths

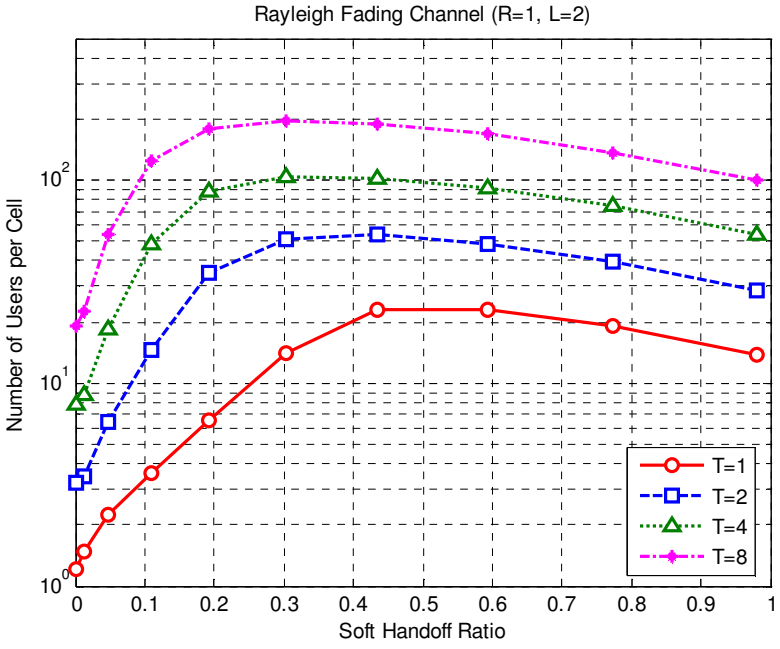

Figure 5.30: Cell capacity vs. soft handoff ratio (considering both power reduction and channel assignment) for different number of transmit antennas and two resolvable multipaths

Next, let us investigate when transmit diversity is implemented at BS and receive diversity is implemented at MS. It is assumed that only two receive antennas are implemented at MS, taking into account the small size of handheld devices. On the other hand, BS is assumed to be able to be equipped with up to eight transmit antennas. Figure 5.31 shows cell capacity versus soft handoff ratio, for different number of transmit antennas, taking into account only the reduction of the fractional power of BS by soft handoff. It is assumed that there is only one resolvable multipath component. It can be observed that because of receive diversity at MS the supportable number of users significantly improves for the same number of transmit diversity as compared with the results without receive diversity shown in from Figure 5.23 to Figure 5.30. Similarly, the cell capacity reaches a limit above a certain soft handoff ratio in a cell.

Figure 5.32 shows cell capacity versus soft handoff ratio, for different number of transmit antennas, where both the reduction of the fractional power of BSs and the consumption of multiple channel resources by one MS during soft handoff are taken into account. As seen in other plot, the capacity is a convex function of the soft handoff ratio. It is also observed that the soft handoff ratio for the maximum capacity is changed as compared with the results shown in Figure 5.26, where only transmit diversity is implemented at BS without implementing receive diversity at MS. In this result, the soft handoff ratios for the maximum cell capacity are observed to be shifted to a lower value as compared with those in Figure 5.26 for the same number of transmit diversity.

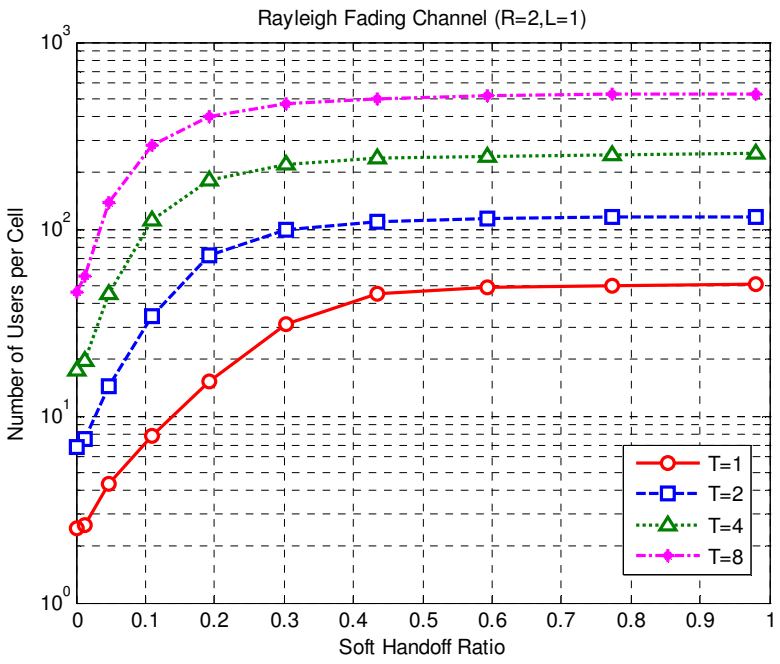

Figure 5.31: Cell capacity vs. soft handoff ratio (considering only power reduction by soft handoff) for different number of transmit antennas and two receive antennas

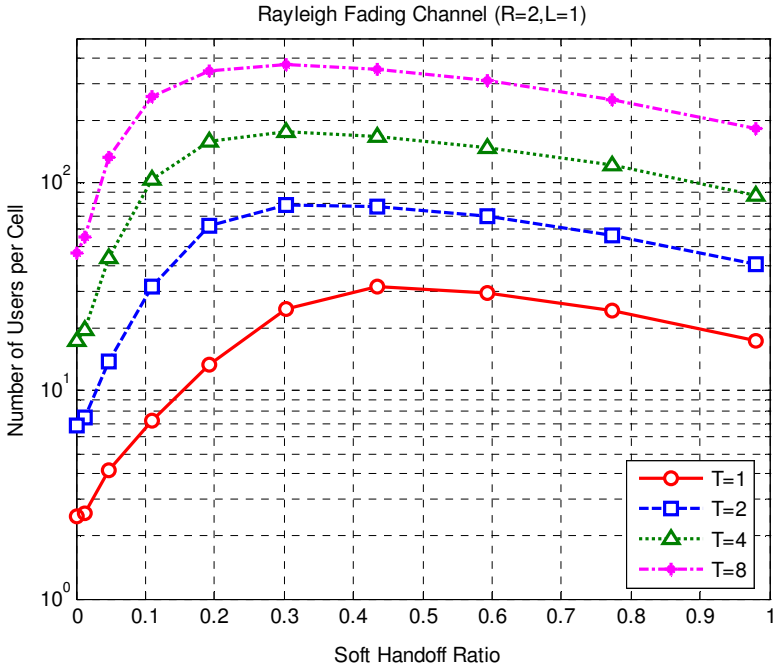

Figure 5.32: Cell capacity vs. soft handoff ratio (considering both power reduction and channel assignment) for different number of transmit antennas and two receive antennas

Figure 5.33 shows cell capacity versus soft handoff ratio for varying number of transmit antennas, two receive antennas and two resolvable multipath components. Because of multipath diversity, the performance of transmit diversity is degraded as compared with those with one resolvable multipath component. However, due to the receive diversity, the supportable number of users with a small number of transmit antennas (T=1 and T=2) increases, when compared with the results shown in Figure 5.31. On the other hand, capacity is observed to be reduced with large number of transmit antennas (T=4 and T=8), when compared with the results shown in Figure 5.31. From these results, it is concluded that the capacity degradation of transmit diversity is small when there receive diversity implemented. However, when the transmit diversity order is larger than the receive diversity order, the capacity degradation of transmit diversity is more distinct. Furthermore, it is observed that the relative improvements by increasing transmit diversity are reduced when compared with the results shown in Figure 5.31 because of the additional multipath diversity.

Figure 5.34 shows capacity versus soft handoff ratio, taking into account both the reduction of fractional power of BS allocated to MS and the consumption of multiple channel resources by an MS in soft handoff. As before, it can be observed that the cell capacity is a convex function of the soft handoff ratio. However, because of the receive diversity and multipath diversity, it is observed that the soft handoff ratio for the maximum cell capacity is shifted to lower value as compared with the results shown in Figure 5.32.

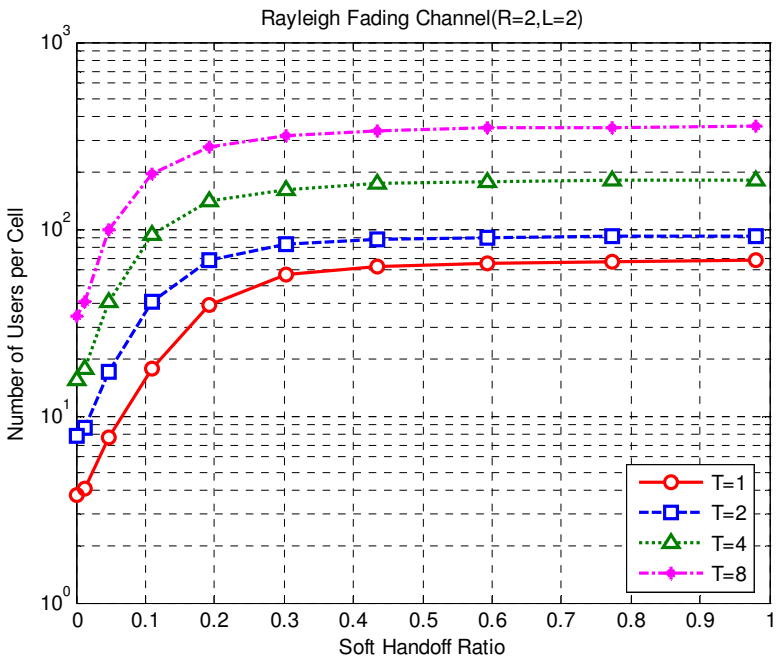

Figure 5.33: Cell capacity vs. soft handoff ratio (considering only power reduction by soft handoff) for different number of transmit antennas, two receive antennas and two resolvable multipaths

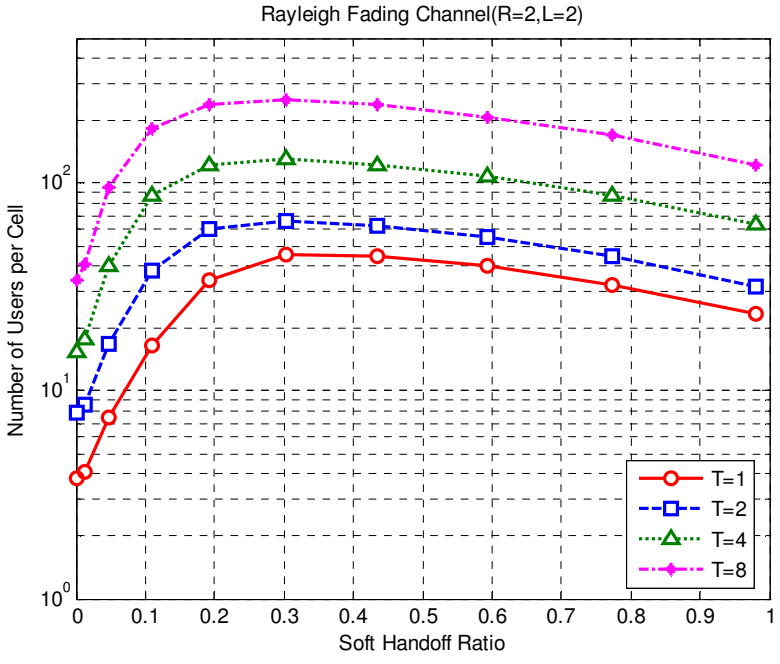

Figure 5.34: Cell capacity vs. soft handoff ratio (considering both power reduction and channel assignment) for different number of transmit antennas and two receive antennas and two resolvable multipaths

Finally, let us investigate the downlink system capacity with the different path loss exponent. In the uplink, it was observed that the larger path loss exponent increases the propagation loss from the interferer to the BS. Similar to the uplink, in the downlink, the larger path loss exponent will also increase the propagation loss from the interferer to the MS. In addition, the signal power will be maintained at the required level by power control. Hence, the received SIR improves, which results in the capacity improvement. Figure 5.35 shows the normalized capacity achieved by receive diversity, for different soft handoff ratio and with the path loss exponent of '5'. It is observed that the system capacities achieved by the receive diversity with the path loss exponent of '5' are larger than those with the path loss exponent of '4' shown in Figure 5.24. Also, Figure 5.36 shows that the system capacities achieved by transmit diversity with the path loss exponent of '5' are larger than those with the path loss exponent of '4'. Therefore, the system capacity in the environment with the smaller path loss exponents will be reduced by the increased interference.

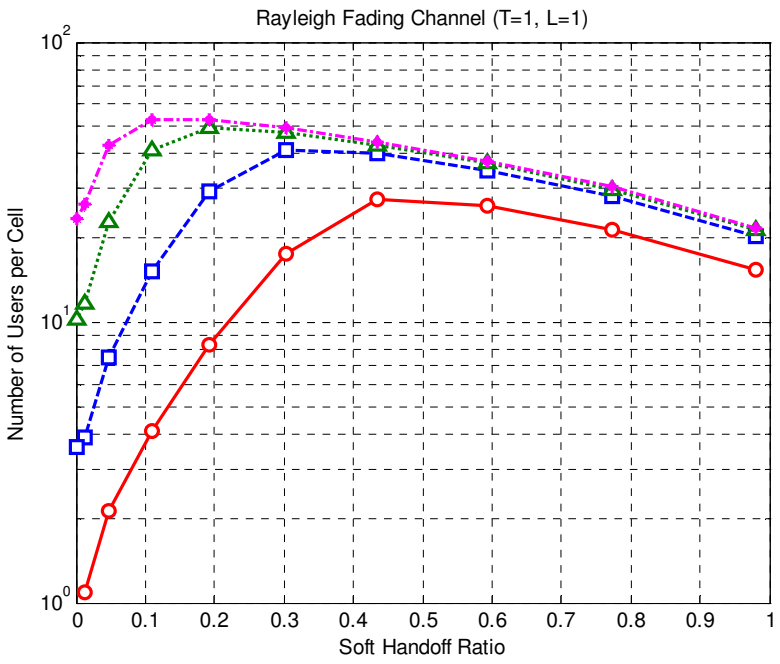

Figure 5.35: Cell capacity vs. soft handoff ratio with path loss exponent of '5' for different number of transmit antennas, two receive antennas and two resolvable multipaths

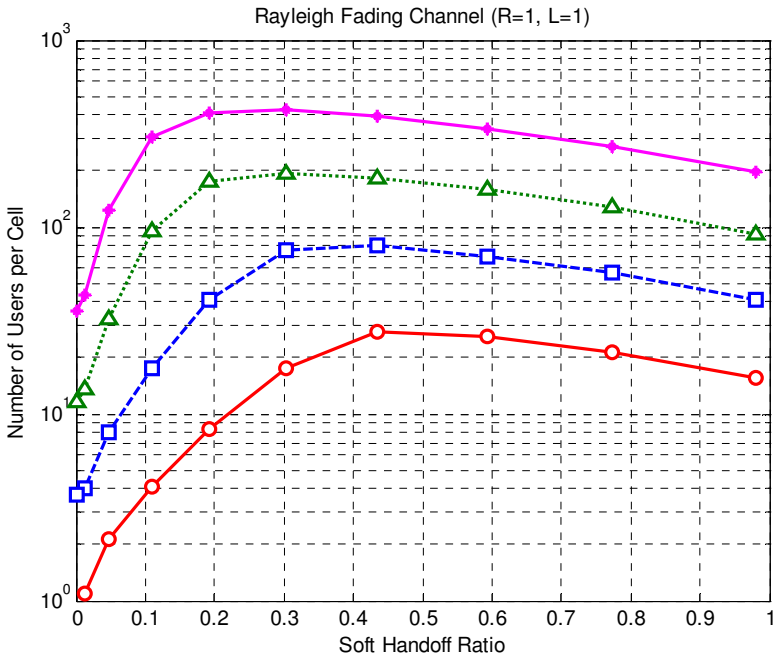

Figure 5.36: Cell capacity vs. soft handoff ratio with path loss exponent of '5' for different number of transmit antennas and two receive antennas and two resolvable multipaths

5.6 Chapter Summary

In this chapter, we have investigated the impact of MIMO and soft handoff on system capacity of the downlink DS/CDMA cellular. In the downlink, system outage is defined as when the sum of the fractional powers of BS allocated to the MSs exceeds the available power of BS. Since soft handoff in the downlink allocates multiple channel resources to an MS, it has been known to have a negative impact on system capacity of the downlink. However, the analysis in this chapter shows:

- Combining the signals from multiple BSs and fast power control along with controlling the soft handoff ratio can improve the system capacity. That is, the system capacity is observed to be a convex function of the soft handoff ratio in a cell.
- Using MIMO in conjunction with fast power control can significantly improve the system capacity of the downlink by reducing the mean and variance of interference.
- Employing maximal ratio transmit diversity, implemented by closed loop transmit diversity in this analysis, provides better performance than the receive diversity due to its ability to reject intracell interference.

The analytical framework for the downlink is derived based on the outage probability of the system. The analytical expression for the fractional power of BS is derived taking into account MIMO, soft handoff process and fast downlink power control. Furthermore, it is shown that the fractional power of BS allocated to an MS in downlink is well approximated by log-normal distribution, which makes it simple and efficient to analyze the outage probability of the system.

Chapter

6 System Performances of DS/CDMA Cellular Systems with MIMO Diversity in Degenerate MIMO Channel

6.1 Introduction

Multiple-input multiple-output (MIMO) systems have drawn a considerable attention in the area of wireless communication because of their potential capabilities – combating multipath fading and co-channel interference, and providing large channel capacities. However, significant capacity gain is only achievable when the sub-channels connecting each transmit antenna to each receive antenna are independent. It is well known that *correlation* between antenna elements from the imperfect separation of antenna elements is a major obstacle in achieving in the benefits of a MIMO systems. Correlation between antenna elements is known to limit the degrees of freedom of the MIMO channel; hence, the diversity gain and capacity diminish if there is rank deficiency of the MIMO channel. Recently, however, it has been reported that the rank or the diversity order of MIMO

channel could degenerate even without any correlation between antenna elements [79-91]. This degeneracy of MIMO channel is referred to as *the keyhole effect* and the degenerate MIMO channel has the property of uncorrelated elements and low channel rank. The negative impact upon spatial multiplexing has been shown through mathematical analysis [79, 80, 84-86, 90] and empirical results [87-89, 91]. In addition, it has been shown that the keyhole effect can significantly reduce the spatial diversity gain [81-83]. It is interesting to note that so far all the analysis and experimental results have been performed based on the point-to-point communications without considering the impact of keyhole channels on the overall networks.

- ***Contributions***

In this chapter, the impact of keyhole effect on the MIMO performance is investigated in both the uplink and the downlink of DS/CDMA cellular systems by using the framework developed in Chapter 3 and Chapter 5.

- ***Organization***

The remainder of this chapter is organized as follows. In section 6.2, the concept of keyhole effect is briefly reviewed and several realizations of keyhole effect in real environments are introduced. In section 6.3 and section 6.4, the degeneracy of MIMO channel and MISO / SIMO channel, respectively, is investigated in terms of the channel capacity and diversity performance of point-to-point communication. In section 6.5, the system level performance is evaluated in the degenerate MIMO channel. Finally, the main points of this chapter are summarized in section 6.6.

6.2 Keyhole Effects

In this section, the concept of keyhole (or pinhole) effect of degenerate MIMO channel is briefly reviewed and several realizations in practical MIMO systems are introduced.

6.2.1 Fundamentals

Let us take into account a simple but elegant example of 2×2 MIMO channel in rich multipath environment where all the components of the matrix channel are represented by uncorrelated complex Gaussian random variables. This channel has two degrees of freedom and can be transformed into two 'virtual' parallel independent channels through the singular value decomposition (SVD) / QR decomposition or layered coding at the transmitter with appropriate decoding and signal processing at the receiver [92]. This transformation of MIMO channel has been popularly exploited for spatial multiplexing independent data streams into each virtual channel; hence, twice the data rate can be achieved without any loss of channel bandwidth.

Now, let us place a screen with a small hole (referred to as keyhole or pinhole) between transmit and receive antenna arrays as shown in Figure 6.1. The only way for the radio wave to propagate from the transmitter to the receiver is to pass through this keyhole. The channel matrix in this case takes the following form [85].

$$\mathbf{H} = \begin{pmatrix} b_1 \\ b_2 \end{pmatrix} \sigma \begin{pmatrix} a_1 & a_2 \end{pmatrix} = \sigma \begin{pmatrix} a_1 b_1 & a_2 b_1 \\ a_1 b_2 & a_2 b_2 \end{pmatrix} \tag{1.1}$$

where a_1 and a_2 are the channel coefficients from the transmit antenna array to the keyhole, b_1 and b_2 are the channel coefficients from the keyhole to the receive antenna array, σ is the scattering cross-section of the keyhole which is assumed to ideally reradiate the captured energy. Apparently, the entries of $\mathbf{H}$ are uncorrelated since a_i and b_i $(i = 1,2)$ are uncorrelated complex Gaussian random variables. However, this channel has only one non-zero singular value (by construction, the first row is dependent of the second row) and, hence there is only one degree of freedom, meaning that the channel capacity is low. Such a channel may be referred to as a degenerate channel, also known as uncorrelated low rank (ULR) in contrast to the uncorrelated high rank (UHR) channel corresponding to the normal MIMO channel. Comparing with the usual case (normal MIMO channel), each entry of $\mathbf{H}$ are distributed not as complex Gaussian but as a

product of two complex Gaussians. The probability distribution $f(p)$ of power p for such a process may be shown to be [85]

$$f(p) = \frac{2}{b^2} K_0\left(\frac{2\sqrt{p}}{b}\right) \tag{1.2}$$

where b is the average power and K_0 is the modified Bessel function. Some more realistic examples of such channel have been discussed in [84, 85, 87-89], which are also summarized in the following section.

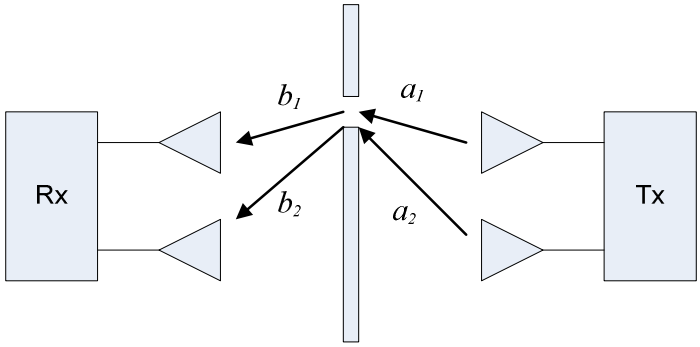

Figure 6.1: Example of a degenerate 2×2 channel with a keyhole.

6.2.2 Keyhole effects in real world

In this section, several examples of a degenerate MIMO channel in practical communication systems are introduced for better understanding the importance of keyhole effect on MIMO communication systems.

- ***Indoor hallway or tunnel / street canyon***

Keyhole effects are mostly explained by a waveguide model. For example, the indoor hallway at microwave frequencies may be thought of as an overmoded waveguide. In outdoor environments, the tunnel / street canyon can behave as a waveguide. In such practical environments, due to the losses at the boundary (usually made from dielectric materials) of waveguide, the higher-order modes becomes less significant, which in turn limits the achievable channel capacity [90]. In addition, the coupling among the decomposed modes reduces the channel matrix rank [85]. Several measurement

campaigns of MIMO channel in indoor hallways show that the channel capacity significantly decreases due to the reduced rank of measured MIMO channel as well as the losses at the boundaries of the hallways [87-89]. Figure 6.2 shows the possible scenario of the waveguide in outdoor environments.

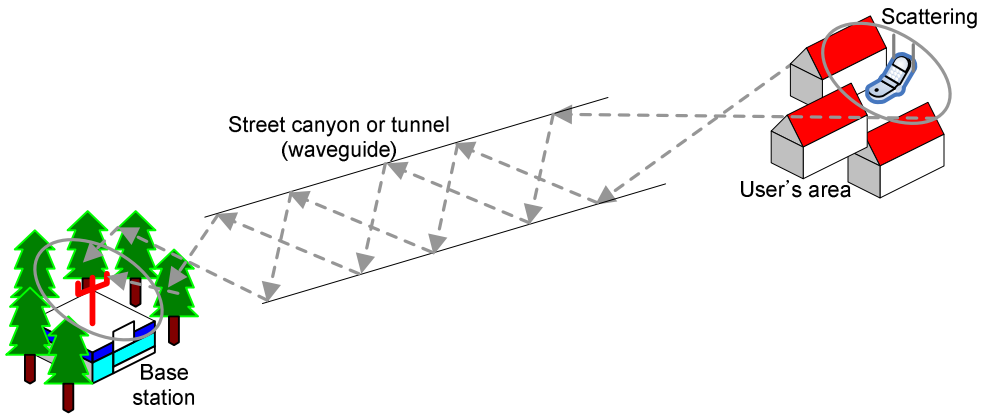

Figure 6.2: Waveguide in outdoor environments

- ***Narrow air pipe***

The pinhole realization can be occurred through thin air pipe as shown in Figure 6.3. This pinhole realization is analogous to that occurred in the communication through the indoor hallway. However, in contrast to the indoor hallway, this pinhole realization can be occurred without any concrete and visible waveguide. For example, reflections around the base transmitter stations and subscribers create lots of multipath and cause locally uncorrelated fading. However, all multipath components from the transmitter merge before they, again, split up into received multipath components. Hence, if the scatter rings are too small as compared to the separation between the two rings, the channel rank may become low [84, 93].

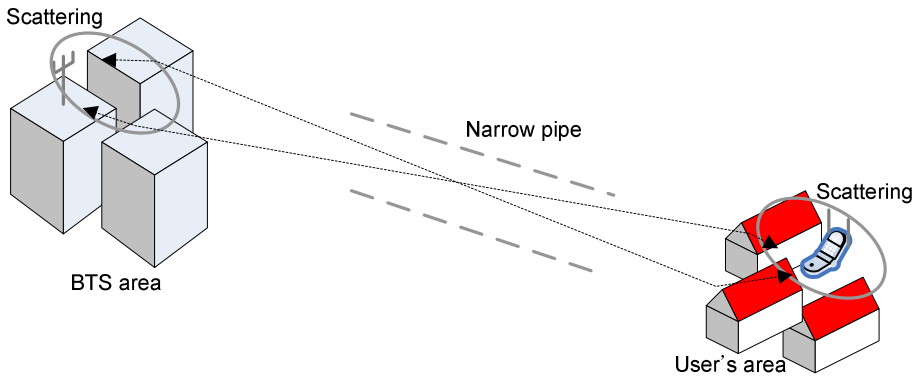

Figure 6.3: Thin air pipe effect

- ***Diffraction at rooftop edge***

In outdoor environments, the receiver is often obstructed from the transmitter by a diffracting edge, such as a roof edge, or a building corner. If the dominant path from the transmitter to the receiver is via diffraction at the roof edge, the diffracting edge acts as an equivalent horizontal line source with varying current strength along its length as shown in Figure 6.4. If the base antennas are vertically separated, the richness of the perceived channel is collapsed, and a keyhole is formed [85]. In this case, increasing the vertical separation of antenna arrays would be useless. This may be remedied by placing the base antennas in a horizontal array [91].

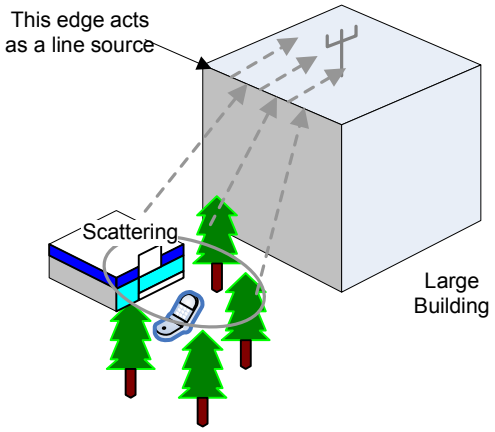

Figure 6.4: Diffraction at rooftop edge

6.3 Degenerate MIMO Channel

The characteristics of the degenerate MIMO channel created by the keyhole effect can be readily described by the cumulative distribution function of the channel capacity or the eigenvalue (or eigenmode) of $\mathbf{H}\mathbf{H}^{+}$, where $\mathbf{H}$ is the MIMO channel matrix. For spatial multiplexing application, the channel capacity may be an important measure, while for the spatial diversity application, the eigenvalue distribution will an important measure.

Let us first examine the channel capacity of both the degenerate MIMO channel and the normal MIMO channel. The channel capacity is given by

$$C = \log_2\left[\det\left(\mathbf{I}_M + \frac{\rho}{N}\mathbf{H}\mathbf{H}^{+}\right)\right] \tag{1.3}$$

where $\mathbf{H}$ is the $M \times N$ channel matrix, $\mathbf{I}_M$ denotes the identity matrix of size M, and ρ is the average signal-to-noise ratio (SNR) at each receiver antenna. Note that since $\mathbf{H}$ is random, C will be random as well. Assuming a piece-wise constant fading model (block-fading model) and coding over many independent fading intervals, $C_s = E_{\mathbf{H}}[C]$ will be the Shannon capacity of the random MIMO channel. In practice, the cumulative distribution function (cdf) of C is often used to characterize the outage properties of the MIMO channel [94]. Figure 6.5 shows the outage distributions of channel capacity for 2×2 channel. It is observed that the capacity of the degenerate MIMO channel is lower than that of the normal MIMO channel due to the rank deficiency as mentioned in the previous section. This rank deficiency can be easily observed in the eigenvalues of $\mathbf{H}\mathbf{H}^{+}$. Figure 6.6 and Figure 6.7 show the eigenvalues of $\mathbf{H}\mathbf{H}^{+}$ for the normal MIMO channel and the degenerate MIMO channel, respectively, with 2×2 configuration. For the full rank of the normal 2×2 channel, two eigenvalues are observed as shown in Figure 6.6; hence two independent spatial channels are available for the spatial multiplexing; However, for the degenerate 2×2 channel, due to the rank deficiency, one large eigenvalue and one small eigenvalue are observed in Figure 6.7; hence, there is only one spatial channel available for the transmission, which results in the lower channel capacity than that of the normal MIMO channel as shown in Figure 6.5 for an SNR of 10 dB.

On the other hand, for the spatial diversity application, the statistical property of the transmission path providing the largest eigenvalue is more important: mean and variance, corresponding to *array gain* and *diversity gain*, respectively. The array gain represents the energy capturing ability of the diversity system, thus means SNR improvement. The diversity gain implies the ability of diversity system to flatten fading channel fluctuation. Let us suppose that MIMO diversity is implemented by the receive diversity with MRC and MRT diversity. Assuming that the power of each channel is normalized to be one, and that AWGN is identical and independent distributed with zero mean and unit variance, the array gain is approximated as

$$G_A = \mathbb{E}\left[\lambda_{\max}(\mathbf{H}\mathbf{H}^{+})\right] \tag{1.4}$$

On the other hand, the diversity gain can be estimated by the normalized standard deviation (NSD) [95] or the effective fading figure (EFF) [83] of the largest eigenvalue of the channel matrix square ($\lambda_{\max}(\mathbf{H}\mathbf{H}^{+})$). Note that the EFF is just the square of the NSD. Hence, the EFF is calculated as

$$EFF = \left(\frac{\sqrt{\mathbb{V}\mathrm{ar}\left[\lambda_{\max}(\mathbf{H}\mathbf{H}^{+})\right]}}{\mathbb{E}\left[\lambda_{\max}(\mathbf{H}\mathbf{H}^{+})\right]}\right)^2 = \frac{\mathbb{V}\mathrm{ar}\left[\lambda_{\max}(\mathbf{H}\mathbf{H}^{+})\right]}{\mathbb{E}\left[\lambda_{\max}(\mathbf{H}\mathbf{H}^{+})\right]^2} \tag{1.5}$$

which is also referred as the variance-to-mean-square ratio (VMSR) being frequently used to assess the severity of fading and the effectiveness of diversity system on reducing signal fluctuations.

In Figure 6.6 and Figure 6.7, it can be observed that the mean of the largest eigenvalue in the degenerate MIMO channel is larger than that in the normal MIMO channel. The rank deficiency of the degenerate MIMO channel causes the channel energy to be concentrated on one channel; hence, the full array gain can be obtained in the degenerate MIMO channel. However, in terms of the diversity gain, it can be observed that the largest eigenvalue of the degenerate MIMO channel has larger variance than that of the normal MIMO channel. This is explained by both the fading distribution and the diversity gain of MIMO channel. Since each transmission path of the degenerate MIMO channel follows the distribution of a product of two complex Gaussian random variables, fading

distribution will be more severe than that of the normal MIMO channel. In the normal MIMO channel, each transmission path follows the distribution of single complex Gaussian random variable and its power follows a Gamma distribution. The power distributions of the transmission paths for both the degenerate MIMO channel and the normal MIMO channel are plotted in Figure 6.8. It is observed that the variance of the degenerate MIMO channel is larger than that of the normal MIMO channel. Although it is difficult to find the exact expression for the largest eigenvalue of the channel square matrix, $\lambda_{\max}(\mathbf{HH}^{+})$ with MIMO, a bound on $\lambda_{\max}(\mathbf{HH}^{+})$ can be easily found using the property that the sum of all eigenvalues is equal to the trace of the matrix $\mathbf{HH}^{+}$. Hence, for the normal MIMO channel, $\lambda_{\max}(\mathbf{HH}^{+})$ is bounded as

$$\frac{1}{n_T}\sum_{i=1}^{n_R}\sum_{j=1}^{n_T}\left|h_{ij}\right|^2 < \lambda_{\max}(\mathbf{HH}^{+}) \le \sum_{i=1}^{n_R}\sum_{j=1}^{n_T}\left|h_{ij}\right|^2 \tag{1.6}$$

and for the degenerate MIMO channel, $\lambda_{\max}(\mathbf{HH}^{+})$ is bounded as

$$\frac{1}{n_T}\left(\sum_{j=1}^{n_T}\left|h_j\right|^2\right)\cdot\left(\sum_{i=1}^{n_R}\left|h_i\right|^2\right) < \lambda_{\max}(\mathbf{HH}^{+}) \le \left(\sum_{j=1}^{n_T}\left|h_j\right|^2\right)\cdot\left(\sum_{i=1}^{n_R}\left|h_i\right|^2\right) \tag{1.7}$$

From these bounds, it is expected that the diversity gain of the degenerate MIMO channel is limited by the minimum among the number of transmit antennas and the number of receive antennas. On the other hand, the diversity gain of the normal MIMO channel linearly increases as either the number of transmit antennas or the number of receive antennas increases.

Diversity gain can be also expressed by the *diversity order* which can be estimated by the slope of the bit error probability (BEP) or the symbol error probability (SEP) curves [63, 94] with MIMO. Generally, the normal MIMO channel has the diversity order of the product of the number of transmit antennas and the number of receive antennas ($=n_T \times n_R$), while the degenerate MIMO channel has the diversity order of the minimum value among the number of transmit antennas and the number of receive antennas

$(=\min\{n_T, n_R\})$ [83, 84][6]. Hence, the slope of the BEP or SEP will not change for the same diversity order but the different antenna configurations. Therefore, the achievable diversity order of the degenerate MIMO channel is always less than that of the normal MIMO channel. Finally, it can be concluded that the diversity system in the degenerate MIMO channel provides the higher array gain but the smaller diversity gain than that in the normal MIMO channel.

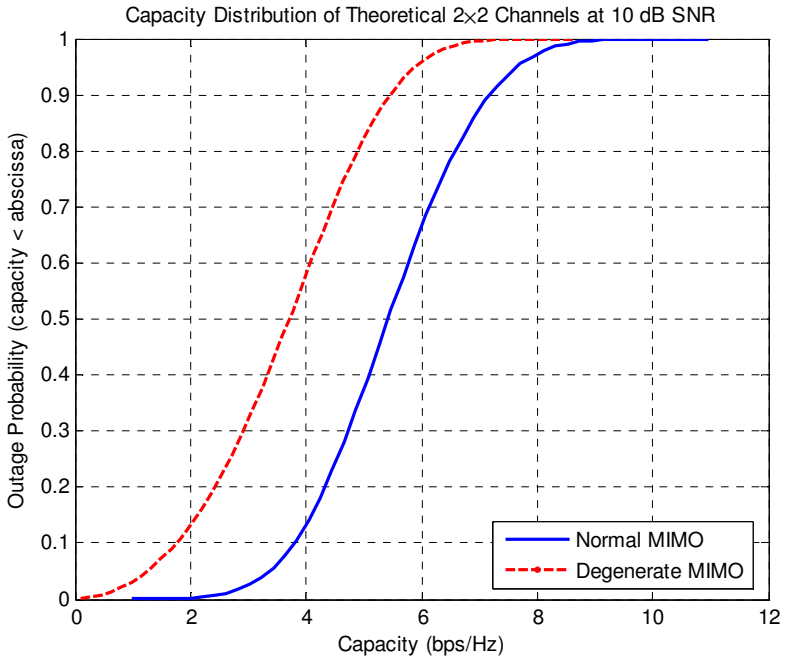

Figure 6.5: Channel capacity of both normal and degenerate MIMO channel (2×2)

[6] The derivation of the diversity order in MIMO channel is beyond the objective of this research and can be found in other literatures [63, 83, 94].

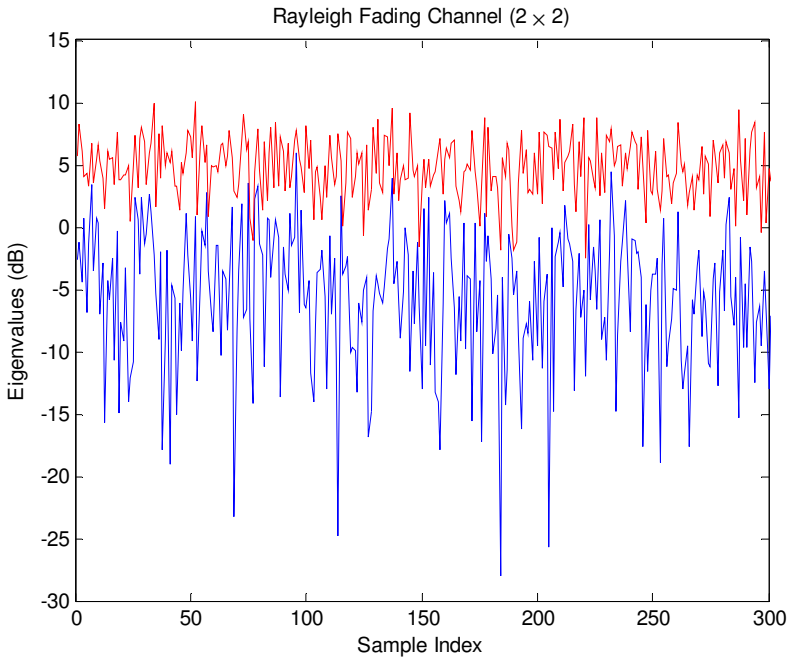

Figure 6.6: Eigenvalues of normal MIMO channel (2×2)

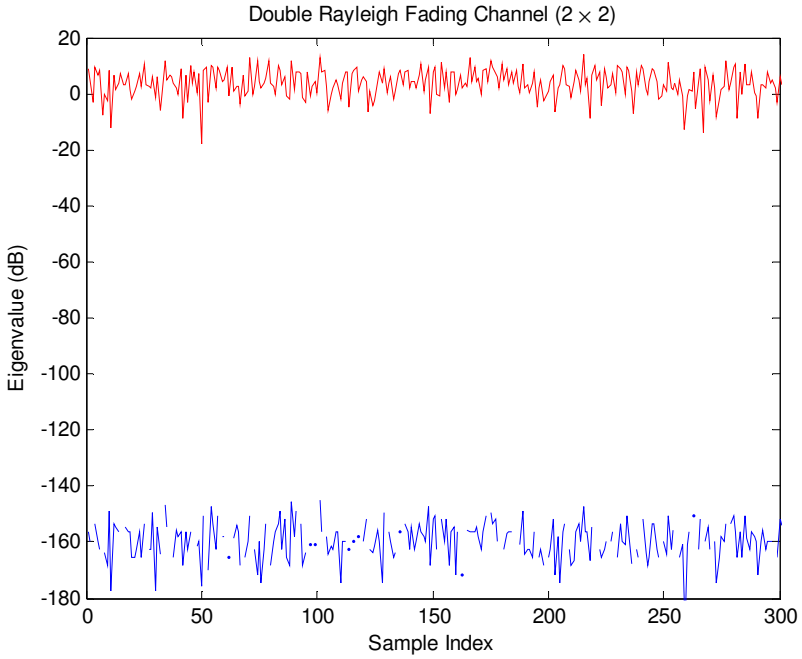

Figure 6.7: Eigenvalues of degenerate MIMO channel (2×2)

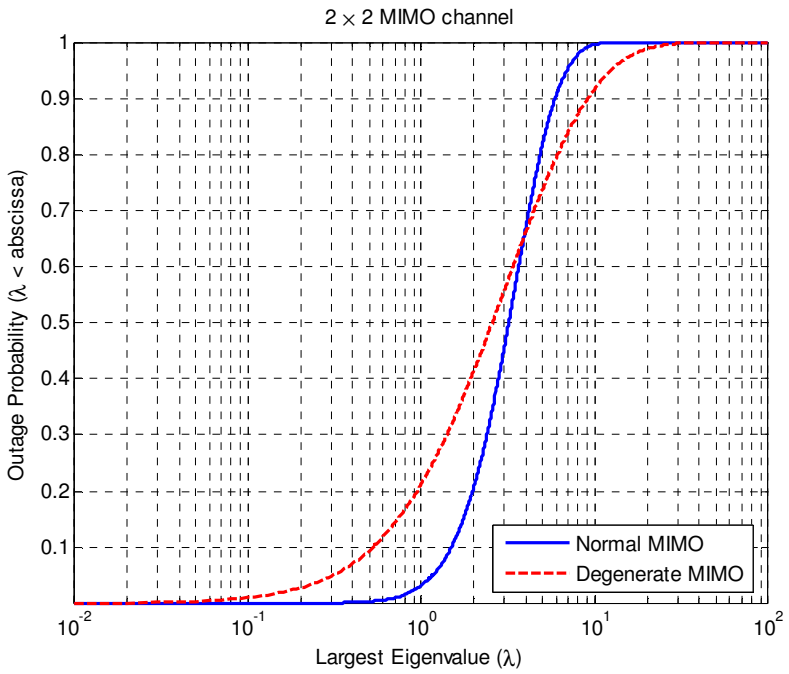

Figure 6.8: CDF of the largest eigenvalue of both normal and degenerate MIMO channel (2×2)

6.4 Degenerate MISO / SIMO channel

In this section, the degenerate multiple input single output (MISO) or single input multiple output (SIMO) channel is investigated. While the degenerate MIMO channel still provides the diversity gain (though reduced as compared with the normal channel) as well as the array gain, the degenerate MISO / SIMO channel will not provide any diversity gain because the diversity order of the degenerate MIMO channel is determined as the minimum between the number of transmit antennas and the number of receive antennas. However, the degenerate MISO / SIMO channel still provide array gain due to the rank reduction. Figure 6.9 and Figure 6.10 show the eigenvalues of the degenerate MISO channel and the normal MISO channel, respectively, for 4×1 antenna configuration. It can be observed that one large eigenvalue and three small eigenvalues in both the degenerate and the normal MISO channels. Hence, both channels provide only one spatial transmission path. Even so, the outage probability of channel capacity is observed to be better in the normal MISO channel than that in the degenerate MISO

channel as shown in Figure 6.11. It is due to that the normal MISO channel can provide additional diversity gain while the diversity gain of the degenerate MISO channel is very small as compared to that of the normal MISO channel. As mentioned in the degenerate MIMO channel, the diversity gain can be observed by investigating the EFF. It can be easily shown that the EFF of the degenerate MISO channel is always greater than one. In Equation (1.7), let us suppose that the number of receive antennas n_R be one and the number of transmit antennas n_T be arbitrarily large. Then, the variance of the largest eigenvalue will depend only on the channel power of $|h_1|^2$ at receive antenna. Figure 6.12 shows the EFF reduction for both the degenerate and the normal MISO channel as the number of transmit antennas increases given the number of receive antennas of one.

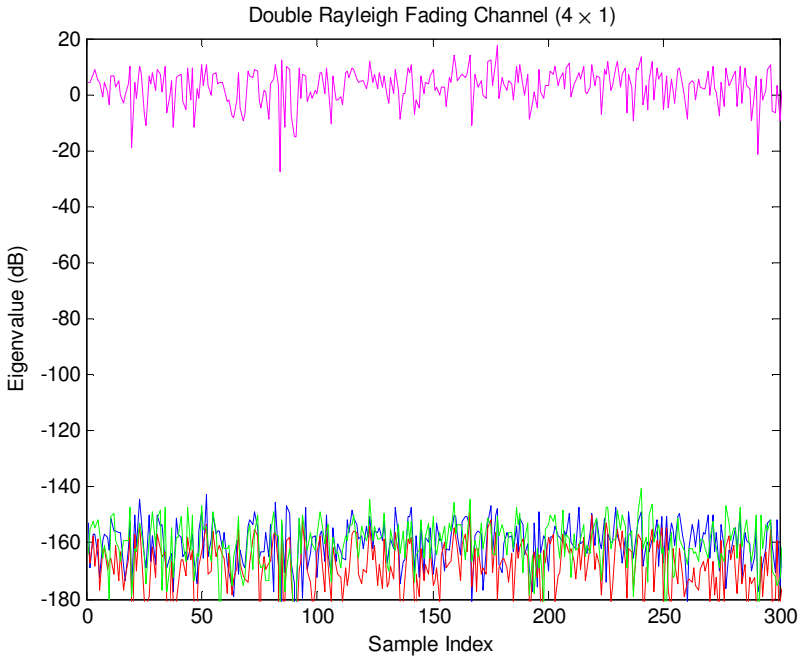

Figure 6.9: Eigenvalues of the degenerate MISO / SIMO channel (4×1)

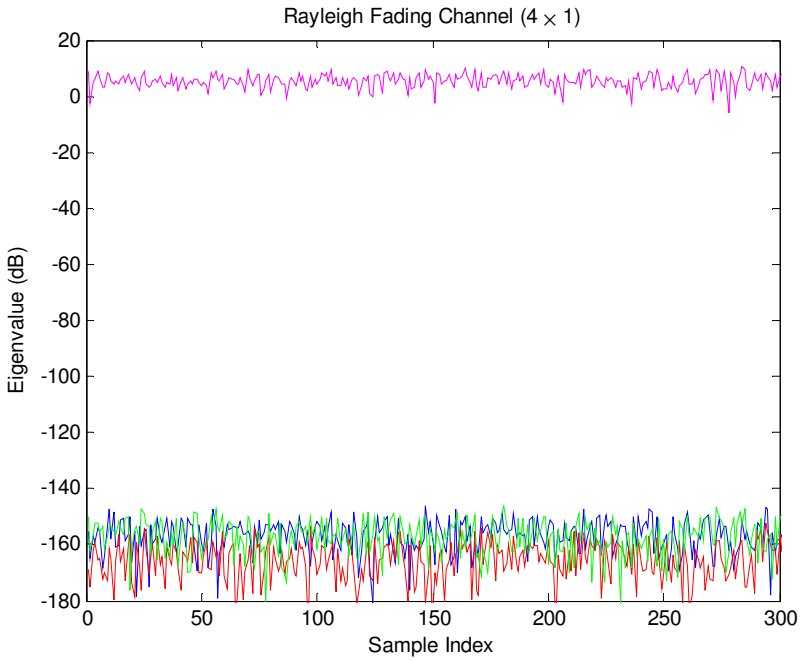

Figure 6.10: Eigenvalues of normal MISO/SIMO channel (4×1)

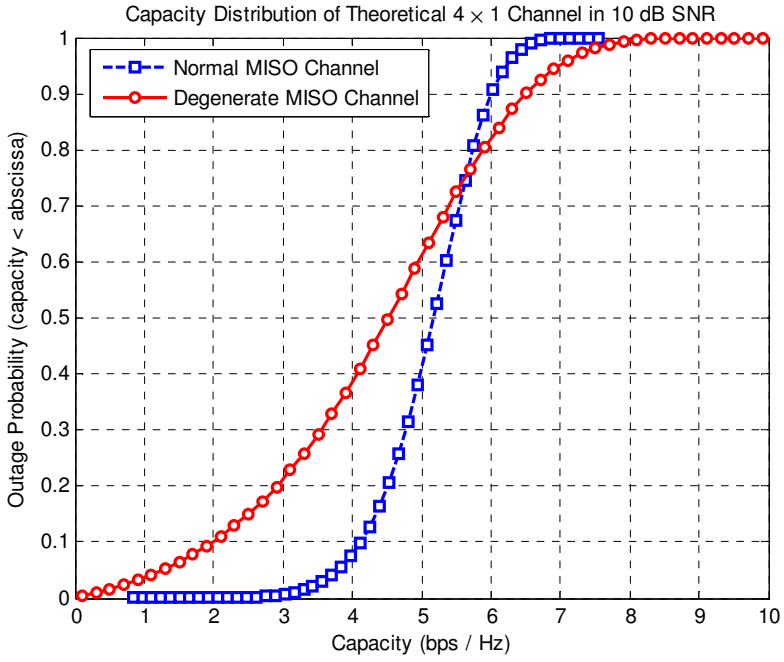

Figure 6.11: Channel capacity of both degenerate and normal MISO channels (4×1)

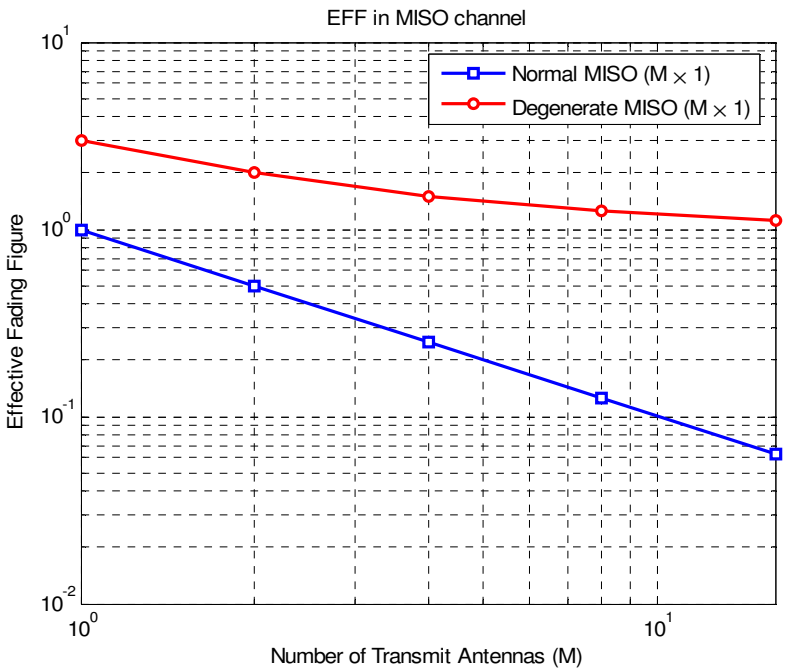

Figure 6.12: Effective fading figure in MISO channel ($M \times 1$)

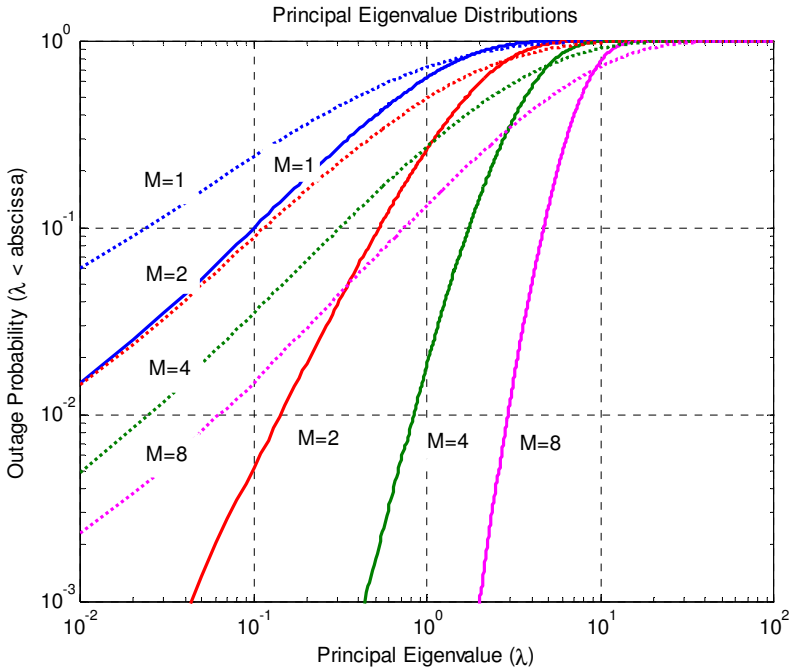

Figure 6.13: CDF of the largest eigenvalue of MISO channel for different number of transmit antennas (Dotted line: degenerate MISO channel, solid line: normal MISO channel)

Figure 6.13 shows the cdfs of the largest eigenvalue of both the degenerate MISO channel (the dotted line) and the normal MISO channel (the solid line) for different number of transmit antennas. It can be observed that the outage probability of the largest eigenvalue improves with the number of transmit antennas in both the degenerate and the normal MISO channel. However, because of more severe channel power distribution in the degenerate channel than that in the normal channel, the outage probability in the degenerate MISO channel is worse than that in the normal MISO channel for the same number of transmit antennas.

Now, let us investigate the impact of the diversity order increment in the degenerate channel. The diversity order can be increased simply by adding antenna arrays at the receiver in the MISO channel, and vice versa for the degenerate SIMO channel. That is, the diversity order can be increased by converting the MISO / SIMO channel into MIMO channel. Figure 6.14 shows the cdf of the largest eigenvalue of the degenerate MISO and MIMO channel. It can be observed that the outage probability can be significantly improved by adding the antenna array at the opposite side in the degenerate MISO / SIMO channel. Furthermore, given the outage probability of 10^{-2}, a 2×2 antenna configuration shows the better outage probability than 8×1 antenna configuration due to the diversity order increment even though 8×1 antenna configuration provide higher array gain than 2×2 antenna configuration. In contrast, in the normal MISO channel, the outage probability of 2×2 antenna configuration is worse than 4×1 antenna configuration as shown in Figure 6.15. This results from that the array gain in 2×2 antenna configuration is smaller than that in 4×1 antenna configuration even though the diversity order is the same in both configurations. Note that the channel powers are spread over two transmission paths in 2×2 antenna configuration while it is concentrated on one transmission path in 4×1 antenna configuration.

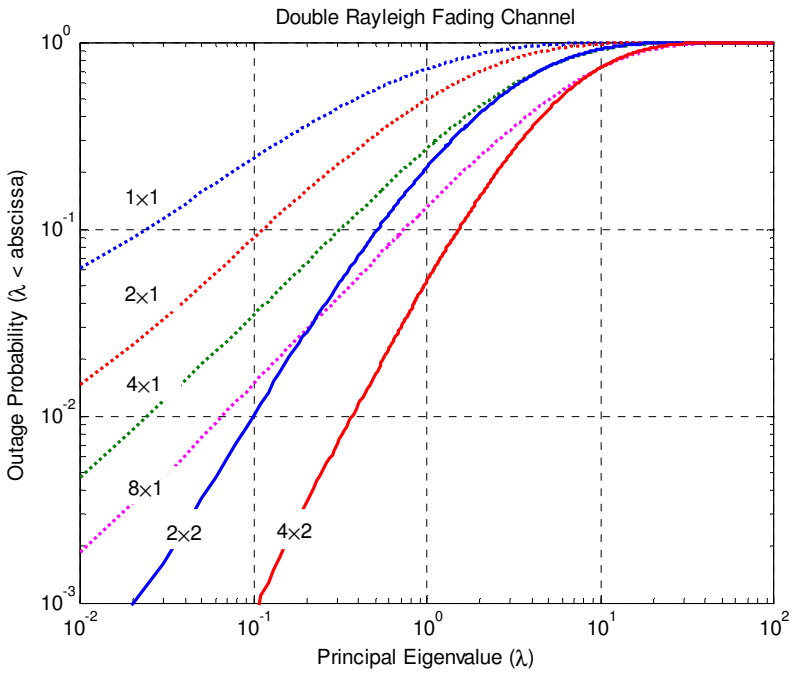

Figure 6.14: CDF of the largest eigenvalue of degenerate MISO/MIMO channel

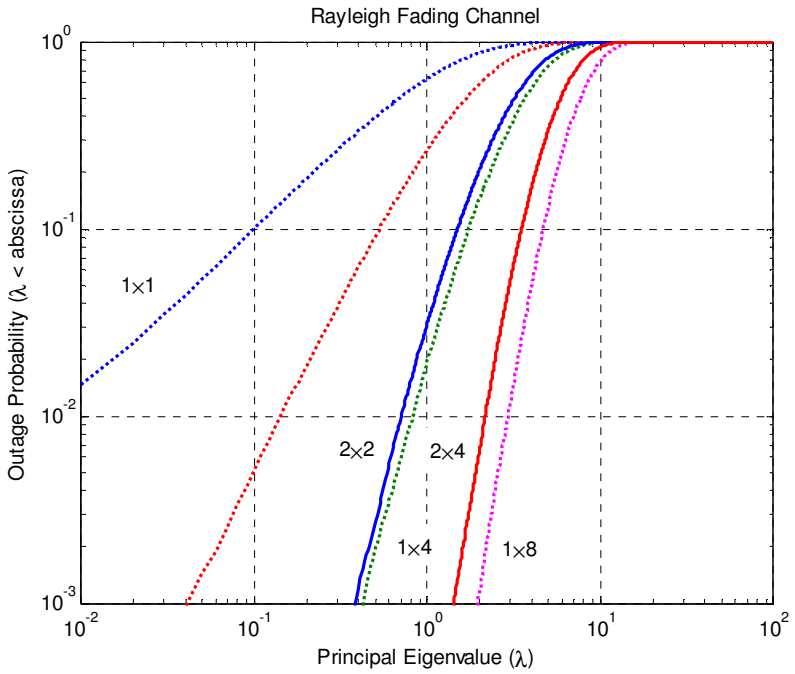

Figure 6.15: CDF of the largest eigenvalue of the normal MISO/MIMO channel.

6.5 System Performances of DS/CDMA Cellular Systems

Thus far, the characteristics of the degenerate MISO channel are investigated in the viewpoint of the point-to-point communications. However, as observed in the previous chapters, the system level performances are not directly translated from the link level performance. Hence, in this section, the system level performance of DS/CDMA cellular systems are briefly investigated for degenerate MISO, SIMO, and MIMO channels in terms of system capacity. System parameters assumed in the following analysis for both the downlink and uplink are summarized in Table 5.1. All the results shown in this section are generated by the framework developed in the previous chapters; however, the statistics of the interference-to-signal ratio are collected using Monte Carlo simulations.

Table 6.1: System Parameters

Parameters	Value
Spreading bandwidth (W)	1.25 MHz
Data Rate (R_b)	8 Kbps
Voice activity (ν)	0.4
Target E_b / I_0	5.6 dB
Shadowing correlation between BSs	0.5
Log-normal shadowing	$\sigma = 8\text{dB},\ m = 0$
Path loss exponent	$u = 4$
Soft handoff	3-way
Diversity order (M)	1, 2, 4, 8

6.5.1 Uplink performances

First, let us take into account the system capacity of the uplink DS/CDMA cellular systems with spatial diversity for the degenerate MIMO channel. The system capacity can be determined in terms of the number of users per cell for a given outage probability. Figure 6.16 shows the outage probabilities versus the number of users per cell for different number of transmit antennas with one or two receive antennas. It is assumed that the number of resolvable multipath component is one, and the fade margin is 20 dB. It can be observed that the outage probability improves as the number of transmit antennas increases for one receive antenna. However, the relative improvements by adding the additional transmit antennas significantly diminish as the number of transmit antenna increases in contrast to the results shown in Chapter 3, section 4.7. As shown in previous chapters, the system performance improvement is closely related to how much the interference is reduced by any interference reduction technique. However, note that for uplink DS/CDMA there is no intracell interference reduction by transmit diversity. Furthermore, the diversity gain may be very small in the degenerate MISO channel as shown in the previous section. Therefore, the improvement in outage probability by increasing the number of transmit antennas primarily comes from improved array gain. This is confirmed by the mean and variance of interference provided in Table 6.2.

On the other hand, it can be observed that the outage probability can be significantly improved just by implementing two receive antennas with two transmit antennas. It can be observed that the outage probability of the 2×2 antenna configurations is better than that of the 8×1 antenna configurations. This improvement in outage probability is due to the diversity gain from the added receive antenna increment and the intracell interference reduction by the added receive diversity.

Table 6.2: Interference statistics in the degenerate MISO channel

	Intracell interference		Intercell interference	
	Mean	Variance	Mean	Variance
T=1, R=1	0.372	0.266	2.358	310.31
T=2, R=1	0.373	0.269	1.105	101.85
T=4, R=1	0.374	0.270	0.469	64.32
T=8, R=1	0.374	0.270	0.261	55.13
T=2, R=2	0.187	0.100	0.210	11.71
T=4, R=2	0.187	0.100	0.069	0.498

In Figure 6.17, the outage probability versus the number of users is plotted for different number of receive antennas with one or two transmit antennas for the degenerate SIMO channel. It can be observed that the outage probability is improved by adding the receive antenna is larger than by adding a transmit antenna as shown in Figure 6.16. This is due to the intracell interference reduction by the receive diversity implementation. Furthermore, it is observed that the outage probability of 2×2 antenna configuration is observed to be better than that of 8×1 antenna configuration. Therefore, it is expected that the impact of diversity gain on the system performance is larger than that of array gain in the uplink with the degenerate MIMO channel. It can be further observed that the outage probability of the 2×4 antenna configuration is better than that of the 4×2 antenna configuration due to the larger interference reduction afforded by the 2×4 antenna configuration than by the 4×2 antenna configuration.

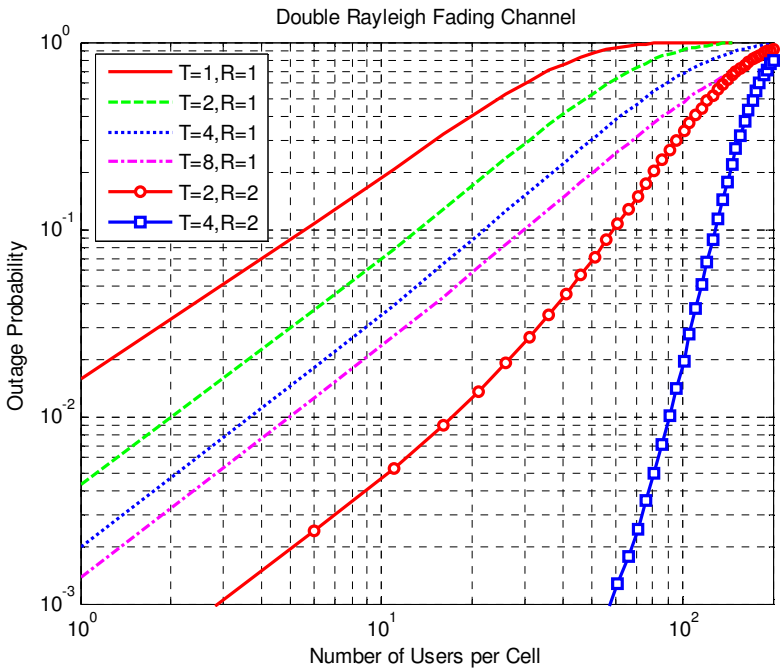

Figure 6.16: Outage probability vs. the number of users per cell for different number of transmit antennas with one or two receive antennas

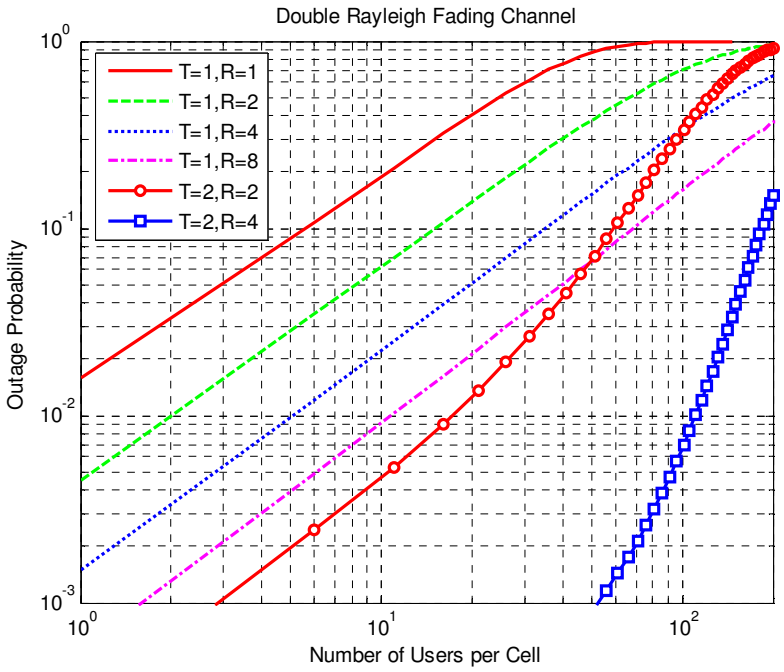

Figure 6.17: Outage probability vs. the number of users per cell for different number of receive antennas with one or two transmit antennas

6.5.2 Downlink performances

Now, let us investigate the system performance of the downlink DS/CDMA. For the simple illustrations, the system performances in the degenerate MIMO channel are presented with all MSs either in hard handoff or in soft handoff.

Figure 6.18 shows the outage probability versus the number of users per cell, for different number of receive antennas, and with either one or two transmit antennas. It is assumed that the number of resolvable multipath components is one and all MSs in a cell are in hard handoff. As expected, the outage performances are severely degraded in the degenerate SIMO channel as compared with those in the normal SIMO channel shown in Chapter 5. However, it can be still observed that the outage probability improves as the number of receive antennas increases. In addition, similar to the results shown in the uplink performance in the degenerate MIMO channel, the outage probability of 2×2 antenna configuration is better than that of 1×8 antenna configuration because of the improvement in diversity gain.

Figure 6.19 shows the outage probability versus the number of users per cell for varying number of transmit antennas and with either one or two receive antennas. It is assumed that the number of resolvable multipath components is one and all MSs in a cell are in hard handoff. Similar results to those shown in Figure 6.18 can be observed:

- The outage performance is severely degraded in the degenerate SIMO channel as compared with the normal SIMO channel discussed in Chapter 5.
- The outage probability improves as the number of receive antennas increases due to the array gain.
- The outage probability of 2×2 antenna configuration is better than that of 1×8 antenna configuration because of the improvement in diversity gain.

However, it is observed that the outage performance of the downlink with transmit diversity is similar to receive diversity in the degenerate MIMO channel. This trend is different from the result shown in Chapter 5. Note that, in Chapter 5, transmit diversity shows the better outage performance than the receive diversity in the normal MIMO channel since the intracell interference are reduced only by transmit diversity. Thus, in the degenerate MIMO channel, it is expected that the impact of intracell interference reduction by transmit diversity is insignificant due to the large intercell interference.

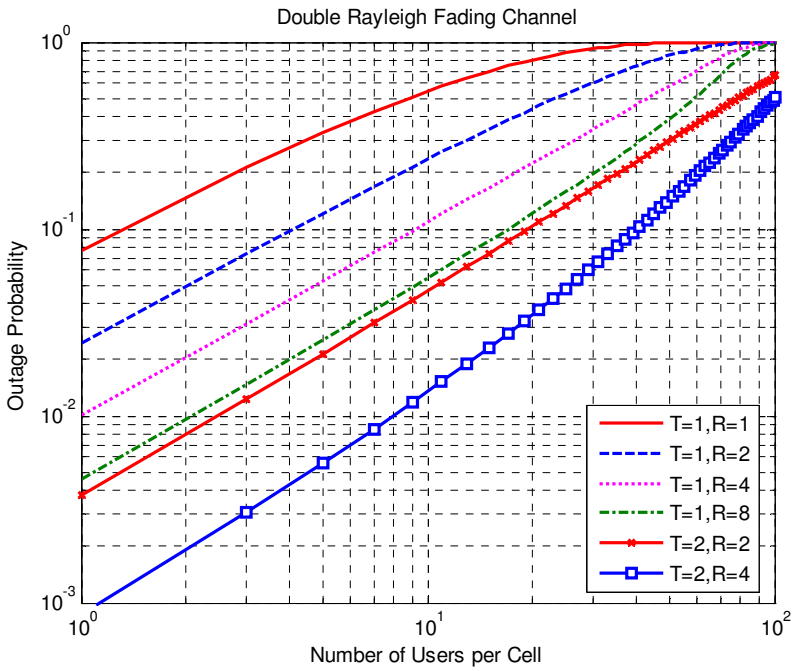

Figure 6.18: Outage probability vs. the number of users per cell for different number of receive antennas with one or two transmit antennas (hard handoff)

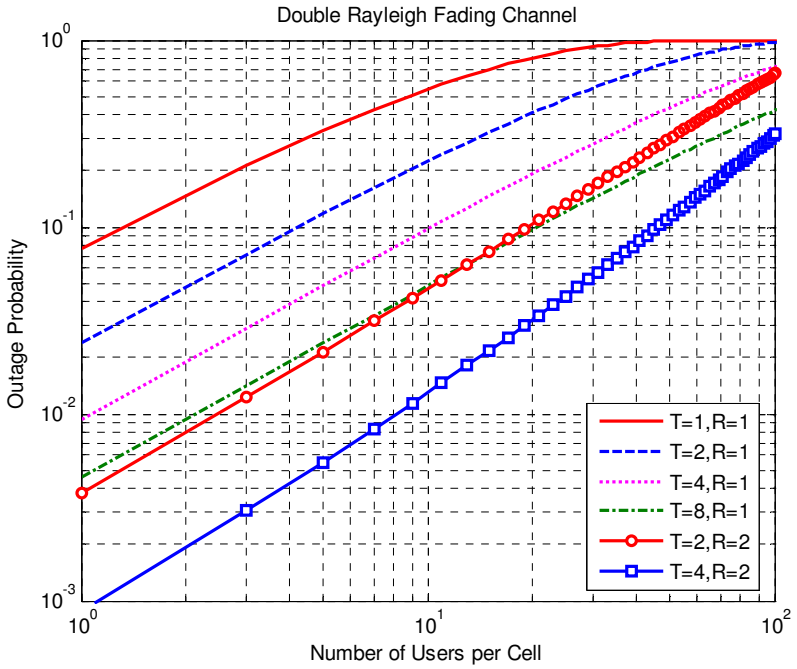

Figure 6.19: Outage probability vs. the number of users per cell for different number of transmit antennas with one or two receive antennas (hard handoff)

Finally, let us take into account the outage performance of the downlink of DS/CDMA cellular systems with soft handoff in the degenerate MIMO channel. Figure 6.20 shows the outage probability versus the number of users per cell, for different number of receive antennas, and with either one or two transmit antennas. It is assumed that all MSs in a cell are in 3-way soft handoff and the number of resolvable multipath components is one. The number of users per cell is normalized by the number of BSs in soft handoff since all BSs allocate their fractional power to the same user in soft handoff. It can be observed that the outage probability significantly improves compared with the results shown in Figure 6.18 as the number of receive antennas increases due to the power reduction by the soft handoff combining process. However, still diversity gain achieved by increasing the number of receive antennas is smaller compared with the diversity gain obtained from increasing the number of transmit antennas. Therefore, the outage performance of the 2×2 antenna configuration is better than the outage performance of the 8×1 antenna configuration.

Figure 6.21 shows the outage probability versus the number of users per cell, for different number of transmit antennas, and with either one or two receive antennas. It is assumed that all MSs in a cell are in 3-way soft handoff and the number of resolvable multipath components is one. The number of users per cell is normalized by the number of BSs in soft handoff since all BSs allocate their fractional power to the same user in soft handoff. In the case where as single receive antenna is implemented at MS, it can be observed that the outage probability significantly improves as the number of transmit antennas increases even though the diversity gain in the degenerate MIMO channel is small. That is, the impact of the intracell interference reduction by transmit diversity is more pronounced since the intercell interference is sufficiently suppressed by the soft handoff. Hence, the outage performance of the 4×1 antenna configuration is similar to the outage performance of the 2×2 antenna configuration and the outage performance of the 8×1 antenna configuration is better than the 4×2 antenna configuration.

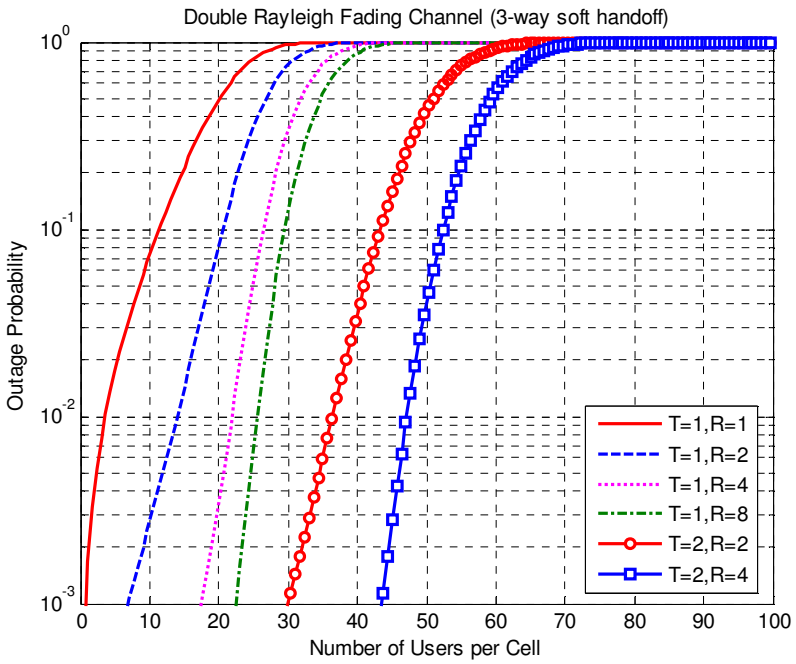

Figure 6.20: Outage probability vs. the number of users per cell for different number of receive antennas with one or two transmit antennas (soft handoff)

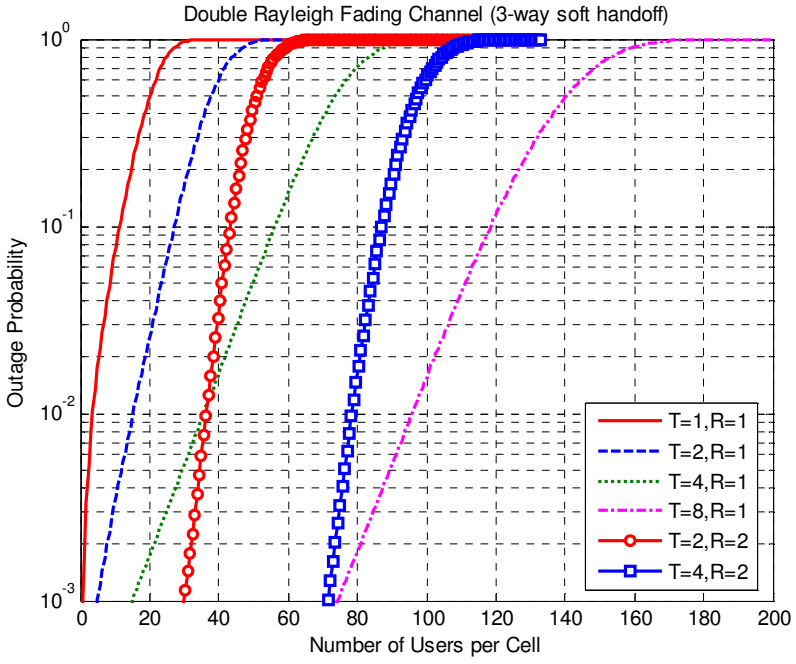

Figure 6.21: Outage probability vs. the number of users per cell for different number of transmit antennas with one or two receive antennas (soft handoff)

6.6 Chapter Summary

In this chapter, the degeneracy of the MIMO channel, known as keyhole effect, is briefly reviewed and its impact on the system performance of DS/CDMA with MIMO diversity are investigated in terms of the outage probability as a function of the number of users per cell. In the degenerate MIMO channel, the channel matrix $\mathbf{H}$ has a single degree of freedom, even though its entries are uncorrelated. The low rank property makes the channel capacity low. Furthermore, the diversity performance is known to be limited by the smaller number between the number of transmit antennas and the number of receive antennas. However, it can be observed that increasing the antenna array size at either side can still provide an array gain. Thus, it has been observed that

- In both the uplink and downlink, outage performance improves as the number of transmit antenna or receive antennas increases, respectively, regardless of poor diversity gain.
- For the uplink, increasing diversity order by implementing the antenna array at both sides always shows the better performance than increasing array size at only transmitter or receiver.
- For the downlink with soft handoff, the array gain by increasing transmit antenna array shows a similar or larger impact on the system outage performance than increasing the receive antenna array because the intercell interference is sufficiently suppressed by soft handoff.

Chapter

7 Conclusions

This dissertation presents an analytical framework to evaluate the performance of Direct Sequence Code Division Multiple Access (DS/CDMA) cellular systems equipped with antenna arrays performing spatial diversity at both the base station (BS) and the mobile station (MS).

In Chapter 2, a comprehensive mathematical framework was developed to analyze the impact of transmit diversity at the MS on the uplink system capacity. The transmit diversity was observed to improve the system capacity by reducing mean and variance of the intercell interference. In addition, the capacity achieved by transmit diversity was found to be greater when the system employs fast power control than when the system employs slow power control. This implies that system capacity is more sensitive to interference variation caused by other user signals that have not been completely compensated for by either power control or diversity processing than to total interference generated by occasional high power transmission from other users due to power control. Correlation among diversity branches was also observed to have a more significant negative impact on the capacity of a system employing slow power control than that of a system using fast power control.

In Chapter 3, the framework developed in Chapter 2 was generalized to incorporate the receive diversity at the BS and to investigate the impact of MIMO on capacity and

coverage. System outage was observed to depend on the desired signal statistics for a small number of users per cell and on the interference statistics for a large number of users per cell. The receive diversity at the BS was also shown to reduce both the intercell interference and intracell interference in the uplink while transmit diversity at the MS reduces only the intercell interference. Hence, receive diversity provides greater capacity improvement than transmit diversity. Furthermore, MIMO enables significant improvements in both capacity and coverage of the uplink and can provide capacity improvement without loss of coverage and vice versa. MIMO can also overcome a capacity limit.

In Chapter 4, a system level simulator was developed to evaluate the analytical results from Chapter 2 and 3 and to evaluate the impact of several realistic implementation issues, such as the feedback delay of closed loop operation of transmit diversity and power control, user mobility, and resolvable multipath combining, on the uplink system capacity. Those realistic implementation issues were observed to cause the actual system performance to deviate from the analytical results. However, performance trends observed in the analytical results were insignificantly changed. Therefore, the simulation can fine-tune the rough estimates of system performances provided by the analytical results.

In Chapter 5, we investigated the impact of MIMO on system capacity and soft handoff capability in the downlink. Combining the signals from multiple BSs and fast downlink power control was shown to improve the system capacity if the percentage of the MS in soft handoff is properly controlled. Also, MIMO in conjunction with fast power control was shown to significantly improve the system capacity of the downlink by reducing the mean and variance of interference. Furthermore, maximal ratio transmit diversity, implemented by closed loop transmit diversity, enabled the intracell interference rejection to provide better performance than the receive diversity with MRC.

In Chapter 6, the impact of the degenerate MIMO channel on the system performances of both the uplink and downlink was examined. In the degenerate MIMO channel, the

channel matrix **H** has a single degree of freedom even though its entries are uncorrelated. This results in low channel capacity and and poor diversity performance. For the uplink, implementing antenna array elements at *both* the MS and the BS always shows the better performance than implementing antenna array elements at either the MS or the BS. However, in the downlink with soft handoff, the array gain achieved by increasing transmit antenna array elements shows a similar or larger impact on the system outage performance than increasing the receive antenna array elements because the intercell interference is suppressed.

Finally, although this dissertation has mainly focused on investigating the efficiency of spatial diversity techniques in DS/CDMA cellular networks, the framework explored can be extended to the analysis and design of other cellular networks using MIMO. Future research directions using the framework developed in this dissertation include the following three concepts. First, assessing the performances of various MIMO techniques in cellular networks by modifying the SIR expressions is a critical step in the designing process of wireless communication systems to be able to choose the best MIMO technique. Secondly, investigating possible interactions between MIMO techniques at the physical layer implementation with upper layer protocol is essential for the system optimization. Lastly, evaluating system performance under various situations and environments by changing parameters such as channel statistics, user distributions, and MIMO configuration, gives valuable in the system deployment choices.

Appendix

A Calculation of Received Signal-to-Interference-plus-Noise Ratio with MIMO implementation

In this section, the procedure to obtain the received signal-to-interference-plus-noise ratio (SINR) is presented when employing the closed loop transmit diversity with maximal ratio combining of signals from multiple receive antennas.

Let us start with Equation (2.22). Assuming that the interference-plus-noise term is a non-white process, we apply the diagonalization theorem for maximum likelihood detection before calculating the received SINR. Since the noise covariance matrix is positive semi-definite, it can be decomposed as

$$\mathbf{R}_n = \mathbf{U}\mathbf{D}\mathbf{U}^H = \left(\mathbf{U}\sqrt{\mathbf{D}}\right)\left(\mathbf{U}\sqrt{\mathbf{D}}\right)^H = \mathbf{B}\mathbf{B}^H \tag{A.1}$$

where $\mathbf{D}$ is a diagonal matrix whose diagonal terms are eigenvalues of $\mathbf{R}_n$ and $\mathbf{U}$ is the eigenvectors corresponding to each diagonal term. By multiplying both sides of Equation (2.22) by $\mathbf{B}^{-1}$, the received signal is expressed as

$$\mathbf{B}^{-1}\mathbf{r} = \mathbf{B}^{-1}\mathbf{H}\mathbf{w} \cdot x + \mathbf{B}^{-1}\mathbf{n} \tag{A.2}$$

For the channel compensation, multiplying both sides by $\left(\mathbf{B}^{-1}\mathbf{H}\mathbf{w}\right)^H$ results in

$$\begin{aligned}\left(\mathbf{B}^{-1}\mathbf{H}\mathbf{w}\right)^{H}\mathbf{B}^{-1}\mathbf{r} &= \left(\mathbf{B}^{-1}\mathbf{H}\mathbf{w}\right)^{H}\mathbf{B}^{-1}\mathbf{H}\mathbf{w}\cdot x+\left(\mathbf{B}^{-1}\mathbf{H}\mathbf{w}\right)^{H}\mathbf{B}^{-1}\mathbf{n}\\ &= \mathbf{w}^{H}\mathbf{H}^{H}\left(\mathbf{B}^{-1}\right)^{H}\mathbf{B}^{-1}\mathbf{H}\mathbf{w}\cdot x+\mathbf{w}^{H}\mathbf{H}^{H}\left(\mathbf{B}^{-1}\right)^{H}\mathbf{B}^{-1}\mathbf{n}\end{aligned} \tag{A.3}$$

Thus, the received SINR is calculated as

$$\begin{aligned}SINR &= \frac{E\left[\left(\mathbf{w}^{H}\mathbf{H}^{H}\left(\mathbf{B}\mathbf{B}^{H}\right)^{-1}\mathbf{H}\mathbf{w}x\right)\left(\mathbf{w}^{H}\mathbf{H}^{H}\left(\mathbf{B}\mathbf{B}^{H}\right)^{-1}\mathbf{H}\mathbf{w}x\right)^{H}\right]}{E\left[\left(\mathbf{w}^{H}\mathbf{H}^{H}\mathbf{B}^{-H}\mathbf{B}^{-1}\mathbf{n}\right)\left(\mathbf{w}^{H}\mathbf{H}^{H}\mathbf{B}^{-H}\mathbf{B}^{-1}\mathbf{n}\right)^{H}\right]}\\ &= \frac{\mathbf{w}^{H}\mathbf{H}^{H}\mathbf{R}_{n}^{-1}\mathbf{H}\mathbf{w}\,|x|^{2}\,\mathbf{w}^{H}\mathbf{H}^{H}\mathbf{R}_{n}^{-1}\mathbf{H}\mathbf{w}}{\mathbf{w}^{H}\mathbf{H}^{H}\mathbf{R}_{n}^{-1}\mathbf{H}\mathbf{w}}\\ &= \mathbf{w}^{H}\mathbf{H}^{H}\mathbf{R}_{n}^{-1}\mathbf{H}\mathbf{w}\cdot|x|^{2}\end{aligned} \tag{A.4}$$

This result is used in section 2.2.3.

Appendix

B Calculation of Received Signal-to-Interference-plus-Noise Ratio with MIMO implementation

In this section, the procedure to obtain the coefficients for the partial fraction expansion of moment generating function (MGF) of Nakagami-*m* fade distribution with MIMO diversity is shown. Let us take into account the following MGF given in Equation (2.57).

$$\begin{aligned}\phi_X(s) &= \prod_{k=1}^{L_m}\left(1+\frac{\Omega_k}{m}s\right)^{-mL_tL_r} \\ &= \sum_{k=1}^{L_m}\sum_{l=1}^{mL_tL_r}\frac{A_{k,l}}{(1+(\Omega_k/m)s)^l}\end{aligned} \tag{B.1}$$

Let $\lambda_k = \Omega_k / m$. Then, the coefficients, $A_{k,l}$, are calculated as

$$
\begin{aligned}
A_{k,M} &= (1+\lambda_k s)^M \phi_X(s)\Big|_{s=-1/\lambda_k} \\
A_{k,M-1} &= \frac{1}{\lambda_k}\frac{d}{ds}(1+\lambda_k s)^M \phi_X(s)\Big|_{s=-1/\lambda_k} \\
A_{k,M-2} &= \frac{1}{2}\frac{1}{(\lambda_k)^2}\frac{d^2}{ds^2}(1+\lambda_k s)^M \phi_X(s)\Big|_{s=-1/\lambda_k} \\
A_{k,M-3} &= \frac{1}{3\cdot 2}\frac{1}{(\lambda_k)^3}\frac{d^3}{ds^3}(1+\lambda_k s)^M \phi_X(s)\Big|_{s=-1/\lambda_k} \\
&\vdots \\
A_{k,l} &= \frac{1}{(M-l)!}\frac{1}{(\lambda_k)^{M-l}}\frac{d^{M-l}}{ds^{M-l}}(1+\lambda_k s)^M \phi_X(s)\Big|_{s=-1/\lambda_k}
\end{aligned}
\tag{B.2}
$$

That is,

$$
A_{k,l} = \frac{1}{(M-l)!}\frac{1}{(\lambda_k)^{M-l}}\frac{d^{M-l}}{ds^{M-l}}(1+\lambda_k s)^M \phi_X(s)\Big|_{s=-1/\lambda_k} \tag{B.3}
$$

where the n^{th} derivative of $(1+\lambda_k s)^M \phi_X(s)$ is calculated by the following differentiation identity:

$$
\frac{d^n(u\cdot v)}{ds^n} = \sum_{k=0}^{n}\binom{n}{k}\frac{d^k}{ds^k}v\frac{d^{n-k}}{ds^{n-k}}u \tag{B.4}
$$

Let $n_0 = M - l$

$$
\begin{aligned}
&\frac{d^{n_0}}{ds^{n_0}}(1+\lambda_k s)^M \phi_X(s) \\
&= \frac{d^{n_0}}{ds^{n_0}}\prod_{j=1,j\neq k}^{L}\phi_j(s) \\
&= \sum_{n_1=0}^{n_0}\binom{n_0}{n_1}\frac{d^{n_1}}{ds^{n_1}}\phi_1(s)\frac{d^{n_0-n_1}}{ds^{n_0-n_1}}\phi_2(s)\cdots\phi_L(s) \\
&= \sum_{n_1=0}^{n_0}\binom{n_0}{n_1}\frac{d^{n_1}}{ds^{n_1}}\phi_1(s)\sum_{n_2=0}^{n_0-n_1}\binom{n_0-n_1}{n_2}\frac{d^{n_2}}{ds^{n_2}}\phi_2(s)\frac{d^{n_0-n_1-n_2}}{ds^{n_0-n_1-n_2}}\phi_3(s)\cdots\phi_L(s) \\
&\vdots \\
&= \sum_{n_1=0}^{n_0}\binom{n_0}{n_1}\frac{d^{n_1}}{ds^{n_1}}\phi_1(s)\sum_{n_2=0}^{n_0-n_1}\binom{n_0-n_1}{n_2}\frac{d^{n_2}}{ds^{n_2}}\phi_2(s)\cdots \\
&\qquad \sum_{n_{L-2}=0}^{n_0\cdots-n_{L-3}}\binom{n_0\cdots-n_{L-3}}{n_{L-2}}\frac{d^{n_{L-2}}}{ds^{n_{L-2}}}\phi_{L-1}(s)\frac{d^{n_0\cdots-n_{L-2}}}{ds^{n_0\cdots-n_{L-2}}}\phi_L(s)
\end{aligned}
\tag{B.5}
$$

Let $n_0 - \cdots - n_{L-2} = n_{L-1}$, then, $n_0 = n_1 + n_2 + \cdots + n_{L-1}$ and Equation (B.5) is given by

$$
\frac{d^{n_0}}{ds^{n_0}}\prod_{j=1,j\neq k}^{L}\phi_j(s) = \sum_{n_1=0}^{n_0}\sum_{n_2=0}^{n_0-n_1}\cdots\sum_{n_{L-2}=0}^{n_0\cdots-n_{L-3}}\binom{n_0}{n_1,n_2,\cdots,n_{L-1}}\frac{d^{n_1}}{ds^{n_1}}\phi_1(s)\frac{d^{n_2}}{ds^{n_2}}\phi_2(s)\cdots\frac{d^{n_{L-1}}}{ds^{n_{L-1}}}\phi_L(s) \tag{B.6}
$$

The n th derivative of ϕ_i is

$$\begin{aligned}
\phi_i(s) &= (1+\lambda_i s)^{-M} \\
\frac{d}{ds}\phi_i(s) &= (-M)(\lambda_i)(1+\lambda_i s)^{-M-1} \\
\frac{d^2}{ds^2}\phi_i(s) &= (-M)(-M-1)(\lambda_i)^2(1+\lambda_i s)^{-M-2} \\
&\vdots \\
\frac{d^n}{ds^n}\phi_i(s) &= \frac{(M+n-1)!}{(M-1)!}(-1)^n(\lambda_i)^n(1+\lambda_i s)^{-M-n}
\end{aligned} \tag{B.7}$$

By plugging Equation (B.7) into Equation (B.6), we obtain

$$\begin{aligned}
\frac{d^{n_0}}{ds^{n_0}}\prod_{j=1,j\neq k}^{L}\phi_j(s) = \sum_{n_1=0}^{n_0}\sum_{n_2=0}^{n_0-n_1}\cdots\sum_{n_{L-2}=0}^{n_0\cdots-n_{L-3}} n_0!\binom{M+n_1-1}{n_1}\cdots\binom{M+n_{L-1}-1}{n_{L-1}} \\
(-1)^n\prod_{i,u=1,i\neq k}^{L,L-1}\frac{\lambda_i^{n_u}}{(1+\lambda_i s)^{M+n_u}}
\end{aligned} \tag{B.8}$$

Finally, the coefficient of partial fraction expansion is obtained by plugging Equation (B.8) into Equation (B.3).

$$A_{k,l} = \frac{1}{(-\lambda_k)^{n_0}}\sum_{n_1=0}^{n_0}\sum_{n_2=0}^{n_0-n_1}\cdots\sum_{n_{L-2}=0}^{n_0\cdots-n_{L-3}}\prod_{i,u=1,i\neq k}^{L,L-1}\binom{M+n_u-1}{n_u}\frac{\lambda_i^{n_u}}{(1-\lambda_i/\lambda_k)^{M+n_u}} \tag{B.9}$$

This result is used in section 2.3.2.

Appendix

C Simple Comparison of Received SIR of Intracell Interference in Uplink of DS/CDMA cellular systems with Antenna Arrays

In this section, signal-to-interference ratios of intracell interference in the uplink of DS/CDMA cellular systems employing perfect power control are derived and compared for a system equipped with simple single-input single-output (SISO), multiple-input single-output (MISO), and single-input multiple output (SIMO) configurations. From these results, it is clearly observed that receive diversity with maximal ratio combining implemented at BS shows the better performance than maximal ratio transmit diversity implemented at MS in the uplink.

C.1 Single-Input Single-Output

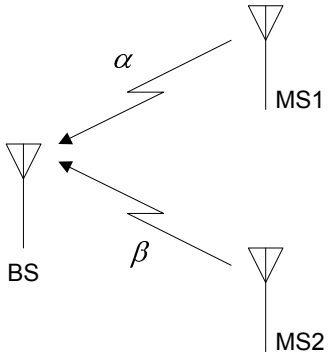

Figure C.1: Single-input single-output system

Let us suppose that there are one BS and two MSs, and both MSs are communicating with the BS as shown in Figure C.1. Let MS1 be the desired user and MS2 the interference source to MS1. The channel between MS1 and BS is defined as α, and channel between MS2 and BS is defined as β. Furthermore, the transmit power of MS1 is denoted by P_1 and the transmit power of MS2 is denoted by P_2. If the perfect power control based on the channel strength is implemented, $P_1 = |\alpha|^{-2}$, and $P_2 = |\beta|^{-2}$. Then, the received signal at BS without additive white Gaussian noise can be expressed as

$$r = \alpha \cdot \sqrt{P_1} \cdot s_1 + \beta \cdot \sqrt{P_2} \cdot s_2 \tag{C.1}$$

where s_1 and s_2 are the transmit symbol data from MS1 and MS2, respectively. Then, the desired signal can be demodulated by the channel compensation with α as follows

$$\hat{r} = \alpha^* \cdot r = |\alpha|^2 \sqrt{P_1} \cdot s_1 + \alpha^* \beta \sqrt{P_2} \cdot s_2 \tag{C.2}$$

From this equation, the signal-to-interference ratio can be expressed as

$$SIR = \frac{P_s}{P_i} = \frac{\left|\,|\alpha|^2 \sqrt{P_1} \cdot s_1\right|^2}{\left|\alpha^* \beta \sqrt{P_2} \cdot s_2\right|^2} = \frac{|\alpha|^2 P_1}{|\beta|^2 P_2} = 1 \tag{C.3}$$

where it is assumed that $|s_i|^2 = 1,\ i = 1,2$. That is, the intracell interference is always a constant, '1' in SISO systems, a commonly used assumption in other studies.

C.2 Multiple-Input Single-Output

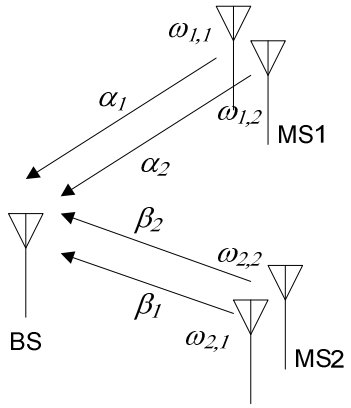

Figure C.2: Multiple-input single output system

In the multiple-input single-output configuration, the channel of each antenna is distinguished by the subscript. The signal from each transmit antenna is transmitted after being multiplied by each antenna weight, $w_{1,1}$ and $w_{1,2}$ for MS1, and $w_{2,1}$ and $w_{2,2}$ for MS2. For the maximal ratio transmit diversity, the weight coefficients are

$$\begin{bmatrix} w_{1,1} \\ w_{1,2} \end{bmatrix} = \frac{1}{\sqrt{|\alpha|^2 + |\alpha|^2}} \begin{bmatrix} \alpha_1^* \\ \alpha_2^* \end{bmatrix} \tag{C.4}$$

$$\begin{bmatrix} w_{2,1} \\ w_{2,2} \end{bmatrix} = \frac{1}{\sqrt{|\beta|^2 + |\beta|^2}} \begin{bmatrix} \beta_1^* \\ \beta_2^* \end{bmatrix} \tag{C.5}$$

The transmit power with the perfect power control based on the channel strength is determined as

$$P_1 = \left(|\alpha_1|^2 + |\alpha_2|^2\right)^{-1} \text{ and } P_2 = \left(|\beta_1|^2 + |\beta_2|^2\right)^{-1} \tag{C.6}$$

Now, the received signal at BS becomes

$$\begin{aligned} r &= \left(w_{1,1}\alpha_1 + w_{1,2}\alpha_2\right) \cdot \sqrt{P_1} \cdot s_1 + \left(w_{2,1}\beta_1 + w_{2,2}\beta_2\right) \cdot \sqrt{P_2} \cdot s_2 \\ &= \frac{|\alpha|^2 + |\alpha|^2}{\sqrt{|\alpha|^2 + |\alpha|^2}} \cdot \sqrt{P_1} \cdot s_1 + \frac{|\beta|^2 + |\beta|^2}{\sqrt{|\beta|^2 + |\beta|^2}} \cdot \sqrt{P_2} \cdot s_2 \end{aligned} \tag{C.7}$$

The demodulated signal of MS1 after channel compensations expressed as

$$\hat{r} = \left| \frac{|\alpha|^2 + |\alpha|^2}{\sqrt{|\alpha|^2 + |\alpha|^2}} \right|^2 \cdot \sqrt{P_1} \cdot s_1 + \left(\frac{|\alpha|^2 + |\alpha|^2}{\sqrt{|\alpha|^2 + |\alpha|^2}} \right)^* \frac{|\beta|^2 + |\beta|^2}{\sqrt{|\beta|^2 + |\beta|^2}} \cdot \sqrt{P_2} \cdot s_2 \tag{C.8}$$

Thus, the signal-to-interference ratio can be calculated as

$$SIR = \frac{\left| \left| \frac{|\alpha|^2 + |\alpha|^2}{\sqrt{|\alpha|^2 + |\alpha|^2}} \right|^2 \cdot \sqrt{P_1} \cdot s_1 \right|^2}{\left| \left(\frac{|\alpha|^2 + |\alpha|^2}{\sqrt{|\alpha|^2 + |\alpha|^2}} \right)^* \frac{|\beta|^2 + |\beta|^2}{\sqrt{|\beta|^2 + |\beta|^2}} \cdot \sqrt{P_2} \cdot s_2 \right|^2} = \frac{\left| \frac{|\alpha|^2 + |\alpha|^2}{\sqrt{|\alpha|^2 + |\alpha|^2}} \right|^2 \cdot P_1}{\left| \frac{|\beta|^2 + |\beta|^2}{\sqrt{|\beta|^2 + |\beta|^2}} \right|^2 \cdot P_2} = 1 \tag{C.9}$$

where it is assumed that $|s_i|^2 = 1,\ i = 1,2$. Hence, the intracell interference in MISO systems is also a constant '1' just as with the SISO system. This result can also easily be generalized for MISO in multipath channel.

C.3 Single-Input Multiple-Output

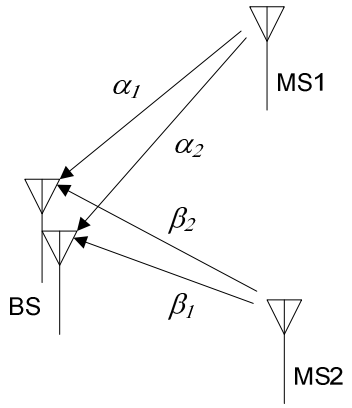

Figure C.3: Single-input multiple-output system

Consider the single-input multiple-output system. In the single-input multiple-output configuration, channels between each MS and BS are distinguished by the subscripts. For two receive antennas, the transmit power of each MS with perfect power control based on the channel strength is expressed as

$$P_1 = \left(|\alpha_1|^2 + |\alpha_2|^2\right)^{-1} \text{ and } P_2 = \left(|\beta_1|^2 + |\beta_2|^2\right)^{-1} \tag{C.10}$$

Then, the received signal at the i^{th} branch is represented by

$$r_i = \alpha_i \sqrt{P_1} \cdot s_1 + \beta_i \sqrt{P_2} \cdot s_2 \tag{C.11}$$

The demodulation can be performed by combining two signals from each antenna after channel compensation, resulting in

$$\hat{r} = \alpha_1^* r_1 + \alpha_2^* r_2 = \left(|\alpha_1|^2 + |\alpha_2|^2\right)\sqrt{P_1} \cdot s_1 + \left(\alpha_1^* \beta_1 + \alpha_2^* \beta_2\right)\sqrt{P_2} \cdot s_2 \tag{C.12}$$

Now, the signal-to-interference ratio can be calculated as

$$\begin{aligned} SIR &= \frac{\left||\alpha_1|^2 + |\alpha_2|^2\right|^2 P_1 \cdot |s_1|^2}{\left|\alpha_1^* \beta_1 + \alpha_2^* \beta_2\right|^2 P_2 \cdot |s_2|^2} \\ &= \frac{\left(|\alpha_1|^2 + |\alpha_2|^2\right)\left(|\beta_1|^2 + |\beta_2|^2\right)}{\left|\alpha_1^* \beta_1 + \alpha_2^* \beta_2\right|^2} \\ &\geq 1 \end{aligned} \tag{C.13}$$

where it is assumed that $|s_i|^2 = 1,\ i = 1,\ 2$. The last inequality in Equation (C.13) comes from *Cauchy-Schwarz inequality*. Hence, the signal-to-interference ratio with SIMO is better than SISO and MISO in the uplink.

Appendix

D Simple Comparison of Received SIR of Intracell Interference in Downlink of DS/CDMA cellular systems with Antenna Arrays

In this section, the signal-to-interference ratio of intracell interference in the downlink DS/CDMA cellular systems employing perfect power control will be derived and compared for simple single-input single-output (SISO), multiple-input single-output (MISO), and single-input multiple output (SIMO) configurations. From these results, it is clearly observed that maximal ratio transmit diversity implemented at the BS shows the better performance than receive diversity employing MRC implemented at the MS in the downlink of DS/CDMA cellular system.

D.1 Single-Input Single-Output

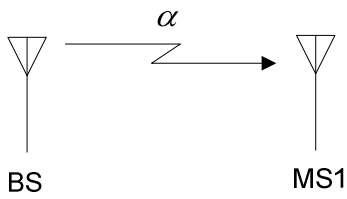

Figure D.1: Single-input single-output system

Let us suppose that MS1 is served by BS in the system by single transmit and single receive antennas as shown in Figure D.1. To simplify the analysis, let us also suppose the followings:

- There is only one resolvable multipath fading channel, α, but orthogonality among other user's signals is not preserved due to many unresolvable multipath components.
- BS transmits at full power, P_T, which is sum of the fractional power of BS allocated to MSs served by the BS.

The received signal can be expressed as

$$r = \alpha\sqrt{P_T} + n \tag{D.1}$$

where n is additive white Gaussian noise (AWGN). Let us assume that the AWGN is negligible as compared to the received signal from BS and that the fractional power of BS allocated to each MS is very small. Then, the total transmit power of BS can be approximated as the intracell interference. Finally, the received signal to interference ratio at MS1 is calculated as

$$\gamma_{SISO} = \frac{P_S}{P_I} = \frac{\left|\sqrt{N_T}\,|\alpha|^2\right|^2}{\left|\sqrt{P_T}\,|\alpha|^2\right|^2} = \frac{N_T}{P_T} \tag{D.2}$$

D.2 Single-Input Multiple-output

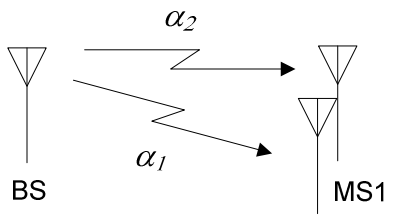

Figure D.2: Single-input multiple-output system

Let us suppose that MS1 is served by BS in the system by single transmit and two receive antennas as shown in Figure D.2. Let us also suppose the followings:

- There is only one resolvable multipath fading channel thus gains α_1 and α_2 are seen at each receive antenna. Orthogonality among other user's signals is not preserved due to many unresolvable multipath components.
- BS transmits at full power, P_T, which is sum of the fractional power of BS allocated to MSs served by the BS.

The received signal at each receive antenna can be expressed as

$$\begin{aligned} r_1 &= \alpha_1\sqrt{P_T} + n_1 \\ r_2 &= \alpha_2\sqrt{P_T} + n_2 \end{aligned} \tag{D.3}$$

From these received signals, the demodulated signal can be expressed as

$$\hat{r} = \left(|\alpha_1|^2 + |\alpha_2|^2\right)\cdot\sqrt{N_T}\cdot s_1 + \alpha_1^* n_1 + \alpha_2^* n_2 \tag{D.4}$$

where s_1 is the transmit symbol for MS1 from BS. Assuming that the AWGN is negligible as compared to the received signal from BS and that the fractional power of BS allocated to each MS is very small due to many users served by BS. Then, total transmit power of BS can be approximated as the intracell interference. Finally, the received signal-to-interference ratio can be calculated as

$$\gamma_{SIMO} = \frac{P_S}{P_I} = \frac{\left||\alpha_1|^2 + |\alpha_2|^2\right|^2\cdot N_T\cdot|s_1|^2}{\left||\alpha_1|^2 + |\alpha_2|^2\right|^2\cdot P_T} = \frac{N_T}{P_T} \tag{D.5}$$

where it is assumed that $|s_1|^2 = 1$. This result is the same as that of SISO system.

D.3 Multiple-Input Single-Output

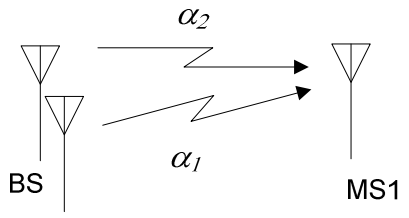

Figure D.3: Multiple-input single-output

Consider multiple-input single-output system in the downlink employing maximal ratio transmit diversity. Let us also presume the followings:

- There is only one resolvable multipath fading channel thus gains α_1 and α_2 are seen at each receive antenna. Orthogonality among other user's signals is not preserved due to many unresolvable multipath components.
- BS transmits at full power, P_T, which is sum of the fractional power of BS allocated to MSs served by the BS.
- Total transmit power of BS is uniformly distributed across each transmit antennas

The received signal at MS can be expressed as

$$r = (\alpha_1 + \alpha_2)\sqrt{\frac{P_T}{2}} + n_1 \tag{D.6}$$

The demodulated signal can be expressed as

$$\hat{r} = \left| \frac{|\alpha_1|^2 + |\alpha_1|^2}{\sqrt{|\alpha_1|^2 + |\alpha_1|^2}} \right|^2 \cdot \sqrt{N_T} \cdot s_1 + (\alpha_1 + \alpha_2)^* n_1 \tag{D.7}$$

Assuming that the AWGN is negligible as compared to the received signal from BS and that the fractional power of BS allocated to each MS is small due to many users served by BS. Then, total transmit power of the BS can be approximated as the intracell interference, the received signal-to-interference can be calculated as

$$\begin{aligned}\gamma_{MISO} = \frac{P_S}{P_I} &= \frac{\left|\left|\frac{|\alpha_1|^2+|\alpha_1|^2}{\sqrt{|\alpha_1|^2+|\alpha_1|^2}}\right|^2 \cdot \sqrt{N_T}\cdot s_1\right|^2}{\left|\left(\frac{|\alpha_1|^2+|\alpha_1|^2}{\sqrt{|\alpha_1|^2+|\alpha_1|^2}}\right)^* (\alpha_1+\alpha_2)\sqrt{\frac{P_T}{2}}\right|^2} \\ &= \frac{\left||\alpha_1|^2+|\alpha_1|^2\right|^2 \cdot N_T \cdot |s_1|^2}{\left|\left(\frac{|\alpha_1|^2+|\alpha_1|^2}{\sqrt{|\alpha_1|^2+|\alpha_1|^2}}\right)^* (\alpha_1+\alpha_2)\right|^2 \frac{P_T}{2}} \\ &= 2\cdot\frac{|\alpha_1|^2+|\alpha_1|^2}{|\alpha_1+\alpha_2|^2}\frac{N_T}{P_T}\end{aligned} \tag{D.8}$$

From Cauchy-Schwarz inequality as follows,

$$|\alpha_1+\alpha_2|^2 \le 2\cdot\left(|\alpha_1|^2+|\alpha_2|^2\right) \tag{D.9}$$

Thus, Equation (D.8) can be simplified as

$$\gamma_{MISO} = 2\cdot\frac{|\alpha_1|^2+|\alpha_1|^2}{|\alpha_1+\alpha_2|^2}\frac{N_T}{P_T} \ge \frac{N_T}{P_T} \tag{D.10}$$

Hence, the received signal-to-interference ratio with MISO is observed to be significantly better than that with either SISO or SIMO in the downlink.

Bibliography

[1] J. H. Reed, *Software radio: a modern approach to radio engineering*: Prentice Hall, 2001.

[2] R. Mostafa, *Feasibility of Smart Antennas for the Small Wireless Terminals*. Blacksburg: Ph.D, Virginia Tech, 2003.

[3] M. Kahn and J. Klein, "Adaptive Transmit Diversity in Handsets for Performance Enhancement of CDMA Cellular Networks," in *RFDESIGN Magazine*, 2003, pp. 50-58.

[4] 3GPP TS 25.211, *Physical channels and mapping of transport channels onto physical channels (FDD)*, 2003.

[5] P. Viswanath, D. N. C. Tse, and R. Laroia, "Opportunistic beamforming using dumb antennas," *IEEE Transactions on Information Theory,* vol. 48, pp. 1277-1294, 2002.

[6] J. Jing, R. M. Buehrer, and W. H. Tranter, "Antenna diversity in multiuser data networks," *IEEE Transactions on Communications,* vol. 52, pp. 490-497, 2004.

[7] F. Kronestedt and S. Anderson, "Adaptive antennas in frequency hopping GSM," *Proceedings of IEEE International Conference on Universal Personal Communications,* vol. 1, pp. 325-329 vol.1, 1998.

[8] S. Anderson, B. Hagerman, H. Dam, U. Forssen, J. Karlsson, F. Kronestedt, S. Mazur, and K. J. Molnar, "Adaptive antennas for GSM and TDMA systems," *IEEE Wireless Communications,* vol. 6, pp. 74-86, 1999.

[9] W. H. Tranter, K. S. Shanmugan, T. S. Rappaport, and K. L. Kosbar, *Principles of Communication Systems Simulation with Wireless Applications*: Prentice Hall, 2004.

[10] K. S. Gilhousen, I. M. Jacobs, R. Padovani, A. J. Viterbi, L. A. Weaver, Jr., and C. E. Wheatley, III, "On the capacity of a cellular CDMA system," *IEEE Transactions on Vehicular Technology,* vol. 40, pp. 303-312, 1991.

[11] A. J. Viterbi, *Principles of Spread Spectrum Communication*: Addison-Wesley, 1995.

[12] B. Hashem and E. S. Sousa, "Reverse link capacity and interference statistics of a fixed-step power-controlled DS/CDMA system under slow multipath fading," *IEEE Transactions on Communications,* vol. 47, pp. 1905-1912, 1999.

[13] B. Hashem and E. S. Sousa, "On the capacity of cellular DS/CDMA systems under slow Rician/Rayleigh-fading channels," *IEEE Transactions on Vehicular Technology,* vol. 49, pp. 1752-1759, 2000.

[14] J. M. Romero-Jerez, M. Ruiz-Garcia, and A. Diaz-Estrella, "Interference statistics of cellular DS/CDMA systems with base station diversity under multipath fading," *IEEE Transactions on Wireless Communications,* vol. 2, pp. 1109-1113, 2003.

[15] M. Chopra, K. Rohani, and J. D. Reed, "Analysis of CDMA range extension due to soft handoff," in *IEEE 45th Vehicular Technology Conference*, 1995, pp. 917-921 vol.2.

[16] K. M. Rege, S. Nanda, C. F. Weaver, and W. C. Peng, "Analysis of fade margins for soft and hard handoffs," in *IEEE Int. Symp. Personal, Indoor and Mobile Radio Communications*, 1995, pp. 829-835 vol.2.

[17] S. Chi Wan, "Analysis of fade margins for soft and hard handoffs in cellular CDMA systems," *IEEE Transactions on Wireless Communications,* vol. 2, pp. 431-435, 2003.

[18] L. Yi-Bing and P. Ai-Chun, "Comparing soft and hard handoffs," *IEEE Transactions on Vehicular Technology,* vol. 49, pp. 792-798, 2000.

[19] C. Wan and K. Jin Young, "Forward-link capacity of a DS/CDMA system with mixed multirate sources," *IEEE Transactions on Vehicular Technology,* vol. 50, pp. 737-749, 2001.

[20] M. Ruiz-Garcia, J. M. Romero-Jerez, F. Bravo-Encinas, and C. Tellez-Labao, "Forward link capacity analysis of CDMA systems," 2004, pp. 459-463 Vol.1.

[21] J. Y. Kim and G. L. Stuber, "CDMA soft handoff analysis in the presence of power control error and shadowing correlation," *IEEE Transactions on Wireless Communications,* vol. 1, pp. 245-255, 2002.

[22] L. Jalloul and K. Rohani, "CDMA forward link capacity and coverage in a multipath fading channel," 1997, pp. 1440-1444 vol.3.

[23] H. S. Dugin LYU, and Fumiyuki ADACHI, "Capacity Evaluation of a Forward Link DS/CDMA Cellular System with Fast TPC Based on SIR," *IEICE Trans. Commun.,* vol. E83-B, Jan. 2000 2000.

[24] L. Dongdong and V. K. Prabhu, "Effects of the BS power and soft handoff on the outage and capacity in the forward link of an SIR-based power-controlled CDMA system," *IEEE Transactions on Wireless Communications,* vol. 5, pp. 1987-1992, 2006.

[25] M. Ahmed and K. Rohani, "Effect of fast power control on CDMA forward link performance," *Proceedings of IEEE VTC 2000-Spring,* vol. 3, pp. 1955-1959 vol.3, 2000.

[26] D. J. Shyy and J. Dunyak, "Capacity enhancement of cdma networks using interference cancellation techniques," *IEEE Communications Magazine,* vol. 44, pp. 86-92, 2006.

[27] A. M. Viterbi and A. J. Viterbi, "Erlang capacity of a power controlled CDMA system," *IEEE Journal on Selected Areas in Communications,* vol. 11, pp. 892-900, 1993.

[28] A. J. Viterbi, A. M. Viterbi, K. S. Gilhousen, and E. Zehavi, "Soft handoff extends CDMA cell coverage and increases reverse link capacity," *IEEE Journal on Selected Areas in Communications,* vol. 12, pp. 1281-1288, 1994.

[29] S. Qiang and W. A. Krzymien, "The effect of fading on the Erlang capacity of the IS-95 CDMA cellular system," in *IEEE International Conference on Communications*, 1996, pp. 1829-1833 vol.3.

[30] D. K. Kim and F. Adachi, "Theoretical analysis of reverse link capacity for an SIR-based power-controlled cellular CDMA system in a multipath fading environment," *IEEE Transactions on Vehicular Technology,* vol. 50, pp. 452-464, 2001.

[31] A. A. Abu-Dayya and N. C. Beaulieu, "Microdiversity on Rician fading channels," *IEEE Transactions on Communications,* vol. 42, pp. 2258-2267, 1994.

[32] 3GPP TR25.896 v2.0.0, *Feasibility Study for Enhanced Uplink for UTRA FDD (Release 6)*, 2004.

[33] S. M. Alamouti, "A simple transmit diversity technique for wireless communications," *IEEE Journal on Selected Areas in Communications,* vol. 16, pp. 1451-1458, 1998.

[34] C.S0002-A, *Physical Layer Standard for cdma2000 Spread Spectrum Systems*, 1999.

[35] T. K. Y. Lo, "Maximum ratio transmission," *IEEE Transactions on Communications,* vol. 47, pp. 1458-1461, 1999.

[36] P. A. Dighe, R. K. Mallik, and S. S. Jamuar, "Analysis of transmit-receive diversity in Rayleigh fading," *IEEE Transactions on Communications,* vol. 51, pp. 694-703, 2003.

[37] K. Ming and M. S. Alouini, "Largest eigenvalue of complex Wishart matrices and performance analysis of MIMO MRC systems," *IEEE Journal on Selected Areas in Communications,* vol. 21, pp. 418-426, 2003.

[38] M. Sandell, "Analytical analysis of transmit diversity in WCDMA on fading multipath channels," in *IEEE Int. Symp. Personal, Indoor and Mobile Radio Communications*, 1999.

[39] S. Ariyavisitakul and C. Li Fung, "Signal and interference statistics of a CDMA system with feedback power control," *IEEE Transactions on Communications,* vol. 41, pp. 1626-1634, 1993.

[40] J. Abate and W. Whitt, "Numerical inversion of Laplace transforms of probability distribution," *ORSA J. Computing,* vol. 7, pp. 36-43, 1995.

[41] K. S. Vanganuru and A. Annamalai, "Combined transmit and receive diversity schemes for WCDMA in multipath fading channels," *Electronics Letters,* vol. 38, pp. 1471-1472, 2002.

[42] A. Annamalai, C. Tellambura, and V. K. Bhargava, "Simple and accurate methods for outage analysis in cellular mobile radio systems-a unified approach," *IEEE Transactions on Communications,* vol. 49, pp. 303-316, 2001.

[43] A. Popoulis, *Probability, Random Variables, and Stochastic Process*, 3rd ed.: McGraw-Hill, 1991.

[44] J. S. Evans and D. Everitt, "Effective bandwidth-based admission control for multiservice CDMA cellular networks," *IEEE Transactions on Vehicular Technology,* vol. 48, pp. 36-46, 1999.

[45] T. S. Rappaport, *Wireless Communications: Principles and Practice*, 2nd Edition ed.: Pearson Education, 1996.

[46] Z. Qinqing and Y. On-Ching, "UMTS air interface voice/data capacity-part 1: reverse link analysis," in *IEEE VTS 53rd Vehicular Technology Conference*, 2001, pp. 2725-2729 vol.4.

[47] D. Ling and J. S. Lehnert, "Calculation of Erlang capacity for cellular CDMA uplink systems," in *IEEE Wireless Communications and Networking Conference*, 2000, pp. 338-342 vol.1.

[48] R. P. Narrainen and F. Takawira, "Performance analysis of soft handoff in CDMA cellular networks," *IEEE Transactions on Vehicular Technology,* vol. 50, pp. 1507-1517, 2001.

[49] D. Bertsekas and R. Gallager, *Data Networks*, 2nd Edition ed.: Prentice Hall, 1992.

[50] TIA/EIA/IS-95 Intermin Standard, *Mobile Station - Base Station Compatibility Standard for Dual-Mode Wideband Spread Spectrum Cellular System*: Telecommunication Industry Association, 1993.

[51] M. Gudmundson, "Correlation model for shadow fading in mobile radio systems," *Electronics Letters,* vol. 27, pp. 2145-2146, 1991.

[52] H. Rong and J. H. Reed, "Cell average carrier-to-interference coverage improvement by using DSP interference rejection techniques," in *IEEE 47th Vehicular Technology Conference*, 1997, pp. 1079-1083 vol.2.

[53] A. A. Abu-Dayya and N. C. Beaulieu, "Outage probabilities of diversity cellular systems with cochannel interference in Nakagami fading," *IEEE Transactions on Vehicular Technology,* vol. 41, pp. 343-355, 1992.

[54] Q. T. Zhang and X. W. Cui, "Outage probability for optimum combining of arbitrarily faded signals in the presence of correlated Rayleigh interferers," *IEEE Transactions on Vehicular Technology,* vol. 53, pp. 1043-1051, 2004.

[55] C. Jian and A. U. H. Sheikh, "Outage probability of cellular radio systems using maximal ratio combining in the presence of multiple interferers," *IEEE Transactions on Communications,* vol. 47, pp. 1121-1124, 1999.

[56] Z. Yan, F. Chin, L. Ying-Chang, and K. Chi-Chung, "Performance comparison of transmit diversity and beamforming for the downlink of DS-CDMA system," *IEEE Transactions on Wireless Communications,* vol. 2, pp. 320-334, 2003.

[57] D. G. Brennan, "Linear diversity combining techniques," *Proceedings of the IEEE,* vol. 91, pp. 331-356, 2003.

[58] T. Eng and L. B. Milstein, "Coherent DS-CDMA performance in Nakagami multipath fading," *IEEE Transactions on Communications,* vol. 43, pp. 1134-1143, 1995.

[59] M. Pursley, "Performance Evaluation for Phase-Coded Spread-Spectrum Multiple-Access Communication--Part I: System Analysis," *IEEE Transactions on Communications [legacy, pre - 1988],* vol. 25, pp. 795-799, 1977.

[60] A. F. Naguib and A. Paulraj, "Performance of wireless CDMA with M-ary orthogonal modulation and cell site antenna arrays," *IEEE Journal on Selected Areas in Communications,* vol. 14, pp. 1770-1783, 1996.

[61] A. A. Abu-Dayya and N. C. Beaulieu, "Outage probabilities in the presence of correlated lognormal interferers," *IEEE Transactions on Vehicular Technology,* vol. 43, pp. 164-173, 1994.

[62] G. L. Stuber, *Principles of Mobile Communication*, 2nd Edition ed.: Kluwer Academic Publishers, 2001.

[63] D. J. Love and R. W. Heath, Jr., "Equal gain transmission in multiple-input multiple-output wireless systems," *IEEE Transactions on Communications,* vol. 51, pp. 1102-1110, 2003.

[64] K. C. Hwang and K. B. Lee, "Efficient weight vector representation for closed-loop transmit diversity," *IEEE Transactions on Communications,* vol. 52, pp. 9-16, 2004.

[65] 3GPP2 WG5 Evaluation AHG, *1xEV-DV Evaluation Methodology*, 2001.

[66] V. Graziano, "Propagation correlations at 900 MHz," *IEEE Transactions on Vehicular Technology,* vol. 27, pp. 182-189, 1978.

[67] S. R. Saunders and B. G. Evans, "The spatial correlation of shadow fading in macrocellular mobile radio systems," *Proceedings of IEE Colloquium on Propagation Aspects of Future Mobile Systems,* Oct. 1996.

[68] J. Zhang and V. Aalo, "Performance analysis of a multicell DS-CDMA system with base station diversity," *IEE Proceddings - Communications,* vol. 148, pp. 112-118, 2001.

[69] B. Natarajan, C. R. Nassar, and V. Chandrasekhar, "Generation of correlated Rayleigh fading envelopes for spread spectrum applications," *IEEE Communications Letters,* vol. 4, pp. 9-11, 2000.

[70] 3GPP2 C.S0025, *Markov Service Option (MSO) for cdma2000 Spread Spectrum Systems*, 2000.

[71] Y. H. Kwon, D. C. Lee, and W. Park, "Capacity analysis of forward link with deterministic power model in CDMA systems with adaptive antenna array and soft handoff," *Proceedings of VTC 2002-Spring,* vol. 1, pp. 335-339 vol.1, 2002.

[72] A. Sathyendran, K. W. Sowerby, and M. Shafi, "Capacity estimation for 3rd generation CDMA cellular systems," 1999, pp. 356-360 vol.1.

[73] A. Seeger, M. Sikora, and A. Klein, "Variable orthogonality factor: a simple interface between link and system level simulation for high speed downlink packet access," 2003, pp. 2531-2534 Vol.4.

[74] K. I. Pedersen and P. E. Mogensen, "The downlink orthogonality factors influence on WCDMA system performance," 2002, pp. 2061-2065 vol.4.

[75] M. Hunukumbure, M. Beach, and B. Allen, "Downlink orthogonality factor in UTRA FDD systems," *Electronics Letters,* vol. 38, pp. 196-197, 2002.

[76] A. Shah and A. M. Haimovich, "Performance analysis of maximal ratio combining and comparison with optimum combining for mobile radio communications with cochannel interference," *IEEE Transactions on Vehicular Technology,* vol. 49, pp. 1454-1463, 2000.

[77] X. W. Cui, Q. T. Zhang, and Z. M. Feng, "Outage performance for maximal ratio combiner in the presence of unequal-power co-channel interferers," *IEEE Communications Letters,* vol. 8, pp. 289-291, 2004.

[78] S. D. Dubey, "A Theorem on a Ratio of Random Variables," *Operations Research,* vol. 13, pp. 476-477, May - Jun. 1965.

[79] H. Shin and J. H. Lee, "Capacity of multiple-antenna fading channels: spatial fading correlation, double scattering, and keyhole," *IEEE Transactions on Information Theory,* vol. 49, pp. 2636-2647, 2003.

[80] H. Shin, M. Z. Win, J. H. Lee, and M. Chiani, "On the Capacity of Doubly Correlated MIMO Channels," *To appear in the IEEE Transactions on Wireless Communications*.

[81] H. Shin and J. H. Lee, "Effect of keyholes on the symbol error rate of space-time block codes," *IEEE Communications Letters,* vol. 7, pp. 27-29, 2003.

[82] H. Shin and J. H. Lee, "Performance analysis of space-time block codes over keyhole Nakagami-m fading channels," *IEEE Transactions on Vehicular Technology,* vol. 53, pp. 351-362, 2004.

[83] H. Shin and M. Z. Win, "MIMO Diversity in the Presence of Double Scattering," *To appear in the IEEE Transactions on Information Theory*.

[84] D. Gesbert, H. Bolcskei, D. A. Gore, and A. J. Paulraj, "Outdoor MIMO wireless channels: models and performance prediction," *IEEE Transactions on Communications,* vol. 50, pp. 1926-1934, 2002.

[85] D. Chizhik, G. J. Foschini, M. J. Gans, and R. A. Valenzuela, "Keyholes, correlations, and capacities of multielement transmit and receive antennas," *IEEE Transactions on Wireless Communications,* vol. 1, pp. 361-368, 2002.

[86] S. Loyka and A. Kouki, "On MIMO channel capacity, correlations, and keyholes: analysis of degenerate channels," *IEEE Transactions on Communications,* vol. 50, pp. 1886-1888, 2002.

[87] P. Almers, F. Tufvesson, and A. F. Molisch, "Measurement of keyhole effect in a wireless multiple-input multiple-output (MIMO) channel," *IEEE Communications Letters,* vol. 7, pp. 373-375, 2003.

[88] S. W. Ellingson and D. W. Taylor, "Measurement of MIMO Capacity in a Hallway at 2.4 GHz," *Proceedings of IEEE Antennas and Propagation Society International Symposium,* pp. 4811-4814, 2006.

[89] D. Porrat, P. Kyritsi, and D. C. Cox, "MIMO capacity in hallways and adjacent rooms," *Proceedings of Global Telecommunications Conference,* vol. 2, pp. 1930-1934 vol.2, 2002.

[90] P. Kyritsi and D. C. Cox, "Modal analysis of MIMO capacity in a hallway," *Proceedings of IEEE Global Telecommunications Conference,* vol. 1, pp. 567-571 vol.1, 2001.

[91] D. Chizhik, F. Rashid-Farrokhi, J. Ling, and A. Lozano, "Effect of antenna separation on the capacity of BLAST in correlated channels," *IEEE Communications Letters* vol. 4, pp. 337-339, 2000.

[92] G. J. Foschini and M. J. Gans, "On limits of wireless communications in a fading environment when using multiple antennas," *Wireless Pers. Commun.,* vol. 6, pp. 311-335, Mar. 1998.

[93] M. A. Jensen and J. W. Wallace, "A review of antennas and propagation for MIMO wireless communications," *IEEE Transactions on Antennas and Propagation,* vol. 52, pp. 2810-2824, 2004.

[94] E. Biglieri, J. Proakis, and S. Shamai, "Fading channels: information-theoretic and communications aspects," *IEEE Transactions on Information Theory,* vol. 44, pp. 2619-2692, 1998.

[95] M. Z. Win and J. H. Winters, "Analysis of hybrid selection/maximal-ratio combining in Rayleigh fading," *Proceedings of IEEE International Conference on Communications 1999,* vol. 1, pp. 6-10 vol.1., 1999.

Vita

Jong Han Kim received the B.S. and M.S. degrees, both in electronic engineering, from Korea University in Seoul, Korea, in 1995 and 1997, respectively. From 1997 to 2002, he was a Senior Engineer with Samsung Electronics, Korea, and was involved in the design of cdma2000 1x mobile modem series. Since 2003, he has been pursuing his Ph.D. degree at Virginia Tech, and working in the area of performance analysis of antenna array processing with Prof. Jeffrey H. Reed, and Prof. A. Annamalai. His research interests include multiple input/multiple output (MIMO) systems and efficient implementation of communication systems.